

Cancer Dissemination Pathways
Series Editor: Daniele Regge

Nicola Sverzellati
Mario Silva *Editors*

The Thorax

Cancer Dissemination Pathways

Daniele Regge

University of Torino, Torino, Italy

Candiolo Cancer Centre, Torino, Italy *Series Editor*

This series aims to describe pathways of cancer dissemination in a practical and clinically driven approach that will enable the reader to define cancer dissemination accurately and thus to predict patient outcome and select the best therapeutic option. Each volume will include an introduction on the role of morphopathological and genetic drivers of cancer spread, followed by a chapter describing the anatomy, pathways of diffusion, and signs of disease. The subsequent chapters will include a systematic review of pathways of dissemination of each neoplasm. The content will be presented in an extremely schematic way, with high-quality illustrations and images obtained with different modalities (US, CT, MRI, and PET). The clinical significance of findings and possible therapeutic options will also be discussed whenever significant. Dynamic images will be included in the online version.

More information about this series at <http://www.springer.com/series/13608>

Nicola Sverzellati

Mario Silva

Editors

The Thorax

Editors

Nicola Sverzellati

Scienze Radiologiche – Department of
Medicine and Surgery (DiMeC)
University of Parma
Parma, Italy

Mario Silva

Scienze Radiologiche – Department of
Medicine and Surgery (DiMeC)
University of Parma
Parma, Italy

ISSN 2510-3474

ISSN 2510-3482 (electronic)

Cancer Dissemination Pathways

ISBN 978-3-030-27232-6

ISBN 978-3-030-27233-3 (eBook)

<https://doi.org/10.1007/978-3-030-27233-3>

© Springer Nature Switzerland AG 2020

This work is subject to copyright. All rights are reserved by the Publisher, whether the whole or part of the material is concerned, specifically the rights of translation, reprinting, reuse of illustrations, recitation, broadcasting, reproduction on microfilms or in any other physical way, and transmission or information storage and retrieval, electronic adaptation, computer software, or by similar or dissimilar methodology now known or hereafter developed.

The use of general descriptive names, registered names, trademarks, service marks, etc. in this publication does not imply, even in the absence of a specific statement, that such names are exempt from the relevant protective laws and regulations and therefore free for general use.

The publisher, the authors, and the editors are safe to assume that the advice and information in this book are believed to be true and accurate at the date of publication. Neither the publisher nor the authors or the editors give a warranty, expressed or implied, with respect to the material contained herein or for any errors or omissions that may have been made. The publisher remains neutral with regard to jurisdictional claims in published maps and institutional affiliations.

This Springer imprint is published by the registered company Springer Nature Switzerland AG
The registered company address is: Gewerbestrasse 11, 6330 Cham, Switzerland

To the past, the present, and the future collaborators who make our profession so special and keep bringing intellectual input in the continuous strain toward excellence.

To my wife, Martina, and daughter, Alice.

– Nicola Sverzellati

To my daughters, Agata and Adele, but mostly to my brilliant wife and best friend, Monica. Your support, love, and laughter are everything to me.

– Mario Silva

Preface

Thoracic tumors represent a heterogeneous group of benign and malignant lesions. Primary tumors can originate from each of the various components of the thorax, including the lungs, airways, pleura, mediastinum, and all the tissue components of the chest wall. Furthermore, similar involvement is also seen in thoracic dissemination of malignancies, either from thoracic or extrathoracic primary tumors.

This book has been written to provide radiologists, physicians, pathologists, and thoracic surgeons with a one-volume account of imaging findings that represent the patterns of dissemination of the primary thoracic malignancies. In particular, integrated review of the radiological appearances encountered in these tumors and their most common differential by a clinical streamline approach is granted by comprehensive description of the clinical scenario for each topic, along with

detailed findings by the most recent imaging techniques.

An easy-to-read format including introductory sections (e.g., epidemiology, pathology, imaging features, staging, treatment) and patterns of dissemination has been applied to each chapter dealing with individual tumors.

This book is meant as a resource for radiologists seeking comprehensive and translational understanding of both common and uncommon patterns of thoracic tumors dissemination. It is intended for guidance in clinical practice with the most accurate assessment of the disease staging with the accompaniment of pathological background. The most synergistic coupling of radiology and pathology spectra is provided for comprehensive description of the clinical behavior of thoracic tumors and systematic clinical assessment, according to likelihood rank.

Nicola Sverzellati

Mario Silva

Parma, Italy

Contents

1	Mechanisms of Tumor Dissemination in Thoracic Neoplasms	1
	<i>Francesca Locatelli, Francesca Ambrosi, and Giulio Rossi</i>	
2	Radiological Signs of Tumor Dissemination	35
	<i>Lucian Beer, Felicitas Oberndorfer, Mario Silva, and Helmut Prosch</i>	
3	Non-Small Cell Lung Cancer: Common Types	47
	<i>Cristiano Rampinelli, Antonio Passaro, Monica Casiraghi, and Cristiana Fanciullo</i>	
4	Non-Small Cell Lung Cancer: Rare Types	63
	<i>Andrea Borghesi, Silvia Michelini, and Andrea Tironi</i>	
5	Pulmonary Neuroendocrine Neoplasms	87
	<i>Anna Rita Larici, Giuseppe Cicchetti, Giulia D'Ambra, Rosa D'Abronzo, Annemilia del Ciello, Lucio Calandriello, Alessandra Farchione, Riccardo Manfredi, and Guido Rindi</i>	
6	Tumors of the Thymus	105
	<i>Carlotta Sartorio, Andrea Ciuni, and Gianluca Milanese</i>	
7	Other Mediastinal Tumors	127
	<i>Francesca Milone, Gianluca Taronna, Letizia Gnetti, and Mario Silva</i>	
8	Primary Tumors of the Pleura	159
	<i>Roberta Eufrasia Ledda, Claudia Commisso, Luciano Cardinale, and Nicola Sverzellati</i>	
9	Tumors of the Chest Wall	181
	<i>Elisa Baratella, Ilaria Fiorese, Sundeep M. Nayak, and Stefano Lovadina</i>	

Contributors

Francesca Ambrosi

Pathology Unit, Department of Experimental,
Diagnostic and Specialty Medicine
University of Bologna
Bologna, Italy
francesca.ambrosi@unibo.it

Elisa Baratella

Department of Radiology
Azienda Sanitaria Universitaria Integrata di
Trieste (ASUITS)
Trieste, Italy
elisa.baratella@gmail.com

Lucian Beer

Department of Biomedical Imaging and
Image-guided Therapy
Medical University of Vienna
Wien, Austria

Department of Radiology and Cancer Research
UK Cambridge Center
University of Cambridge
Cambridge, UK
lucian.beer@meduniwien.ac.at

Andrea Borghesi

Department of Radiology
University and ASST Spedali Civili of Brescia
Brescia, Italy
andrea.borghesi@unibs.it

Lucio Calandriello

Fondazione Policlinico Universitario "A. Gemelli"
IRCCS – Dipartimento Diagnostica per
Immagini, Radioterapia Oncologica ed
Ematologia
Rome, Italy
lucio.calandriello@policlinicogemelli.it

Luciano Cardinale

SCDU Radiodiagnostica e Medicina Nucleare
Azienda Ospedaliero-Universitaria S Luigi
Gonzaga
Orbassano, Italy
luciano.cardinale@gmail.com

Monica Casiraghi

Division of Thoracic Surgery
European Institute of Oncology, IRCCS
Milan, Italy
monica.casiraghi@ieo.it

Giuseppe Cicchetti

Fondazione Policlinico Universitario "A. Gemelli"
IRCCS – Università Cattolica del Sacro Cuore –
Dipartimento Diagnostica per Immagini,
Radioterapia Oncologica ed Ematologia –
Istituto di Radiologia
Rome, Italy
cicchetti.giuseppe88@gmail.com

Andrea Ciuni

Scienze Radiologiche – Department of
Medicine and Surgery (DiMeC)
University of Parma
Parma, Italy
andrea.ciuni@studenti.unipr.it

Claudia Comisso

Scienze Radiologiche – Department of
Medicine and Surgery (DiMeC)
University of Parma
Parma, Italy
comissoclaudia@gmail.com

Rosa D'Abronzo

Fondazione Policlinico Universitario "A. Gemelli"
IRCCS – Università Cattolica del Sacro Cuore –
Dipartimento Diagnostica per Immagini,
Radioterapia Oncologica ed Ematologia –
Istituto di Radiologia
Rome, Italy
rosadabronzo@hotmail.it

Giulia D'Ambra

Fondazione Policlinico Universitario "A. Gemelli"
IRCCS – Università Cattolica del Sacro Cuore –
Dipartimento Diagnostica per Immagini,
Radioterapia Oncologica ed Ematologia –
Istituto di Radiologia
Rome, Italy
dambragiulia@gmail.com

Annemilia del Ciello

Fondazione Policlinico Universitario "A. Gemelli"
IRCCS – Dipartimento Diagnostica per
Immagini, Radioterapia Oncologica ed
Ematologia
Rome, Italy
annemilia.delciello@policlinicogemelli.it

Cristiana Fanciullo

School of Medicine
University of Milan
Milan, Italy
fanciullo.cristiana@gmail.com

Alessandra Farchione

Fondazione Policlinico Universitario "A. Gemelli"
IRCCS – Dipartimento Diagnostica per
Immagini, Radioterapia Oncologica ed
Ematologia
Rome, Italy
alessandra.farchione@policlinicogemelli.it

Ilaria Fiorese

Department of Medicine, Surgery
and Health Science
University of Trieste
Trieste, Italy
fiorese.ilaria@gmail.com

Letizia Gnetti

Pathology Section
University Hospital of Parma
Parma, Italy
letizia.gnetti@unipr.it

Anna Rita Larici

Fondazione Policlinico Universitario "A. Gemelli"
IRCCS – Università Cattolica del Sacro Cuore –
Dipartimento Diagnostica per Immagini,
Radioterapia Oncologica ed Ematologia –
Istituto di Radiologia
Rome, Italy
annarita.larici@unicatt.it

Roberta Eufrasia Ledda

Scienze Radiologiche – Department of
Medicine and Surgery (DiMeC)
University of Parma
Parma, Italy
roberta.ledda@hotmail.com

Francesca Locatelli

Operative Unit of Pathologic Anatomy, Azienda
USL della Romagna, Hospital degli Infermi
Rimini, Italy
francesca.locatelli@auslromagna.it

Stefano Lovadina

Thoracic Surgery Unit, ASUITS
Trieste, Italy
stelova@hotmail.com

Riccardo Manfredi

Fondazione Policlinico Universitario "A. Gemelli"
IRCCS – Università Cattolica del Sacro Cuore –
Dipartimento Diagnostica per Immagini,
Radioterapia Oncologica ed Ematologia –
Istituto di Radiologia
Rome, Italy
riccardo.manfredi@unicatt.it

Silvia Michelini

Department of Radiology
Fondazione Poliambulanza Istituto Ospedaliero
Brescia, Italy
silviamichelini2015@gmail.com

Gianluca Milanese

Scienze Radiologiche – Department of
Medicine and Surgery (DiMeC)
University of Parma
Parma, Italy
gianluca.milanese@studenti.unipr.it

Francesca Milone

Scienze Radiologiche – Department of
Medicine and Surgery (DiMeC)
University of Parma
Parma, Italy
francesca.milone1@gmail.com

Sundeep M. Nayak

Department of Radiology
Kaiser Permanente Northern California
San Leandro, CA, USA
sundeep.nayak@gmail.com

Felicitas Oberndorfer

Department of Pathology
Medical University of Vienna
Wien, Austria
felicitas.oberndorfer@meduniwien.ac.at

Antonio Passaro

Division of Thoracic Oncology
European Institute of Oncology, IRCCS
Milan, Italy
antonio.passaro@ieo.it

Helmut Prosch

Department of Biomedical Imaging and
Image-guided Therapy
Medical University of Vienna
Wien, Austria
helmut.prosch@meduniwien.ac.at

Cristiano Rampinelli

Division of Radiology
European Institute of Oncology, IRCCS
Milan, Italy
cristiano.rampinelli@ieo.it

Guido Rindi

Fondazione Policlinico Universitario "A. Gemelli"
IRCCS – Università Cattolica del Sacro Cuore –
Dipartimento Scienze della Salute della Donna
e del Bambino e di Sanità Pubblica – Istituto di
Anatomia Patologica
Rome, Italy
guido.rindi@unicatt.it

Giulio Rossi

Operative Unit of Pathologic Anatomy
Azienda USL della Romagna, Hospital S. Maria
delle Croci
Ravenna, Italy
giurossi68@gmail.com

Carlotta Sartorio

Scienze Radiologiche – Department of
Medicine and Surgery (DiMeC)
University of Parma
Parma, Italy
carlotta.sartorio@studenti.unipr.it

Mario Silva

Scienze Radiologiche – Department of
Medicine and Surgery (DiMeC)
University of Parma
Parma, Italy
mario.silva@unipr.it

Nicola Sverzellati

Scienze Radiologiche – Department
of Medicine and Surgery (DiMeC)
University of Parma
Parma, Italy
nicola.sverzellati@unipr.it

Gianluca Taronna

Scienze Radiologiche – Department of
Medicine and Surgery (DiMeC)
University of Parma
Parma, Italy
gianluca.taronna@gmail.com

Andrea Tironi

Department of Pathology
ASST Spedali Civili of Brescia
Brescia, Italy
ndr.tironi@gmail.com



Mechanisms of Tumor Dissemination in Thoracic Neoplasms

Francesca Locatelli, Francesca Ambrosi, and Giulio Rossi

- 1.1 Introduction – 2**
- 1.2 Shared Dissemination Pathways of Primary and Secondary Malignancies of the Thorax – 3**
- 1.3 Tumor Dissemination in Primary Malignant Lung Tumors and Metastases – 4**
 - 1.3.1 Radiopathologic Correlation of Ancillary Signs of Thoracic Malignancy – 8
- 1.4 Tumor Dissemination and Oncogenic Driver Gene Alterations in Primary Lung Cancer and Metastases – 22**
- 1.5 Primary Malignant Tumors Mimicking Metastatic Lesions and Vice Versa – 23**
- 1.6 Tumor Dissemination in Secondary Benign Neoplasms – 23**
- 1.7 Tumor Dissemination in Mesothelioma – 25**
- 1.8 Tumor Dissemination in Other Primary Thoracic Neoplasms – 26**
 - 1.8.1 Soft Tissue Tumors – 26
 - 1.8.2 Lymphomas of the Thorax – 26
 - 1.8.3 Thymic Neoplasms – 28
- 1.9 Conclusion – 29**
- References – 29**

1.1 Introduction

Tumors commonly show several patterns of spread due to direct growth into adjacent structures, as well as lymphatic and hematogenous dissemination. However, the lung represents a peculiar site both for primary cancer and metastatic malignancies. In particular, the singularity of lung dissemination is found in aerogenous spread, an old concept recently reintroduced under the definition of “spread through airspaces (STAS).” STAS is basically related to the unique architecture of the lung where airspaces can be traveled across relatively easily by cells. Although this is a characteristic feature of adenocarcinomas (ADC) (formerly known as bronchioloalveolar carcinoma, BAC), even other histological types may show this dissemination pathway. Of note, aerogenous dissemination justifies some unusual imaging findings mimicking benign diseases, such as miliary pattern or ground-glass opacities (GGO).

Beyond STAS in lung cancer, further primary neoplasms of the thorax show patterns of local growth by direct invasion into adjacent structures and organs, including pleura, mediastinum, chest wall, and spine.

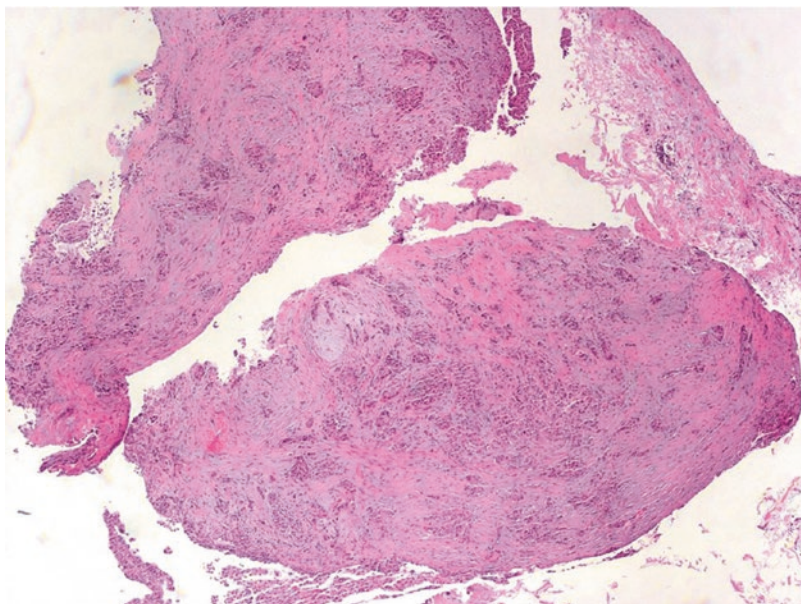
Pleural invasion is the effect of direct extension of tumor growth into the pleura rather than seeding from hematogenous or lymphatic pathway. Demonstration of pleural invasion from lung cancer is highlighted by desmoplastic fibroblastic stroma or

disruption of elastic tissue. Growth of tumor cells on the pleural surface may mimic mesothelioma; this phenomenon is also known as pseudo-mesotheliomatous adenocarcinoma (■ Fig. 1.1). Pleural effusion may be due to pleural seeding; nonetheless, lymphatic or pulmonary venous obstruction as well as inflammatory reaction by the tumor cells can display such evolution.

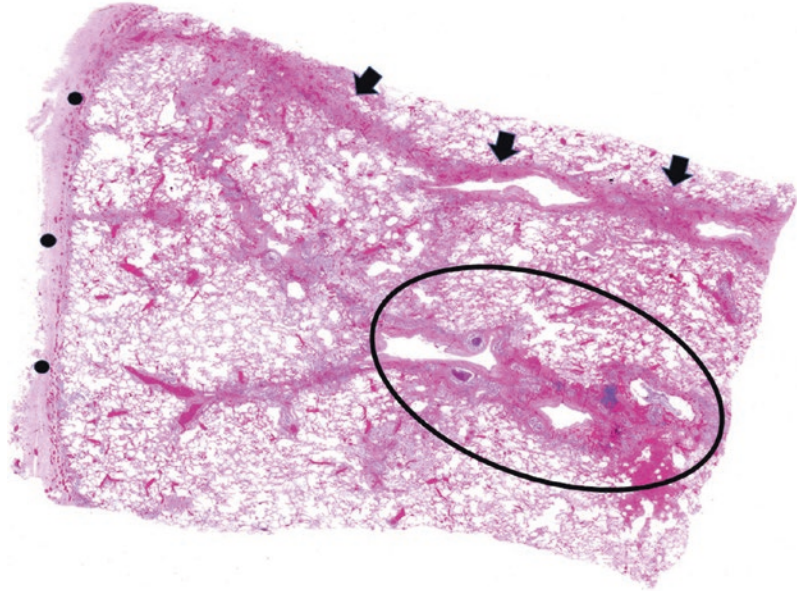
Lymphatic dissemination is very common, particularly in lung cancer with adenocarcinoma histology. Lymphatics represent a main structural network within the intangible texture of the lung; the anatomic distribution of lymphatic drainage is diffuse from the pleura to the bronchial structures, namely, from the very periphery to the hila, including a tight network throughout. Lymphatic dissemination in lung cancer becomes a determinant of therapeutic approach (e.g., surgery or medical therapy), and it represents a major prognostic factor, as deployed in lung cancer staging system. Tumor spread through lymphatic channels is also characteristic of other neoplasms beyond lung cancer, notably lymphoproliferative diseases and metastatic tumors (■ Fig. 1.2).

Finally, vascular invasion is extremely common in carcinomas, involving large or small vessels, veins, or arteries. Vascular invasion translates into hematogenous dissemination leading to systemic tumor cell dissemination to extrathoracic sites. Massive lymphatic/hematogenous invasion is the cause of neoplastic thrombotic microangi-

■ Fig. 1.1 Generous pleuroscopy biopsy of a pseudo-mesotheliomatous adenocarcinoma of the lung manifesting as a prominent pleura-based neoplasm mimicking mesothelioma growth pattern



■ **Fig. 1.2** A low magnification of lung parenchyma with lymphangitic carcinomatosis involving the interlobular septa (arrows), pleural surface (dots), and bronchovascular bundles (circle)



opathy often simulating interstitial lung diseases on pathology as well as on imaging. Notably, this pattern is becoming more and more challenging in the evolving scenario of medical oncology because adverse events to new agents are increasingly common (sometimes asymptomatic) and their imaging pattern might substantially overlap signs of tumor progression. Different mechanisms of metastasis in primary and secondary neoplasms are here presented.

1.2 Shared Dissemination Pathways of Primary and Secondary Malignancies of the Thorax

Growth and spread of primary and secondary thoracic neoplasms mainly depend on the peculiar anatomy of the thoracic region (in particular the pulmonary structure), the type of tumor, and the colonized tissue.

The most common category of tumors in the lung parenchyma is metastatic malignancies [1]. This fact can be explained by two pivotal anatomic characteristics of the lung: the whole venous and lymphatic drainage of the body is collected into the right heart toward the lungs. Namely, systemic bloodstream and lymphatics of most organs are in parallel with one another, but lung is in series. Therefore, any organ is drained into the lung, which ultimately can filter out metabolic derivate

as well as becomes a first stop site of neoplastic cells that are filtered through its exceptionally dense capillary bed. Noteworthy, such rich capillary bed provides abundant oxygen to early metastasis, which will thereafter be supplied by bronchial arteries [2].

Lung metastasis and primary lung tumors share the same dissemination pathways. Hematogenous dissemination, either arterial or venous, is the most common pathway, followed by lymphatics, endobronchial, pleural, and aerogenic diffusion, and direct extension. A combination of the above pathways is quite common in lung cancer at the time of diagnosis [1, 2].

Primary lung carcinomas mainly disseminate by lymphatic channels or airway dissemination, while pulmonary metastases from carcinoma, sarcoma, and lymphoma metastasize to the lung via the bloodstream [3]. As expected, adenocarcinoma from any organ is the most common subgroup of lung metastasis because of its epidemic incidence, notably from the breast, digestive tract, kidney, head/neck region, pancreato-biliary region, uterine leiomyosarcoma, and lung itself [2–6].

Similar spreading routes can determine similar histopathologic patterns of spread in both primary lung cancer and secondary thoracic malignancy. Patterns of spread are classified into infiltrative/destructive, interstitial, lepidic, and alveolar filling [1–4]. Such pathways rely on the structure of the secondary lobule: a polygonal unit, sized 1–2 cm in

diameter, consisting of acinar structures with peripheral boundary by the pleura and/or connective tissue of interlobular septa, the latter including lymphatics and venules [7, 8]. The center of the lobule is represented by the bronchovascular bundle made up of bronchioles and arterioles; it is usually larger than the peripheral veno-lymphatic complex. Indeed, it is also depicted on computed tomography, whereas the lobule periphery is seen only in case of abnormal thickening. The most volume of the secondary lobule is represented by alveoli surrounded by intralobular septa that contain the smallest branches of arterioles and venules and the capillary network [7–9]. Lung metastasis can simulate primary tumors both grossly and microscopically, and sometimes the differential diagnosis can be challenging and critical, even at pathology. Radiologists and clinicians must be aware that an independent primary lung tumor should always be considered in a patient with metastatic disease and vice versa. The detailed description of both radiologic and histopathologic findings in cancer patients allows accurate image interpretation throughout its wide spectrum of display and robust reasoning toward diagnosis. Immunohistochemistry and extractive molecular biology can become relevant for assisting the pathologist to refine the differential and drive the final diagnosis.

1.3 Tumor Dissemination in Primary Malignant Lung Tumors and Metastases

Primary lung tumor typically exhibits a histologic infiltrative/destructive pattern. It occurs more frequently as solitary nodule in the upper lobes and shows infiltrative dissemination to the surrounding lung parenchyma. In the destructive pattern, general characteristics such as site, location, and multicentricity, together with the clinical history, can suggest the distinction between primary lung tumor and metastasis, but unusual presentation can occur. Expansive borders are seen as the second most common dissemination pathway across the intangible pulmonary texture. There are exceptions to the aforementioned dissemination pathways; notably some adenocarcinomas (e.g., lepidic adenocarcinoma) happen to show dissemination by cellular leaning over alveolar epithelium (pulmonary structure is preserved).

Most primary lung tumors are represented by non-small-cell lung cancer (NSCLC) into either adenocarcinoma (ADC) or squamous cell carcinoma (SCC) histology and neuroendocrine tumors (NET) including carcinoid tumors and high-grade neuroendocrine tumor such as large-cell (LCNEC) and small-cell-lung carcinoma (SCLC). Primary invasive ADC of the lung and roughly one third of primary SCC present as a peripheral solitary nodule or mass, more frequently involving the upper lobes [2, 3]. A large peripheral mass is more commonly an ADC, while a hilar mass is more commonly a SCC or a SCLC [1], and they usually associate with lymph node involvement, either unilateral or bilateral. SCLC is an aggressive, smoking-related, high-grade NET that characteristically presents as a large hilar mass with bulky mediastinal lymph nodes. Unlike NSCLC, SCLC tends to involve adjacent structures by direct invasion, and it translates into frequent onset of superior vena cava syndrome. Occasionally, SCLC can occur as a predominant endobronchial mass and in about 5% of cases can be detected by CT screening as a peripheral nodule, even node-negative [2, 3]; however, the outcome of SCLC remains poor even with screening [10]. LCNEC occurs more frequently peripherally, and it is seldom associated with bulky intrathoracic lymph nodes. Signs, symptoms, and imaging findings of other rarer histological types mostly overlap with NSCLC.

Unlike primary lung cancer, metastases are more frequently multiple and bilateral and show a random nodular distribution. Metastases used to be overall smaller than primary lung cancer; notably, they show heterogeneous size depending on the temporal evolution of spread or on the type of “soil,” according to Paget’s theory [6]. Furthermore, hematogenous metastases to the lung usually appear as well-delimited findings with smooth margins; they mostly are round, oval, or lobulated in shape. Like most primary lung ADC, metastases tend to be peripherally located, but unlike ADC they prefer the lower or middle lung fields according to perfusion gradient [1, 2]. Metastases have usually a rapid growth, substantially faster than primary adenocarcinoma. The most common spreading patterns in primary lung cancer and metastatic tumors to the lungs are reported in [Table 1.1](#).

Table 1.1 Tumor cell dissemination in lung primary and metastasis

Spreading features	Primary lung tumor	Metastasis
Multiple or solitary peripheral located	Multiple peripheral nodules are usually mucinous invasive adenocarcinoma or lepidic/papillary/micropapillary adenocarcinoma; intrapulmonary metastases by adenocarcinoma may occur Peripheral solitary nodules in the upper lobes are usually adenocarcinoma, more often TRU type Carcinoid tumors Squamous cell carcinoma in pulmonary fibrosis	Usually multiple, bilateral, peripheral, and randomly distributed nodules with rounded, well-defined margins and variable size Sometimes solitary nodules: Colorectal carcinomas Malignant melanoma Skeletal sarcoma Testicular carcinoma Other adenocarcinomas
Centrally located hilar/peri-hilar and endobronchial	Squamous cell carcinoma Small cell carcinoma Bronchial-type adenocarcinoma Carcinosarcoma Salivary gland tumors Carcinoid tumor	Breast cancer Anaplastic thyroid carcinoma Colorectal carcinoma Renal cell carcinoma Lymphoma/plasmacytoma Sarcomas
Hilar and mediastinal intrathoracic nodes	Small cell carcinoma > centrally located adenocarcinoma Squamous cell carcinoma	Prostatic cancer Breast carcinoma Renal cell carcinoma Testicular tumor Pancreatic carcinoma from the tail Papillary thyroid carcinoma
Cavitation	Squamous cell carcinoma Mucinous adenocarcinoma (pseudocavitation) Pleomorphic, spindle cell, and giant cell carcinoma Sarcoma	Sarcoma
Calcification	Pulmonary hamartoma Chondroma Mucinous adenocarcinoma Primary tumors with necrosis	Colorectal adenocarcinoma Mucinous metastatic carcinoma Osteosarcoma Condrosarcoma Treated metastatic choriocarcinoma
Cystic spaces	Tumors of ectopic origin Erdheim-Chester disease LAM	Choriocarcinoma Endometrial stromal sarcoma Benign metastasizing leiomyoma Leiomyosarcoma Cellular fibrous histiocytoma
Lepidic pattern	Lepidic adenocarcinoma	Pancreatic adenocarcinoma Colorectal adenocarcinoma Melanoma Mesothelioma
Aerogenous	Mucinous invasive adenocarcinoma Micropapillary and papillary adenocarcinoma Epithelioid hemangioendothelioma	Mucinous invasive carcinoma

(continued)

Table 1.1 (continued)

Spreading features	Primary lung tumor	Metastasis
Interstitial/septal	Adenocarcinoma with lymphangitic spread Kaposi sarcoma Angiosarcoma Intravascular lymphoma Erdheim-Chester disease	Lymphangitic carcinomatous: Gastric carcinoma Breast cancer Pancreatic carcinoma Kaposi sarcoma Angiosarcoma Cervical carcinoma Melanoma Lymphomas
Miliary/nodular pattern	Adenocarcinoma DIPNECH Meningotheliomatosis	Thyroid papillary carcinoma Medullary carcinoma Melanoma Renal cell carcinoma Ovarian cancer Osteosarcoma Trophoblastic tumors, especially choriocarcinoma
Pleural spreading	Diffuse malignant mesothelioma Peripheral adenocarcinoma	Lymphoproliferative disorders Benign/malignant mesenchymal tumors

Abbreviations: TRU terminal respiratory unit, LAM lymphangioleiomyomatosis, DIPNECH diffuse idiopathic pulmonary neuroendocrine cell hyperplasia

However, exceptions to this rule can occur, such as solitary lung metastasis or multiple primary lung tumors. Solitary lung metastases are reported in 3–9% of the cases [2]; they can present as large cannon ball, even larger than 5 cm, formerly frequent event from colorectal carcinoma [2]. Solitary metastases to the lung are also seen in melanoma, sarcoma, testicular carcinoma, and extrathoracic ADC [2]. Metastases to the lung are also seen in young age, with sarcoma and germ cell neoplasms being the most frequent cause of hematogenous dissemination [3, 4]. Lung metastases are expected to follow a clinical history of extrapulmonary neoplasms; however, it happens in 20–54% of cases. Otherwise, in 15–25% of cases, the lung is the only site of the so-called anachronous metastasis, be they solitary or multiple [2].

Nonetheless, clinicians must be aware that solitary lung nodules in patients with extrathoracic neoplasms can also be a primary tumor. According to Filderman, this situation is more likely to occur in cancers of the lung (e.g., second primary), breast, stomach, prostate, and head and neck. Conversely, primary lung cancer is less fre-

quent in case of melanomas and sarcoma. Lung solitary nodules in patients with carcinomas of kidneys, colon, or testes have the same probability to be either primary or secondary [11].

Unfortunately, there is no perfect panel of immunostains to distinguish a primary from a metastatic tumor; hence, careful clinico-radiological correlation is mandatory. This is especially true for the differential diagnosis between a primary SCC and a metastatic SCC of head and neck, esophagus, or cervix origin. The comparative use of p16 and p53 immunostaining status can sometimes be helpful to the purpose of histological differential [2, 3]: the association of SCC from head and neck with HPV/p16 is more straightforward than its pulmonary counterpart. Finally, SCC should be distinguished from metastatic urothelial carcinoma, which is positive for GATA3 [2, 3, 12–16] (■ Fig. 1.3). A practical list of the most important immunostains involved in the diagnosis of primary versus secondary malignancy is summarized in ■ Table 1.2.

Multiple primary lung cancers are not uncommon, especially invasive mucinous ADC and lepidic ADC, formerly known as bronchioloalveolar

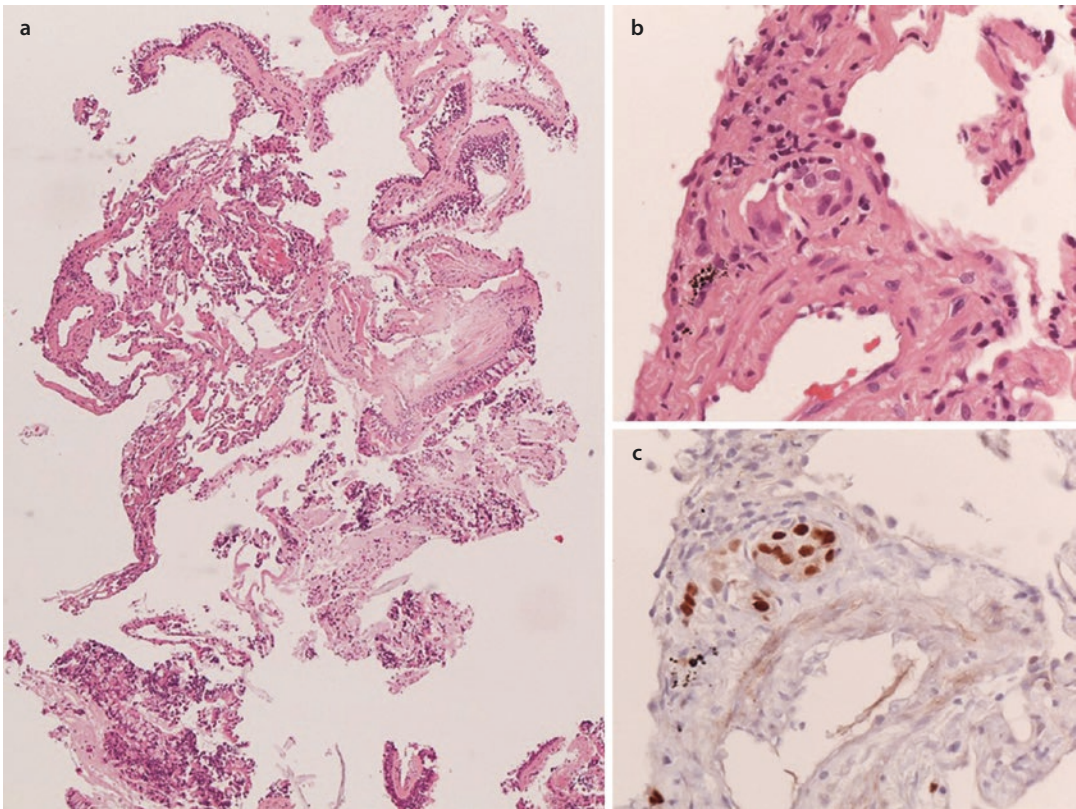


Fig. 1.3 Transbronchial biopsy **a** showing a tiny aggregate of tumor cells into a lymphatic channel **b**. Positive anamnesis of mammary neoplasm and expression

of estrogen receptors **c** supported the diagnosis of pulmonary dissemination/metastasis from breast cancer

Table 1.2 Practical summary of the most important immunohistochemical stains in the identification of cell differentiation of various primary/metastatic neoplasms

Tumors	Positive primary antibodies
Primary adenocarcinoma (except mucinous carcinoma)	TTF-1 (clone 8G7G3/1 more specific than SPT24 and SP141), napsin A (monoclonal more specific than polyclonal), CK7
Colorectal adenocarcinoma	CK20, CDX2+ (positive in a subset of primary adenocarcinoma of the lung with goblet/colloid/enteric morphology), SATB2 (particularly helpful in mucinous type)
Breast carcinoma	ER/PgR, GCDFP15, GATA3 (hormone-dependent), mammaglobin, CK7
Merkel cell carcinoma	CK20 (dot-like), NF, polyomavirus, neuroendocrine markers
Melanoma	S100, HMB45, melan-A, SOX10, tyrosinase, MiTF
Thymic epithelial tumors (thymoma and carcinoma)	CD5 (carcinoma), PAX8, C117 (carcinoma), FOXN1, CD205, p63/p40
Squamous cell carcinoma	p63/p40 The presence of HPV/p16 is suggestive of a metastasis from head/neck region or uterine cervix, except primary squamous cell carcinoma arising in papillomatosis) High-molecular-weight cytokeratins (34betaE12, CK903, CK5/6), desmocollin, and desmoglein

(continued)

Table 1.2 (continued)

Tumors	Positive primary antibodies
Urothelial carcinoma	CK7, p40, GATA3, uroplakin 2/3
Germ cell tumors	CD30, alpha-FP, CKs, SALL4, PLAP, beta-HCG, OCT3–4, CD117
Prostatic adenocarcinoma	PSA, PSAP, AR, NKX3.1
Vascular neoplasms	CD31, CD34, FLI1, ERG, factor VIII, HHV8 (Kaposi sarcoma), CAMPTA-1 (epithelioid hemangioendothelioma)
Papillary and follicular thyroid cancer	TTF-1, thyroglobulin, HBME1, PAX8, CK7, CEA, calcitonin, and neuroendocrine markers in medullary carcinoma
Renal cell carcinoma	CK7, CD10, EMA, RCC, TFE3, SDH-B, HMB45 (PEComas)
Neuroendocrine neoplasm	Synaptophysin, chromogranin A, CD56, ASH-1
Mesothelioma	BAP1, CK7, HMBE1, calretinin, D2–40, WT1, CK5/6
Sarcomas other than vascular	Smooth-muscle actin, desmin, myogenin, STAT6 (solitary fibrous tumor); H3K27me3 (malignant peripheral nerve sheath tumor), S100, MDM2 (dedifferentiated liposarcoma); WT1, ETV4, TFE3 (synovial sarcoma), ALK (inflammatory myofibroblastic tumor), CDK4 (liposarcoma), SMARCB1 and SMARCA4, beta-catenin (desmoid/fibromatosis), NKX2.2, MUC4 (low-grade fibromyxoid sarcoma), INI1
Gynecological tumors	WT1, p63, p16, ER, inhibin, napsin A
Biliary/pancreas	CK7/CK20, CDX2, MUC1, CK17, CK19, CEA
Lymphoma and plasmacytoma	LCA, B-cell (CD20, CD79a, PAX5, CD10, bcl6, MUM1, MNDA, cyclin D1, SOX11), T-cell (CD2, CD3, CD4, CD5, CD7, CD8), bcl2, CD30, CD15, c-myc, BOB-1, ALK, TdT, CD56, CD57, CD38 and CD138 (plasma cells), light chains K and lambda, EBV, HHV8, BRAF (hairly cell leukemia), CD23 and CD35 (follicular dendritic cells), CD68 (macrophages), CD1a and Langerin (Langerhans cell histiocytosis), CD123 (plasmacytoid dendritic cells)

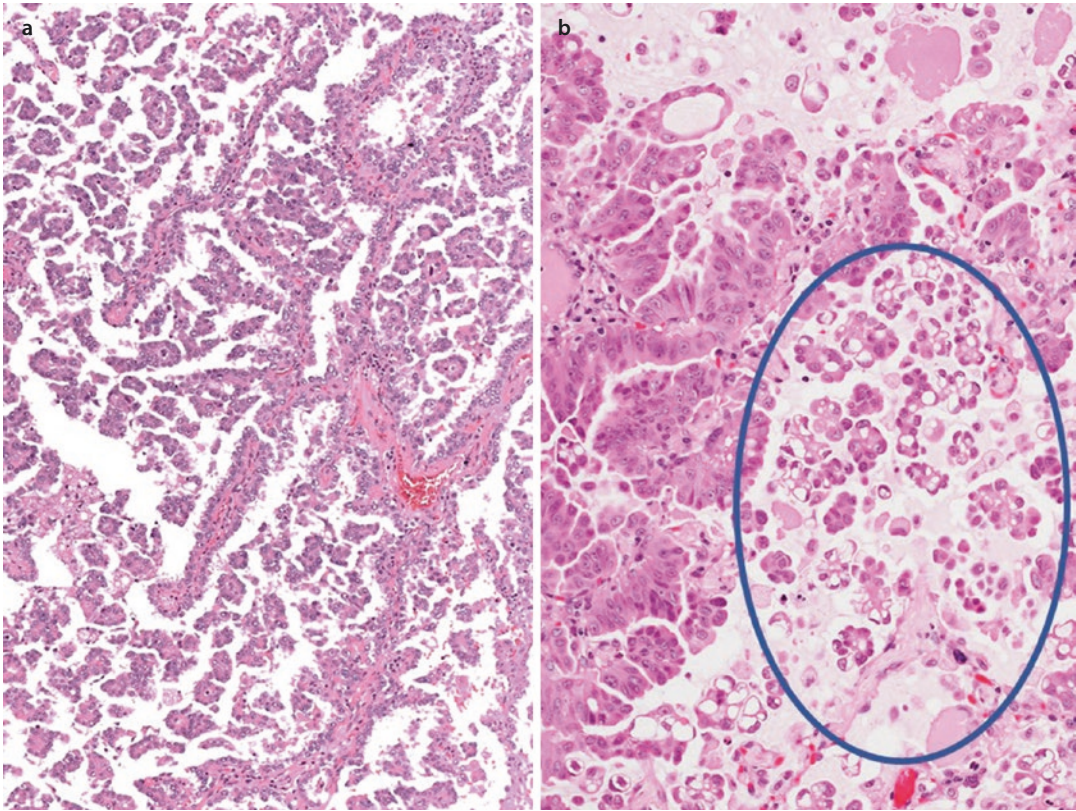
Abbreviations: IHC immunohistochemistry, TTF-1 thyroid transcription factor-1, CK cytokeratin, CDX caudal-type homeobox, ER estrogen, PGR progesterone, GCDFFP gross cystic disease fluid protein, NF neurofilament, PAX8 paired box gene 8, alpha-FP alpha fetoprotein, SALL4 Sal-like protein 4, PLAP placental alkaline phosphatase, HCG: human chorionic gonadotropin, PSA prostate-specific antigen, PSAP prostate-specific acid phosphatase, AR androgen receptor, FLI1 Friend leukemia integration, HBME1 Hector Battifora mesothelial-1, LMW low molecular weight, HMW high molecular weight, EMA epithelial membrane antigen, RCC renal cell carcinoma, PEComas perivascular epithelioid cell tumors, NSE neuron-specific enolase

carcinomas (BAC). Such histology tends to be multicentric, bilateral, and usually peripheral. The differential between multiple synchronous primary ADC and alveolar/aerogenous spread is quite challenging both at pathology and imaging. Synchronous intrapulmonary metastases from primary lung cancer can also manifest as multiple nodules or masses and should be differentiated from a primary tumor because of substantially different clinical management and prognosis. The comprehensive histologic subtyping, characteriza-

tion of cytology (clear cells or signet ring features), and stromal features (desmoplasia or inflammation) are most useful in case of multiple ADC.

1.3.1 Radiopathologic Correlation of Ancillary Signs of Thoracic Malignancy

Both primary and metastatic malignancies of the lung can occur with ancillary radiologic findings



■ Fig. 1.4 Lung adenocarcinoma with micropapillary pattern a and dissemination of tumor cells through airspaces (b, circle)

such as cavitation, calcification, hemorrhage, and cyst, which, together with other clinical characteristics, can suggest the proper diagnosis. The pathological counterpart of such radiological signs explains the heterogeneity of pulmonary malignancies, either primary or secondary, and the variable confidence in the differential. The radio-pathologic parallel is thereafter given.

1.3.1.1 Alveolar Pattern

Peculiar patterns of spread in the lung are the lepidic growth, the alveolar filling, and a recently recognized aerogenous (airspace) spread known as STAS. All these kinds of spread can be radiologically classified in the field of alveolar pattern [1, 2, 7]. Two signs can reflect the alveolar pattern on computed tomography: ground glass opacities (GGO) and parenchymal consolidation, the latter also typical of pneumonia. In histology, they are seen as filling of airspaces that ranges from partial (GGO) to complete (consolidation) [1, 2, 7] (■ Fig. 1.4).

In particular, the alveolar pattern is most commonly encountered in primary lung cancer with lepidic and mucinous ADC histology, respectively, associated with ground glass opacity and pneumonia-like consolidation [1, 2]. Papillary and micropapillary invasive ADC can also present with this pattern. As an aerogenous spread, this pattern of dissemination is oftentimes associated with multifocal and multilobar tumors, without a dominant nodule, and is characterized by the presence of satellite discontinuous neoplastic foci along the airspaces and airways around the tumor or, at distant, even in the contralateral lung [17, 18]. A very unusual variant of is represented by discohesive tumor cells filling and engulfing the alveolar spaces mimicking desquamative interstitial pneumonia (DIP), then called “malignant DIP” [19] (■ Fig. 1.5).

Lepidic Growth

Lepidic growth is considered a grade I histological pattern of invasive lung ADC [20], mucinous or not. The lepidic spreading is characterized by the

Fig. 1.5 An unusual pattern of tumor cell dissemination in lung adenocarcinoma with intra-alveolar growth of discohesive tumor cells with signet ring cell features mimicking macrophages in desquamative interstitial pneumonia

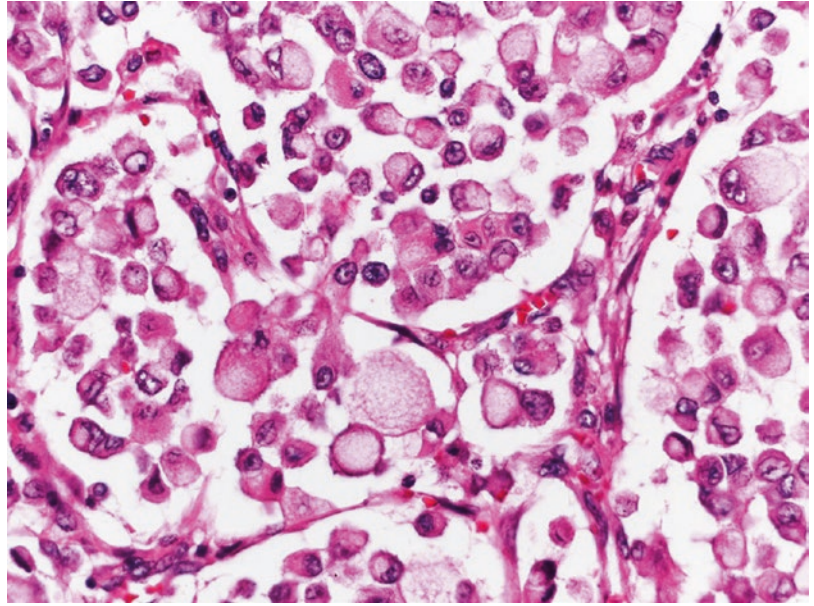
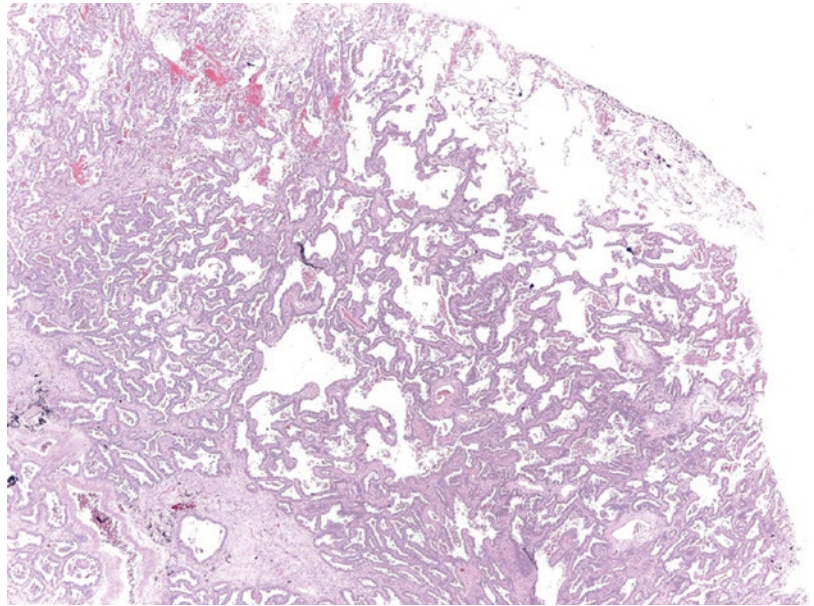


Fig. 1.6 Lung adenocarcinoma with lepidic growth characterized by preservation of the pulmonary alveolar architecture



growth of the neoplastic cells along the intact alveolar walls like *Lepidoptera* on a fence. It respects the microscopic structure of alveoli, without displacing or destroying the adjacent lung (■ Fig. 1.6). Pure lepidic or predominantly lepidic pattern is a mandatory criterion for the diagnosis of in situ ADC (AIS) and minimally invasive ADC, respectively. This definition applies to solitary and discrete tumor up to 3 cm in diam-

eter. The radiological counterpart of AIS is non-solid nodule (sole GGO component), while minimally invasive ADC is associated with part-solid nodules with solid component up to 5 mm.

Rarely, metastatic ADC to the lungs may show a lepidic pattern, but they do not typically express TTF-1 and type II pneumocytes and/or club (Clara) cell morphology [21]. Examples of metastatic melanoma were described with an alveolar/

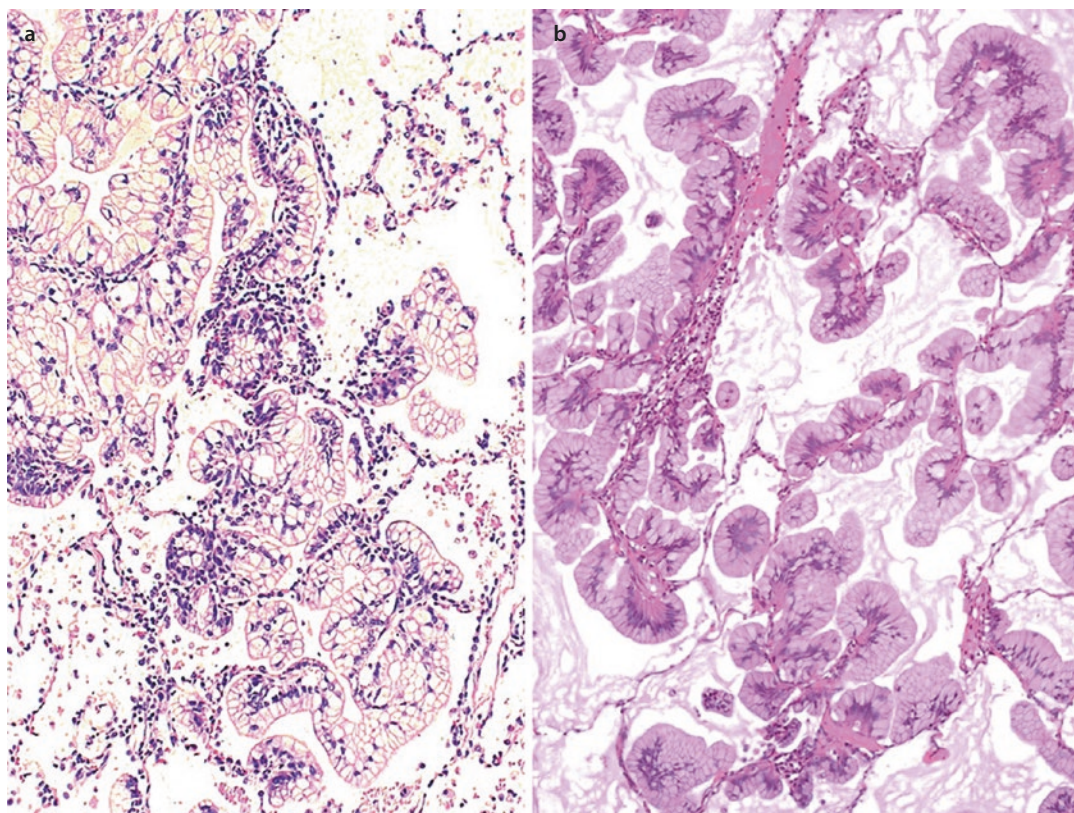


Fig. 1.7 Pulmonary metastasis from pancreatic cancer **a** and primary mucinous invasive adenocarcinoma **b** showing an identical growth pattern with mucin-rich tumor cells lining the alveoli forming papillary projection

interstitial growth, mimicking primary ADC and thus relatively insidious at differential [1, 2]. Metastases from pancreato-biliary or colorectal ADC also may grow in a lepidic fashion [21] (Fig. 1.7).

Mucinous invasive ADC can be radiologically characterized by consolidation that must be differentiated from both lipidic and obstructive pneumonia. Furthermore, mucinous invasive ADC is also characterized by the so-called bubble-like lucencies or pseudo-cavitations that are frequently described on computed tomography. The pathological counterpart of bubble-like lucencies is dilation of bronchioles from a valve mechanism of bronchiolar obstruction or desmoplastic traction or expression of spared pulmonary lobules. The bubble-like lucency can also present as pseudo-cavitation, which however must be distinguished from real cavitation [1, 2]. Lepidic growth of primary mucinous ADC comes into the differential with primary lung colloid ADC (characterized by abundant extracellular mucin that destroys

and replaces the parenchyma) and with metastases from pancreatic, biliary, colorectal, gastric, and breast carcinoma. Immunohistochemistry can help in such differential [3, 4, 22].

Intra-alveolar Pattern of Growth

Intra-alveolar pattern of growth is typical of epithelioid hemangioendothelioma, described previously as intravascular bronchioloalveolar tumor, usually a multifocal vascular neoplasm typical of young female that can have a nodular pattern in the lung; it is histologically characterized by nodular aggregates of epithelioid cells with intracytoplasmic lumina embedded in a myxochondroid or hyaline stroma, simulating ADC, sarcoma, metastatic cardiac myxoma, or sclerosing pneumocytoma.

Spread Through Airspaces

Recently, the term “spread through airspaces” (STAS) has been reintroduced by Kadota et al. [23] to define the presence of micropapillary clus-

ters, solid nests, or single cells in alveolar spaces beyond the edge of the main tumor and within the surrounding lung parenchyma. STAS probably contributes to the significantly increased risk of recurrences for patients with small stage I ADC who undergo limited resections and to the worse survival observed by others. Kadota et al. [23] found STAS to be significantly associated with any recurrence in small (≤ 2 cm) stage I lung ADC treated by limited resection, compared with lobectomy. After the validation of STAS in two studies [24, 25], the 2015 WHO classification introduced it as a fourth type of invasion of ADC beyond lepidic pattern (such as acinar, papillary, micropapillary, solid, colloid, or enteric), tumor cells within myofibroblast stroma, and vascular or pleural invasion. STAS is indeed considered an exclusion criterion for the diagnosis of minimally invasive ADC, together with tumor necrosis and vascular or pleural invasion [3, 4]. Unfortunately, there is no presurgical noninvasive parameter for direct measurement of STAS, the risk which can only be rated by solid proportion on computed tomography. Its prognostic value is however debated by who considers STAS not an *in vivo* effect but an artifact induced by the cutting that, in fact, was proved to increase the extension of the tumor cells at the lung periphery. Tumor islands, originally described by Onozato in 2013 [26] as isolated, large collection of cells, with no clear micropapillary configuration, distant at least a few alveoli by the main tumor, are considered the forerunner of the solid-type STAS and a subset of spread proved to exist by three-dimensional reconstruction study. They have been correlated to smoking, solid or micropapillary high-grade pattern, K-RAS mutations, and a higher nuclear grade and have been associated with low recurrence-free survival. Despite that the distance of STAS has been defined in different ways according to different studies, up to now, all studies have demonstrated its prognostic value independently from the extent and its relevance both in ADC and SCC [27], and in the latter it is considered a new unfavorable prognostic parameter together with cell nest size, nuclear diameter, and tumor budding. Importantly, STAS resulted to be a significant prognostic factor independent from lymph vascular invasion and predominant pattern but dependent from stage. Of note, micropapillary STAS has been associated with lymph

vascular invasion, recurrence-free survival, and mortality, so much that tumor cells within airspaces in a micropapillary feature should be assigned to a micropapillary pattern, which is known to be associated with poor prognosis even in small amounts.

The exact reason for the association of STAS with prognosis is unknown, but we can speculate that STAS could be the epiphenomenon of the tumor diffusion between interalveolar pores of Kohn and bronchiole-alveolar communications of Lambert that normally guarantee the collateral ventilation, and this is why tumor cells could remain undetected in alveolar spaces beyond the surgical margin. Another possible explanation is that tumor cells may reenter in the interstitium around the terminal bronchioles.

For the aforementioned reasons, the inclusion of STAS in pathology report could have potential implication on treatment decisions, therapy, and surveillance, including meticulous radiological follow-up of recurrence, even if more studies on margin distance are warranted. Of note, more recently, the prognostic role of STAS phenomenon has been reported even in primary NET of the lung [28].

1.3.1.2 Halo Sign

Peripheral halo of ground-glass (aka halo sign) can be seen by computed tomography in both primary and secondary malignancies of the lung. Hemorrhage is the pathological counterpart of halo sign, which can be associated both with neoplastic and benign conditions (e.g., angioinvasive aspergillosis). Metastases with halo sign are mostly reported in choriocarcinoma and angiosarcoma. Nonetheless, it can also be observed in nonhemorrhagic metastases with a peri-nodular lepidic growth [9].

1.3.1.3 Cavitation

Cavitation is radiologically characterized by a lucent cavity surrounded by solid wall of varying thickness [1, 7, 9]. Cavitation occurs more frequently in primary lung carcinomas and in particular in lung SCC, where it reflects tumor necrosis in the core of the lesion where angiogenic stimuli and metabolic demand substantially mismatch. However, cavitation is not exclusive to primary lung SCC; indeed, it is also seen in metastases and in nonneoplastic conditions such as

infections, Langerhans cell histiocytosis, necrobiotic rheumatoid nodules, granulomatosis with polyangiitis, and septic embolism. Therefore, oncologic perspective should not fail to recognize further conditions associated with nodule/mass cavitation, especially in case of known malignancy and potentially overlapping nonneoplastic disorder. The erosion of necrotic cavitation into the pleura can be responsible for pneumothorax or bronchopleural fistula. This scenario is reported to be relatively common in pediatric metastases from sarcoma of the bone, which accounts for 70% of lung malignancies in pediatric age, the most frequent being osteosarcoma [1, 2]. Further thoracic malignancies to bear in mind for pediatric population are pulmonary metastases from rhabdomyosarcoma, Wilms' tumor, Ewing's sarcoma, and neuroblastoma. Primary lung sarcoma is a very rare malignant tumor, accounting for less than 0.5% of all lung tumors, and a secondary origin must be first considered, including leiomyosarcoma, undifferentiated high-grade pleomorphic sarcoma, and synovial sarcoma [1, 2]. Cavitation must be distinguished from bubble-like lucencies (pseudo-cavitation) that is usually associated with mucinous ADC [9].

1.3.1.4 Cystic Pattern

Cysts on computed tomography are seen as areas of hyperlucency with a thin regular boundary. Cystic pattern is a known mechanism of local neoplastic growth of metastasis. The pattern shows different pathological explanations, including a check-valve mechanism with obstruction of small airways, lepidic growth of ADC in emphysema/bullae, and cyst formation of tumor. The pattern is often associated with metastases by ADC histology from non-thoracic malignancy [41]. Further primary neoplasms with cystic pulmonary metastases are uterine leiomyosarcoma, stromal endometrial sarcomas, cellular fibrous histiocytoma, and benign metastasizing leiomyoma. Cysts are also a common presentation of tumors of ectopic origin (e.g., teratoma).

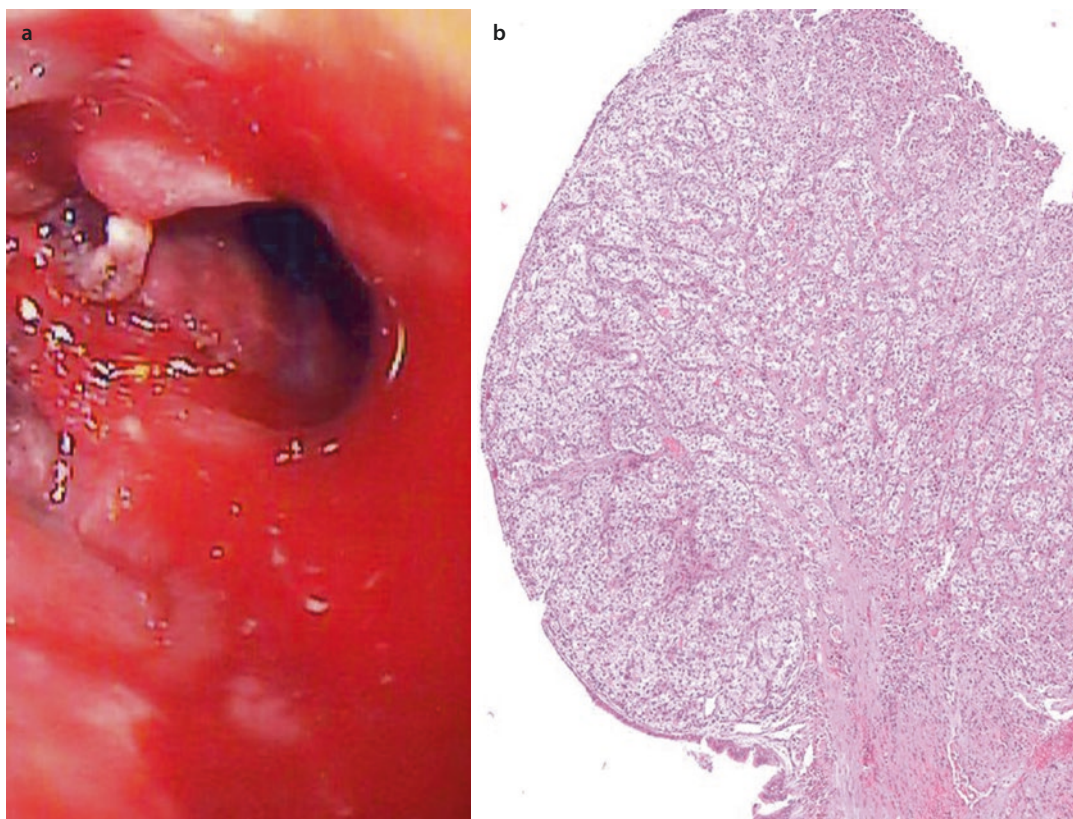
1.3.1.5 Endobronchial Growth

The endobronchial growth is characterized by the neoplastic spread along bronchial and bronchiolar wall, with invasion of bronchial lumen [9]. Central tumors present more often a hilar/peri-hilar growth around the main or lobar bronchus, and

they commonly show an endobronchial component. Primary thoracic neoplasms with such dissemination pathway are SCC, carcinosarcoma, and lung carcinoid tumor, including typical and atypical carcinoid. Endobronchial growth is also reported in rare salivary-gland-type tumors, such as mucoepidermoid carcinoma, adenoid cystic carcinoma, epithelial-myoeepithelial carcinoma, and pleomorphic adenoma. Of note, primary salivary gland tumors of the lung and the rare primary melanoma of the lung are bronchus-associated, unlike the corresponding metastases [1, 2]. Laryngotracheal papillomatosis is also a rare tracheobronchial HPV-related disease of childhood that can spread from larynx and eventually to the alveolar parenchyma, where it can degenerate into a SCC and can be differentiated from a well-differentiated SCC by the absence of invasion [3, 4, 29].

Endobronchial metastases can have the same clinical and radiologic appearance of primary endobronchial tumors presenting with obstructive respiratory symptoms related to tumor mass, including cough, hemoptysis, dyspnea, chest pain, and wheezing. At imaging, they can present with hilar and mediastinal mass, single peripheral nodules, atelectasis, or pleural effusion associated with pneumonitis. Endobronchial metastases can be the result of lymphatic or hematogenous spread rather than representing the extension from a parenchymal or mediastinal/hilar metastasis. Bronchial aspiration of tumor cells has also been described [1, 2, 30]. Interestingly, 5% of endobronchial metastases represent the first presentation of the extrathoracic neoplasm [30]. The latency may be very long, such as in renal cell carcinomas, which are known to have all kinds of pulmonary spread and the ability to extend directly into the right ventricle [1, 2]. Breast cancer is reported to be the most common primary tumor presenting with endobronchial metastases, followed by colorectal carcinoma, renal cell carcinoma, gastric carcinoma, prostate cancer, and melanoma [30] (■ Fig. 1.8). Virtually all types of solid tumors can spread to the bronchial tree, including spermatic cord liposarcoma, malignant fibrous tumor, leiomyosarcoma, meningioma, thymic tumor, germ cell tumor, and lymphoproliferative neoplasm (lymphoma and plasmacytoma).

Multiple peripheral carcinoids may be associated with numerous endobronchial tumorlets



■ **Fig. 1.8** Endobronchial metastasis from clear cell carcinoma of the kidney manifesting as polypoid lesion of the bronchus **a** at bronchoscopy and histology **b**

in the context of diffuse idiopathic pulmonary neuroendocrine cell hyperplasia (DIPNECH) showing a miliary pattern that should not be confused with intrapulmonary metastases (■ Fig. 1.9).

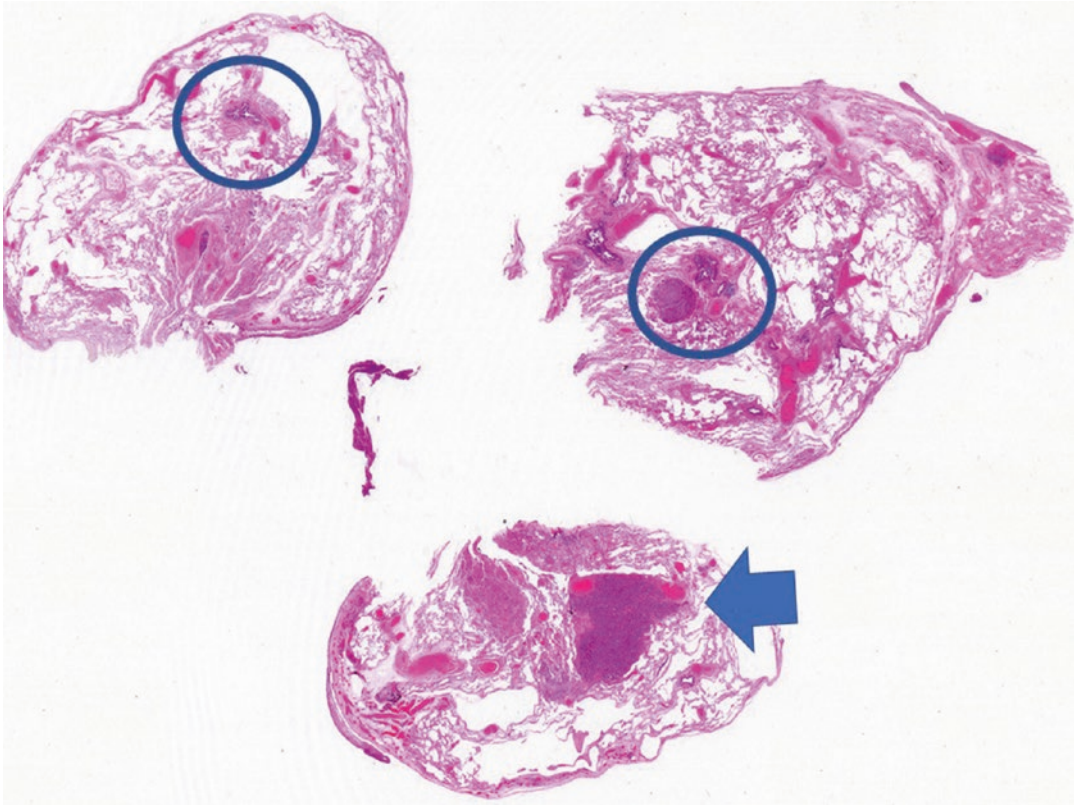
Endobronchial dissemination can also result from lymphatic metastases to peribronchial lymph nodes. The dissemination from a primary tumor to peribronchial lymph nodes can happen in several ways including infiltration of pleural lymphatics or directly through the lymphatic drainage from the retroperitoneum and periaortic nodes. For instance, testicular tumor can display mediastinal involvement in posterior and sub-carinal mediastinal lymph nodes all the way from retroperitoneal lymphatic network. The same mechanism happens to determine hilar and mediastinal lymph node from pancreatic carcinoma of the tail, whereas it happens seldom in pancreatic cancer of the head. Thyroid carcinomas, in particular the papillary type, are also a frequent source of hilar and mediastinal nodes, usually

associated with lung metastasis in 50% of cases [1, 2]. Surprisingly, prostate cancer has a tropism for mediastinal lymph nodes, and radiolabeled choline (18F-Fcholine) may be helpful in differential diagnosis [31].

1.3.1.6 Interstitial Pattern of Growth

Interstitial dissemination pathway is seen at imaging with reticulation (potentially beaded) variably associated with ground-glass opacity; its differential with nonneoplastic interstitial abnormality is oftentimes challenging especially during medical therapy or after radiation therapy. Pathology describes distribution of neoplastic cells inside the pulmonary lymphatics including interlobular and intralobular septa, visceral pleura, fibrovascular bundles, and capillaries. Transbronchial biopsy has high diagnostic yield in recognizing lymphangitic dissemination [32].

The understanding of radiologic pattern in lymphatic spread can be helped by the prototypical patterns described in Yang and Lin series [33]:



■ **Fig. 1.9** Low magnification of a surgical lung biopsy showing three histologic sections including a typical carcinoid (arrow) with multiple bronchiolocentric

proliferations of neuroendocrine tumor cells (circles) in a case of DIPNECH

- Anterograde route by progressive linear and bilateral infiltrates without hilar enlargement or tumor masses; this is mostly reported in gastric carcinoma that spreads through the diaphragm and pleural surface.
- Retrograde spread by radiating linear lines from enlarged hilar masses; this is due to the inverted lymphatic drainage caused by lymphatic obstruction up to complete blockade. It is more often reported in gastric, cervical, and breast carcinomas.
- Focal spread from centrally or peripherally located primary lung carcinoma [35].

Such dissemination pathway is seen in malignant vascular neoplasms, such as Kaposi sarcoma and angiosarcoma; lymphoproliferative disorders, such as intravascular lymphoma; and primary lung tumors (SCC and sarcomatoid spindle cell carcinoma) or metastasis [1, 2, 34] (■ Fig. 1.10).

Kaposi sarcoma rarely occurs in the lungs either as primary or metastatic neoplasm in HIV-positive and severely immunocompromised patients. It spreads around vessels and into the interstitial spaces leading to hemorrhagic areas that appear as ground glass opacities and can evolve into interstitial fibrotic disease. Intravascular lymphoma is a rare and aggressive subtype of extranodal large B-cell lymphoma (■ Fig. 1.11) characterized by the systemic presence of tumor cells almost exclusively inside the lumen of small vessels such as capillaries. The diagnosis of extranodal large B-cell lymphoma is often delayed because of imaging findings overlapping interstitial lung disease: nodules of variable size superimposed on ground-glass opacities from interstitial thickening. Symptoms are also not specific, while the diagnosis might be suspected by high level of serum lactate dehydrogenase (LDH). This condition conveys a poor prognosis and sometimes can cause sudden death.

Fig. 1.10 Pulmonary squamous cell carcinoma showing a peculiar interstitial growth pattern dissecting the alveoli showing hyperplastic type II pneumocytes

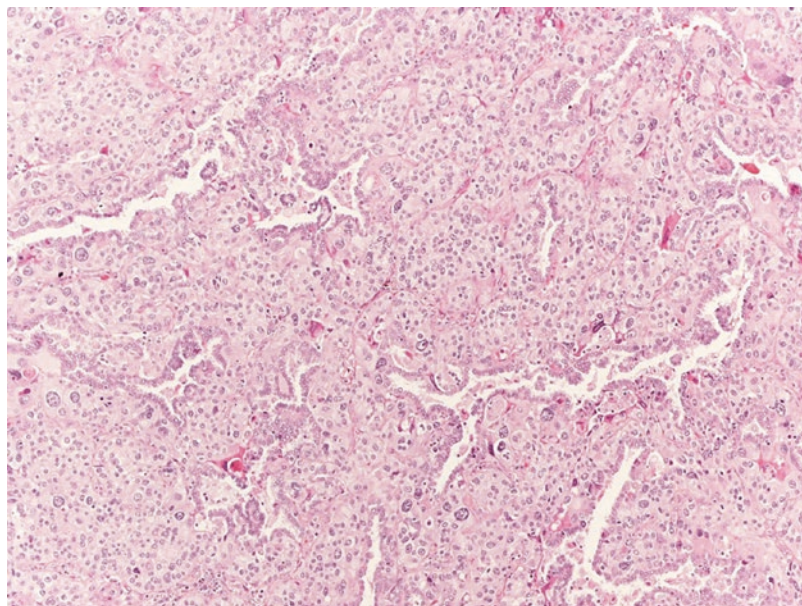
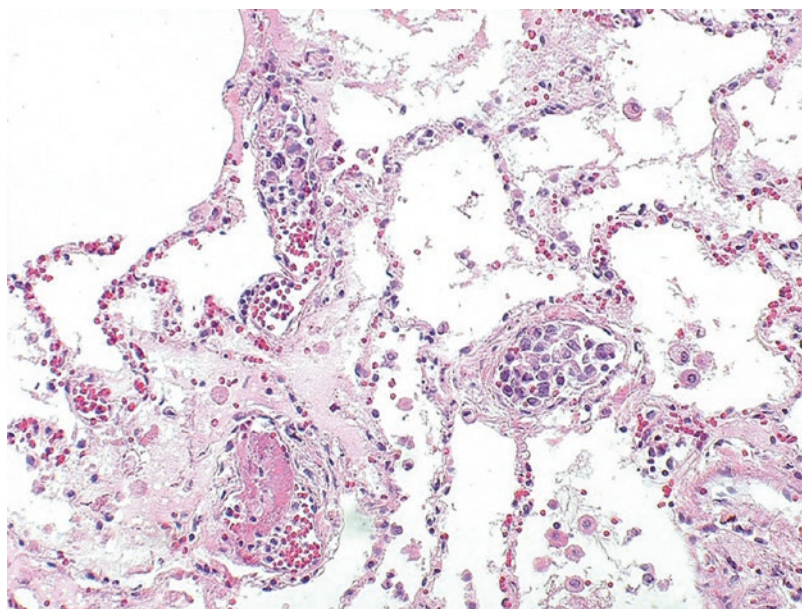
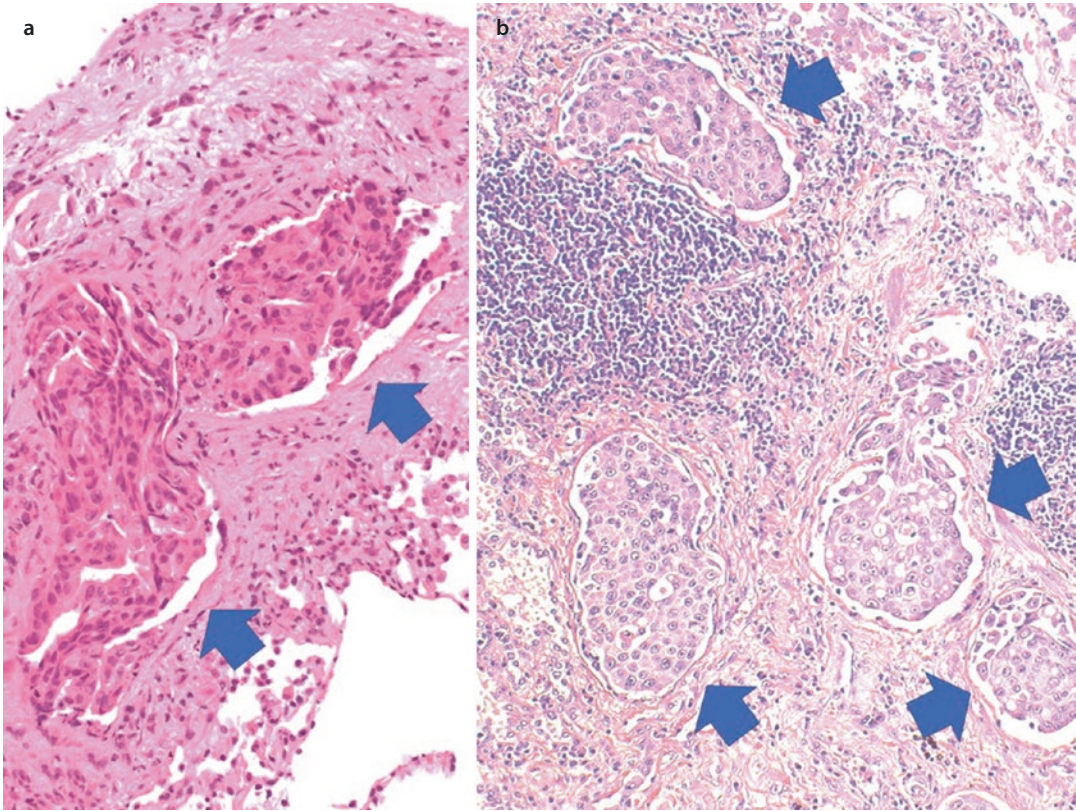


Fig. 1.11 Intravascular large B-cell lymphoma with large discohesive tumor cells growing and filling into the interstitial alveolar capillaries



Carcinomatous lymphangitis is a peculiar pattern with interstitial dissemination pathway; this is rendered by beaded reticulation with ground-glass opacity at computed tomography. Innumerable and diffuse neoplastic emboli from cell clusters are seen on histological slides, even at gross examination. It is estimated to be the presentation of 6–8% of lung metastases and is often caused by either primary pulmonary or extrathoracic ADC, as well as mesothelioma. Metastases from the stomach, breast, and

pancreas are more likely to present this dissemination pathway [1, 2] (Fig. 1.12). Other sources of carcinomatous lymphangitis include the thyroid, cervix, prostate, larynx, choriocarcinoma, melanoma, and metastatic ADC from an unknown primary cancer. Bilateral involvement is more common than unilateral lymphangitic spread in metastatic disease, while unilateral involvement occurs more frequently in breast cancer than in other malignancies [1, 2]. Symptoms correlated to lymphangitic



■ **Fig. 1.12** Interstitial lymphatic dissemination of pulmonary adenocarcinoma (arrows) in a transbronchial biopsy **a** and lung resection **b**

spread are similar independent from the cause, a persistent dry cough and dyspnea being frequent, sometimes with a severe respiratory failure.

Metastatic uterine leiomyosarcoma may also grow in the interstitium and enclosed bronchioles [3], as well as meningotheliomatosis and metastatic meningioma (■ Fig. 1.13). Fifty percent of carcinomatous lymphangitis can present with normal radiographs, while high-resolution computed tomography is the most sensitive imaging tool and can reveal the beaded septum sign, consisting in the reticular or reticulonodular interstitial markings, usually with an irregular contour and thickening of interlobular septa (Kerley B lines) and the peribronchovascular sheaths, reminiscent of a row of beads. Interestingly, the interstitial lymphatic septal thickening of carcinomatous lymphangitis is reported to be greater than lymphangitic lymphomas and sarcoidosis, where the beaded sign can be observed in 15–20% of patients and is usually associated with a more common pattern characterized by micronodules in a perilymphatic

distribution (avid of pleura) and by bilateral, symmetric lymph node enlargement.

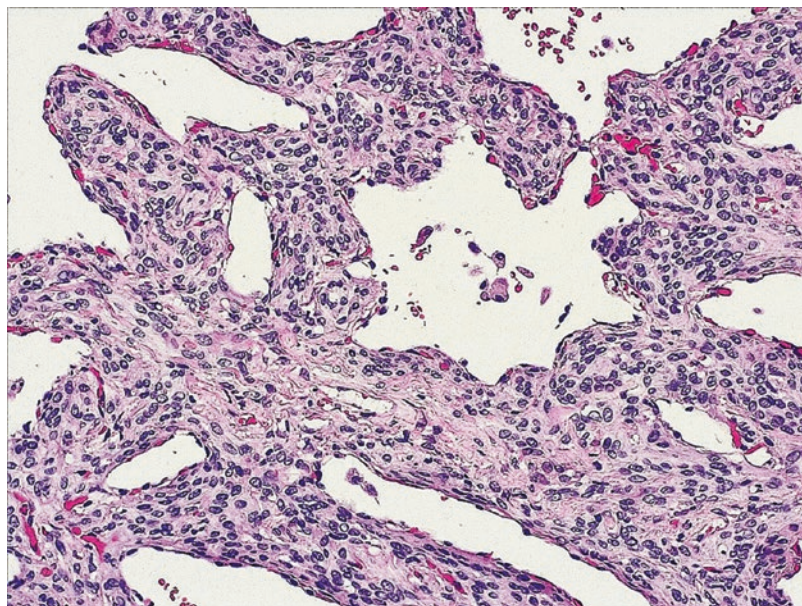
1.3.1.7 Miliary Pattern

The *miliary pattern* is the result of hematogenous spread that determines multiple, sharply defined, and tiny (3–5 mm) nodules. Such pattern is reported in primary lung tumor, such as adenocarcinoma (■ Fig. 1.14), as well as in metastatic neoplasms including medullary carcinoma, melanoma, renal cell carcinoma, ovarian cancer, osteosarcoma, and choriocarcinoma [1, 2].

1.3.1.8 Pulmonary Tumor Thrombotic Microangiopathy

Pulmonary tumor thrombotic microangiopathy (PTTM) leads to radiologic display of consolidation, ground-glass opacity, small nodules, and tree-in-bud appearance associated with multiple small perfusion deficiencies. Its differential is quite challenging before pathology, though it should be suspected when acute respiratory

■ **Fig. 1.13** Interstitial growth of bland-looking meningothelial cells in a case of pulmonary metastatic meningioma



■ **Fig. 1.14** Surgical lung resection showing multiple subcentimetric whitish nodules involving the pleura in a primary lung adenocarcinoma with miliary pattern of tumor cell dissemination



failure is accompanied by hypercoagulable condition without embolism in pulmonary arteries. PTTM is a unique, rare, and fatal form of pulmonary arterial tumor embolism by tumor cells; this is seen in massive pulmonary dissemination by gastric cancer and associates with elevated levels of vascular endothelial growth factor (VEGF) [35, 36] (■ Fig. 1.15). Emboli in large pulmonary

vessels can cause infarction and, potentially, acute pulmonary hypertension, followed by right heart failure.

Small vessel emboli can be responsible for unexplained dyspnea with subacute onset until right heart failure by established chronic pulmonary hypertension (■ Fig. 1.16). Isolated single small tumor embolus at pathology should not be

Fig. 1.15 Gastric adenocarcinoma presenting as thrombotic microangiopathy with nests of tumor cells filling the interstitial vessels leading to respiratory failure

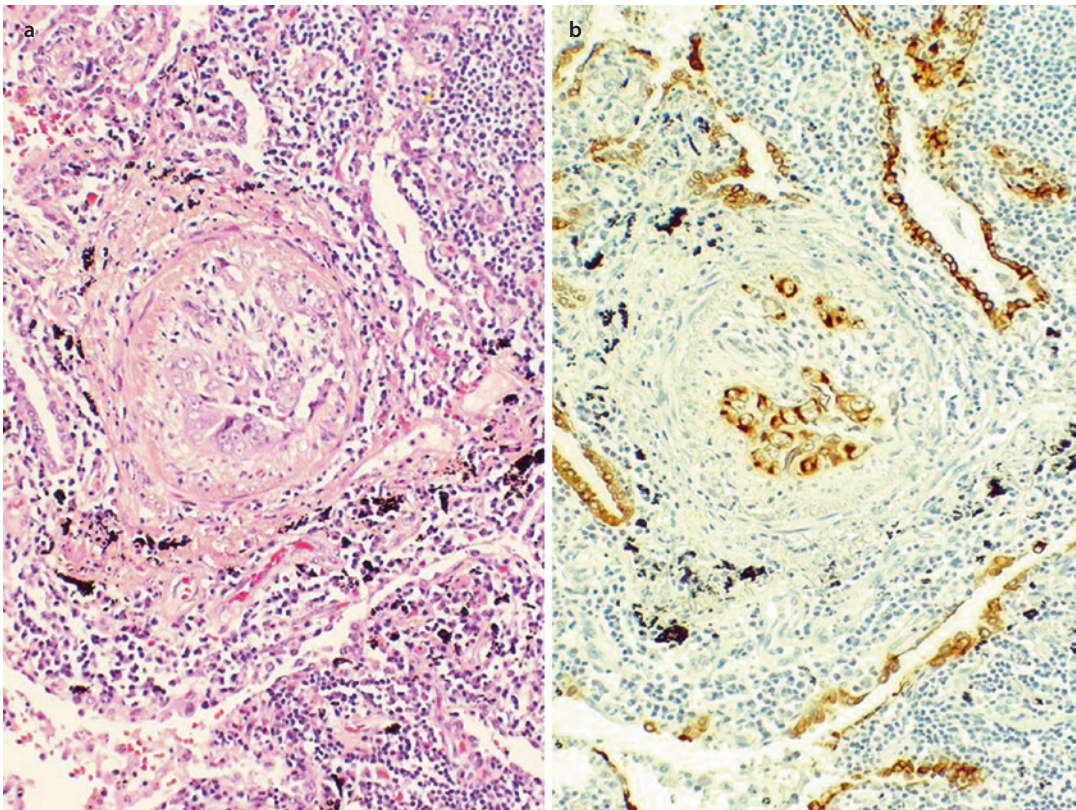
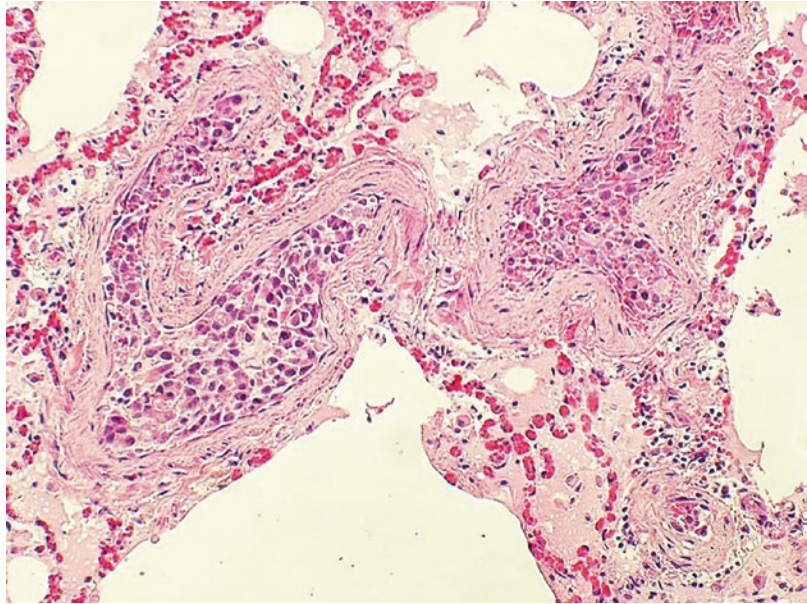
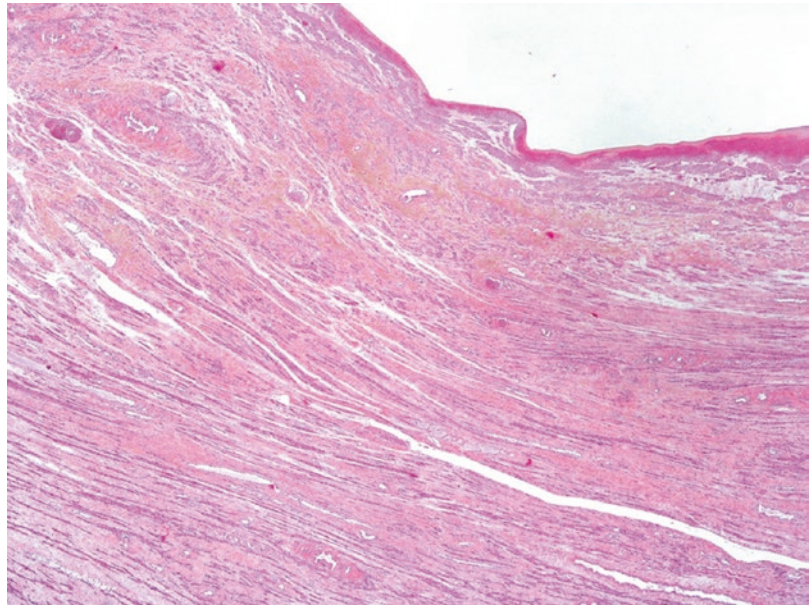


Fig. 1.16 Vascular infiltration by spindle cell sarcomatoid carcinoma. A subtle tumor cell proliferation **a** is better highlighted by expression of pan-cytokeratins into small arterioles (**b**, immunohistochemistry)

Fig. 1.17 Pulmonary artery sarcoma mural type characterized by proliferation of spindle tumor cells into the wall of pulmonary artery



diagnosed as a metastasis because most small emboli will not become a metastasis but rather resolve leaving a thrombus, which eventually forms a fibrotic scar or a calcification [1, 2]. Such microscopic pattern is rendered by radiological “vascular tree in bud” [1, 2, 7].

A peculiar and poorly recognizable pattern of microvascular dissemination is related to the rare occurrence of pulmonary artery and vein sarcomas (Fig. 1.17). These malignancies arise from subendothelium or vascular wall of major pulmonary vessels (either artery or vein) and classically manifest with chronic thromboembolic disease with intraluminal growth and organized thrombi (embolic metastasis), finally invading the lung parenchyma and producing multiple nodular lesions simulating pulmonary emboli. Subtle symptoms in the early phase of such neoplasm ought to delay diagnosis. Unexplained sudden death is not infrequent in these cases [37]. The characterization of these tumors is extremely difficult even at pathology by small biopsy; hence, surgical specimens are often mandatory to reach the final diagnosis.

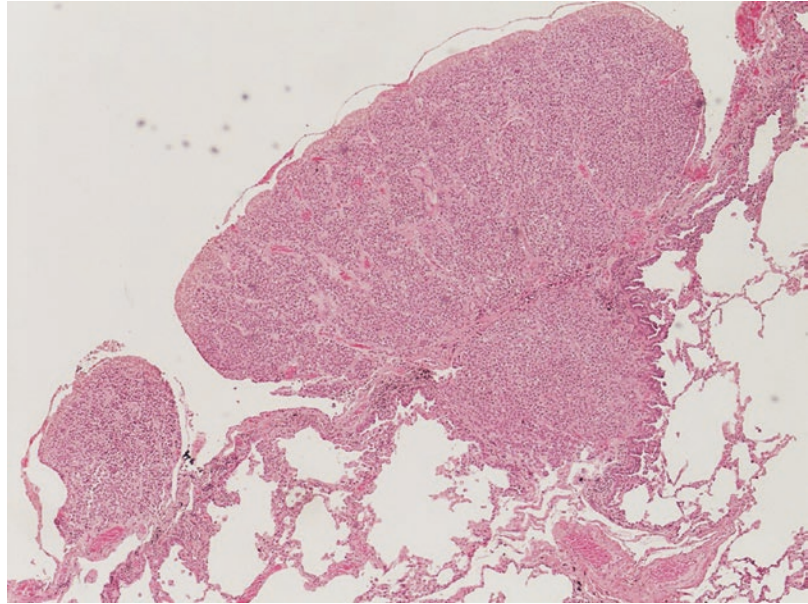
1.3.1.9 Pleural Involvement

Pleura is a common target of tumor dissemination by a large variety of neoplasms including primary pleural tumor, primary lung tumor, metastasis, and hematologic neoplasms. Pleural

effusion is the most common radiological sign of pleural dissemination, with or without a pleural mass (Fig. 1.18). Pleural effusion in malignancies may be due to pleural seeding of tumor cells, lymphatic obstruction, pulmonary venous obstruction, or mesothelial cell reactive proliferation. Peripheral ADC of the lung is the most common type of primary lung tumor involving the pleura, followed by SCC, SCLC, LCNEC, and, rarely, carcinosarcoma. Extrathoracic malignancies with pleural dissemination encompass breast, renal, gastrointestinal, and gynecological carcinomas. Even lymphoproliferative diseases (lymphomas, plasmacytoma, and leukemia) may involve the pleura leading to effusion.

Of note, peripheral ADC may spread along the pleural surface either in a continuous way as a “thick rind” or through “skip lesions” via lymphatic channels or implants on pleural surface from viable neoplastic cells floating in effusion. The rind pattern must be grossly differentiated from mesothelioma proliferation; indeed, it is also known as *pseudo-mesotheliomatous adenocarcinoma*. Other primary and metastatic tumors that may show this gross and radiologic pattern of tumor dissemination include epithelioid heman-gioendothelioma, epithelioid angiosarcoma, intra-pleural thymoma, melanoma, lymphoma, synovial sarcoma, multiple myeloma, and leukemia [38, 39].

■ **Fig. 1.18** Pleural dissemination of a clear cell sarcoma mimicking nodular growth of mesothelioma



The type of pleural dissemination in primary lung cancer has a key role in determining the disease stage, since involvement/disruption of elastic layer of visceral pleura (score PL1) and overrunning of elastic fibers with involvement of pleural surface (PL2) are associated with pT2 stage. Moreover, involvement of parietal pleura and soft tissue of chest wall (PL3) leads the tumor to stage pT3 [40].

Generally, pleural metastasis is due to lymphangitic or vascular dissemination. However, tumors may metastasize to the pleura by direct extension through the chest wall or diaphragm. In histology, several growth patterns may be appreciated ranging from tiny miliary nests into prominent fibrosis to endolymphatic growth or gross nodules. Pleural metastasis invading and replacing the surface mesothelial cells also forming papillary structures may occur and closely suggests mesothelioma [1, 2].

1.3.1.10 Direct Extension

Another peculiar pattern in thoracic neoplasm is the *direct extension* to the chest wall. Noteworthy, this is a well-defined cause of Pancoast syndrome (lower brachial plexopathy, Horner's syndrome, and shoulder pain). Furthermore, direct extension to major mediastinal structures is paramount in the prognosis of the patient as vascular syndromes happen to be life-threatening. Of note,

venous vessels are more prone to complications from neoplastic growth in the mediastinum, which frequently results in superior vena cava syndrome. Moreover, adherences between the lung and the wall chest can be a bridge for the direct invasion of the ribs and the surrounding soft tissue, and they can also create new lymphatic channels that, together with an inverted lymphatic stream, can cause nodal metastasis in the chest wall or supraclavicular lymph nodes, even without contiguity. A direct infiltration of ribs and vertebrae, mediastinum, hilar structures, heart, pericardium, or diaphragm can also occur. Involvement of the pericardium or the heart may lead to tamponade and sudden death.

1.3.1.11 Calcifications

Calcifications can be seen in primary lung cancer, as well as metastases. Radiologically depicted calcifications reflect pathological evidence of necrotic evolution, deposition of mucoid material, intralesional bony degeneration, or intrinsic characteristics of the primary extrathoracic neoplasm. Extrathoracic tumors expected to render calcification metastases are colorectal cancer, osteosarcoma, chondrosarcoma, and papillary thyroid carcinoma. Noteworthy, colorectal metastases are the most common tumor to undergo benign osseous and must be distinguished from chondroma [1, 2].

1 1.4 Tumor Dissemination and Oncogenic Driver Gene Alterations in Primary Lung Cancer and Metastases

Oncogenic driver gene alterations can determine different tumor dissemination pathways. Mutational state seems to influence tumor spread in resectable lung cancer [41]. ADC consists of a heterogeneous group of tumors that mainly harbor K-RAS and EGFR at molecular analysis. Other gene alterations are BRAF, HER2, and c-MET mutations (frequency range <1–5% of all primary lung ADC), while rearrangements of ALK, ROS-1, RET, and NTRKs have a propensity for solid pattern (in addition to signet ring cells) and aggressive behavior with exceptionally poor prognosis [41]. K-RAS- and EGFR-mutated ADC are the most frequent and distinct tumors, also showing contrasting histologic and clinicopathologic characteristics.

K-RAS-mutated tumors derive more frequently from central region, in heavy/active smokers, and Caucasian patients; they occur preferentially in mucinous TTF-1-negative ADC with a bronchiolar differentiation [42] or poor differentiation, necrosis, cytological atypia, tumor-infiltrating leukocytes, adverse prognostic impact, and resistance to EGFR tyrosine kinase inhibitors and conventional cisplatin-based chemotherapy.

EGFR-mutated tumors are peripherally located and non-mucinous with a lepidic or papillary pattern and occur in non-/light smokers, preferentially in Asian women. Intrapulmonary miliary dissemination by primary ADC mimicking infection disease has been documented, particularly in nonsmoker patients. The tumor is TTF-1 positive and generally lacks necrosis or cytologic atypia [42, 43]. Several of these findings associated to K-RAS and EGFR and K-RAS mutations reflect, respectively, the origin of type II pneumocytes (the putative stem cells for the terminal respiratory unit TRU) from the peripheral compartment or the basal cells of the bronchus in the central airway compartment (not-TRU-type origin). TRU carcinomas, characterized by differentiation to Clara cells, type II pneumocytes or bronchiolar cells, and dome-shaped protruding cytoplasm, are more often peripherally located and do not usually involve bronchi, while non-TRU carcinomas have, instead, a bronchial surface epithelium, mucous

cell or goblet cell morphology, and a central location [44, 45]. According to Wang et al. [41], central ADC are associated with a high risk of lymph node metastasis even at small size with respect to peripheral ones, allegedly due to the thick and flowing lymphatics of the central bronchus and to the proximity to lymph nodes. This could be correlated even with intrinsic properties of the tumors as we know that ADC appears more likely to metastasize than SCC; nevertheless, the latter is more common in the central part and therefore is more likely to invade mediastinal structures. Moreover, EGFR-mutated ADC has a major frequency of skip N2 metastasis probably due to its peripheral location and vascular invasion [41]. In general, lung cancer with early lymphatic and avascular dissemination is characterized by activation of mesenchymal-epithelial transition (EMT) and then exhibits high expression of EpCAM, VEGF, c-MET, E-cadherin, vimentin, and other pro-invasive molecules. EMT develops during cancer progression and indeed contributes to metastatic colonization. EMT endows metastatic properties upon cancer cells by enhancing mobility, invasion, and resistance to apoptotic stimuli. Furthermore, EMT-derived tumor cells acquire stem cell properties and exhibit therapeutic resistance. The disseminated tumor cells recruited to distant organs are suggested to subsequently undergo an EMT reversion through mesenchymal to epithelial transition (MET), which seems necessary for efficient colonization and growth into macroscopic metastasis. Furthermore, tumor microenvironment has a key role in promoting both primary lung tumors and lung metastasis from extrapulmonary neoplasms. Notably, microenvironmental factors involved in tumor dissemination are inflammation, angiogenesis, immune modulation, and response to therapies [46–49].

Among extrapulmonary carcinomas, peculiar pulmonary tropism is seen in breast cancer and melanoma. These neoplasms are associated with specific molecular profiles, such as cancer-specific lung metastasis secretome signatures revealing candidate lung metastasis proteins as nidogen 1 (NID1). Overexpression of NID1 promotes lung metastasis of breast cancer and melanoma, enhancing cancer cell migration and invasion, promoting adhesion to the endothelium, disrupting its integrity, and improving vascular tube formation capacity [50, 51].

1.5 Primary Malignant Tumors Mimicking Metastatic Lesions and Vice Versa

The prototypic presentation of pulmonary metastases from macroscopy and imaging studies relies on multiple, bilateral nodules of variable size and smooth margins, mainly located at the lower lobes. Although this presentation is useful to discriminate primary versus metastatic disease, it is not uncommon to detect primary lung tumors simulating metastases or metastatic tumors mimicking lung primary.

The pattern of growth of primary lung carcinoma suggesting metastatic dissemination at imaging studies and histology is particularly evident in adenocarcinoma presenting with miliary pattern or *tree-in-bud*-like appearance and lymphangitic carcinomatosis. This pattern of tumor dissemination is closely related to upregulation of EMT mechanisms with overexpression of molecules promoting cell-to-cell dis-cohesion, such as e-cadherin, Ep-CAM, MUC1, CDH1, CDH2, VIM, TWIST1, SNAI1, SNAI2, ZEB1, and ZEB2, and downregulation of the systems maintaining cell adhesion.

The presence of multiple nodules in the same or different pulmonary lobes generally favors a metastatic tumor, particularly when patients have a previous history of malignancy elsewhere. Nevertheless, with the dramatic increase of lung adenocarcinomas, it is quite common to face with patients showing different lesions in the lungs.

The examination of conventional morphology demands comprehensive investigation to distinguish primary tumors from metastases of the same histology (particularly adenocarcinomas); several features should be evaluated: growth pattern, cytologic features, patterns of stroma, necrosis, discrete nodularity versus miliary growth, and the presence of unusual characteristics as clear cell, signet ring, mucinous, and fetal-type changes.

Histology matches with molecular determinations in about 90% of cases; however, distinction by genomic profiling may contradict clinicopathologic findings in a significant proportion of cases (up to 20%), greatly influencing staging and therapeutic management of lung cancer patients with multiple tumors [50, 51].

Some tumors metastasizing to the lungs may show a peculiar dissemination pattern mimick-

ing primary lung tumor. It is the case of extrapulmonary adenocarcinomas growing into the lung in a lepidic way, namely, with substantial preservation of the alveolar architecture. This is particularly true in a subset of mucin-rich adenocarcinomas from pancreas that closely mimics primary lung neoplasm, both from a morphologic and immunohistochemical viewpoint. In these cases, the differential between extrapulmonary and pulmonary neoplasms is driven by comparison of histology, immunostains, and molecular features [22, 52].

Another unusual mechanism of extrapulmonary tumor dissemination resembling primary pulmonary neoplasm is endobronchial growth, with/without lymph node. Endobronchial metastases result in solitary nodules vegetating into the bronchial lumen. This peculiar pattern of metastatic tumors should be considered in patients with a previously known history of extrapulmonary malignancies from breast, stomach, kidney, colon, melanoma, and plasmacytoma.

1.6 Tumor Dissemination in Secondary Benign Neoplasms

Several benign/low-grade neoplasms may disseminate to the lungs (► Box 1.1), including pleomorphic adenoma (■ Fig. 1.19), uterine leiomyoma (■ Fig. 1.20), fibrous histiocytoma/dermatofibroma, and some fibro-epithelial lesions of the breast.

Pleomorphic adenoma is a benign tumor composed of epithelial, modified myoepithelial cells admixed in chondroid matrix. Usually, it occurs in parotid salivary gland, and it is classified as low-grade tumor with a low potential to metastasize. It is rare in the lungs, and around 20 cases have been reported [53]. Pleomorphic adenoma

Box 1.1 Benign Tumors Metastasizing to the Lungs

- Benign metastasizing leiomyoma
- Pleomorphic adenoma (mixed tumor)
- Fibrous histiocytoma/dermatofibroma
- Giant cell tumor of bone
- Mammary adenomyoepithelioma
- Hemangiomas

Fig. 1.19 Pulmonary metastasis from a benign pleomorphic adenoma of the parotid

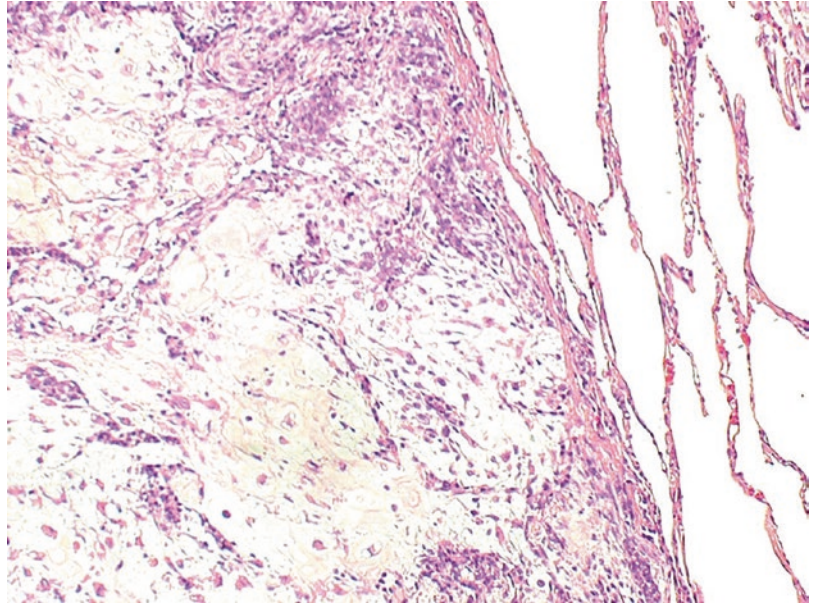
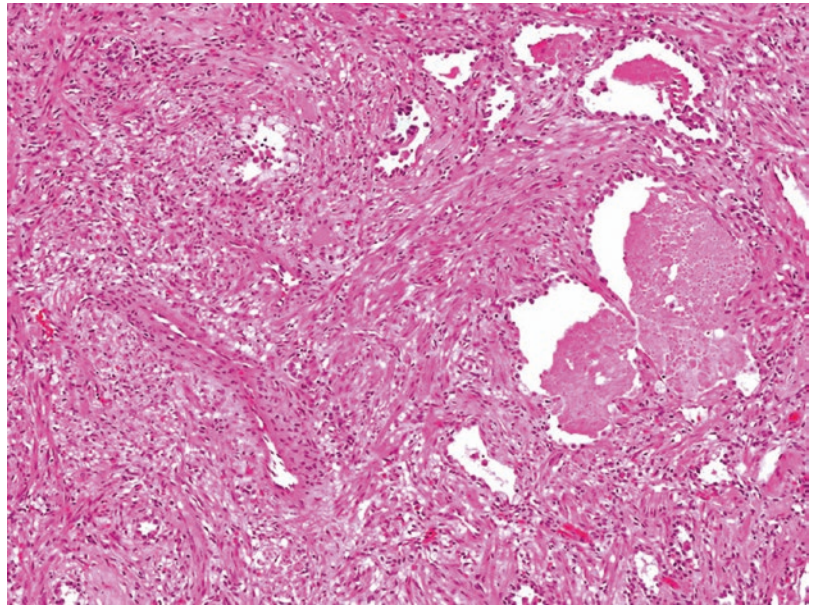


Fig. 1.20 Benign metastasizing leiomyoma with entrapment of alveolar pneumocytes

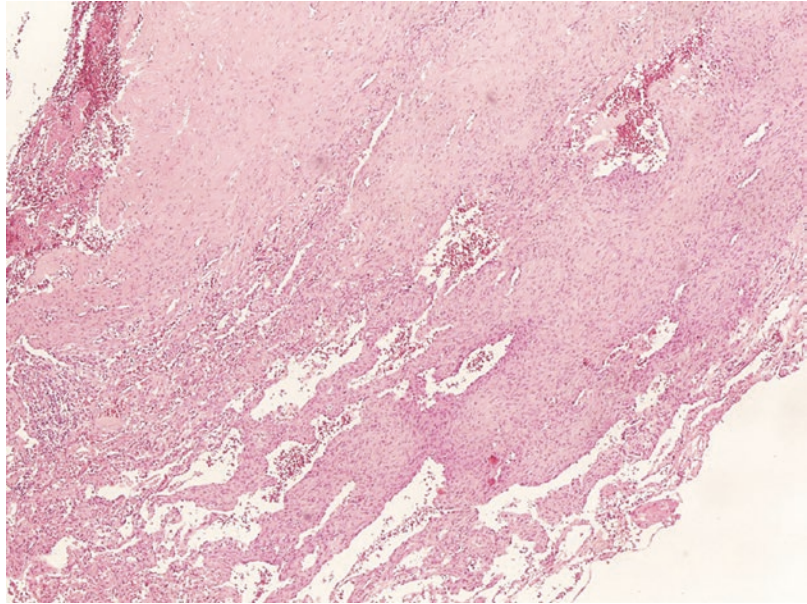


appears as a small, solitary, and well-circumscribed tumor; however, metastases have been reported especially in cases with slight atypia and infiltrative margins [54]. Differential diagnosis with metastatic lesions from mixed tumors of the salivary glands and other biphasic pulmonary neoplasms such as blastoma and carcinosarcoma is mandatory.

Benign metastasizing leiomyoma is a rare phenomenon with approximately 161 cases so

far described in the literature [55]. This occurrence is usually asymptomatic at presentation and is incidentally found in the lungs of women with a history of hysterectomy for leiomyomas. Nodules variably range in size and may be observed from 3 months to 20 years after hysterectomy [56a, b]. Its mechanism of dissemination is still unclear, allegedly referred to as multifocal leiomyomatosis, hematogenous extension following uterine surgical procedures, or metastasis

■ **Fig. 1.21** Desmoplastic-type mesothelioma growing along the pleural surface and invading the lung parenchyma



from a very-low-grade uterine leiomyosarcoma [57]. Malignant transformation has been reported in anecdotal cases [58]. Metastasizing leiomyoma may occur as a solitary pulmonary lesion rather than multiple bilateral nodules. Solid nodules with perilesional traction emphysema should suggest the hypothesis of metastases from benign metastasizing leiomyoma [57]. The differential diagnosis includes primary lung tumor, metastatic disease, infections, and interstitial lung disease with nodular appearance [57].

The mechanism of dissemination of benign metastasizing leiomyoma is still unclear.

Myoepithelial tumors are benign/low-grade neoplasms showing a predominately myoepithelial differentiation [58] that may metastasize to the lungs, and their recognition is based on knowledge of clinical history and detection of EWSR1 gene rearrangements [59].

Even adenomyoepithelioma, a biphasic benign tumor, arising from salivary glands, soft tissue, and breast, may metastasize to the lung, thus representing another example of tumor that can metastasize in the absence of histologic features that would suggest malignant behavior [60].

Primary pulmonary meningioma is extremely rare and entirely identical to conventional counterpart of central nervous system [61, 62], while meningioma metastasizing to the lungs is another unusual condition leading to a challenging differential diagnosis, mainly including sclerosing

hemangioma, intrapulmonary fibrous tumor, lymphangioliomyomatosis, and spindle cell carcinoid. The final diagnosis relies on pathological examination coupled to immunohistochemical coordinated expression of EMA, progesterone receptor, and CD56 [63]. Other benign tumors rarely metastasizing to the lungs and pleura are cutaneous fibrous histiocytoma/dermatofibroma [64, 65], giant cell tumor of the bone, giant cell tumor of the tendon sheath [66], and hemangiomas (especially in patients with Kasabach-Merritt syndrome) [67, 68].

1.7 Tumor Dissemination in Mesothelioma

Mesothelioma is the most common primary neoplasm of the pleura. The 2015 WHO classification recognizes four major histologic subtypes of diffuse malignant mesothelioma: epithelioid, biphasic, sarcomatoid, and desmoplastic [3, 4] (■ Fig. 1.21). The majority of malignant pleural mesothelioma arises from the parietal and diaphragmatic pleura, and, therefore, extrapleural N2 nodes rather than intrapleural N1 nodes might be the first draining station.

Lymph nodes are the most common site of distant dissemination from malignant pleural mesothelioma, followed by intra-abdominal disease and contralateral lung [69].

Metastatic spread often occurs late in the course of the disease, but postmortem examinations showed distant spread in over half of pleural diffuse malignant mesothelioma patients at the time of death. Metastatic spread of mesothelioma is often underrecognized as demonstrated by 55% prevalence in a large postmortem series of 350 patients.

Recently, a large study of 165 patients showed bone metastases in 20%, peritoneal and omental disease in 24%, and ascites in 16% [70]. An emerging pattern of dissemination pathway from mesothelioma is the intrapulmonary growth leading to miliary pattern or interstitial pattern of dissemination (about 11% of cases) [71]. Visceral metastases were found in 15% of cases, with a prevalence in the liver (78% of their series) but also in adrenals, spleen, and kidneys. Another metastatic site was the brain, where only 3% were symptomatic, within a median overall survival of 24.2 months. Case reports show brain metastases of mesothelioma presenting with hemorrhagic clinical presentation [69] or leptomeningeal involvement [72]. Other uncommon sites of metastatic mesothelioma include the breast [73], skin [74], kidney [75], and oral mucosa [76, 77].

1.8 Tumor Dissemination in Other Primary Thoracic Neoplasms

1.8.1 Soft Tissue Tumors

According to the current WHO classification [3, 4, 78], primary sarcomas of the thorax are rare and consist of a large group of tumors arising from the lung, mediastinum, pleura, chest wall, and heart. Primary thoracic sarcomas commonly manifest as large, heterogeneous masses that can appear in a variety of radiological presentation, such as solitary pulmonary nodule, multiple pleuropulmonary masses, central endobronchial tumor, and even intraluminal masses within the pulmonary arteries. The most common soft tissue neoplasms of the thorax are epithelioid hemangioendothelioma, angiosarcoma, synovial sarcoma, and solitary fibrous tumor (SFT).

Epithelioid hemangioendothelioma arises more commonly from the pleura but often simultaneously involves the lungs in young women, and it is prone to lymph node as well as distant

metastases in the contralateral lung, bone, and skin [1–4, 79, 80]. According to 2015 WHO classification [1–4], negative prognostic factors are extensive intrapulmonary and pleural spread, weight loss, anemia, and hemorrhagic pleural effusions. The tumor may mimic mesothelioma when presenting with diffuse thickening of the pleura rather than infection or metastatic disease in case of multiple, tiny nodules filling the alveolar spaces.

In contrast, angiosarcoma is a high-grade and more aggressive vascular neoplasm harbored in the great vessels of mediastinum [1–4, 81] or from the chest wall as well as from the pleural surface [82, 83]. The disease tends to rapidly diffuse through the hematogenous route and may appear as bilateral solid nodules and cystic or bullous lesions sometimes associated with spontaneous hemopneumothorax [84].

Although rare, involvement of the thoracic region by synovial sarcoma represents the most common visceral site of origin of this sarcoma [85–87]. As in soft tissue, synovial sarcoma may show the monophasic spindle cell form and the biphasic and poorly differentiated variants. Immunohistochemical stains overlap with carcinomas and mesothelioma, while molecular detection of the translocation involving SYT-SSX2 genes is quite specific leading to a confirmatory diagnosis [88, 89]. The tumor generally appears as solitary or multiple masses originating from the pleura/mediastinum, solitary lung mass, or pseudo-mesotheliomatous pleural thickening.

Solitary fibrous tumor (SFT) commonly arises in the pleura and sometimes in the lungs (intrapulmonary SFT possibly originating from pulmonary fissure) (■ Fig. 1.22). The majority of SFT have a benign/low-grade behavior and manifest as solitary large mass, but local recurrences may occur particularly when the tumor has a sessile growth pattern and arises from the parietal pleura [90]. Distant metastasis has been reported anecdotally [91, 92].

1.8.2 Lymphomas of the Thorax

All lymphoproliferative neoplasms reported in the most recent WHO classification [93] may involve the lung, mediastinum, and pleura. Among others, primary mediastinal large B-cell lymphomas

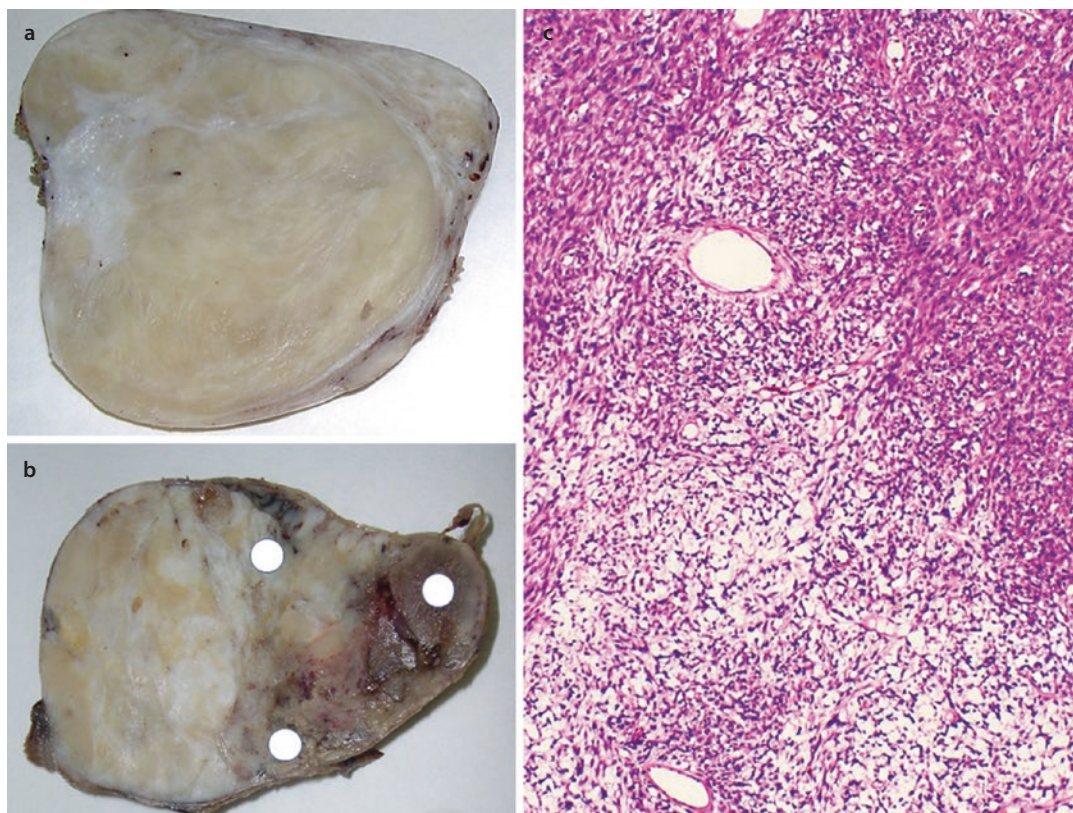


Fig. 1.22 Solitary fibrous tumor with gross benign features evidenced by lardaceous whitish tissue **a** and malignant aspects, as necrotic and hemorrhagic areas **(b)**,

white dots). At histology, the tumor alternates hypocellular fibrotic areas (**c**, at the bottom) and hypercellular zones (**c**, at the top)

are exclusively present in the mediastinum and associated with a more favorable survival than the germinal center B-cell and activated B-cell subtypes of diffuse large B-cell lymphoma (DLBCL) [93–95]. This lymphoma arises from the thymus and presents as a large mass of the anterosuperior mediastinum, possibly extending to the pleura and the lung. Mediastinal involvement is most frequently seen in the nodular-sclerosis subtype of classical Hodgkin's lymphoma. The malignancy presents as an irregular mass involving mediastinal lymph nodes. Other common lymphomas occurring in the mediastinum and showing a mass-forming pattern of dissemination consist of lymphoblastic lymphoma, anaplastic lymphoma, and plasmacytoma.

The pleura is the primary site of some peculiar lymphomas, namely, diffuse large B-cell lymphoma associated with chronic inflammation (formerly known as pyothorax-associated lymphoma) and primary effusion lymphoma (PEL) [96]. The

former presents as *tumor masses* in patients with long-standing (>20 years) pyothorax and is associated with EBV, which is likely facilitated by local immunodeficiency conditions. Otherwise, PEL is also a large B-cell lymphoma, but it presents as *effusion without masses*; it is a human herpesvirus 8 (HHV8)-associated lymphoma developing in the context of severe immunodeficiency showing a dismal prognosis [97, 98].

Primary pulmonary lymphoma mainly consists of marginal zone, mucosa-associated lymphoid tissue (MALT) lymphoma, possibly transforming to DLBCL in <10% of cases. MALT-type lymphoma has a protean spectrum of dissemination, including lymphatic, interstitial, miliary, and direct extension patterns as well as cystic changes with calcification. Its development is slow and insidious having no specific clinical symptoms and imaging findings [99, 100].

Lymphomatoid granulomatosis (LYG) is a rare T-cell-rich large B-cell lymphoma driven by

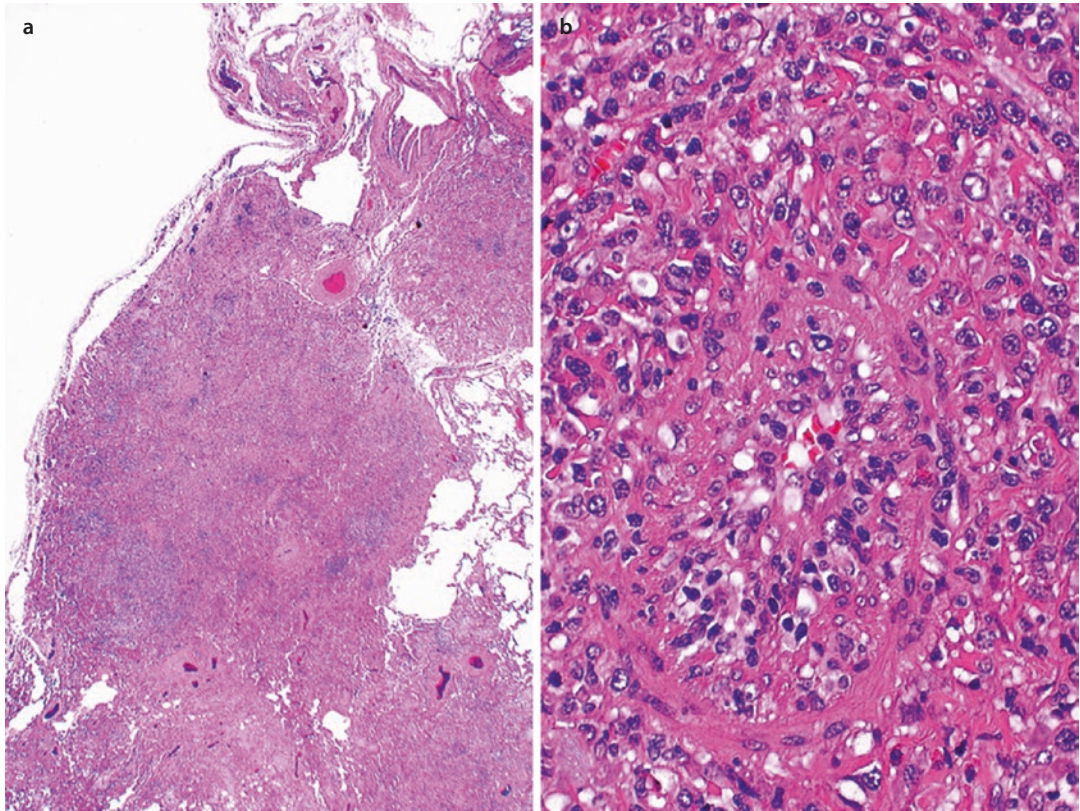


Fig. 1.23 Lymphomatoid granulomatosis showing solid nodules at low magnification **a** and angiocentric proliferation of a mixed inflammatory infiltrate with scattered large cells **b**

Epstein-Barr virus infection. The disease may mimic pulmonary vasculitis histologically showing a peculiar angiocentric pattern, often revealed by systemic symptoms. Involvement of vessel wall is common into the hematogenous dissemination of disease to the lung, reflected by bilateral pulmonary nodules and ground-glass opacities (Fig. 1.23). The diagnostic clue is the identification of large CD20- and EBV-positive B-cell showing vascular infiltration in the context of a mixed mononuclear cell infiltrate that shows numerous T-cells [101].

1.8.3 Thymic Neoplasms

Thymic epithelial tumors (thymomas and carcinomas) are generally characterized by a common mass-forming dissemination pattern. Thymomas, from medullary type A to cortical B2 type, consist of an encapsulated mass with well-defined margins. The International Thymic Malignancies

Interest Group (ITMIG) recommends that anterior mediastinal nodules be removed routinely along with the thymus and encourages a systematic sampling of deep nodes (paratracheal, aortopulmonary window, subcarinal lymph nodes) during resection of thymomas with invasion of pericardium or lungs. For thymic carcinoma, a systematic removal of both N1 and N2 nodes is recommended during curative-intent resection [102]; however, thymic carcinomas are often unresectable due to local invasion of adjacent structures (pleura, lung, vessels, pericardium). Survival of patients with thymoma is significantly related to tumor stage and margin-free surgery [103].

Furthermore, thymoma may show an unpredictable clinical behavior characterized by local recurrences and metastasis to neighboring organs or distant sites (e.g., bone, liver, and brain) [104].

The most common pattern of metastatic dissemination of thymic carcinoma is represented by subpleural nodules (visceral or parietal), as well as pericardial nodules. Occasionally, intrapa-

renchymal pulmonary nodules (nodules of the visceral pleura) are seen but also in the bone, liver, and brain [105, 106]. Thymic carcinoma shows higher stage, lower resectability, lower overall survival and progression-free survival, more distant metastases, and earlier relapses compared with thymoma [105].

Finally, the mediastinum is the site for other unusual epithelial malignancy such as carcinoma with NUT translocation, basaloid carcinoma, mucoepidermoid carcinoma, sarcomatoid carcinoma, adenocarcinoma, neuroendocrine tumors, and undifferentiated malignancies. These uncommon tumors reflect the pulmonary counterpart, and their dissemination pattern is characterized by solid growth of heterogeneous masses occupying the anterosuperior mediastinum with compression of the adjacent structures possibly leading to superior vena cava syndrome [1–4].

1.9 Conclusion

As in many other anatomic districts, the main mechanisms of tumor dissemination in thoracic malignancies include direct invasion of neighboring structures and lymphatic and hematogenous spread. Noteworthy, lung cancer has a peculiar growth pattern with tumor cells infiltrating and propagating through the airways, recently defined as “spread through airspaces (STAS).” The finding of STAS seems to be significantly associated with higher rate of local recurrence and prognosis, and although originally identified in adenocarcinoma histology, it is also recognized in squamous cell and neuroendocrine carcinomas.

The prototypical presentation of lung metastasis is characterized by bilateral nodules of variable size with well-defined borders; nonetheless, radiologists should be aware that gross appearance of primary tumors may often simulate metastatic growth (i.e., miliary pattern), while metastatic diseases may closely simulate lung primary (i.e., endobronchial polypoid growth, solitary nodule, pneumonia-like consolidation, or ground-glass opacities).

Again, extrathoracic metastatic malignancies not infrequently involve the mediastinum as unique huge mass or the pleura with diffuse pleural thickening resembling primary neoplasms (i.e., pseudo-mesotheliomatous adenocarcinoma

from the lung or other extrapulmonary primary). On the other hand, localized or intrapulmonary mesothelioma strikingly mimics primary lung cancer and interstitial lung diseases.

The diagnosis by pathologist relies on large biopsies to discriminate primary from metastatic tumors, while careful analysis of histopathologic features together with selected panels of immunohistochemical stains or molecular investigations should be often ordered to better classify malignancies involving the thoracic region. Nonsurgical biopsies, such as transbronchial and percutaneous biopsies, have a high diagnostic yield, particularly when tumor shows a lymphatic/airway-filling pattern or peripheral masses, respectively.

References

1. Colby TV, Koss MN, Travis WD. Tumors of the lower respiratory tract: atlas of tumor pathology, Third Series, Fascicle 13. Washington, DC: Armed Forces Institute of Pathology; 1995.
2. Dail and Hammar's Pulmonary Pathology Volume II. Neoplastic lung disease. 3rd ed. Heidelberg: Springer, Berlin, New York; 2008.
3. Travis WD, Brambilla E, Burke AP, Marx A, Nicholson AG. WHO classification of tumours of the lung, pleura, thymus and heart. Lyon: International Agency for Research on Cancer; 2015.
4. Travis WD, Brambilla E, Nicholson AG, Yatabe Y, Austin JHM, Beasley MB, Chirieac LR, Dacic S, Duhig E, Flieder DB, Geisinger K, Hirsch FR, Ishikawa Y, Kerr KM, Noguchi M, Pelosi G, Powell CA, Tsao MS, Wistuba I, Panel WHO. The 2015 World Health Organization Classification of lung tumors: Impact of genetic, clinical and radiologic advances since the 2004 classification. *J Thorac Oncol.* 2015;10(9):1243–60.
5. Chambers AF, Groom AC, MacDonald IC. Dissemination and growth of cancer cells in metastatic sites. *Nat Rev Cancer.* 2002;2(8):563–72.
6. Akhtar M, Haider A, Rashid S, Al-Nabet ADMH. Paget's “seed and soil” theory of cancer metastasis: an idea whose time has come. *Adv Anat Pathol.* 2019;26(1):69–74.
7. Colby TV, Swensen SJ. Anatomic distribution and histopathologic patterns in diffuse lung disease: correlation with HRCT. *J Thorac Imaging.* 1996 Winter;11(1):1–26.
8. Colby TV, Yousem SA. Pulmonary histology for the surgical pathologist. *Am J Surg Pathol.* 1988;12(3):223–39.
9. Dalpiaz G, Cancellieri A, editors. Atlas of diffuse lung diseases. A multidisciplinary approach. Springer; 2017.
10. Silva M, Galeone C, Sverzellati N, et al. Screening with low-dose computed tomography does not improve survival of small cell lung cancer. *J Thorac Oncol.* 2016;11:187–93.

11. Filderman AE, Shaw C, Matthay RA. Lung cancer. Part II. Staging and therapy. *Investig Radiol.* 1986;21(2): 173–85.
12. Rossi G, Tiseo M, Cavazza A, Colby TV. Is immunohistochemistry always required to diagnose lung cancer? *Adv Anat Pathol.* 2013;20(5):327–33.
13. Gruver AM, Amin MB, Luthringer DJ, Westfall D, Arora K, Farver CF, Osunkoya AO, McKenney JK, Hansel DE. Selective immunohistochemical markers to distinguish between metastatic high-grade urothelial carcinoma and primary poorly differentiated invasive squamous cell carcinoma of the lung. *Arch Pathol Lab Med.* 2012 Nov;136(11):1339–46.
14. Zhang J, Xiang C, Han Y, Teng H, Li X, Shao J, Zhu L, Han-Zhang H, Ye J, Yu K. Differential diagnosis of pulmonary enteric adenocarcinoma and metastatic colorectal carcinoma with the assistance of next-generation sequencing and immunohistochemistry. *J Cancer Res Clin Oncol.* 2019;145(1): 269–79.
- 15a. Patel SB, Kadi W, Walts AE, Marchevsky AM, Pao A, Aguiluz A, Mudalige T, Liu Z, Deng N, Lopategui J. Next-generation sequencing: a novel approach to distinguish multifocal primary lung adenocarcinomas from intrapulmonary metastases. *J Mol Diagn.* 2017;19(6):870–80.
- 15b. Girard N, Ostrovskaya I, Lau C, Park B, Ladanyi M, Finley D, Deshpande C, Rusch V, Orlow I, Travis WD, Pao W, Begg CB. Genomic and mutational profiling to assess clonal relationships between multiple non-small cell lung cancers. *Clin Cancer Res.* 2009;15(16):5184–90.
16. Thunnissen E, Borczuk AC, Flieder DB, Witte B, Beasley MB, Chung JH, Dacic S, Lantuejoul S, Russell PA, den Bakker M, Botling J, Brambilla E, de Cuba E, Geisinger KR, Hiroshima K, Marchevsky AM, Minami Y, Moreira A, Nicholson AG, Yoshida A, Tsao MS, Warth A, Duhig E, Chen G, Matsuno Y, Travis WD, Butnor K, Cooper W, Mino-Kenudson M, Motoi N, Poleri C, Pelosi G, Kerr K, Aisner SC, Ishikawa Y, Buettner RH, Keino N, Yatabe Y, Noguchi M. The use of immunohistochemistry improves the diagnosis of small cell lung cancer and its differential diagnosis. An international reproducibility study in a demanding set of cases. *J Thorac Oncol.* 2017;12(2):334–46.
17. Truini A, Santos Pereira P, Cavazza A, Spagnolo P, Nosseir S, Longo L, Jukna A, Lococo F, Vincenzi G, Bogina G, Tiseo M, Rossi G. Classification of different patterns of pulmonary adenocarcinomas. *Expert Rev Respir Med.* 2015;9(5):571–86.
18. Kuhn E, Morbini P, Cancellieri A, Damiani S, Cavazza A, Comin CE. Adenocarcinoma classification: patterns and prognosis. *Pathologica.* 2018;110(1):5–11.
19. Raparia K, Ketterer J, Dalurzo ML, Chang YH, Colby TV, Leslie KO. Lung tumors masquerading as desquamate interstitial pneumonia (DIP): report of 7 cases and review of the literature. *Am J Surg Pathol.* 2014;38(7):921–4.
20. Sica G, Yoshizawa A, Sima CS, Azzoli CG, Downey RJ, Rusch VW, Travis WD, Moreira AL. A grading system of lung adenocarcinomas based on histologic pattern is predictive of disease recurrence in stage I tumors. *Am J Surg Pathol.* 2010;34(8):1155–62.
21. Suster S, Moran CA. Malignant thymic neoplasms that may mimic benign conditions. *Semin Diagn Pathol.* 1995;12(1):98–104.
22. Rossi G, Murer B, Cavazza A, Losi L, Natali P, Marchioni A, Migaldi M, Capitanio G, Brambilla E. Primary mucinous (so-called colloid) carcinomas of the lung: a clinicopathologic and immunohistochemical study with special reference to CDX-2 homeobox gene and MUC2 expression. *Am J Surg Pathol.* 2004;28(4): 442–52.
23. Kadota K, Nitadori J, Sima CS, et al. Tumor spread through air spaces is an important pattern of invasion and impacts the frequency and location of recurrences after limited resection for small stage I lung adenocarcinoma. *J Thorac Oncol.* 2015;10:806–14.
24. Warth A, Beasley MB, Kenudson MM. Breaking new ground: the evolving concept of Spread through Air Spaces (STAS). *J Thorac Oncol.* 12:334.
25. Warth A, Muley T, Kossakowski CA, et al. Prognostic impact of intra-alveolar tumor spread in pulmonary adenocarcinoma. *Am J Surg Pathol.* 2015;39:793–801.
26. Onozato ML, Kovach AE, Yap BY, et al. Tumor island in resected early-stage lung adenocarcinoma are associated with unique clinicopathologic and molecular characteristic and worse prognosis. *Am J Surg Pathol.* 2013;37:287–94.
27. Onozato ML, Klepeis VE, Yagi Y, et al. A role of three dimensional (3D)-reconstruction in the classification of lung adenocarcinoma. *Anal Cell Pathol.* 2012;35: 79–84.
28. Aly RG, Rekhman N, Li X, Takahashi Y, Eguchi T, Tan KS, Rudin CM, Adusumilli PS, Travis WD. Spread Through Air Spaces (STAS) is prognostic in atypical carcinoid, large cell neuroendocrine carcinoma, and small cell carcinoma of the lung. *J Thorac Oncol.* 2019; <https://doi.org/10.1016/j.jtho.2019.05.009>. pii: S1556-0864(19)30375-2. [Epub ahead of print].
29. Mitsumoto GL, Bernardi FDC, Paes JF, Villa LL, Mello B, Pozzan G. Juvenile-onset recurrent respiratory papillomatosis with pulmonary involvement and carcinomatous transformation. *Autops Case Rep.* 2018;8(3):e2018035.
30. Marchioni A, Lasagni A, Busca A, Cavazza A, Agostini L, Migaldi M, Corradini P, Rossi G. Endobronchial metastasis: an epidemiologic and clinicopathologic study of 174 consecutive cases. *Lung Cancer.* 2014;84(3):222–8.
31. Rossi G, Nannini N, Casali C, Longo L, Mengoli MC, Cavazza A. Peribronchial lymph node metastasis from prostate cancer in pulmonary lobectomy for primary lung adenocarcinomas: a possible source of pitfall with therapeutic consequences. *Histopathology.* 2011;58(6):996–8.
32. Colby TV. The pathologist's approach to bronchoscopic biopsies. *Pathologica.* 2010;102(6):432–42.
33. Yang SP, Lin CC. Lymphangitic carcinomatosis of the lungs. The clinical significance of its roentgenologic classification. *Chest.* 1972;62(2):179–87; Lu S, Tan KS, Kadota K, et al. Spread through air spaces (STAS) is an independent predictor of recurrence and lung cancer-specific death in squamous cell carcinoma. *J Thorac Oncol.* 2017;12:223–34.

34. Colby TV. Malignancies in the lung and pleura mimicking benign processes. *Semin Diagn Pathol.* 1995;12(1):30–44.
35. Uruga H, Fujii T, Kurosaki A, Hanada S, Takaya H, Miyamoto A, Morokawa N, Homma S, Kishi K. Pulmonary tumor thrombotic microangiopathy: a clinical analysis of 30 autopsy cases. *Intern Med.* 2013;52(12):1317–23.
36. Sato Y, Marutsuka K, Asada Y, Yamada M, Setoguchi T, Sumiyoshi A. Pulmonary tumor thrombotic microangiopathy. *Pathol Int.* 1995;45(6):436–40.
37. Ushioda R, Kitahara H, Ise H, Koichi Y, Wakabayashi N, Tanaka C, Nakanishi S, Ishikawa N, Kamiya H. A case of pulmonary artery sarcoma that was initially misdiagnosed as pulmonary embolism. *J Surg Case Rep.* 2019;2019(3):rjz078.
38. Exarchos GD, Attanoos RL. Pseudomesotheliomatous small-cell neuroendocrine carcinoma of the lung with calretinin expression. *Histopathology.* 2015;66(6):895.
39. Attanoos RL, Gibbs AR. 'Pseudomesotheliomatous' carcinomas of the pleura: a 10-year analysis of cases from the Environmental Lung Disease Research Group, Cardiff. *Histopathology.* 2003;43(5):444–52.
40. Rami-Porta R, Bolejack V, Crowley J, Ball D, Kim J, Lyons G, Rice T, Suzuki K, Thomas CF Jr, Travis WD, Wu YL, IASLC Staging and Prognostic Factors Committee, Advisory Boards and Participating Institutions. The IASLC Lung Cancer Staging Project: Proposals for the revisions of the T descriptors in the forthcoming eighth edition of the TNM classification for lung cancer. *J Thorac Oncol.* 2015;10(7):990–1003.
41. Wang Z, Li M, Teng F, Kong L, Yu J. Primary tumor location is an important predictor of survival in pulmonary adenocarcinoma. *Cancer Manag Res.* 2019;11:2269–80.
42. Chilosi M, Murer B. Mixed adenocarcinomas of the lung: place in new proposals in classification, mandatory for target therapy. *Arch Pathol Lab Med.* 2010;134(1):55–65.
43. Rossi G, Graziano P, Leone A, Migaldi M, Califano R. The role of molecular analyses in the diagnosis and treatment of non-small-cell lung carcinomas. *Semin Diagn Pathol.* 2013;30(4):298–312.
44. Takeuchi T, Tomida S, Yatabe Y, Kosaka T, Osada H, Yanagisawa K, Mitsudomi T, Takahashi T. Expression profile-defined classification of lung adenocarcinoma shows close relationship with underlying major genetic changes and clinicopathologic behaviors. *J Clin Oncol.* 2006;24(11):1679–88.
45. Sun F, Wang P, Zheng Y, Jia W, Liu F, Xiao W, Bao J, Wang S, Lu K. Diagnosis, clinicopathological characteristics and prognosis of pulmonary mucinous adenocarcinoma. *Oncol Lett.* 2018;15(1):489–94.
46. Mizuno T, Arimura T, Kuroda H, Sakakura N, Yatabe Y, Sakao Y. Current outcomes of postrecurrence survival in patients after resection of non-small cell lung cancer. *J Thorac Dis.* 2018;10(3):1788–96.
47. Mittal V. Epithelial mesenchymal transition in aggressive lung cancers. *Adv Exp Med Biol.* 2016; 890:37–56.
48. Hamilton G, Rath B. Mesenchymal-epithelial transition and circulating tumor cells in small cell lung cancer. *Adv Exp Med Biol.* 2017;994:229–45.
49. O'Flaherty JD, Gray S, Richard D, Fennell D, O'Leary JJ, Blackhall FH, O'Byrne KJ. Circulating tumour cells, their role in metastasis and their clinical utility in lung cancer. *Lung Cancer.* 2012;76(1):19–25.
50. Altorki NK, Markowitz GJ, Gao D, Port JL, Saxena A, Stiles B, McGraw T, Mittal V. The lung microenvironment: an important regulator of tumour growth and metastasis. *Nat Rev Cancer.* 2019;19(1):9–31.
51. Medeiros B, Allan AL. Molecular mechanisms of breast cancer metastasis to the lung: clinical and experimental perspectives. *Int J Mol Sci.* 2019;20(9). pii: E2272.
52. Girard N, Ostrovskaya I, Lau C, Park B, Ladanyi M, Finley D, Deshpande C, Rusch V, Orlov I, Travis WD, Pao W, Begg CB. Genomic and mutational profiling to assess clonal relationships between multiple non-small cell lung cancers. *Clin Cancer Res.* 2009;15(16):5184–90.
53. Krasinskas AM, Chiosea SI, Pal T, Dacic S. KRAS mutational analysis and immunohistochemical studies can help distinguish pancreatic metastases from primary lung adenocarcinomas. *Mod Pathol.* 2014;27(2): 262–70.
54. Wang Y, Lei L, Jiang GY, Yang LH, Xu HT. Case Report Primary pleomorphic adenoma of the lung with positive staining of TTF-1: a case report and review of literature. *Int J Clin Exp Med.* 2018;11(1):378–83.
55. Wasserman JK, Dickson BC, Smith A, Swanson D, Purgina BM, Weinreb I. Metastasizing pleomorphic adenoma: recurrent PLAG1/HMGA2 rearrangements and identification of a novel HMGA2-TMTC2 fusion. *Am J Surg Pathol.* 2019;43:1145. <https://doi.org/10.1097/PAS.0000000000001280>.
- 56a. Barnaś E, Książek M, Raś R, Skręt A, Skręt-Magierło J, Dmoch-Gajzlerska E. Benign metastasizing leiomyoma: A review of current literature in respect to the time and type of previous gynecological surgery. *PLoS One.* 2017;12(4):e0175875.
- 56b. Ogawa M, Hara M, Ozawa Y, Moriyama S, Yano M, Shimizu S, Shibamoto Y. Benign metastasizing leiomyoma of the lung with malignant transformation mimicking mediastinal tumor. *Clin Imaging.* 2011;35(5):401–4.
57. Abramson S, Gilkeson RC, Goldstein JD, Woodard PK, Eisenberg R, Abramson N. Benign metastasizing leiomyoma: clinical, imaging, and pathologic correlation. *Am J Roentgenol.* 2001;176(6):1409–13.
58. Ofori K, Fernandes H, Cummings M, Colby T, Saqi A. Benign metastasizing leiomyoma presenting with miliary pattern and fatal outcome: Case report with molecular analysis & review of the literature. *Respir Med Case Rep.* 2019;28:100831.
59. Wei J, Yuan X, Yao Y, Sun L, Yao X, Sun A. Primary myoepithelial carcinoma of the lung: a case report and review of literature. *Int J Clin Exp Pathol.* 2015;8(2):2111.
60. Thway K, Fisher C. Tumors with EWSR1-CREB1 and EWSR1-ATF1 fusions: the current status. *Am J Surg Pathol.* 2012;36(7):e1–11.
61. Nadelman CM, Leslie KO, Fishbein MC. "Benign," metastasizing adenomyoepithelioma of the breast: a report of 2 cases. *Arch Pathol Lab Med.* 2006;130(9): 1349–53.

62. Jayaschandran V, Gjorgova-Gjeorgjievski S, Siddique H. An uncommon cause of miliary pattern of pulmonary nodules – diffuse pulmonary meningotheliomatosis. *Respir Case Rep.* 2017;5(4):e00238.
63. Kumar A, Cherian SV, Farver C, Mehta AC. Pulmonary meningotheliomatosis. *Arch Bronconeumol.* 2018;54(2):104–5.
64. Luo JZ, Zhan C, Ni X, Shi Y, Wang Q. Primary pulmonary meningioma mimicking lung metastatic tumor: a case report. *J Cardiothorac Surg.* 2018;13(1):99.
65. Colby TV. Metastasizing dermatofibroma. *Am J Surg Pathol.* 1997;21(8):976.
66. Doyle LA, Fletcher CD. Metastasizing “benign” cutaneous fibrous histiocytoma: a clinicopathologic analysis of 16 cases. *Am J Surg Pathol.* 2013;37(4):484–95.
67. López-Barea F, Rodríguez-Peralto JL, García-Girón J, Guemes-Gordo F. Benign metastasizing giant-cell tumor of the hand. Report of a case and review of the literature. *Clin Orthop Relat Res.* 1992;274:270–4.
68. Zhuang BW, Li W, Chen ZF, Cao CJ, Xie XY, Xie XH. Multiple cavernous hemangiomas of the lung and liver mimicking metastasis: A case report and literature review. *Medicine (Baltimore).* 2018;97(51):e13509.
69. Amin MB, MD, FCAPAJCC Cancer Staging Manual 8th edition; Chicago 2017 (Amin MB, Edge S, Greene F. *AJCC Cancer Staging System: UPDATE.* Cancer AJCC, ed. 2016.)
70. Arslan A, Ozcakir-Tomruk C, Deniz E, Akin O. A case report of metastasis of malignant mesothelioma to the retromolar trigone. *World J Surg Oncol.* 2016;14(1):188.
71. Finn RS, Brims FJ, Gandhi A, Olsen N, Musk AW, Maskell NA, Lee YG. Postmortem findings of malignant pleural mesothelioma: a two-center study of 318 patients. *Chest.* 2012;142(5):1267–73.
72. Hirooka A, Tamiya A, Kanazu M, Nonaka J, Yonezawa T, Asami K, Atagi S. Brain metastasis of pleural mesothelioma after a subarachnoid hemorrhage. *Intern Med.* 2016;55(7):779–81.
73. Wroński M, Burt M. Cerebral metastases in pleural mesothelioma: case report and review of the literature. *J Neuro-Oncol.* 1993;17(1):21–6.
74. Framarino-dei-Malatesta M, Sammartino P, Derme M, Iannini I, Masselli G, Pecorella I. Breast cancer or metastasis? An unusual case of metastatic malignant pleural mesothelioma to the breast. *World J Surg Oncol.* 2015;13(1):79.
75. Maiorana A, Giusti F, Cesinaro AM, Conti A, Rossi G. Cutaneous metastases as the first manifestation of pleural malignant mesothelioma. *J Am Acad Dermatol.* 2006;54(2):363–5.
76. Zardawi SJ, Li BT, Zauderer MG, Wang JW, Atmore BB, Barnes TA, Pavlakis N, Mathur MN, Clarke S. Localized malignant pleural mesothelioma with renal metastasis. *Oxf Med Case Reports.* 2015;2015(1):170–2.
77. Moser S, Beer M, Damerau G, Lübbers HT, Grätz KW, Kruse AL. A case report of metastasis of malignant mesothelioma to the oral gingiva. *Head Neck Oncol.* 2011;3(1):21.
78. Mann S, Khawar S, Moran C, Kalhor N. Revisiting localized malignant mesothelioma. *Ann Diagn Pathol.* 2019;39:74–7.
79. Attanoos RL, Pugh MR. The diagnosis of pleural tumors other than mesothelioma. *Arch Pathol Lab Med.* 2018;142(8):902–13.
80. Gladish GW, Sabloff BM, Munden RF, Truong MT, Erasmus JJ, Chasen MH. Primary thoracic sarcomas. *Radiographics.* 2002;22(3):621–37.
81. Bagan P, Hassan M, Barthes FLP, Peyrard S, Souilamas R, Danel C, Riquet M. Prognostic factors and surgical indications of pulmonary epithelioid hemangioendothelioma: a review of the literature. *Ann Thorac Surg.* 2006;82(6):2010–3.
82. Thalheimer A, Fein M, Geissinger E, Franke S. Intimal angiosarcoma of the aorta: report of a case and review of the literature. *J Vasc Surg.* 2004;40(3):548–53.
83. Suzuki T, Suzuki S, Kitami A, Kamio Y, Hori G, Mitsuya T, Ota H. Angiosarcoma of the chest wall. *Thorac Cardiovasc Surg.* 1996;44(04):213–5.
84. Pramesh CS, Madur BP, Raina S, Desai SB, Mistry RC. Angiosarcoma of the pleura. *Ann Thorac Cardiovasc Surg.* 2004;10(3):187–90.
85. Piciucchi S, Dubini A, Tomassetti S, Sanna S, Ravaglia C, Carloni A, Gurioli C, Gurioli C, Colby TV, Poletti V. Angiosarcoma in the chest: radiologic-pathologic correlation: Case report. *Medicine (Baltimore).* 2016;95(48):e5348.
86. Yano M, Toyooka S, Tsukuda K, Dote H, Morimoto Y, Ohata N, et al. SYT-SSX fusion genes in synovial sarcoma of the thorax. *Lung Cancer.* 2004;44:391–7.
87. Okamoto S, Hisaoka M, Daa T, Hatakeyama K, Iwamasa T, Hashimoto H. Primary pulmonary synovial sarcoma: a clinicopathologic, immunohistochemical, and molecular study of 11 cases. *Hum Pathol.* 2004;35:850–6.
88. Katakura H, Fukuse T, Shiraishi I, Hayatsu E, Nishijo K, Toguchida J, Nakashima Y, Wada H. Mediastinal synovial sarcoma. *Thorac Cardiovasc Surg.* 2009;57(03):183–5.
89. Essary LR, Vargas SO, Fletcher CD. Primary pleuropulmonary synovial sarcoma: reappraisal of a recently described anatomic subset. *Cancer.* 2002;94(2):459–69.
90. de Perrot M, Fischer S, Bründler MA, Sekine Y, Keshevjee S. Solitary fibrous tumors of the pleura. *Ann Thorac Surg.* 2002;74(1):285–93.
91. Ng HK, Choi PC, Wong CW, To KF, Poon WS. Metastatic solitary fibrous tumor of the meninges: case report. *J Neurosurg.* 2000;93(3):490–3.
92. Schirosi L, Lantuejoul S, Cavazza A, Murer B, Yves Brichon P, Migaldi M, Sartori G, Sgambato A, Rossi G. Pleuro-pulmonary solitary fibrous tumors: a clinicopathologic, immunohistochemical, and molecular study of 88 cases confirming the prognostic value of de Perrot staging system and p53 expression, and evaluating the role of c-kit, BRAF, PDGFRs (alpha/beta), c-met, and EGFR. *Am J Surg Pathol.* 2008;32(11):1627–42.
93. Swerdlow SH, Campo E, Pileri SA, Harris NL, Stein H, Siebert R, Advani R, Ghielmini M, Salles GA, Zelenetz AD, Jaffe ES. The 2016 revision of the World Health Organization classification of lymphoid neoplasms. *Blood.* 2016;127(20):2375–90.

94. Martelli M, Ferreri A, Di Rocco A, Ansuinelli M, Johnson PW. Primary mediastinal large B-cell lymphoma. *Crit Rev Oncol Hematol*. 2017;113:318–27.
95. Dunleavy K, Wilson WH. Primary mediastinal B-cell lymphoma and mediastinal gray zone lymphoma: do they require a unique therapeutic approach? *Blood*. 2015;125(1):33–9.
96. Vitolo U, Seymour JF, Martelli M, Illerhaus G, Illidge T, Zucca E, Campo E, Ladetto M. Extranodal diffuse large B-cell lymphoma (DLBCL) and primary mediastinal B-cell lymphoma: ESMO Clinical Practice Guidelines for diagnosis, treatment and follow-up. *Ann Oncol*. 2016;27(suppl_5):v91–102.
97. Borie R, Wislez M, Antoine M, Cadranel J. Lymphoproliferative disorders of the lung. *Respiration*. 2017;94(2):157–75.
98. Nakatsuka SI, Yao M, Hoshida Y, Yamamoto S, Iuchi K, Aozasa K. Pyothorax-associated lymphoma: a review of 106 cases. *J Clin Oncol*. 2002;20(20):4255–60.
99. Narkhede M, Arora S, Ujjani C. Primary effusion lymphoma: current perspectives. *Onco Targets Ther*. 2018;11:3747–54.
100. Kurtin PJ, Myers JL, Adlakha H, Strickler JG, Lohse C, Pankratz VS, Inwards DJ. Pathologic and clinical features of primary pulmonary extranodal marginal zone B-cell lymphoma of MALT type. *Am J Surg Pathol*. 2001;25(8):997–1008.
101. Borie R, Wislez M, Antoine M, Copie-Bergman C, Thieblemont C, Cadranel J. Pulmonary mucosa-associated lymphoid tissue lymphoma revisited. *Eur Respir J*. 2016;47(4):1244–60.
102. Colby TV. Current histological diagnosis of lymphomatoid granulomatosis. *Mod Pathol*. 2012;25(Suppl 1):S39–42.
103. Marx A, Chan JK, Coindre JM, Detterbeck F, Girard N, Harris NL, Jaffe ES, Kurrer MO, Marom EM, Moreira AL, Mukai K. The 2015 World Health Organization classification of tumors of the thymus: continuity and changes. *J Thorac Oncol*. 2015;10(10):1383–95.
104. Kondo K, Monden Y. Lymphogenous and hematogenous metastasis of thymic epithelial tumors. *Ann Thorac Surg*. 2003;76(6):1859–64.
105. Huang J, Rizk NP, Travis WD, Riely GJ, Park BJ, Bains MS, Dycoco J, Flores RM, Downey RJ, Rusch VW. Comparison of patterns of relapse in thymic carcinoma and thymoma. *J Thorac Cardiovasc Surg*. 2009;138(1):26–31.
106. Jain RK, Mehta RJ, Henley JD, Kesler KA, Loehrer PJ, Badve S. WHO types A and AB thymomas: not always benign. *Mod Pathol*. 2010;23(12):1641.



Radiological Signs of Tumor Dissemination

*Lucian Beer, Felicitas Oberndorfer, Mario Silva,
and Helmut Prosch*

- 2.1 Introduction – 36**
- 2.2 Local Spread – 36**
 - 2.2.1 Expansive Growth – 36
 - 2.2.2 Infiltrative Growth – 38
- 2.3 Hematogenous Spread – 40**
- 2.4 Lymphatic Spread – 41**
- 2.5 Bronchogenic and Aero-genic Spread – 43**
- References – 45**

2.1 Introduction

Radiology plays a central role for the assessment of tumor dissemination in a process called “staging.” Precise radiological tumor staging is fundamental for treatment decisions in patients with cancer. Allocating patients to potential curative surgery or to systemic therapy is mainly based on a patient’s clinical features, as well as the molecular and imaging characteristics of the tumor. Tumor assessment includes both the local staging, which focuses mainly on regional tumor extension and potential technical respectability, and the distant staging, to rule out or confirm the presence of metastasis. Staging of thoracic tumors follows the staging system of the International Union Against Cancer (Union internationale contre le cancer, UICC), which was last updated in 2017 [1].

The main imaging modalities used in patients with lung cancer are computed tomography (CT), positron-emission tomography (PET)/CT, magnetic resonance imaging (MRI), and ultrasound (US). Each of these possesses strengths and weaknesses, and the thoughtful combination of these methods enables an optimal diagnostic workup.

Computed tomography (CT) is the primary tool with which to investigate patients with suspected thoracic tumors, as it is sufficient in most patients to detect distant metastases and an extensive infiltration of neighboring structures. However, in patients who are eligible for curative surgery, current guidelines require the acquisition of a ^{18}F -labeled fluoro-2-deoxyglucose (FDG) positron-emission tomography (PET)/CT and a brain magnetic resonance imaging (MRI) (or contrast-enhanced brain CT) to exclude metastasis [2]. PET/CT is requested because it has been shown that PET/CT may detect distant metastases in up to 20% of patients who would otherwise have been surgical candidates [3].

In addition, MRI is frequently performed in lung cancer patients with suspected mediastinal or chest wall infiltration, as its excellent soft tissue contrast allows for a better delineation of the extent of infiltration than CT. MRI is also the method with which to further characterize suspected bone metastases detected on other imaging modalities [2].

Ultrasound has been proven to be an excellent tool for the investigation of an infiltration of the chest wall [4]. Furthermore, ultrasound-guided

biopsies of the supraclavicular lymph nodes are a reliable and safe procedure to confirm an inoperable tumor stage. Last but not least, ultrasound and ultrasound-guided biopsies are often used to further investigate equivocal findings from CT or PET/CT [5, 6].

2.2 Local Spread

Activation of the invasive capacities of tumors is one of the ten hallmarks of cancer [7]. The underlying genomic, genetic, and metabolomic alterations are complex, and the multistep process of invasion and, finally, metastasis has been termed the invasion-metastasis cascade [8]. In particular, a regulatory program, referred to as the “epithelial-mesenchymal transition,” has been shown to broadly regulate invasion and metastasis [9]. While, on a genetic level, the alterations during the progression of these cascades are manifold, the macroscopic changes visible on diagnostic imaging are limited and can only detect relatively late stages of the invasion-metastatic cascade. Advanced imaging technologies, such as hyperpolarized carbon 13 MRI [10], which assesses metabolomic changes, are promising tools that might capture changes in tumor aggressiveness earlier compared to conventional imaging modalities.

2.2.1 Expansive Growth

Measurement of tumor size must be performed in a standardized way, and the current TNM staging system mandates the measurement of the largest unidimensional diameter using thin sections (≤ 1 mm slice thickness) and multiplanar reconstructions (transverse, coronal, and sagittal) (■ Fig. 2.1) [11]. Thin sections provide the least variability, as they suffer from smaller partial volume averaging compared to thicker slices. In addition, all measurements should be performed using a lung window setting with sharp filters, except for partly solid nodules, in which the solid component can also be measured using a narrow (soft tissue or mediastinal) window [11]. For partly solid nodules, the long axis of both the solid and ground-glass components should be measured (■ Fig. 2.2). However, for final staging

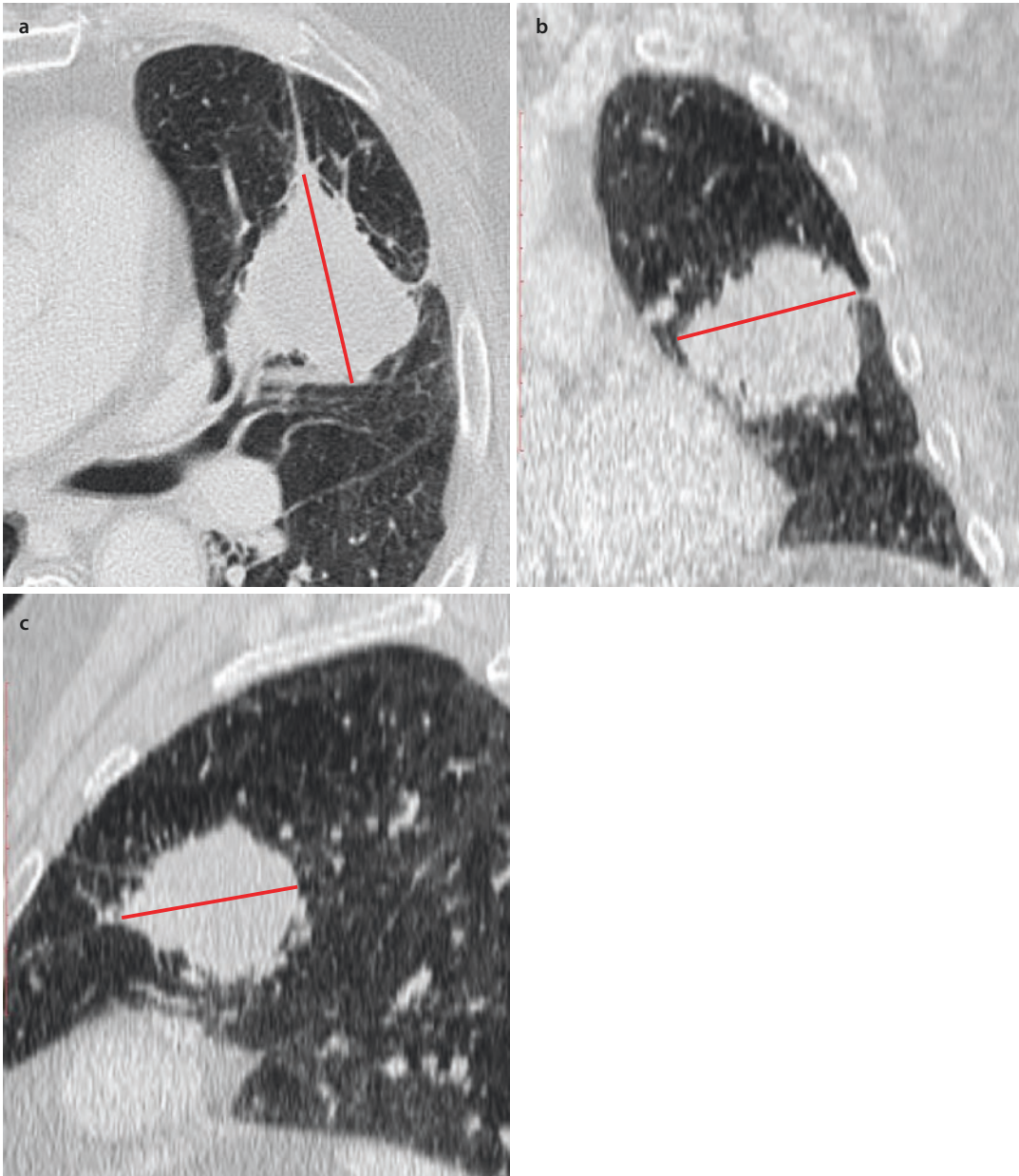


Fig. 2.1 Axial **a**, coronal **b**, and sagittal **c** contrast-enhanced CT of a squamous cell carcinoma in the left upper lobe. The largest tumor diameter should be used

for T staging. In this case, the largest diameters were 5.7 cm, 5.6 cm, and 5.2 cm in the axial, coronal, or sagittal reconstructions, respectively

purposes, only the long-axis dimension of the solid component is used, as this represents the invasive tumor parts [11].

Expansive tumor growth can lead to obliteration of bronchi and the development of postobstructive lung atelectasis or pneumonia. Tumor assessment in atelectatic areas can be challenging at times using CT, in which case FDG PET can be

helpful to differentiate between tumor and collapsed lung, although concomitant pneumonia challenges image interpretation.

A particular type of NSCLC in terms of appearance and treatment is the pneumonic type of adenocarcinoma. These cancers are characterized by a regional distribution of tumor similar to a pneumonia (Fig. 2.3) [12]. They have imaging

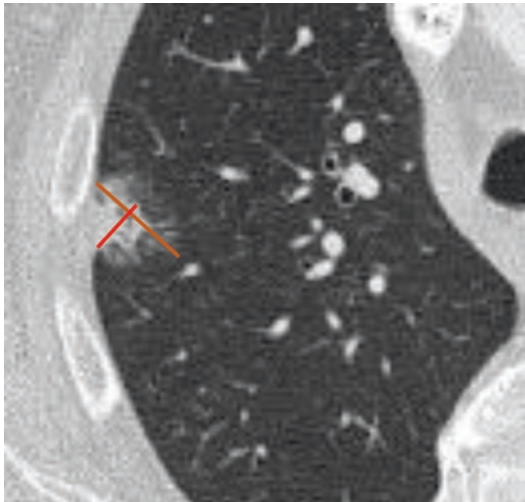


Fig. 2.2 Axial contrast-enhanced CT showing a partly solid nodule in the right upper lobe compatible with a biopsy-proven invasive adenocarcinoma. It is recommended that both the solid (red line) and ground-glass (orange line) tumors be measured. The solid part represents the invasive component of the tumor and should be used to define the T classification for staging. The solid compartment better predicts prognosis than the overall tumor size in lepidic-predominant adenocarcinomas



Fig. 2.3 Axial contrast-enhanced CT scan shows patchy bilateral ground-glass opacities and consolidations without pleural effusions or enlarged lymph nodes, corresponding to a histology-proven pneumonic-type adenocarcinoma of both lungs (cM1a)

similarities to multifocal ground-glass adenocarcinomas, and it has been discussed whether they represent a later stage in the evolution of this entity [13]. In more than 50% of cases, pneumonic-type adenocarcinomas involve both lungs [14]. Nodal or systemic metastases are typically not

present at the time of diagnosis. Correct clinical and pathological staging is important, as double-lung transplantation is an accepted treatment option for selected patients [15, 16].

2.2.2 Infiltrative Growth

Direct infiltration of tumor tissue into adjacent structures is especially important in the lung apices, the mediastinum, and the diaphragm. MRI is favored, compared to CT, to assess the infiltrative growth pattern due to the higher tissue contrast and the ability to perform dynamic examinations.

2.2.2.1 Chest Wall

Reliable criteria for an infiltration of the chest wall include direct evidence of tumor masses infiltrating the chest wall and evidence of rib erosion. Additional signs are a thickening of the pleura or impaired respiratory motion. The latter two signs, however, are less reliable, as inflammatory reactions in the vicinity of malignant tumors may also lead to a thickening of the pleura and an impaired respiratory motion of the tumor in relation to the chest wall. A confident diagnosis of an infiltration of the chest wall is difficult in many cases. Because of the relatively low soft tissue contrast, the sensitivity and specificity of CT are limited. With MRI, one is often able to slightly increase both the sensitivity and specificity of diagnosis.

A particular site of chest wall infiltration is the superior sulcus, the most apical area of the chest cavity. Tumors that infiltrate this area are called Pancoast tumors and most commonly are adenocarcinomas. Anatomically, this area is a highly specific region, as the brachial plexus and the large vessels of the arm and head run through it in close proximity to each other.

CT scans are usually the first imaging procedure performed for Pancoast tumors (Fig. 2.4a). Using multiplanar reformations, in addition to conventional axial images, the relation of the tumor to the great vessels can be depicted. Due to its poor soft tissue contrast, CT, however, has its limitations in depicting the relation of the tumor to the brachial plexus and neural foramina. For a comprehensive preoperative evaluation, additional imaging is almost always necessary. MRI

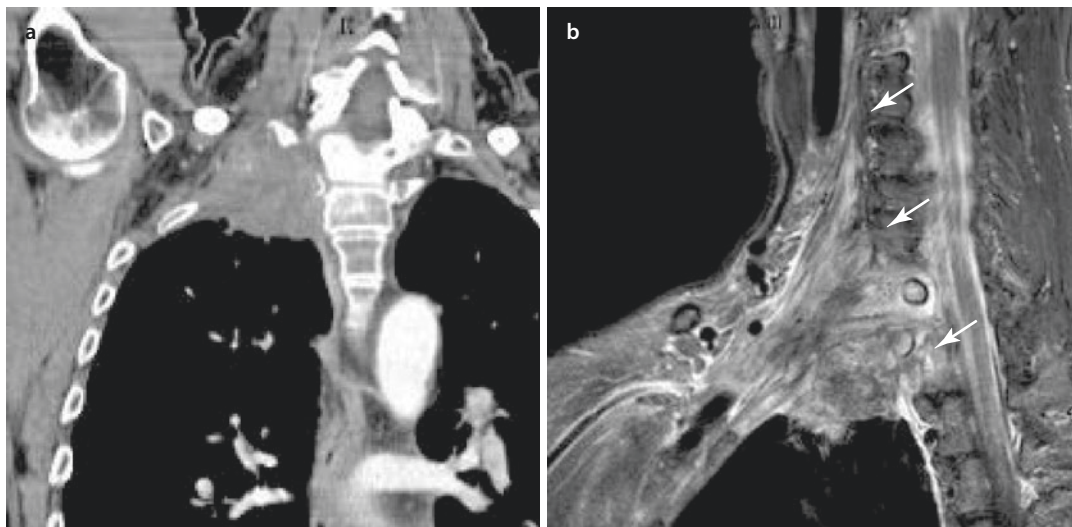


Fig. 2.4 Right-sided Pancoast tumor. **a** Coronal contrast-enhanced CT scan shows a heterogeneous enhancing mass in the right apex with infiltration of the chest wall and infiltration of the second rib. **b** MRI of the

same patient better illustrates tumor extension into the soft tissue, as well as infiltration of the cervical and thoracic nerves

allows a clear visualization of the neural foramina, the brachial plexus, the great vessels, and the vertebral bodies and is thus considered to be essential for surgical treatment planning (Fig. 2.4b) [17]. Changes in tumor size during neoadjuvant treatment do not necessarily reflect histopathological treatment response [18], nor do they correlate with overall survival [19]. While a reduction in tumor size measured by CT is associated with a higher frequency of complete histopathological response, cases of complete histopathological response have even been observed in patients with an increase in tumor volume after neoadjuvant treatment, which is believed to be due to extensive tissue fibrosis [18]. Consequently, the decision to operate on a patient with a Pancoast tumor must be made on the basis of preoperative MRI and, thus, prior to the initiation of neoadjuvant radiochemotherapy.

2.2.2.2 Mediastinum

The sensitivity and specificity of CT for the assessment of mediastinal infiltration are poor, with a range from 25% to 84% and from 57% to 99% (summarized in [20]). Indicators of mediastinal infiltration on CT are an obtuse angle and a length of more than 3 cm contact between the mass and adjacent structures, obliteration of the fat plane, and signs of direct invasion

(Fig. 2.5) [21]. In contrast, MRI using thin slices, or dynamic acquisition sequences, has a higher sensitivity between 85% and 100% and a specificity of 89–92% [20, 22–24]. On dynamic respiration-affected MRI sequences, mediastinal or chest wall infiltration can interrupt the physiological sliding motion between the lung and mediastinum, which can help to identify mediastinal infiltration. False-positive results can emerge in case of fibrous adhesions, which also reduce the sliding motion without invasion of the mediastinum. Therefore, the combination of different features, including signs of direct and indirect (e.g., loss of respiratory sliding motion, angle of contact plane) invasion, should be taken into account. Whether or not contrast-enhanced MRI improves the accuracy in detecting mediastinal tumoral infiltration is still under debate, as the increased contrast between the tumor and surrounding structures can obscure tumor margins and reduce the diagnostic accuracy [22].

2.2.2.3 Diaphragm

Multiphase reconstructions in the sagittal and coronal plane are recommended to assess the diaphragm in CT. MRI is better suited to assess infiltration of the diaphragm, compared to CT, based on the superior soft tissue contrast.

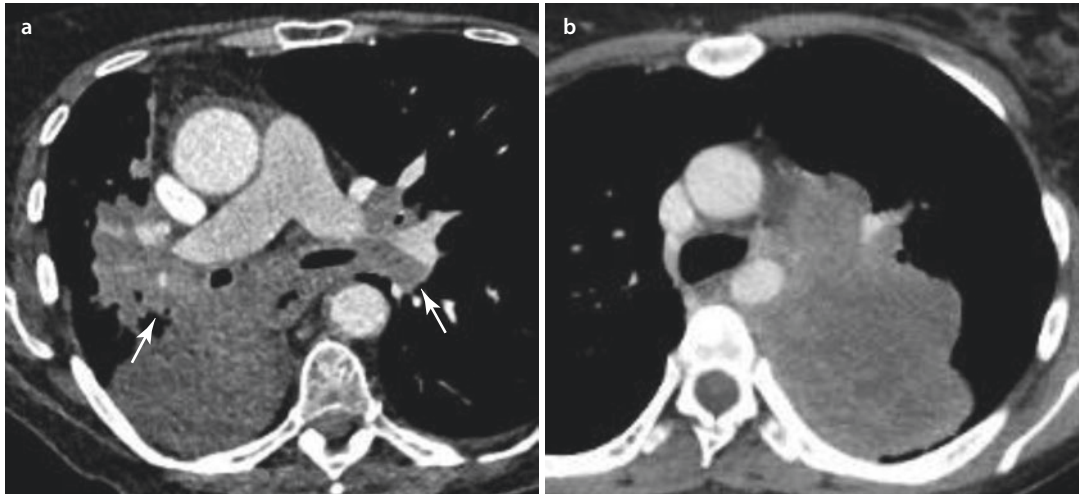


Fig. 2.5 Axial contrast-enhanced CT scans. **a** There is an inhomogeneous enhancing mass presumably arising from the right hilum with extensive infiltration of the mediastinal fat, esophagus, and pulmonary arteries. Both the right and left pulmonary arteries are highly narrowed by the tumor,

and there is no fat plane left between the soft tissue mass and the esophagus. A trace of pericardial effusion is visible, ventral to the ascending aorta (cT4). **b** A different patient with an inhomogeneous enhancing mass arising from the left lower lobe, with signs of direct infiltration of the mediastinum (cT4)

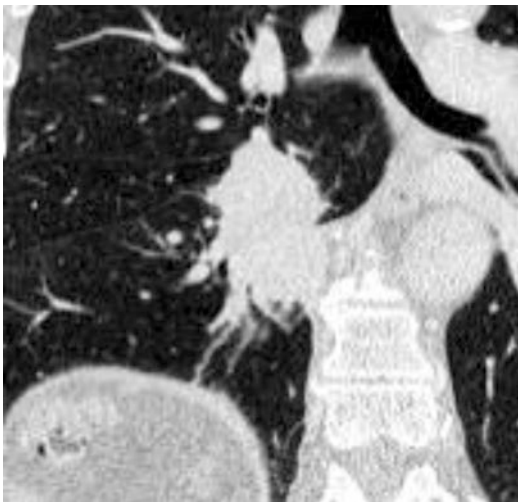


Fig. 2.6 Coronal unenhanced CT showing a centrally located tumor in the right lung probably arising from the middle lobe. The tumor infiltrated the horizontal and oblique fissure, thereby extending into the right upper and lower lobe

2.2.2.4 Transfissural Growth

Although transfissural growth itself does not alter T staging, it commonly affects surgery, as lobectomy is no longer possible. Multiplanar reconstructions should be used to assess transfissural growth (■ Fig. 2.6). Indirect signs of an infiltration of the fissure are a shift of the fissure and broad contact of the fissure.

2.3 Hematogenous Spread

Metastatic dissemination has long been believed to occur during the most advanced stages in cancer progression; however, growing evidence shows that cancer cells can disseminate early [25]. Thoracic tumors can spread hematogenously to intrathoracic as well as extrathoracic sites. The number of distant metastases can vary from single metastases in an organ to innumerable micronodules (military dissemination). The role of imaging is first to detect suspicious lesions and second to differentiate lesions which do not require further evaluation (either because they are clearly malignant or unequivocally benign) from lesions which require histological verification.

For the detection of suspicious lesions, the diagnostic accuracy for the detection of extrathoracic metastasis is higher for PET/CT compared to CT. PET/CT should, therefore, be performed in patients for whom curative surgery is an option [2] in order to reduce the number of unnecessary surgeries (■ Figs. 2.7 and 2.8). MRI is recommended for screening of brain metastases in patients considered for curative therapy [2]. MRI also allows identification and characterization of liver lesions, bone metastasis, and brain metastasis (■ Fig. 2.9). However, MRI is not performed routinely for the former two indications. In the future, whole-body

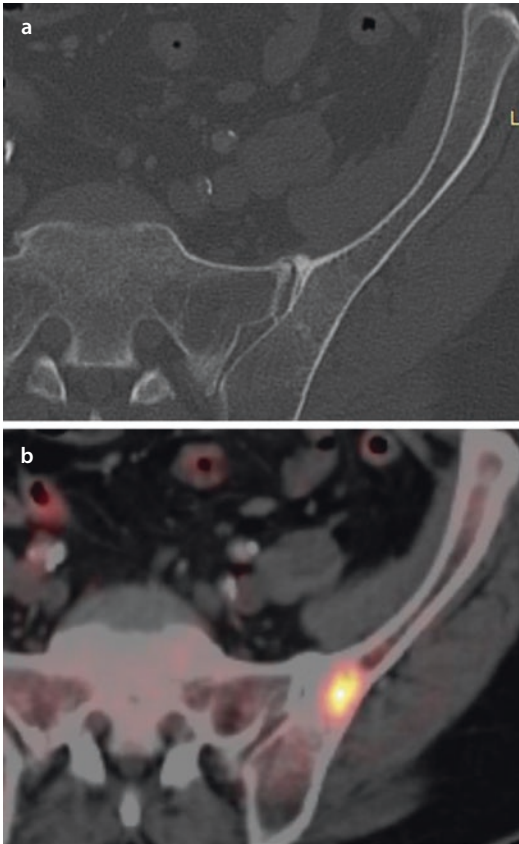


Fig. 2.7 Axial contrast-enhanced CT and FDG PET/CT scan in a patient with newly diagnosed adenocarcinoma. CT scan showed no bone abnormalities, whereas there was a focal increased FDG uptake in the left iliac bone highly suggestive of a bone metastasis. The lesion was proven to be malignant by the pattern of growth in the follow-up examination. There were no further extrathoracic metastases (cM1b). Axial contrast-enhanced CT (a) and FDG PET/CT scan (b)

PET/CT or PET/MRI examination tracers directed against treatment targets, such as the programmed cell death protein 1 (PD-1) [26], might revolutionize imaging and will hopefully enable treatment selection based on imaging studies.

2.4 Lymphatic Spread

Lymphatic spread plays a pivotal role in tumor dissemination. A tumor spread to the pulmonary lymphatic system is called lymphangiosis carcinomatosa. As the pulmonary lymphatics run along the pleura, the interlobular septa, and the bronchovascular bundle, lymphangiosis carcinoma-



Fig. 2.8 Axial and coronal FDG PET/CT scan. a, b Metabolically active, bilateral adrenal gland metastasis (cM1c)

tosa shows on CT as nodular or smooth thickening of these structures (perilymphatic distribution) (Fig. 2.10). Lymphangiosis carcinomatosa can be limited to the edges of a tumor or diffusely involves one lobe or even the lungs on both sides. In contrast to other tumor entities, however, the prognostic role of lymphangiosis carcinomatosa is still unknown and thus not included in the TNM staging system [27].

Of importance, however, is the distinction of lymphangitis from the so-called sarcoid-like reaction. Sarcoid-like reaction is a systemic granulomatous reaction observed in cancer patients undergoing immunotherapy and is radiologically as well as pathologically indistinguishable from sarcoidosis [28, 29]. So far, the immunopathological mechanism of sarcoid-like reaction is not well understood. As sarcoid-like reaction does also present on CT as a nodular disease with a perilymphatic distribution, it may

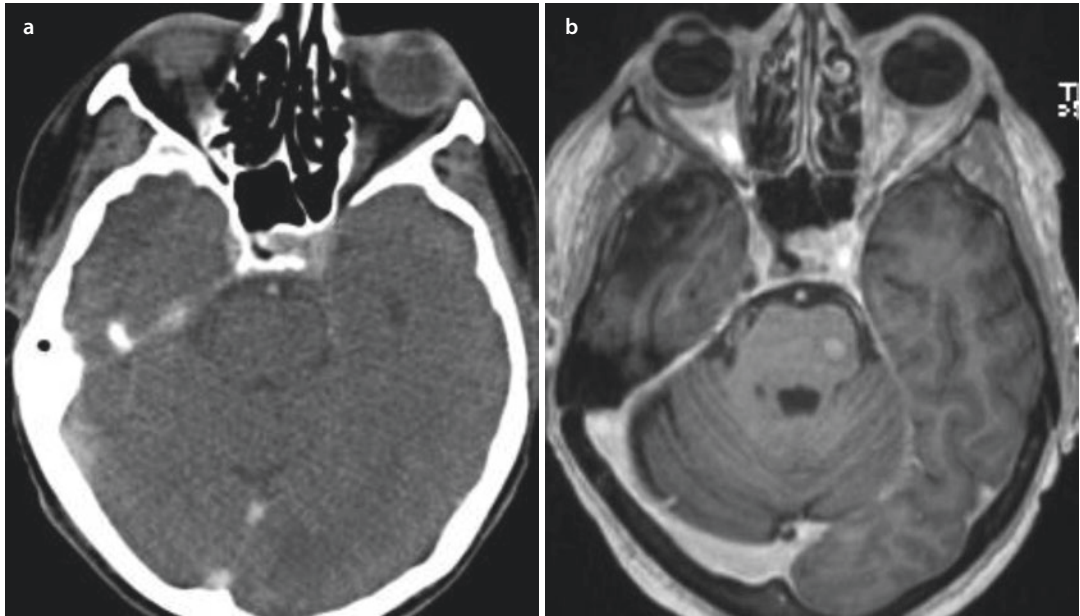


Fig. 2.9 Contrast-enhanced CT **a** and MRI **b** on the same day in a patient with adenocarcinoma of the lung. At the time of the examination, the patient had no neurological symptoms. While CT does not show any

malignant lesion, the MRI shows a 7 mm enhancing metastasis in the left side of the pons. In addition, there was a right-sided adrenal gland metastasis (not shown), which resulted in a cM1c stage

be confused with lymphangiosis carcinomatosa and thus lead to the misdiagnosis of a disease progression. Consequently, cases of presumably newly developed lymphangiosis carcinomatosa in patients undergoing immunotherapy have to be investigated with care. **Table 2.1** summarizes imaging features which might help to distinguish sarcoid-like reactions from lymphangiosis carcinomatosa.

While the prognostic role of lymphangiosis carcinomatosa in lung cancer is not well established, lymph node involvement is the most important prognostic factor in patients with respectable lung cancer [30].

In CT staging, the size of the lymph nodes is the only criterion by which to diagnose lymph node involvement. The cutoff used to differentiate benign from malignant lymph nodes is defined with a maximum short-axis diameter of 1 cm. Unfortunately, as reactive lymph nodes may also reach a considerable size, this criterion is only of limited use in differentiating benign lymph nodes from metastatic nodes. The pooled sensitivity of this criterion has been reported to be as low as 55%, with a specificity of 81% [31]. Notably, 42% of all lymph nodes deemed to be malignant by size criteria are benign instead, and 17% of all

lymph nodes smaller than 1 cm in the short-axis diameter are malignant [32].

One possibility to increase the performance of lymph node staging is the use of PET/CT. In lung cancer staging, the most frequently used tracer is FDG, a labeled glucose analogue [3].

PET scanning alone has reported sensitivities and specificities of 80% and 88% [31, 33], respectively, compared to 55% and 81% with CT alone [31], which demonstrates that PET scanning is more accurate than CT scanning for the staging of lymph nodes in the mediastinum. A PET/CT is currently recommended for all patients who are possible suitable candidates for curative surgery in order to reduce the number of patients who would not benefit from surgery [3, 34]. In case of a positive nodal finding on CT or PET/CT, subsequent tissue confirmation is needed using either endobronchial ultrasound (EBUS)- or endoscopic ultrasound (EUS)-guided tissue sampling [34]. In case of a negative PET and normal-sized mediastinal lymph nodes and a peripheral tumor smaller than 3 cm, no further diagnostic tests are needed. In case of clinical N1 disease or a central tumor larger than 3 cm, tissue sampling using either EBUS, EUS, or video-assisted mediastinoscopy is recommended [34, 35].

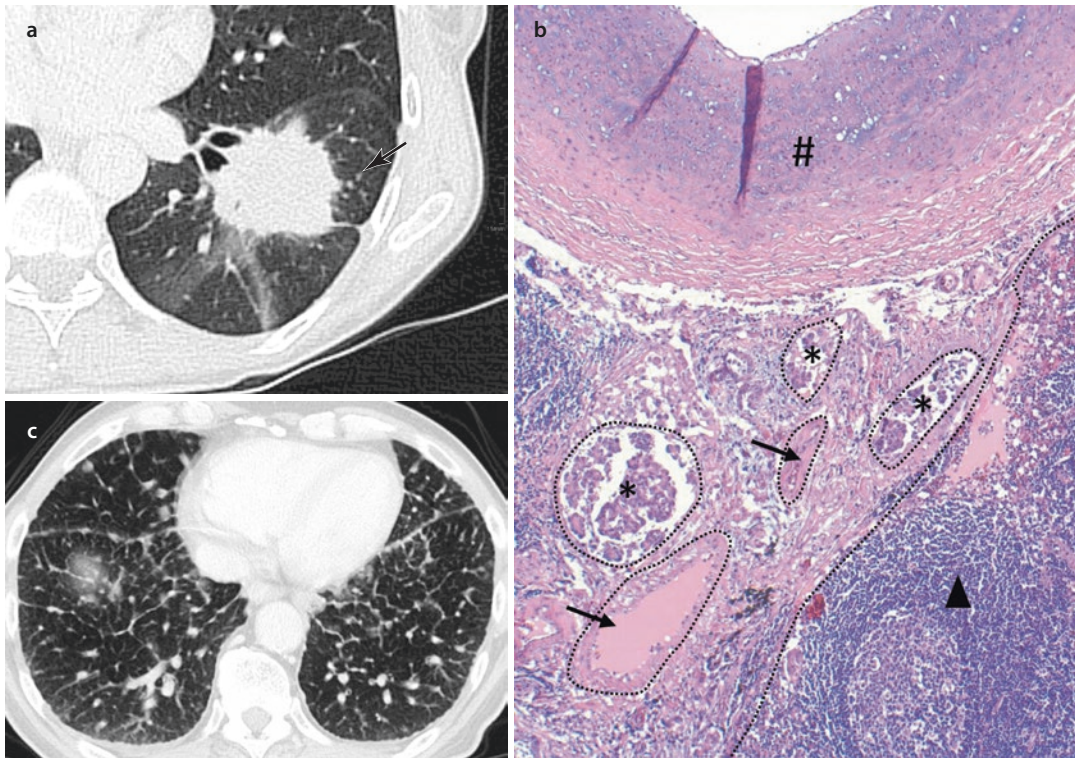


Fig. 2.10 a A 53-year-old female patient with adenocarcinoma of the lung and lymphangiosis carcinomatosa. Axial CT image shows nodular subtle smooth thickening of the interlobular septa and the bronchovascular bundle. b Corresponding histological analysis showed tumor cells with lymphatic invasion (asterisk) but without

involvement of the small vessels/capillaries (arrow). #, pulmonary artery; ▲, lymph node. c A different 64-year-old patient with signet cell cancer of the stomach and lymphangiosis carcinomatosa. Axial CT image shows nodular or smooth thickening of the interlobular septa and the bronchovascular bundle (perilymphatic distribution)

Table 2.1 Radiological imaging findings in lymphangitis and sarcoid-like reaction

Lymphangitis	Sarcoid-like reaction
Nodular or smooth thickening of interlobular septa	± Septal thickening
± Lymphadenopathy (30%)	Symmetric lymphadenopathy
± Pleural effusions (50%)	No pleural effusions
Lobular architecture preserved	Upper lobe predominance

MRI using diffusion weighted imaging has shown to be an alternative to PET/CT for the detection and characterization of mediastinal lymph nodes. The reported sensitivity (77–80%), specificity (84–97%), and accuracy (89–95%) are

comparable to those of the PET/CT [36]. The diagnostic value of MRI can be further improved by using more modern sequences such as STIR turbo SE imaging or FASE sequences [36].

2.5 Bronchogenic and Aerogenic Spread

Adenocarcinomas of the lung sometimes present as rather diffuse consolidations and/or ground glass with positive air bronchogram, which closely resemble the radiological appearance of pneumonias and hence are called “pneumonic-type” lung cancers [13]. On histology, pneumonic-type lung cancers are most frequently invasive mucinous adenocarcinomas and less commonly non-mucinous or mixed [13]. As pneumonic-type adenocarcinomas may spread via airways, they may present with tree-in-bud patterns and centrilobular nodules (Fig. 2.11).

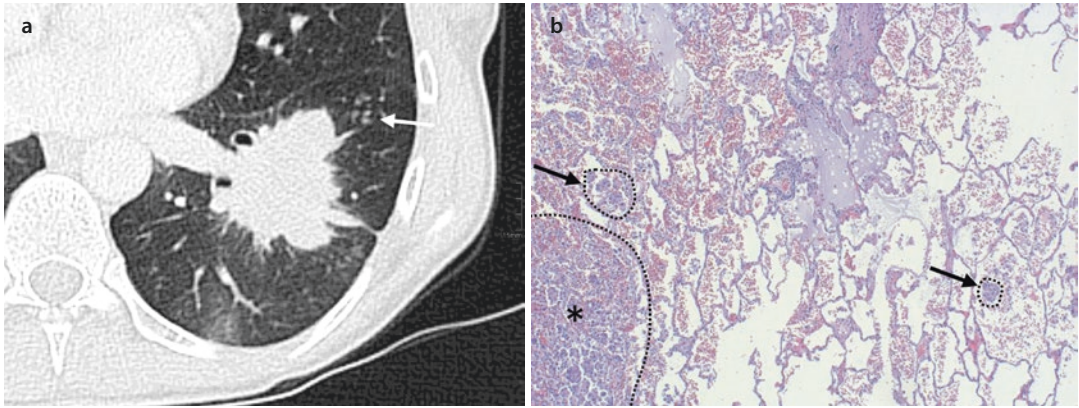


Fig. 2.11 a A 53-year-old female patient with adenocarcinoma of the lung. Axial CT image showed tiny pulmonary nodules surrounding the primary tumor

(arrow) which were histologically confirmed as b airway metastasis (arrow). The primary tumor is marked with an asterisk

A particular type of tumor spread is observed in adenocarcinomas of the lung. This type of tumor spreading is characterized by a spread of “micropapillary clusters, solid nests, or single cells beyond the edge of the tumor” and termed spread through air spaces (STAS) [37]. This particular type of tumor spread has been reported to be associated with a worse recurrence-free survival and overall survival [38–42].

A potential association of STAS with CT features has been only recently investigated. Three studies showed that nodule density correlates the most with the invasion of air by the tumor, demonstrating that the solid component is a risk factor for STAS or, otherwise, that the presence of abundant non-solid component is a good prognostic factor for progression-free survival [43, 44]. Authors have also observed that STAS-positive cancers tend to be larger [43, 44] confirming that the overall nodule size remains a critical feature for tumor prognostication [45]. Nonetheless, any increase in the extent of solid component is associated with higher likelihood of invasiveness [46–49], regardless of the STAS status. Toyokawa et al. reported that STAS-positive lesions exhibit spiculation, pleural indentation, vascular convergence, and nodular notch sign more frequently than STAS-negative cancers [44].

Although these studies showed that there is the opportunity for specific risk stratification of small adenocarcinoma, the direct visualization of STAS is not feasible by CT because this imaging

technique is stuck with several intrinsic limits for this purpose. Indeed, STAS is a microscopic phenomenon, whose direct signs are far beyond the spatial resolution of state-of-the-art CT scanner. Furthermore, there is no evidence of densitometric differentiation between confined clusters of neoplastic cells from STAS and normal cells or microscopic mucus plugging. Contrast enhancement is not expected to make a difference because no microscopic vascularization is described on pathology. In view of these considerations, the refinement of CT diagnostic criteria of STAS is fostered, and validation of its contribution is mandatory before any clinical applicability. Also positron emission tomography is limited for this purpose; to date, there is no data about magnetic resonance approach.

The application of computer-aided diagnosis (CAD) approach is gaining interest among radiologists for standardization of lung cancer characterization [50–52]. Quantitative analyses, including radiomics, have shown a potential in analyzing imaging data beyond the human perception. This perspective is indeed quite sound for investigation of features beyond the conventional method of visual imaging reading. Recently, radiomic approaches to presurgical lung nodule characterization have shown encouraging results toward stratification of malignancy [53]. Should this approach allow accurate rating of STAS is still to be defined and will likely take part within the broad scientific debate of radiomic potential, in the next future.

References

- Brierley J, Gospodarowicz M, Wittekind C. *TNM classification of malignant tumours*. Wiley-Blackwell; 2017.
- Postmus P, Kerr K, Oudkerk M, Senan S, Waller D, Vansteenkiste J, et al. Early and locally advanced non-small-cell lung cancer (NSCLC): ESMO Clinical Practice Guidelines for diagnosis, treatment and follow-up. *Ann Oncol*. 2017;28(suppl_4):iv1-iv21.
- Fischer B, Lassen U, Mortensen J, Larsen S, Loft A, Bertelsen A, et al. Preoperative staging of lung cancer with combined PET-CT. *N Engl J Med*. 2009;361(1):32-9.
- Caroli G, Dell'Amore A, Cassanelli N, Dolci G, Pipitone E, Asadi N, et al. Accuracy of transthoracic ultrasound for the prediction of chest wall infiltration by lung cancer and of lung infiltration by chest wall tumours. *Heart Lung Circ*. 2015;24(10):1020-6.
- Hafez MR, Sobh ES, Elsayy SB, Abo-Elkheir OI. The usefulness of thoracic ultrasonography in diagnosis and staging of bronchogenic carcinoma. *Ultrasound*. 2017;25(4):200-12.
- Cao B-S, Wu J-H, Li X-L, Deng J, Liao G-Q. Sonographically guided transthoracic biopsy of peripheral lung and mediastinal lesions: role of contrast-enhanced sonography. *J Ultrasound Med*. 2011;30(11):1479-90.
- Hanahan D, Weinberg RA. Hallmarks of cancer: the next generation. *Cell*. 2011;144(5):646-74.
- Talmadge JE, Fidler IJ. AACR centennial series: the biology of cancer metastasis: historical perspective. *Cancer Res*. 2010;70(14):5649-69.
- Mittal V. Epithelial mesenchymal transition in tumor metastasis. *Annu Rev Pathol*. 2018;13:395-412.
- Wang ZJ, Ohliger MA, Larson PE, Gordon JW, Bok RA, Slater J, et al. Hyperpolarized ¹³C MRI: State of the Art and Future Directions. *Radiology*. 2019:182391.
- Travis WD, Asamura H, Bankier AA, Beasley MB, Dettnerbeck F, Flieder DB, et al. The IASLC lung cancer staging project: proposals for coding T categories for subsolid nodules and assessment of tumor size in part-solid tumors in the forthcoming eighth edition of the TNM classification of lung cancer. *J Thorac Oncol*. 2016;11(8):1204-23.
- Detterbeck FC, Boffa DJ, Kim AW, Tanoue LT. The eighth edition lung cancer stage classification. *Chest*. 2017;151(1):193-203.
- Detterbeck FC, Marom EM, Arenberg DA, Franklin WA, Nicholson AG, Travis WD, et al. The IASLC Lung Cancer Staging Project: background data and proposals for the application of TNM staging rules to lung cancer presenting as multiple nodules with ground glass or lepidic features or a pneumonic type of involvement in the forthcoming eighth edition of the TNM classification. *J Thorac Oncol*. 2016;11(5):666-80.
- Wislez M, Massiani M-A, Milleron B, Souidi A, Carette M-F, Antoine M, et al. Clinical characteristics of pneumonic-type adenocarcinoma of the lung. *Chest*. 2003;123(6):1868-77.
- Ahmad U, Wang Z, Bryant AS, Kim AW, Kukreja J, Mason DP, et al. Outcomes for lung transplantation for lung cancer in the United Network for Organ Sharing Registry. *Ann Thorac Surg*. 2012;94(3):935-41.
- Kachala SS, Murthy SC. Lung transplantation for multifocal lung adenocarcinoma (multifocal lung carcinoma). *Thorac Surg Clin*. 2014;24(4):485-91.
- Foroulis CN, Zarogoulidis P, Darwiche K, Katsikogiannis N, Machairiotis N, Karapantzou I, et al. Superior sulcus (Pancoast) tumors: current evidence on diagnosis and radical treatment. *J Thorac Dis*. 2013;5(Suppl 4):S342-58.
- Antonoff MB, Hofstetter WL, Correa AM, Bell JM, Sepesi B, Rice DC, et al. Clinical prediction of pathologic complete response in superior sulcus non-small cell lung cancer. *Ann Thorac Surg*. 2016;101(1):211-7.
- Vos CG, Dachele M, van Sornsens de Koste JR, Senan S, Bahce I, Paul MA, et al. Semiautomated volumetric response evaluation as an imaging biomarker in superior sulcus tumors. *Strahlentherapie und Onkologie: Organ der Deutschen Rontgengesellschaft [et al]*. 2014;190(2):204-9.
- Seo JS, Kim YJ, Choi BW, Choe KO. Usefulness of magnetic resonance imaging for evaluation of cardiovascular invasion: evaluation of sliding motion between thoracic mass and adjacent structures on cine MR images. *J Magn Reson Imaging*. 2005;22(2):234-41.
- Quint LE. Lung cancer: assessing resectability. *Cancer Imaging*. 2004;4(1):15.
- Chang S, Hong SR, Kim YJ, Hong YJ, Hur J, Choi BW, et al. Usefulness of thin-section single-shot turbo spin echo with half-fourier acquisition in evaluation of local invasion of lung cancer. *J Magn Reson Imaging*. 2015;41(3):747-54.
- Lee CH, Goo JM, Kim YT, Lee HJ, Park CM, Park E-A, et al. The clinical feasibility of using non-breath-hold real-time MR-echo imaging for the evaluation of mediastinal and chest wall tumor invasion. *Korean J Radiol*. 2010;11(1):37-45.
- Kajiwaru N, Akata S, Uchida O, Usuda J, Ohira T, Kawate N, et al. Cine MRI enables better therapeutic planning than CT in cases of possible lung cancer chest wall invasion. *Lung Cancer*. 2010;69(2):203-8.
- Klein CA. Parallel progression of primary tumours and metastases. *Nat Rev Cancer*. 2009;9(4):302-12.
- Niemeijer A, Leung D, Huisman M, Bahce I, Hoekstra O, van Dongen G, et al. Whole body PD-1 and PD-L1 positron emission tomography in patients with non-small-cell lung cancer. *Nat Commun*. 2018;9(1):4664.
- Rami-Porta R, Bolejack V. Reply to "inclusion of lymphangitis as a descriptor in the new TNM staging of lung cancer: filling up the blank spaces". *J Thorac Oncol*. 2015;10(12):e119-20.
- Gkiozos I, Kopitopoulou A, Kalkanis A, Vamvakaris IN, Judson MA, Syrigos KN. Sarcoidosis-like reactions induced by checkpoint inhibitors. *J Thorac Oncol*. 2018;13(8):1076-82.
- Beer L, Hochmair M, Prosch H. Pitfalls in the radiological response assessment of immunotherapy. *Memo*. 2018;11(2):138-43.
- Truong MT, Viswanathan C, Erasmus JJ. Positron emission tomography/computed tomography in lung

- cancer staging, prognosis, and assessment of therapeutic response. *J Thorac Imaging*. 2011;26(2):132–46.
31. Silvestri GA, Gonzalez AV, Jantz MA, Margolis ML, Gould MK, Tanoue LT, et al. Methods for staging non-small cell lung cancer: diagnosis and management of lung cancer: American College of Chest Physicians evidence-based clinical practice guidelines. *Chest*. 2013;143(5):e2115–e50S.
 32. Alongi F, Ragusa P, Montemaggi P, Bona CM. Combining independent studies of diagnostic fluorodeoxyglucose positron-emission tomography and computed tomography in mediastinal lymph node staging for non-small cell lung cancer. *Tumori*. 2006;92(4):327–33.
 33. Schmidt-Hansen M, Baldwin DR, Hasler E, Zamora J, Abraira V, Roque IFM. PET-CT for assessing mediastinal lymph node involvement in patients with suspected resectable non-small cell lung cancer. *Cochrane Database Syst Rev*. 2014;(11):Cd009519.
 34. Novello S, Barlesi F, Califano R, Cufer T, Ekman S, Levra MG, et al. Metastatic non-small-cell lung cancer: ESMO Clinical Practice Guidelines for diagnosis, treatment and follow-up. *Ann Oncol*. 2016;27(suppl_5):v1–v27.
 35. Reck M, Rabe KF. Precision diagnosis and treatment for advanced non-small-cell lung cancer. *N Engl J Med*. 2017;377(9):849–61.
 36. Ohno Y, Koyama H, Lee HY, Yoshikawa T, Sugimura K. Magnetic Resonance Imaging (MRI) and Positron Emission Tomography (PET)/MRI for lung cancer staging. *J Thorac Imaging*. 2016;31(4):215–27.
 37. Travis WD, Brambilla E, Nicholson AG, Yatabe Y, Austin JH, Beasley MB, et al. The 2015 World Health Organization classification of lung tumors: impact of genetic, clinical and radiologic advances since the 2004 classification. *J Thorac Oncol*. 2015;10(9):1243–60.
 38. Chen D, Mao Y, Wen J, She Y, Zhu E, Zhu F, et al. Tumor spread through air spaces in non-small cell lung cancer: a systematic review and meta-analysis. *Ann Thorac Surg*. 2019;108:945.
 39. Kadota K, Nitadori J-i, Sima CS, Ujiie H, Rizk NP, Jones DR, et al. Tumor spread through air spaces is an important pattern of invasion and impacts the frequency and location of recurrences after limited resection for small stage I lung adenocarcinomas. *J Thorac Oncol*. 2015;10(5):806–14.
 40. Shiono S, Yanagawa N. Spread through air spaces is a predictive factor of recurrence and a prognostic factor in stage I lung adenocarcinoma. *Interact Cardiovasc Thorac Surg*. 2016;23(4):567–72.
 41. Uruga H, Fujii T, Fujimori S, Kohno T, Kishi K. Semiquantitative assessment of tumor spread through air spaces (STAS) in early-stage lung adenocarcinomas. *J Thorac Oncol*. 2017;12(7):1046–51.
 42. Dai C, Xie H, Su H, She Y, Zhu E, Fan Z, et al. Tumor spread through air spaces affects the recurrence and overall survival in patients with lung adenocarcinoma > 2 to 3 cm. *J Thorac Oncol*. 2017;12(7):1052–60.
 43. de Margerie-Mellon C, Onken A, Heidinger BH, VanderLaan PA, Bankier AA. CT manifestations of tumor spread through airspaces in pulmonary adenocarcinomas presenting as subsolid nodules. *J Thorac Imaging*. 2018;33(6):402–8.
 44. Toyokawa G, Yamada Y, Tagawa T, Kamitani T, Yamasaki Y, Shimokawa M, et al. Computed tomography features of resected lung adenocarcinomas with spread through air spaces. *J Thorac Cardiovasc Surg*. 2018;156(4):1670–6. e4.
 45. Larici AR, Farchione A, Franchi P, Ciliberto M, Cicchetti G, Calandriello L, et al. Lung nodules: size still matters. *Eur Respir Rev*. 2017;26(146):170025.
 46. Naidich DP, Bankier AA, MacMahon H, Schaefer-Prokop CM, Pistolesi M, Goo JM, et al. Recommendations for the management of subsolid pulmonary nodules detected at CT: a statement from the Fleischner Society. *Radiology*. 2013;266(1):304–17.
 47. Kamiya S, Iwano S, Umakoshi H, Ito R, Shimamoto H, Nakamura S, et al. Computer-aided volumetry of part-solid lung cancers by using CT: solid component size predicts prognosis. *Radiology*. 2018;287(3):1030–40.
 48. Aokage K, Miyoshi T, Ishii G, Kusumoto M, Nomura S, Katsumata S, et al. Clinical and pathological staging validation in the eighth edition of the TNM classification for lung cancer: correlation between solid size on thin-section computed tomography and invasive size in pathological findings in the new T classification. *J Thorac Oncol*. 2017;12(9):1403–12.
 49. Yanagawa M, Kusumoto M, Johkoh T, Noguchi M, Minami Y, Sakai F, et al. Radiologic–pathologic correlation of solid portions on thin-section CT images in lung adenocarcinoma: a Multicenter Study. *Clin Lung Cancer*. 2018;19(3):e303–e12.
 50. Silva M, Milanese G, Seletti V, Ariani A, Sverzellati N. Pulmonary quantitative CT imaging in focal and diffuse disease: current research and clinical applications. *Br J Radiol*. 2018;91(xxxx):20170644.
 51. Silva M, Schaefer-Prokop CM, Jacobs C, Capretti G, Ciompi F, van Ginneken B, et al. Detection of subsolid nodules in lung cancer screening: complementary sensitivity of visual reading and computer-aided diagnosis. *Investig Radiol*. 2018;53(8):441–9.
 52. Huang W, Xue Y, Wu Y. A CAD system for pulmonary nodule prediction based on deep three-dimensional convolutional neural networks and ensemble learning. *PLoS One*. 2019;14(7):e0219369.
 53. Huang P, Park S, Yan R, Lee J, Chu LC, Lin CT, et al. Added value of computer-aided CT image features for early lung cancer diagnosis with small pulmonary nodules: a matched case-control study. *Radiology*. 2017;286(1):286–95.



Non-Small Cell Lung Cancer: Common Types

Cristiano Rampinelli, Antonio Passaro, Monica Casiraghi, and Cristiana Fanciullo

- 3.1 Overview – 48**
 - 3.1.1 Epidemiology – 48
 - 3.1.2 Risk Factors – 48
 - 3.1.3 Pathology – 48
 - 3.1.4 Staging – 48
 - 3.1.5 Treatment – 48
 - 3.1.6 Prognosis – 50

- 3.2 Patterns of Local Spread – 50**
 - 3.2.1 Heart and Vessel Infiltration – 50
 - 3.2.2 Involvement of Adjacent Structures – 52

- 3.3 Lymph Node Involvement – 54**
 - 3.3.1 Lymphatic Drainage and Lymph Node Involvement – 54
 - 3.3.2 Assessment of Lymph Node Status – 56

- 3.4 Metastatic Spread – 56**
 - References – 58**

3.1 Overview

Squamous cell carcinoma (SCC) and adenocarcinoma (ADC) are the most common types of lung cancer. Even though these common types are different from a histological point of view, they have many aspects in common, with particular regard to risk factors, patterns of local and distant spread, staging, and treatment.

3.1.1 Epidemiology

Lung cancer is the most common cause of tumor-related death in the USA and Europe [1, 2]. In 2019, a total of 228,150 new cases (116,440 in men and 111,710 in women) of lung cancer are estimated to be diagnosed in the USA [1].

The most common histological types of NSCLC are squamous cell carcinoma (25–30%) and non-squamous or adenocarcinoma (70–75%).

3.1.2 Risk Factors

The major risk factor for lung cancer is still smoking cigarettes [3], related inter alia with the development of squamous cell carcinoma more than lung adenocarcinoma. The exposure to certain substances such as radon gas and asbestos has been also associated with a higher risk of developing SCC and ADC [4].

3.1.3 Pathology

Squamous cell carcinoma is defined as a malignant epithelial tumor or an undifferentiated NSCLC with positivity for squamous cell carcinoma markers by immunohistochemistry (IHC).

Adenocarcinoma is characterized by either TTF-1 expression (90–95%) or several DNA/RNA alterations that are of prognostic value, such as epidermal growth factor receptor (EGFR) mutations (10–15%), anaplastic lymphoma kinase (ALK) gene rearrangements (6–8%), ROS1 rearrangements (2%), BRAF mutations (2%), and programmed death (PD-1) receptor expression levels by IHC. Other genetic alterations, such as NTRK gene fusions, RET rearrangements, MET

genetic alterations, and ERBB2 (HER2) mutations, have been reported in 1–2% of cases and may identify oncogenic driver alterations for which effective therapy may be available [5].

3.1.4 Staging

The eighth TNM classification scheme applies for both squamous cell carcinoma and adenocarcinoma, as summarized in Table 3.1 [6].

Computed tomography (CT) is the principal examination in patients with suspected lung cancer, as it is sufficient in most patients to detect distant metastases and an extensive infiltration of neighboring structures. However, in patients who are eligible for curative surgery, current guidelines require the acquisition of a ^{18}F -labeled fluoro-2-deoxyglucose (FDG) positron-emission tomography (PET)/CT and a brain magnetic resonance imaging (MRI) (or contrast-enhanced brain CT) to exclude metastasis [7, 8]. PET/CT is requested because it has been shown that PET/CT may detect distant metastases in up to 20% of patients who would otherwise have been surgical candidates.

In addition, MRI is frequently performed in patients with suspected mediastinal or chest wall infiltration, as its excellent soft tissue contrast allows for a better delineation of the extent of infiltration than CT. MRI is also the method with which to further characterize suspected bone metastases detected on other imaging modalities [9].

Ultrasound has been proven to be an excellent tool for the investigation of chest wall infiltration [10]. Furthermore, ultrasound-guided biopsies of the supraclavicular lymph nodes are a reliable and safe procedure to confirm an inoperable tumor stage. Last but not least, ultrasound and ultrasound-guided biopsies are often used to further investigate equivocal findings from CT or PET/CT [11].

3.1.5 Treatment

3.1.5.1 Surgery

Surgery is the primary therapeutic option for limited disease in both SSC and ADC [12]. The choice of the surgical procedure mostly depends on the

Table 3.1 Eighth edition of the TNM classification for lung cancer

<i>T (primary tumor)</i>	
T0	No primary tumor
Tis	Carcinoma in situ (squamous or adenocarcinoma)
T1	Tumor ≤ 3 cm
T1mi	Minimally invasive adenocarcinoma
T1a	Tumor ≤ 1 cm
T1b	Tumor > 1 but ≤ 2 cm
T1c	Tumor > 2 but ≤ 3 cm
T2	Tumor > 3 but ≤ 5 cm or tumor involving the main bronchus without involving carina; invading visceral pleura; associated with atelectasis or obstructive pneumonitis
T2a	Tumor > 3 but ≤ 4 cm
T2b	Tumor > 4 but ≤ 5 cm
T3	Tumor > 5 but ≤ 7 cm or invading chest wall, pericardium, and phrenic nerve, or separate tumor nodule(s) in the same lobe
T4	Tumor > 7 cm or tumor invading mediastinum, diaphragm, heart, great vessels, recurrent laryngeal nerve, carina, trachea, esophagus, and spine, or tumor nodule(s) in a different ipsilateral lobe
<i>N (regional lymph nodes)</i>	
N0	No regional node metastasis
N1	Metastasis in ipsilateral pulmonary or hilar nodes
N2	Metastasis in ipsilateral mediastinal or subcarinal nodes
N3	Metastasis in contralateral mediastinal, hilar, or supraclavicular nodes
<i>M (distant metastasis)</i>	
M0	No distant metastasis
M1a	Malignant pleural or pericardial effusion or pleural or pericardial nodules or separate tumor nodule(s) in a contralateral lobe
M1b	Single extrathoracic metastasis
M1c	Multiple extrathoracic metastases (1 or > 1 organ)

tumor characteristics (e.g., location, staging) and patient's clinical conditions. There are several surgical procedures, such as wedge resection, segmental resection, lobectomy, or pneumonectomy [12]. Advanced surgical techniques such as minimally invasive surgery and video-assisted thoracoscopic surgery (VATS) may reduce the length of hospitalization and surgical complications.

3.1.5.2 Radiation Therapy

Radiation therapy (RT) may be either radical or palliative and combined with chemotherapy. Definitive RT is considered for early-stage lung cancer with contraindications to surgery or for locally advanced lung cancer. It may be used in both preoperative and postoperative stages or in patients undergoing surgery. Furthermore, it can be used in the treatment of recurrence disease and metastases [12]. There are different RT techniques including intensity-modulated radiation therapy, volumetric modulated arc therapy, image-guided radiation therapy, and proton therapy [13–15].

3.1.5.3 Chemotherapy

Platinum-based chemotherapy is still the standard treatment for both adjuvant and neoadjuvant treatments, regardless of the tumor histology (e.g., for both SSC and ADC) [16]. In advanced or metastatic disease, chemotherapy is the standard of care in patients non-suitable for treatment with targeted therapy or immunotherapy. Cisplatin/carboplatin, docetaxel/paclitaxel, etoposide, gemcitabine, vinorelbine, and pemetrexed (only for non-squamous) still represent the most used chemotherapy drugs [16].

3.1.5.4 Targeted Therapy

The identification of specific molecular biomarkers [17] may allow the use of several anticancer target drugs. These were shown to improve survival in patients with either advanced or recurrent disease [7]. The following agents are approved for the treatment of advanced SSC and ADC [18–23]:

- Bevacizumab and ramucirumab, which are recombinant monoclonal antibodies that target vascular endothelial growth factor (VEGF) or VEGF receptor, respectively.
- Afatinib, dacomitinib, erlotinib, gefitinib, and osimertinib, which are EGFR tyrosine kinase inhibitors approved for patients with EGFR mutations.

- Alectinib, brigatinib, ceritinib, crizotinib, and lorlatinib approved for the treatment of patients with ALK translocations.
- Crizotinib and lorlatinib are approved also for the treatment of ROS1 rearrangement-positive patients.
- Dabrafenib and trametinib are approved for patients with BRAF V600E mutation-positive tumors.

3.1.5.5 Immunotherapy

Immunotherapy has revolutionized the treatment of both SCC and ADC, prolonging the survival in patients with locally advanced or metastatic disease. Surface antigens expressed on tumor cells can be therapeutic targets. Immunotherapy enhances antitumor immune responses by targeting immune cells [24]. In recent years, antibodies against immune checkpoint inhibitors (e.g., nivolumab, pembrolizumab, atezolizumab) have demonstrated their efficacy, in both first line and later lines of therapy [25, 26].

3.1.6 Prognosis

Several factors, notably tumor- and patient-related factors, affect the prognosis of subjects with either SCC or ADC. Only 18% of the subjects with non-small cell lung cancer live 5 years or more after the diagnosis, and the overall 5-year survival rate is 2% for stage IV NSCLC, regardless of histology [27]. The median survival is 8 months [26].

Early-stage disease at diagnosis, good performance status (PS) (ECOG 0, 1), no significant weight loss (<5%), and female gender are considered favorable prognostic factors [28, 29]. Specific mutations, such as KRAS, are also considered reliable biomarkers to predict patient's prognosis [30].

Indeed, the identification of predictive biomarkers of response, particularly detected in adenocarcinoma histology (e.g., EGFR, ALK, ROS1, and BRAF), led to a significant improvement of overall survival, with a median of 30–40 months for patients harboring alterations suitable for target agents. A similar survival achievement can be attained for those patients with high PDL1 receiving immunotherapy [26].

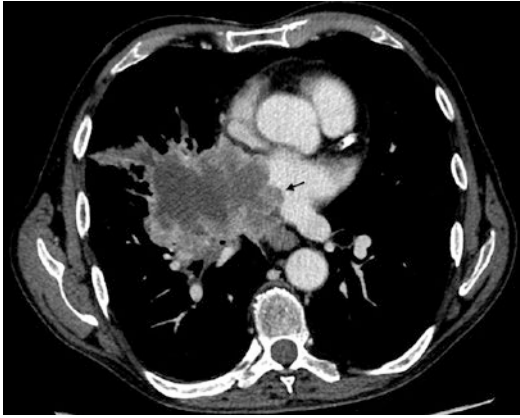
3.2 Patterns of Local Spread

Both SCC and ADC may be highly lethal neoplasms, particularly when diagnosed in advanced stage. Indeed, more than 50% of NSCLC patients present with metastatic disease or unresectable tumors [31]. The neoplasms of the lung usually grow infiltrating tissues or contiguous organs and structures. Locally advanced lung cancer infiltrating adjacent structures such as great vessels, the heart, trachea, esophagus, diaphragm, or vertebral body is classified as T4 according to the eighth TNM edition, whereas the invasion of the chest wall or pericardium is classified as T3 [32]. Even though T4 lung tumors were historically considered unresectable and usually candidates for definitive chemotherapy and/or radiotherapy [33, 34], the advances in surgical techniques and the improvement of anesthesiological skills have challenged this dogma and allowed surgeons to perform extended resection going far beyond the standard surgery for lung cancer. With regard to the oncologic aspects, induction chemotherapy is indicated in the case of T4 NSCLC with the aim to downstage the tumor, increase resectability, and reduce the extension of the resection aside from only improving long-term survival by controlling potential systemic micrometastasis. Although long-term survival could be up to 44% in the case of selected T4 NSCLC with N0–N1 disease, post-operative morbidity (31–53%) and mortality (0.1–19%) are still high, even in highly selected patients [32].

3.2.1 Heart and Vessel Infiltration

3.2.1.1 Left Atrium Invasion

The left atrium may be infiltrated directly by the primary tumor or by tumor emboli protruding from the pulmonary veins. Infiltration of the left atrium can be demonstrated with CT or MRI (■ Fig. 3.1). Patients presenting with SCC and ADC infiltrating the left atrium are normally considered for medical treatments, even if a selected patient's left atrium resection can be achieved by clamping the left atrium and removing the tumor along with the pulmonary veins. In the case of major infiltration of the left atrium, resection on a cardiopulmonary bypass (CPB) after aortic cross-clamping and cardioplegia is mandatory to reduce



■ **Fig. 3.1** CT scan shows a mass of the right lung (squamous cell carcinoma) with extensive infiltration of the left atrium (black arrow)

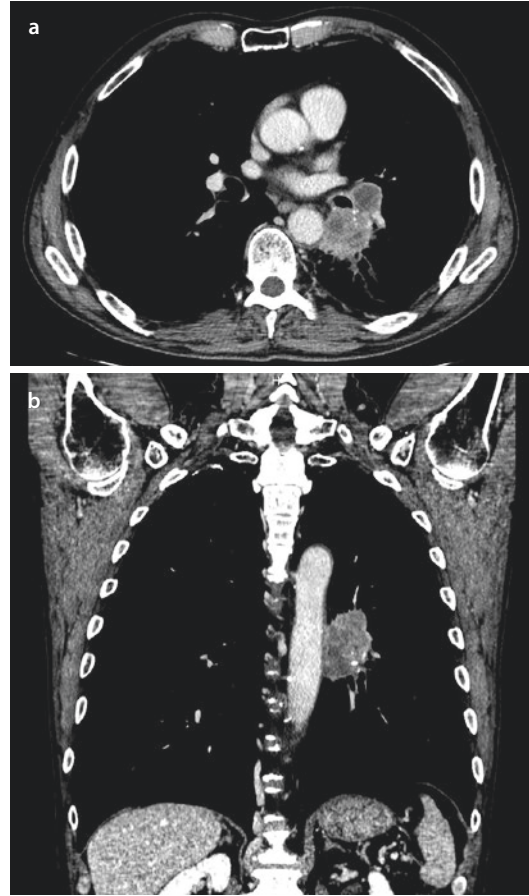
the risk of clamp dislocation and to allow more extended resections with atrium reconstruction by patch; conversely, it increases the risk of bleeding, acute lung injury, and infections [35–38].

Several reports regarding the postoperative outcome of patients with primary lung cancer involving the left atrium concluded that left atrial resection was beneficial for selected patients [36–43]. An overall 5-year survival rate for NSCLC cases invading the atrium usually ranged between 10% and 46% [36–43], but it increased up to 67% in subjects with pathological N0–N1 [44].

3.2.1.2 Thoracic Aorta Invasion

Both SCC and ADC infiltrating the thoracic aorta are considered T4 tumors. Treatment may include some combination of radiation therapy, chemotherapy, and/or surgery. CT and MRI findings suggesting aortic infiltration are as follows: contact between the tumor and aorta extending for more than 3 cm, obliteration of the fat plane between the tumor and aortic wall (■ Fig. 3.2), or contact by the tumor of more than 90° of the aortic circumference [39]. Aortic invasion was seen more frequently reported on the descending tract, and only a small number of subjects needed an aortic arch resection. When indicated, pneumonectomy was often performed in those patients [45–48]. Aortic invasion by NSCLC is usually limited to the adventitia, while the media of the aorta is seldom involved.

The 5-year survival rate after resection ranged from 30% to 60%, but incomplete resection, mediastinal lymph node metastasis, and no



■ **Fig. 3.2** Axial **a** and coronal **b** CT scans show a NSCLC (adenocarcinoma) of left lower lobe with a remarkable contact between the tumor and aortic wall. Invasion of the aorta was confirmed by surgery

perioperative chemotherapy or radiotherapy seem poor prognostic factors [45–48].

3.2.1.3 Superior Vena Cava Invasion

Invasion of the superior vena cava usually arises from SCC and ADC of the right upper lobe (■ Fig. 3.3). According to the eighth TNM edition of lung cancer staging, superior vena cava invasion is classified as T4 and generally is referred for medical treatments.

A precise assessment of the superior vena cava invasion is recommended as it may have important implications on the surgical approach for selected cases. When superior vena cava involvement was less than 50% of the venous circumference, the resection of the tumor and direct repair of the defect using mechanical or hand suture was the preferred technique. In case of larger vascular

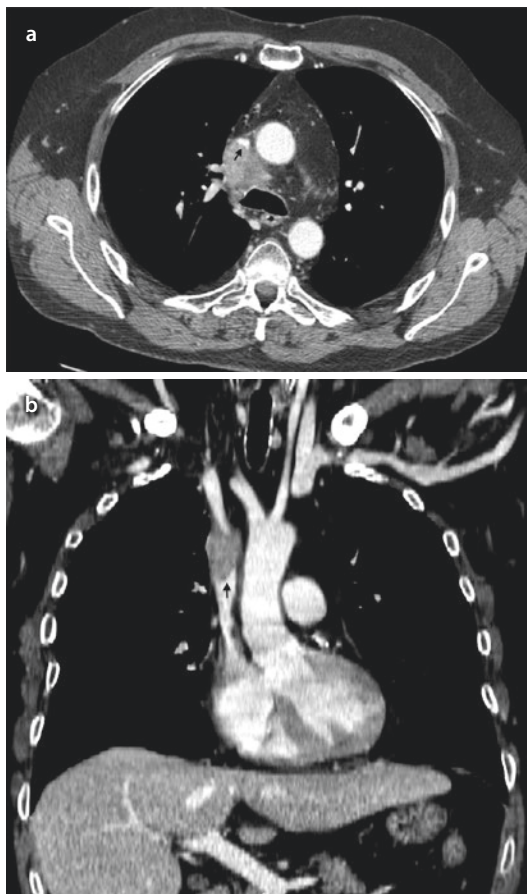


Fig. 3.3 Axial **a** and coronal **b** CT images show a tumor with mediastinal involvement and infiltration of the superior vena cava (black arrow)

resection, an autologous or heterologous pericardial patch is used [49]. When venous infiltration was more than 50% of the circumference, prosthetic vascular replacement by the cross-clamping technique was preferred [49]. Although the operative mortality was about 0–20%, the overall survival was relatively good, especially in patients with N0–N1 and complete resection (R0) [49–53].

3.2.2 Involvement of Adjacent Structures

3.2.2.1 Carina Invasion

When the tumor invades the origin of the main bronchus, the carina, or the distal trachea, a carinal pneumonectomy is required.

CT and MRI are useful in detecting tumors that invade the carina. Multiplanar reconstruc-



Fig. 3.4 Lung adenocarcinoma of the upper right lobe with chest wall invasion (white arrow)

tion imaging and thin slice thickness are essential for the assessment of carina involvement. Suspicious findings are lesions abutting the carina or thickening of the carina wall.

Bronchoscopy is the most important preoperative tool to identify the lesion and to plan the surgical resection. In cases of histologically proven N2 disease, the patients should be candidates for induction chemotherapy and then restaged with total body CT and PET scans to schedule the responders or the patients with stable disease for surgery. However, operative mortality has been reportedly increased from 6.7% to 13% after induction therapy in patients undergoing right carinal pneumonectomy [32, 54–56].

Carinal resection is defined as the resection of the trachea-bronchial bifurcation with lung resection. The 5-year overall survival after carinal resection ranges from 26% to 44% in different series with an improved survival rate of up to 50% in pN0 patients [57, 58], showing the importance of accurate selection of the patient. Another important positive prognostic factor is the completeness of the resection [59].

3.2.2.2 Chest Wall Invasion

The prevalence of chest wall invasion by ADC and SCC is less than 10% [60]. These tumors are given a T3 or T4 designation in the eighth edition TNM staging depending on chest wall or vertebral body invasion.

The most reliable predictor of chest wall invasion is the chest pain, as well as clear evidence of chest wall soft tissue or bone invasion by CT or MRI scans (Fig. 3.4).

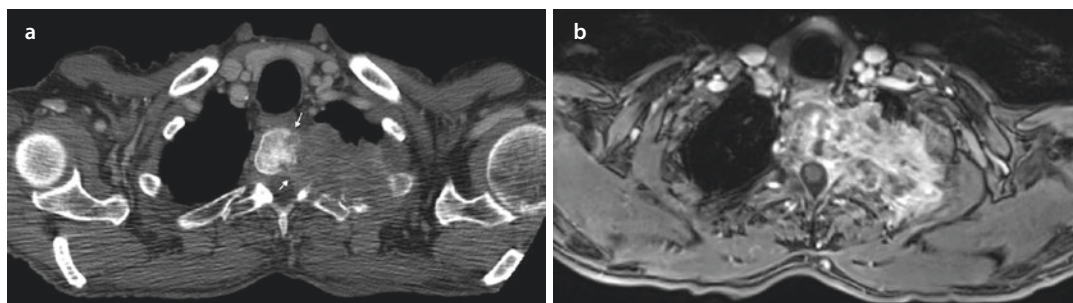


Fig. 3.5 Pancoast tumor of the left upper lobe (squamous cell carcinoma). CT scan **a** shows extensive chest wall and vertebral invasion (white arrows), confirmed by contrast-enhanced MRI **b**

Radiological signs of chest wall invasion are the presence of extrapleural tumor tissue, rib involvement, or vertebral body infiltration.

MRI is at least equal if not superior in the evaluation of chest wall infiltration, with a sensitivity up to 90% and an accuracy of 88% [61]. In particular, MRI is the modality of choice for the evaluation of Pancoast tumors (superior sulcus tumors), with a better assessment of extrapleural fat infiltration, involvement of blood vessels, and brachial plexus.

Chest wall invasion is potentially amenable to radical resection in cases of the absence of distant metastases or contralateral nodal involvement [32]. In these cases, the goal of surgery is the radical resection and reconstruction of the chest wall when necessary. After complete resection, the ideal management of complex chest wall defects is rib cage reconstruction and soft tissue coverage. Long-term survival of those patients has been associated with complete (R0) resection and node-negative disease. Facciolo et al. reported a 5-year overall survival of 18% for T3N2 disease compared with 67% for T3N0 in patients treated with en bloc resection of lung tumors with chest wall invasion [62]. In a series of 201 patients published by Magdeleinat, the 5-year survival of T3N2 patients treated with chest wall en bloc resection was 21%, and there was no survival difference between patients with N1 or N2 disease [63].

3.2.2.3 Vertebral Invasion

Vertebral invasion (T4) can be detected by CT scan and PET/CT scan, though a better assessment of bone involvement can be demonstrated by MRI (■ Fig. 3.5).

SCC and ADC infiltrating the vertebral bodies have usually been considered a contrain-

dication for surgery because of the low likelihood of complete resection (negative margin) and the association with high postoperative morbidity and mortality. However, thanks to innovative approaches and technical developments in performing en bloc partial or total vertebrectomy and spinal reconstruction, 5-year survival rates have been reported in several series ranging between 31% and 61% [64–66], showing encouraging results. Even so, surgical excision alone could be never considered an adequate approach for lung cancer with vertebral involvement and must always be combined with chemoradiotherapy in a multimodality scenario.

3.2.2.4 Diaphragm Invasion

Primary lung cancers infiltrating the diaphragm are less than 0.5% of the patients with locally advanced lung cancer [67]. Invasion of the diaphragm gives a T4 designation in the eighth edition of TNM staging, whereas it was T3 in the seventh TNM edition.

Contrast-enhanced MDCT, with thin slice thickness and fast scan time, is usually able to assess diaphragm invasion even if MRI can better depict its involvement due to the combination of excellent soft tissue contrast with multiplanar information.

In a recent study published in 2014, patients who underwent en bloc lung and diaphragm resection for NSCLC had a mortality rate of 5% and an overall morbidity of 63%; patients with only superficial infiltration of the diaphragm had the best long-term prognoses ($p = 0.04$) [67]. Diaphragm resection is technically feasible and could be a valid therapeutic option with acceptable morbidity and mortality and long-term

survival rate in highly selected patients suffering from NSCLC, when a complete resection is obtained [64, 67].

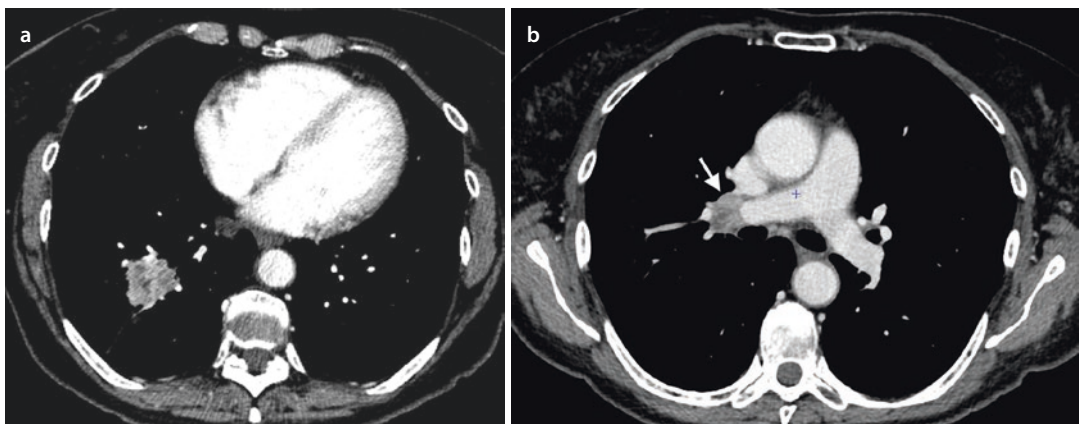
3.3 Lymph Node Involvement

3.3.1 Lymphatic Drainage and Lymph Node Involvement

Lymphatic spread is one of the main pathways of dissemination from SCC and ADC. Tumor cells spread to locoregional lymph nodes through lymphatics of the lung which may be regarded as lymphatic collectors mainly coursing over the surface of the lung (visceral pleural network) and in the connective tissue surrounding the airways and their bronchial artery vascular supply (peribronchovascular collectors) [68]. These two main paths run toward the lung hilum where they generally anastomose with one another, causing ipsilateral hilar lymph nodes as the usual initial station involved in tumor spread from these tumors. The lymphatic collectors then ascend along the bronchial tree and the mediastinum to finally drain the lung lymph into the venous blood circulation either directly by extending upward along the bronchi and trachea and anastomosing into the internal jugulosubclavian venous confluence (cervical lymphovenous portals) [69] or indirectly via the thoracic duct after connecting with it [70]. However, some of the lymphatic collectors of the lower lobes travel downward within the pulmonary ligament, traverse the diaphragm

[71] or the hiatal orifice, and terminate in the juxta-aortic lymph nodes of the celiac region and/or continuing into the thoracic duct at its origin [72]. This might provide the anatomic explanation for celiac region lymph node metastasis from lung cancer derived from the lower lobes.

Along their spread through lymphatic collectors, cancer cells will run up against lymph nodes variably located within the lung and within the mediastinum. The exact identification of the detailed sequence of lymph node invasion and its correlation with patient survival would be of great value in clinical practice. However, the exact pattern of lymph nodal spread is difficult to outline due to the complexity of the anatomical connections between the different lymphatic routes. Within the mediastinal area, cancer cells may run through lymphatic collectors crossing from one side of the trachea to the other, thus reaching contralateral collectors either directly or mostly through lymph nodes located at the level of the carina and bronchi. Moreover, cancer cells may not encounter any lymph nodes along their course through the lymphatic collectors of the lung and may flow directly into mediastinal lymph nodes, perhaps providing the anatomic explanation for “skipped” metastases [73]. Typically, SCC and ADC spread to ipsilateral hilar nodes (■ Fig. 3.6) and then ipsilateral mediastinal, contralateral (■ Fig. 3.7), and supraclavicular nodes, where the latter is the only palpable locoregional lymph node station upon physical examination. Though nodal spread is most often sequential, skip metastases to mediastinal nodes in the absence of



■ Fig. 3.6 a Right lower lobe lung adenocarcinoma. b CT scan shows involvement of ipsilateral hilar lymph node (N1) (white arrow)

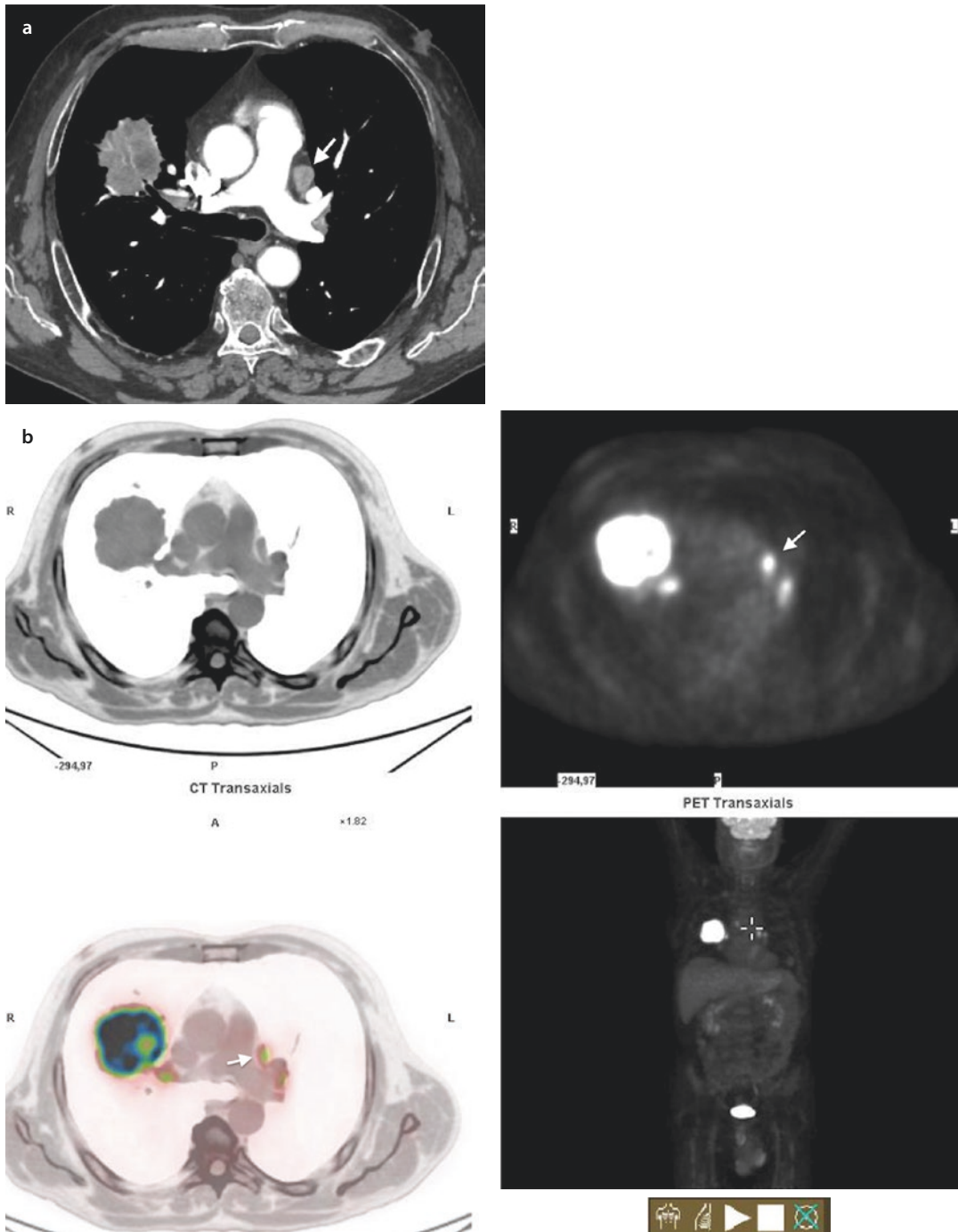


Fig. 3.7 Axial CT scan **a** and PET/CT scan **b** show a right lung adenocarcinoma with contralateral lymph node involvement (white arrows), resulting in an N3 staging

peribronchial or ipsilateral involvement is seen in 20–40% of cases [73–75].

The International Association for the Study of Lung Cancer (IASLC) lymph node map is the most widely used system to define the thoracic

lymph node anatomy. According to this description, the intrapulmonary and mediastinal lymph nodes are classified in 14 stations [76].

Tumors that spread through the lymph vessels, with diffuse interstitial infiltration, can

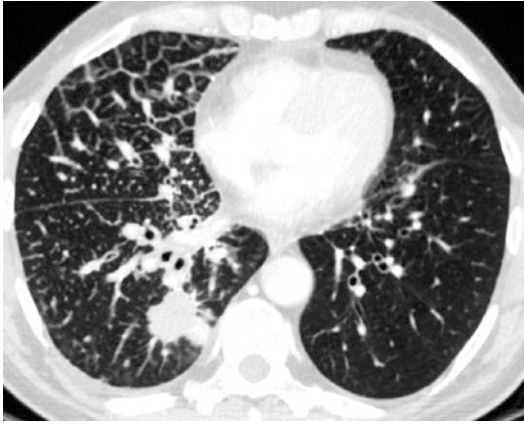


Fig. 3.8 Lymphangitic carcinomatosis. CT scan shows diffuse thickening of interlobular septa and bronchovascular bundles of the right lung in a patient with adenocarcinoma of the right lower lobe

cause a clinical-radiological entity called lymphangitic carcinomatosis. In this case, tumor cells are present within the lymphatic vessels and interstitium, where they cause edema and fibroblast reaction [77–78]. It involves the peripheral lymphatics coursing over the surface of the lung and the interlobular septa, as well as the lymphatics of the bronchovascular interstitium. The typical CT feature is nodular thickening of interlobular septa and bronchovascular bundles, with an overall preserved pulmonary architecture (Fig. 3.8).

3.3.2 Assessment of Lymph Node Status

The diagnosis of mediastinal lymph node metastases from SCC and ADC is a critical point in staging and treatment recommendations. There are no specific measurements or imaging techniques that allow an accurate distinction between benign and malignant lymph nodes.

In patients with suspected NSCLC, the size of the lymph nodes is still the main diagnostic criterion for the assessment of nodal metastases on CT. In particular, a short-axis diameter >10 mm on axial CT images is regarded suspicious for nodal involvement [79]. However, malignant involvement of lymph nodes may also occur in the absence of enlarged mediastinal lymph nodes, thus producing false-negative findings and reducing sensitivity. On the other hand,

enlarged lymph nodes in patients with lung cancer may be due to reactive hyperplasia rather than tumor metastases, thus producing false-positive findings and reducing specificity. Furthermore, lymph nodes may be enlarged from some inflammatory processes (e.g., sarcoidosis), infections (e.g., tuberculosis, histoplasmosis, previous pneumonia, or bronchitis), or other diseases (e.g., lymphoma).

Chest CT is relatively inaccurate for the nodal staging. The pooled sensitivity, specificity, and negative predictive value of chest CT in lymph node assessment were 55% (20–91%), 81% (50–97%), and 83% (54–97%), respectively [79].

Several studies have found that FDG-PET has a higher sensitivity and specificity than CT in mediastinal lymph node assessment. In recent meta-analyses, sensitivities and specificities for evaluating lymph node status were 79–85% and 89–92%, respectively [80, 81]. Moreover, FDG-PET has a high negative predictive value in N staging, which has been estimated at >90% [82].

Although CT alone is not accurate enough to determine the nodal status of a patient with NSCLC, it can be combined with FDG-PET/CT scans or invasive procedures. In patients who have FDG-PET positive and/or enlarged mediastinal nodes (and no distant metastasis), invasive staging of the mediastinum is required [83]; procedures such as endobronchial ultrasound (EBUS), cervical mediastinoscopy (CME), esophageal ultrasound (EUS), and video-assisted thoracic surgery are indicated for nodal sampling.

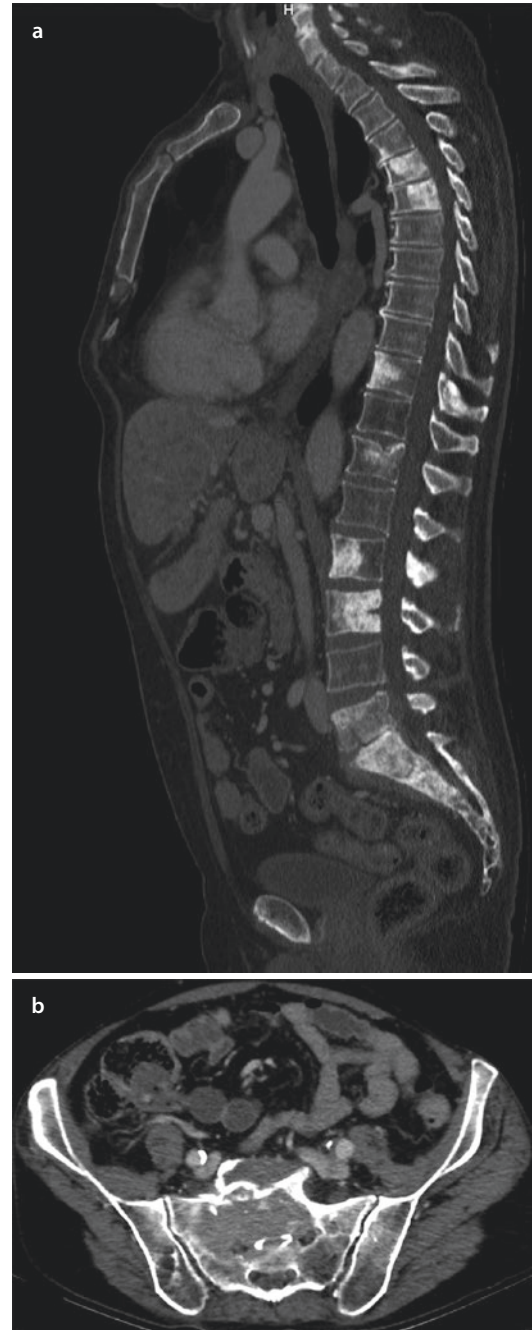
3.4 Metastatic Spread

Metastatic spread of SCC and ADC to distant organs is the most common cause of cancer mortality. Lung cancers can spread when cells break off from the tumor to distant regions of the body. This process can occur through hematogenous, lymphatic, and airborne dissemination.

Sometimes lung cancer can spread with few metastases, and in this case it is defined as oligometastatic disease. Limited site recurrence is also known as oligo-recurrence and may be treated with locoregional therapeutic strategies.

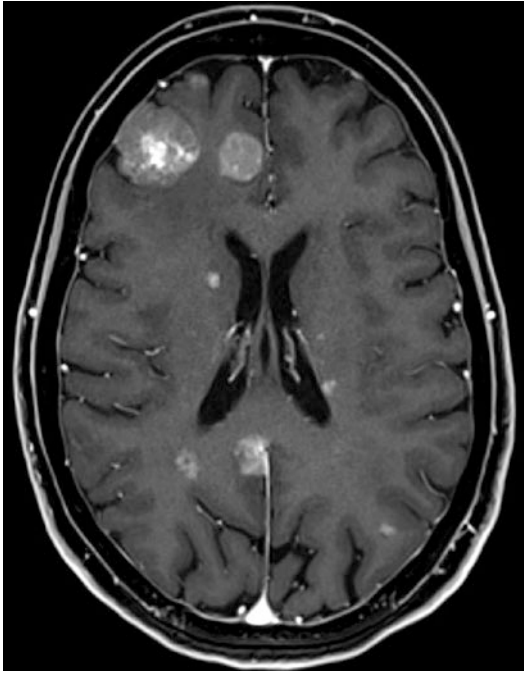
The most common sites for SCC and ADC spread are the lymph nodes, liver, bones, brain, and adrenal glands [84].

- Lymph nodes: As described in the previous paragraph [▶ Sect. 3.3], most lung cancers first spread to the regional or extra-regional lymph nodes.
- Bone: 30–40% of patients with advanced lung cancer have metastatic spread to the bone. Bone metastases from SCC and ADC can be both blastic and lytic, but osteolytic lesions are prevalent (■ Fig. 3.9). The preferential sites of bone metastases are spine and pelvis, and the most common symptom of bone metastases is pain. Some patients can develop pathological fractures that occur with minimal trauma or even during normal daily activities, particularly in case of lytic lesions. The primary goal in the treatment of bone metastases is to reduce pain and to repair or prevent fractures that occur. Options include pain medications, RT, medications, and sometimes surgery.
- Brain: Approximately 10% of newly diagnosed lung cancer and 20–30% of previously diagnosed cancer develop brain metastases. Brain metastases can cause neurological symptoms such as headache, seizure, loss of balance and coordination, vision changes, loss of memory, and personality changes. Brain metastases are usually diagnosed with CT scan or MRI of the brain (■ Fig. 3.10). Treatment is primarily palliative, meaning that the goal is to control symptoms. Steroids may be used to decrease swelling, and RT may be very effective in reducing symptoms. If few brain metastases are present, treatment with either surgery or stereotactic body radiotherapy (SBRT), also known as cyberknife or gamma-knife, has resulted in long-term control of the disease [85].
- Liver: Liver metastases showed an incidence of 6–8% of new diagnosed patients with NSCLC, regardless of histology. Those on CT scans can be either hyperdense or hypodense to liver parenchyma (■ Fig. 3.11). When symptoms are present, they may include pain on the right side, loss of appetite, and nausea. Abdominal ultrasound, a CT scan, MRI, or a PET scan can reveal the presence of liver metastasis. Treatment is usually a systemic therapy, but in rare cases with few lesions, surgery or embolization may be recommended. Particularly, splitting histology into adenocarcinoma and squamous cell carcinoma, we can find that

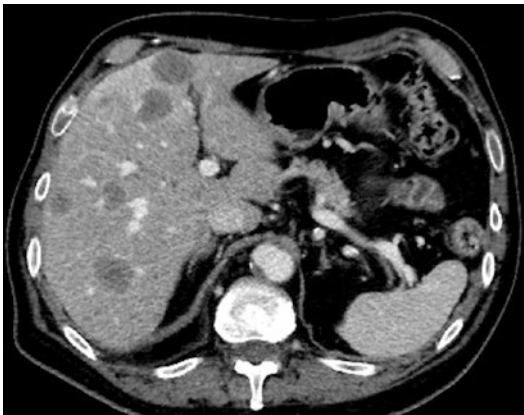


■ Fig. 3.9 a Coronal reformatted CT image shows multiple blastic bone metastases. b Large osteolytic metastasis involving the sacrum on axial CT scan

adenocarcinoma tends to disseminate to liver and adrenal glands (>35% of patient population), differing from squamous cell carcinoma that disseminates to the same metastatic sites in about 20–25% [86].



■ Fig. 3.10 Contrast-enhanced MRI shows multiple bilateral brain metastases from lung adenocarcinoma



■ Fig. 3.11 CT scan shows multiple hypodense liver metastases from squamous cell carcinoma

- Adrenal glands: The incidence of adrenal gland metastases is 2–4% in patients with NSCLC and usually does not cause any symptoms (■ Fig. 3.12). The treatment is generally a systemic therapy, but in some cases surgery can remove the adrenal gland and adrenal metastases with a better long-term survival [86].
- Others: Lung cancer less frequently spreads to other organs such as the stomach, small and large intestines, pancreas, eye, skin, kidney, and breast.



■ Fig. 3.12 Axial CT image shows a right adrenal gland metastasis

References

1. Siegel RL, Miller KD, Jemal A. Cancer statistics. *CA Cancer J Clin.* 2019;69:7–34.
2. Ferlay J, Colombet M, Soerjomataram I, Dyba T, Randi G, Bettio M, Gavin A, Visser O, Bray F. Cancer incidence and mortality patterns in Europe: estimates for 40 countries and 25 major cancers in 2018. *Eur J Cancer.* 2018;103:356–87.
3. Doll R, Peto R. Mortality in relation to smoking: 20 years' observations on male British doctors. *Br Med J.* 1976;2:1525–36.
4. Straif K, Benbrahim-Tallaa L, Baan R, Grosse Y, Secretan B, El Ghissassi F, Bouvard V, Guha N, Freeman C, Galichet L, Cogliano V, WHO International Agency for Research on Cancer Monograph Working Group. A review of human carcinogens – part C: metals, arsenic, dusts, and fibres. *Lancet Oncol.* 2009;10: 453–4.
5. Dugay F, Llamas-Gutierrez F, Gournay M, Medane S, Mazet F, Chiforeanu DC, Becker E, Lamy R, Léna H, Rioux-Leclercq N, Belaud-Rotureau MA, Cabillic F. Clinicopathological characteristics of ROS1- and RET-rearranged NSCLC in caucasian patients: data from a cohort of 713 non-squamous NSCLC lacking KRAS/EGFR/HER2/BRAF/PIK3CA/ALK alterations. *Oncotarget.* 2017;8:53336–51.
6. Rami-Porta R, Bolejack V, Giroux DJ, Chansky K, Crowley J, Asamura H, Goldstraw P. The IASLC Lung Cancer Staging Project: the new database to inform the 8th edition of the TNM classification of lung cancer. *J Thorac Oncol.* 2014;9:1618–24.
7. Postmus PE, Kerr KM, Oudkerk M, Senan S, Waller DA, Vansteenkiste J, Escriu C, Peters S. ESMO Guidelines Committee. Early and locally advanced non-small-cell lung cancer (NSCLC): ESMO Clinical Practice Guidelines for diagnosis, treatment and follow-up. *Ann Oncol.* 2017;28(Suppl_4):iv1–iv21.
8. NCCN – Clinical Practice Guidelines in Oncology. Version 2. 2018. <https://www.nccn.org/>.

9. Ciliberto M, Kishida Y, Seki S, Yoshikawa T, Ohno Y. Update of MR imaging for evaluation of lung cancer. *Radiol Clin N Am.* 2018;56(3):437–69.
10. Caroli G, Dell'Amore A, Cassanelli N, Dolci G, Pipitone E, Asadi N, et al. Accuracy of transthoracic ultrasound for the prediction of chest wall infiltration by lung cancer and of lung infiltration by chest wall tumours. *Heart Lung Circ.* 2015;24(10):1020–6.
11. Hafez MR, Sobh ES, Elsayy SB, Abo-Elkheir OI. The usefulness of thoracic ultrasonography in diagnosis and staging of bronchogenic carcinoma. *Ultrasound.* 2017;25(4):200–12.
12. Howington JA, Blum MG, Chang AC, Balekian AA, Murthy SC. Treatment of stage I and II non-small cell lung cancer: diagnosis and management of lung cancer, 3rd ed: American College of Chest Physicians evidence-based clinical practice guidelines. *Chest.* 2013;143:e278S–313S.
13. Lutz ST, Jones J, Chow E. Role of radiation therapy in palliative care of the patient with cancer. *J Clin Oncol.* 2014;32:2913–9.
14. Prezzano KM, Ma SJ, Hermann GM, Rivers CI, Gomez-Suescun JA, Singh AK. Stereotactic body radiation therapy for non-small cell lung cancer: a review. *World J Clin Oncol.* 2019;10(1):14–27.
15. Ricardi U, Badellino S, Filippi AR. Stereotactic body radiotherapy for early stage lung cancer: history and updated role. *Lung Cancer.* 2015;90(3):388–96.
16. Hirsch FR, Scagliotti GV, Mulshine JL, Kwon R, Curran WJ Jr, Wu YL, Paz-Ares L. Lung cancer: current therapies and new targeted treatments. *Lancet.* 2017;389(10066):299–311.
17. Passaro A, Palazzo A, Trenta P, Mancini ML, Morano F, Cortesi E. Molecular and clinical analysis of predictive biomarkers in non-small-cell lung cancer. *Curr Med Chem.* 2012;19(22):3689–700.
18. Kurzrock R, Stewart DJ. Exploring the benefit/risk associated with antiangiogenic agents for the treatment of non-small cell lung cancer patients. *Clin Cancer Res.* 2017;23(5):1137–48.
19. Tan CS, Cho BC, Soo RA. Next-generation epidermal growth factor receptor tyrosine kinase inhibitors in epidermal growth factor receptor-mutant non-small cell lung cancer. *Lung Cancer.* 2016;93:59–68.
20. Passaro A, Guerini-Rocco E, Pochesci A, Vacirca D, Spitaleri G, Catania CM, Rappa A, Barberis M, de Marinis F. Targeting EGFR T790M mutation in NSCLC: from biology to evaluation and treatment. *Pharmacol Res.* 2017;117:406–15.
21. Passaro A, Lazzari C, Karachaliou N, Spitaleri G, Pochesci A, Catania C, Rosell R, de Marinis F. Personalized treatment in advanced ALK-positive non-small cell lung cancer: from bench to clinical practice. *Oncotargets Ther.* 2016;17(9):6361–76.
22. Facchinetti F, Rossi G, Bria E, Soria JC, Besse B, Minari R, Friboulet L, Tiseo M. Oncogene addiction in non-small cell lung cancer: focus on ROS1 inhibition. *Cancer Treat Rev.* 2017;55:83–95.
23. Kelly RJ. Dabrafenib and trametinib for the treatment of non-small cell lung cancer. *Expert Rev Anticancer Ther.* 2018;18(11):1063–8.
24. Weiner LM, Murray JC, Shuptrine CW. Antibody-based immunotherapy of cancer. *Cell.* 2012;148(6):1081–4.
25. Pochesci A, Passaro A, Catania C, Noberasco C, Del Signore E, Spitaleri G, De Marinis F. Immunotherapy in non-small cell lung cancer: evolution of knowledge and clinical advances. *Recent Prog Med.* 2016;107(4):186–92.
26. Attili I, Passaro A, Pavan A, Conte P, De Marinis F, Bonanno L. Combination immunotherapy strategies in advanced non-small cell lung cancer (NSCLC): does biological rationale meet clinical needs? *Crit Rev Oncol Hematol.* 2017;119:30–9.
27. Woodard GA, Jones KD, Jablons DM. Lung cancer staging and prognosis. *Cancer Treat Res.* 2016;170:47–75.
28. Simmons CP, Koinis F, Fallon MT, et al. Prognosis in advanced lung cancer – a prospective study examining key clinicopathological factors. *Lung Cancer.* 2015;88(3):304–9.
29. Nakamura H, Ando K, Shinmyo T, Morita K, Mochizuki A, Kurimoto N, Tatsunami S. Female gender is an independent prognostic factor in non-small-cell lung cancer: a meta-analysis. *Ann Thorac Cardiovasc Surg.* 2011;17(5):469–80.
30. Timár J. The clinical relevance of KRAS gene mutation in non-small-cell lung cancer. *Curr Opin Oncol.* 2014;26(2):138–44.
31. Ferlay J, Soerjomataram I, Dikshit R, Eser S, Mathers C, Rebelo M, Parkin DM, Forman D, Bray F. Cancer incidence and mortality worldwide: sources, methods and major patterns in GLOBOCAN 2012. *Int J Cancer.* 2014;136:E359–86.
32. Chansky K, Detterbeck FC, Nicholson AG, Rusch VW, Vallières E, Groome P, Kennedy C, Krasnik M, Peake M, Shemanski L, Bolejack V, Crowley JJ, Asamura H, Ramiporta R, IASLC Staging and Prognostic Factors Committee, Advisory Boards, and Participating Institutions. The IASLC Lung Cancer Staging Project: External validation of the revision of the TNM Stage Groupings in the Eighth Edition of the TNM classification of lung cancer. *J Thorac Oncol.* 2017;12(7):1109–21.
33. Patterson GA. Extended pulmonary resection. In: Pearson FG, Cooper JD, et al., editors. *Thoracic surgery*, vol. 1. 2nd ed. New York: Churchill- Livingstone; 2002. p. 1045–61.
34. Borri A, Leo F, Veronesi G, Solli P, Galetta D, Gasparri R, Petrella F, Scanagatta P, Radice D, Spaggiari L. Extended pneumonectomy for non-small cell lung cancer: morbidity, mortality, and long-term results. *J Thorac Cardiovasc Surg.* 2007;134(5):1266–72.
35. Shirakusa T, Kimura M. Partial atrial resection in advanced lung carcinoma with and without cardiopulmonary bypass. *Thorax.* 1991;46:484–7.
36. Tsuchiya R, Asamura H, Kondo H, Goya T, Naruke T. Extended resection of the left atrium, great vessels, or both for lung cancer. *Ann Thorac Surg.* 1994;57:960–5.
37. Ratto GB, Costa R, Vassallo G, Alloisio A, Maineri P, Bruzzi P. Twelve-year experience with left atrial resection in the treatment of non-small cell lung cancer. *Ann Thorac Surg.* 2004;78(1):234–7.
38. Bobbio A, Carbognani P, Grapeggia M, Rusca M, Sartori F, Bobbio P, Rea F. Surgical outcome of combined pulmonary and atrial resection for lung cancer. *Thorac Cardiovasc Surg.* 2004;52(3):180–2.

39. Spaggiari L, D' Aiuto M, Veronesi G, Pelosi G, de Pas T, Catalano G, de Braud F. Extended pneumonectomy with partial resection of the left atrium, without cardiopulmonary bypass, for lung cancer. *Ann Thorac Surg.* 2005;79:234–40.
40. Wu L, Xu Z, Zhao X, Zhong L, Pang T, Wu B. Surgical treatment of lung cancer invading the left atrium or base of the pulmonary vein. *World J Surg.* 2009;33:492–6.
41. Kuehl A, Lindner M, Hornung HM, Winter H, Jauch KW, Hatz RA, Graeb C. Atrial resection for lung cancer: morbidity, mortality, and long-term follow-up. *World J Surg.* 2010;34:2233–9.
42. Stella F, Dell'Amore A, Caroli G, Dolci G, Cassanelli N, Luciano G, Davoli F, Bini A. Surgical results and long-term follow-up of T(4)-non-small cell lung cancer invading the left atrium or the intrapericardial base of the pulmonary veins. *Interact Cardiovasc Thorac Surg.* 2012;14:415–9.
43. Galvaing G, Tardy MM, Cassagnes L, Da Costa V, Chadeyras JB, Naamee A, Bailly P, Filaire E, Pereira B, Filaire M. Left atrial resection for T4 lung cancer without cardiopulmonary bypass: technical aspects and outcomes. *Ann Thorac Surg.* 2014;97:1708–13.
44. Tsukioka T, Takahama M, Nakajima R, Kimura M, Inoue H, Yamamoto R. Surgical outcome of patients with lung cancer involving the left atrium. *Int J Clin Oncol.* 2016;21(6):1046–50.
45. Fukuse T, Wada H, Hitomi S. Extended operations for non-small cell lung cancers invading great vessels and left atrium. *Eur J Cardiothorac Surg.* 1997;11:664–9.
46. Ohta M, Hirabayashi H, Shiono H, Minami M, Maeda H, Takano H, Miyoshi S, Matsuda H. Surgical resection for lung cancer with infiltration of the thoracic aorta. *J Thorac Cardiovasc Surg.* 2005;129:804–8.
47. Collaud S, Waddell TK, Yasufuku K, Oreopoulos G, Rampersaud R, Rubin B, Roche-Nagle G, Keshavjee S, de Perrot M. Thoracic aortic endografting facilitates the resection of tumors infiltrating the aorta. *J Thorac Cardiovasc Surg.* 2014;147:1178–82.
48. Kusumoto H, Shintani Y, Funaki S, Inoue M, Okumura M, Kuratani T, Sawa Y. Combined resection of great vessels or the heart for non-small lung cancer. *Ann Thorac Cardiovasc Surg.* 2015;21:332–7.
49. Spaggiari L, Leo F, Veronesi G, Solli P, Galetta D, Tatani B, Petrella F, Radice D. Superior vena cava resection for lung and mediastinal malignancies: a single-center experience with 70 cases. *Ann Thorac Surg.* 2007;83:223–9.
50. Dartevielle PG, Mitilian D, Fadel E. Extended surgery for T4 lung cancer: a 30 years' experience. *Gen Thorac Cardiovasc Surg.* 2017;65:321–8.
51. Lanuti M, De Delva PE, Gaissert HA, Wright CD, Wain JC, Allan JS, Donahue DM, Mathisen DJ. Review of superior vena cava resection in the management of benign disease and pulmonary or mediastinal malignancies. *Ann Thorac Surg.* 2009;88:392–7.
52. Shargall Y, de Perrot M, Keshavjee S, Darling G, Ginsberg R, Johnston M, Pierre A, Waddell TK. 15 years single center experience with surgical resection of the superior vena cava for non-small cell lung cancer. *Lung Cancer.* 2004;45:357–63.
53. Suzuki K, Asamura H, Watanabe S, Tsuchiya R. Combined resection of superior vena cava for lung carcinoma: prognostic significance of patterns of superior vena cava invasion. *Ann Thorac Surg.* 2004;78:1184–9.
54. de Perrot M, Fadel E, Mercier O, Mussot S, Chapelier A, Dartevielle P. Long-term results after carinal resection for carcinoma: does the benefit warrant the risk? *J Thorac Cardiovasc Surg.* 2006;131(1):81–9.
55. Martin J, Ginsberg RJ, Abolhoda A, Bains MS, Downey RJ, Korst RJ, Weigel TL, Kris MG, Venkatraman ES, Rusch VW. Morbidity and mortality after neoadjuvant therapy for lung cancer: the risks of right pneumonectomy. *Ann Thorac Surg.* 2001;72:1149–54.
56. Tapias LF, Ott HC, Mathisen DJ. Complications following carinal resections, sleeve resections. *Thorac Surg Clin.* 2015;25(4):435–47.
57. Shin S, Park JS, Shim YM, Kim HJ, Kim J. Carinal resection and reconstruction in thoracic malignancies. *J Surg Oncol.* 2014;110(3):239–44.
58. Weder W, Inci I. Carinal resection and sleeve pneumonectomy. *Thorac Surg Clin.* 2014;24(1):77–83.
59. Regnard JF, Perrotin C, Giovannetti R, Schussler O, Petino A, Spaggiari L, Alifano M, Magdeleinat P. Resection for tumors with carinal involvement: technical aspects, results, and prognostic factors. *Ann Thorac Surg.* 2005;80:1841–6.
60. Lanuti M. Surgical management of lung cancer involving the chest wall. *Thorac Surg Clin.* 2017;27(2):195–9.
61. Reimer P, Parizel PM, Meaney JFM, Stichnoth F. *Clinical MR imaging: a practical approach.* 3rd ed. Springer Science & Business Media; 2010. p. 501–2.
62. Facciolo F, Cardillo G, Lopergolo M, Pallone G, Sera F, Martelli M. Chest wall invasion in non-small cell lung carcinoma: a rationale for en bloc resection. *J Thorac Cardiovasc Surg.* 2001;121(4):649–56.
63. Magdeleinat P, Alifano M, Benbrahem C, Spaggiari L, Porrello C, Puyo P, Levasseur P, Regnard JF. Surgical treatment of lung cancer invading the chest wall: results and prognostic factors. *Ann Thorac Surg.* 2001;71(4):1094–9.
64. Yokoi K, Taniguchi T, Usami N, Kawaguchi K, Fukui T, Ishiguro F. Surgical management of locally advanced lung cancer. *Gen Thorac Cardiovasc Surg.* 2014;62(9):522–30.
65. Schirren J, Donges T, Melzer M, Schonmayr R, Eberlein M, Bolukbas S. En bloc resection of non-small-cell lung cancer invading the spine. *Eur J Cardiothorac Surg.* 2011;40:647–55.
66. Grunenwald DH, Mazel C, Girard P, Veronesi G, Spaggiari L, Gossot D, Debrosse D, Caliandro R, Le Guillou JL, Le Chevalier T. Radical en bloc resection for lung cancer invading the spine. *J Thorac Cardiovasc Surg.* 2002;123:271–9.
67. Galetta D, Borri A, Casiraghi M, Gasparri R, Petrella F, Tessitore A, Serra M, Guarize J, Spaggiari L. Outcome and prognostic factors of resected non-small-cell lung cancer invading the diaphragm. *Interact Cardiovasc Thorac Surg.* 2014;19(4):632–6.
68. Lauweryns JM, Baert JH. Alveolar clearance and the role of the pulmonary lymphatics. *Am Rev Respir Dis.* 1977;115:625–83.

69. Le Pimpec Barthes F, Riquet M, Hartl D, Hubsch JP, Hidden G. Cervical venous anastomoses of pulmonary lymphatic vessels. *Surg Radiol Anat.* 1997;19:53–5.
70. Riquet M, Le Pimpec Barthes F, Souilamas R, Hidden G. Thoracic duct tributaries from intrathoracic organs. *Ann Thorac Surg.* 2002;73(3):892–9.
71. Meyer KK. Direct lymphatic connections from the lower lobes of the lung to the abdomen. *J Thorac Surg.* 1958;35(6):726–33.
72. Riquet M, Hidden G, Debesse B. Abdominal nodal connexions of the lymphatics of the lung. *Surg Radiol Anat.* 1988;10(3):251–2.
73. Riquet M, Hidden G, Debesse B. Direct lymphatic drainage of lung segments to the mediastinal nodes. An anatomic study on 260 adults. *J Thorac Cardiovasc Surg.* 1989;97(4):623–32.
74. Ilic N, Petricevic A, Arar D, Kotarac S, Banovic J, Ilic NF, Tripkovic A, Grandic L. Skip mediastinal nodal metastases in the IIIa/N2 non-small cell lung cancer. *J Thorac Oncol.* 2007;2(11):1018–21.
75. Yoshino I, Yokoyama H, Yano T, Ueda T, Takai E, Mizutani K, et al. Skip metastasis to the mediastinal lymph nodes in non-small cell lung cancer. *Ann Thorac Surg.* 1996;62:1021–5.
76. Rusch VW, Asamura H, Watanabe H, Giroux DJ, Rami-Porta R, Goldstraw P, Members of IASLC Staging Committee. The IASLC lung cancer staging project: a proposal for a new international lymph node map in the forthcoming seventh edition of the TNM classification for lung cancer. *J Thorac Oncol.* 2009;4(5):568–77.
77. Johkoh T, Ikezoe J, Tomiyama N, Nagareda T, Kohno N, Takeuchi N, Yamagami H, Kido S, Takashima S, Arisawa J. CT findings in lymphangitic carcinomatosis of the lung: correlation with histologic findings and pulmonary function tests. *AJR Am J Roentgenol.* 1992;158(6):1217–22.
78. Ikezoe J, Godwin JD, Hunt KJ, Marglin SI. Pulmonary lymphangitic carcinomatosis: chronicity of radiographic findings in long-term survivors. *AJR Am J Roentgenol.* 1995;165(1):49–52.
79. Silvestri GA, Gonzalez AV, Jantz MA, Margolis ML, Gould MK, Tanoue LT, Harris LJ, Detterbeck FC. Methods for staging non-small cell lung cancer: diagnosis and management of lung cancer, 3rd ed: American College of Chest Physicians evidence-based clinical practice guidelines. *Chest.* 2013;143:e211S–50S.
80. Birim O, Kappetein AP, Stijnen T, Bogers AJ. Meta-analysis of positron emission tomographic and computed tomographic imaging in detecting mediastinal lymph node metastases in nonsmall cell lung cancer. *Ann Thorac Surg.* 2005;79:375–82.
81. Gould MK, Kuschner WG, Rydzak CE, Maclean CC, Demas AN, Shigemitsu H, Chan JK, Owens DK. Test performance of positron emission tomography and computed tomography for mediastinal staging in patients with non-small cell lung cancer: a meta-analysis. *Ann Intern Med.* 2003;139:879–92.
82. Schrevels L, Lorent N, Dooms C, Vansteenkiste J. The role of PET scan in diagnosis, staging, and management of non-small cell lung cancer. *Oncologist.* 2004;9:633–43.
83. Stamatidis G. Staging of lung cancer: the role of noninvasive, minimally invasive and invasive techniques. *Eur Respir J.* 2015;46(2):521–31.
84. Riihimäki M, Hemminki A, Fallah M, Thomsen H, Sundquist K, Sundquist J, Hemminki K. Metastatic sites and survival in lung cancer. *Lung Cancer.* 2014;86(1):78–84.
85. D'Antonio C, Passaro A, Gori B, Del Signore E, Migliorino MR, Ricciardi S, Fulvi A, de Marinis F. Bone and brain metastasis in lung cancer: recent advances in therapeutic strategies. *Ther Adv Med Oncol.* 2014;6(3):101–14.
86. Milovanovic IS, Stjepanovic M, Mitrovic D. Distribution patterns of the metastases of the lung carcinoma in relation to histological type of the primary tumor: an autopsy study. *Ann Thorac Med.* 2017;12(3):191–8.



Non-Small Cell Lung Cancer: Rare Types

Andrea Borghesi, Silvia Michelini, and Andrea Tironi

- 4.1 Introduction – 64**
- 4.2 Rare Epithelial Malignant Lung Tumors – 64**
 - 4.2.1 Pulmonary Sarcomatoid Carcinoma – 65
 - 4.2.2 Salivary Gland-Type Carcinomas of the Lung – 68
- 4.3 Mesenchymal Malignant Lung Tumors – 73**
 - 4.3.1 Epithelioid Hemangioendothelioma – 73
 - 4.3.2 Synovial Sarcoma – 77
 - 4.3.3 Pulmonary Artery Intimal Sarcoma – 79
- 4.4 Lymphoid Malignant Lung Tumors – 81**
 - 4.4.1 MALT Lymphoma – 81
- References – 83**

4.1 Introduction

The 2015 World Health Organization (WHO) classification of malignant lung tumors includes broad categories of common and uncommon lesions with different histological features. While the common types of non-small-cell lung cancer (NSCLC) are well-known and well-studied entities, there are other types of NSCLC that are seldom encountered in the clinical routine.

Based on their histological origin, these uncommon malignant lung tumors can be divided into three main groups [1] (Table 4.1):

- Epithelial
- Mesenchymal
- Lymphoid

4.2 Rare Epithelial Malignant Lung Tumors

Rare carcinomas of the lung include sarcomatoid carcinoma, salivary gland-type carcinoma (PSGC), and other/unclassified carcinoma (Table 4.1). This latter group consists of lymphoepithelioma-like carcinoma and nuclear protein in testis (NUT)

Table 4.1 Rare malignant lung tumors: 2015 WHO classification of lung tumor [1]

Histology group	Histologic type and subtypes	ICDO code
Epithelial	Sarcomatoid carcinomas	
	Pleomorphic carcinoma	8022/3
	Spindle cell carcinoma	8032/3
	Giant cell carcinoma	8031/3
	Carcinosarcoma	8980/3
	Pulmonary blastoma	8972/3
	Salivary gland-type carcinomas	
	Mucoepidermoid carcinoma	8430/3
	Adenoid cystic carcinoma	8200/3
	Epithelial-myoepithelial carcinoma	8562/3
	Other and unclassified carcinomas	
	Lymphoepithelioma-like carcinoma	8082/3
	NUT carcinoma	8023/3
Mesenchymal	Epithelioid hemangioendothelioma	9133/3
	Pulmonary synovial sarcoma	9040/3
	Pulmonary artery intimal sarcoma	9137/3
	Pulmonary myxoid sarcoma with <i>EWSR1-CREB1</i> translocation	8842/3
	Myoepithelial carcinoma	8982/3
	Malignant PEComa	8714/3
Lymphoid	MALT lymphoma	9699/3
	Diffuse large cell lymphoma	9680/3
	Intravascular large B-cell lymphoma	9712/3

WHO World Health Organization, ICDO International Classification of Disease for Oncology, NUT nuclear protein in testis, MALT mucosa-associated lymphoid tissue

carcinoma. NUT carcinoma is extremely rare in the lungs and usually occurs in midline structures [2]. Similarly, pulmonary lymphoepithelioma-like carcinoma is very rare in Western populations, and no more than 20 cases have been published in the literature [3]. Based on their extremely low incidence in the lungs, NUT and lymphoepithelioma-like carcinomas will not be discussed in this chapter.

4.2.1 Pulmonary Sarcomatoid Carcinoma

4.2.1.1 Overview

Pulmonary sarcomatoid carcinoma (PSC) is a rare and aggressive histological subtype of NSCLC [4], accounting for less than 3% of all NSCLCs [5–7]. According to the WHO classification, PSCs are defined as a group of poorly differentiated NSCLCs containing a sarcomatoid or sarcoma-like (spindle and/or giant cell) component [1, 8]. This uncommon group of NSCLCs includes the following five histological subtypes, thereafter reported according to occurrence rate [1, 5]:

- Pleomorphic carcinoma
- Carcinosarcoma
- Spindle cell carcinoma
- Giant cell carcinoma
- Pulmonary blastoma

Pleomorphic carcinoma, carcinosarcoma, spindle cell carcinoma, and giant cell carcinoma are predominantly observed in men, with a male-to-female ratio of approximately 4:1 [4, 5]. The diagnosis of this group of PSCs usually occurs between the sixth and seventh decades of life [4, 5, 8, 9].

In contrast to these subtypes of carcinoma, pulmonary blastoma does not exhibit a gender propensity, and it occurs mostly in the fourth decade of life [5, 8, 9].

PSCs are frequently associated with a history of moderate to heavy cigarette smoking [4, 5, 8–10]. Some cases of PSC seem to be related to asbestos exposure; however, this association remains indeterminate [5].

The clinical signs and symptoms of PSCs are not specific and are usually related to the involvement of adjacent anatomical structures, such as the bronchial system, pleura, mediastinum, and chest wall [5]. Presenting signs and symptoms

may include cough, hemoptysis, chest pain, dyspnea, fever, and weight loss [5].

PSC is an aggressive type of cancer with high metastatic potential and a very poor prognosis [6, 8, 10]. The 5-year survival rate is approximately 20–25% [6, 8, 10]. The prognosis is significantly related to the size of the tumor and its stage [10]. Therefore, early diagnosis and short-term treatment are two critical aspects for improving the prognosis of patients with PSCs.

From a prognostic point of view, the best treatment for PSC is surgical resection [4, 5, 8]. Therefore, PSCs at an early stage have a better likelihood of complete resection and thereby a better prognosis. However, PSCs are often diagnosed belatedly and in advanced tumor-node-metastasis (TNM) stages. The role of neoadjuvant or adjuvant chemotherapy and new targeted therapies is still unclear [4–10]. However, some authors report that neoadjuvant or adjuvant chemotherapy may significantly improve the prognosis of PSCs [4, 8, 10].

4.2.1.2 Pathology

The diagnosis of PSC can be confirmed only by pathological examination [4, 8]. Noteworthy, the diagnosis of PSC and its subtypes cannot be made on cytology or small biopsies [1, 8, 11]; therefore, a surgical specimen is required for the final diagnosis.

Certain subtypes of PSC may be recognized on hematoxylin and eosin staining; however, additional immunohistochemical and molecular characterization methods may be useful for a more accurate distinction from other malignant tumors [4].

Pleomorphic carcinoma is the most frequent subtype of PSC, and, as the name implies, it is represented by a mixture of epithelial component (similar to conventional NSCLC, usually adenocarcinoma or squamous cell carcinoma) and sarcomatoid component with spindle and/or giant cells (corresponding to 10% or more of the tumor) [1, 5, 12]. Alternatively, the term pleomorphic carcinoma is also assigned to tumors consisting exclusively of spindle and giant cells, without epithelial components [1, 5, 12]. In contrast, carcinomas consisting of only a pure spindle or giant cell component are defined as spindle cell carcinoma or giant cell carcinoma, respectively [1, 5, 12].

Table 4.2 Rare epithelial malignant lung tumors: key imaging features and main differential diagnoses

Tumor type	Key features on CT and PET/CT	Main differential diagnoses
Sarcomatoid carcinoma	Solitary large mass in the upper lobes Heterogeneous contrast enhancement High ^{18}F FDG uptake Hilar/mediastinal lymph node metastasis	Other high-grade NSCLCs
Mucoepidermoid carcinoma	Solitary nodule in the lobar/segmental bronchi Round or oval shape Well-defined margins Heterogeneous ^{18}F FDG uptake	Endobronchial carcinoid Other bronchogenic NSCLCs
Adenoid cystic carcinoma	Solitary nodule in the trachea/main/lobar bronchi Polypoid shape or circumferential thickening Poorly defined margins Extraluminal extension Heterogeneous ^{18}F FDG uptake	Other bronchogenic NSCLCs Endobronchial carcinoid

FDG 18-fluorodeoxyglucose, NSCLC non-small-cell lung cancer

Carcinosarcoma is defined by a mixture of conventional NSCLCs (typically adenocarcinoma or squamous cell carcinoma) and sarcoma components containing heterologous elements of rhabdomyosarcoma, osteosarcoma, or chondrosarcoma [1, 5, 12].

Pulmonary blastoma, the less common subtype of PSC, is a biphasic malignant tumor containing a combination of fetal adenocarcinoma and primitive mesenchymal stroma with occasional foci of rhabdomyosarcoma, osteosarcoma, or chondrosarcoma [1, 5, 12].

4.2.1.3 Imaging

Although computed tomography (CT) and positron emission tomography (PET)/CT imaging can provide information useful to formulate a provisional diagnosis of PSC, the preoperative diagnosis of this rare entity is challenging. Nonetheless, these tumors exhibit some distinctive features on CT and PET/CT imaging that should be known to improve the differential diagnosis with other NSCLCs (Table 4.2).

At the time of diagnosis, most PSCs present with a solitary pulmonary mass located at the periphery of the upper lobes (i.e., more than 2 cm from the main bronchi) (Fig. 4.1) [4, 11–14].

The mass is usually large with a diameter greater than 4–5 cm (Fig. 4.2) [4, 11, 13]. The margins of the lesions can be smooth (Fig. 4.1), lobulated, or spiculated (Fig. 4.2) [4, 11–14].

On contrast-enhanced CT, PSCs exhibit heterogeneous enhancement with central low density. Cavitation may occur reflecting intralobular hemorrhage and necrosis (Fig. 4.2) [4, 11–14]. Pleural indentation and pleural thickening may be observed, mainly with large masses (Fig. 4.2). The literature also reports that the standardized uptake value (SUV) of 18-fluorodeoxyglucose (^{18}F FDG) on PET/CT imaging is significantly higher in PSCs than in other NSCLCs (SUVmax 15.2 vs 8.3) (Figs. 4.1 and 4.2) [8, 11, 15, 16].

Therefore, in cases of a large mass located in the upper lobes with or without cavitation and with high ^{18}F FDG uptake on PET/CT imaging, a provisional diagnosis of PSC should be formulated.

4.2.1.4 Local Spread and Metastatic Dissemination

The local spread of PSCs depends on their location within the lung. As generally peripheral lesions, PSCs tend to spread into adjacent struc-

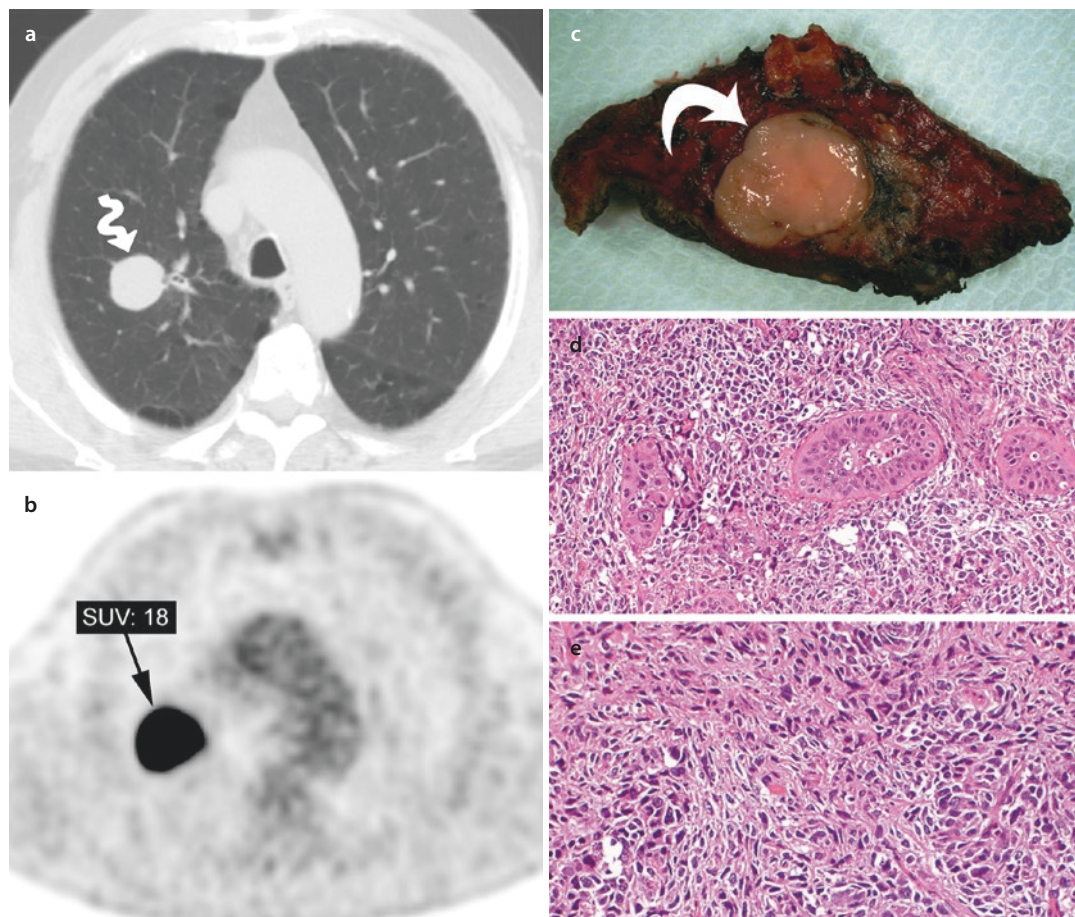


Fig. 4.1 Sarcomatoid carcinoma (pleomorphic subtype) in a 70-year-old man who is heavy smoker. **a** Axial CT image with lung window setting reveals a mass with smooth margins in the right upper lobe (*wavy arrow*). **b** Axial PET image displays the intense ^{18}F FDG uptake of the pulmonary mass (*black arrow*). **c** Gross image of the

resected pulmonary tissue containing the mass (*curved arrow*). **d, e** Histological hematoxylin and eosin (H-E) images showing a mixture of an epithelial component with squamous cell differentiation and an undifferentiated component with spindle cell features (H-E 20 \times)

tures, such as the pleura, chest wall, and diaphragm [17]. Chest wall invasion is more often observed in pleomorphic carcinoma than in other subtypes [12]. Central PSCs, with or without endobronchial involvement, tend to infiltrate the mediastinum and hilum; this pattern of local diffusion may be observed in all PSCs, and it is more frequent in carcinosarcoma [12].

Lymphatic and vascular invasion are common in PSC and reflect its high metastatic potential (Fig. 4.2) [12, 15]. The invasion of lymphatic system and blood vessels brings PSC to metastasize toward the same anatomical organs/structures as conventional NSCLCs do (i.e., bone, brain, lung, liver, and adrenal glands); however,

metastatic diffusion seems to be faster with PSCs than with other NSCLCs [4].

Hilar and/or mediastinal lymph node metastases and distant metastases are observed frequently; in particular, more than 50% of PSCs with parenchymal invasion also exhibit lymph node metastases (Fig. 4.2) [4, 11, 15, 16]. In contrast with other NSCLCs, PSCs show an increased incidence of gastrointestinal tract involvement, notably of the small bowel [5, 12, 18].

Moreover, metastatic lymph nodes and distant metastases exhibit high uptake on ^{18}F FDG PET/CT imaging, substantially overlapping the pattern of the primary lesion (Fig. 4.2) [11, 15].

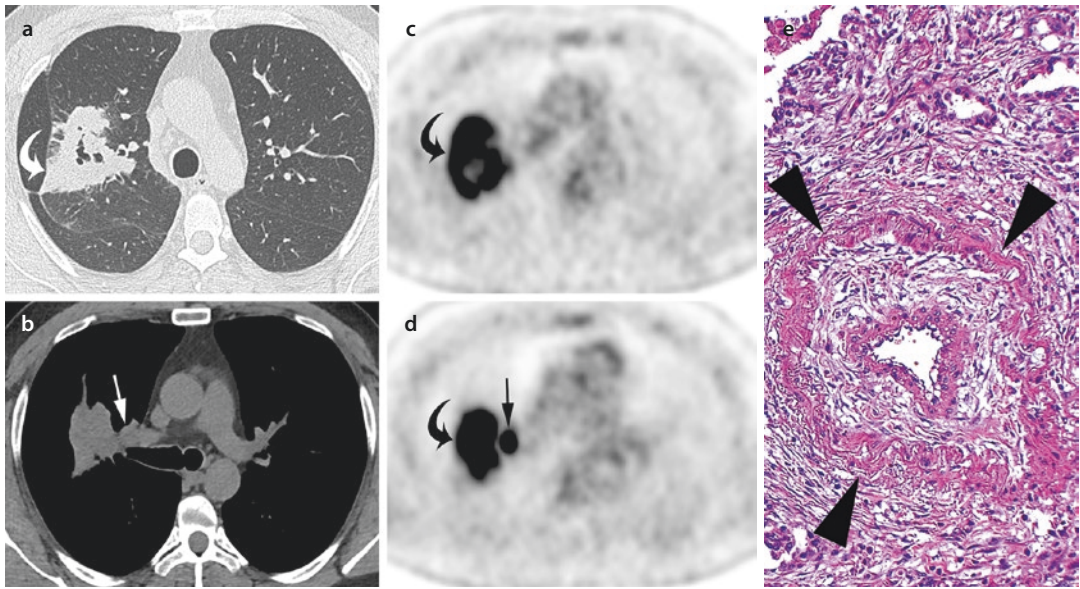


Fig. 4.2 Sarcomatoid carcinoma (spindle cell subtype) in a 54-year-old man who is heavy smoker. **a** Axial CT image with lung window setting shows an irregular mass with cavitation, pleural indentation, and pleural thickening (*curved arrow*) in the right upper lobe. **b** Axial CT image with mediastinal window setting reveals a hilar

lymphadenopathy (*arrow*). **c, d** Axial PET images demonstrate similar intense ^{18}F FDG uptake within the pulmonary mass (*curved arrow*) and hilar adenopathy (*arrow*). **e** Typical vascular invasion of the wall of an artery by spindle cell carcinoma (*arrowheads*) (H-E 10 \times)

4.2.2 Salivary Gland-Type Carcinomas of the Lung

4.2.2.1 Overview

Carcinoma of the salivary gland is an uncommon entity outside of the head and neck region [19]. The literature reports that this type of carcinoma may occur in other anatomic areas, such as the lung, breast, skin, and cervix [19]. Primary pulmonary salivary gland-type carcinomas (PSGCs) represent a small but distinct group of cancers that are thought to arise from the bronchial glands of the central airways [19, 20]. PSGCs are extremely rare, slow-growing, and low-grade malignant tumors, accounting for less than 0.5% of all lung cancers [19–22]. Based on the WHO classification of lung tumors [1], PSGCs include the following three histological subtypes, thereafter reported according to occurrence rate (Table 4.1) [19, 20]:

- Mucoepidermoid carcinoma
- Adenoid cystic carcinoma
- Epithelial-myoepithelial carcinoma

Adenoid cystic carcinoma is also the second most common primary malignancy of the trachea after squamous cell carcinoma [20].

The most uncommon subtype is epithelial-myoepithelial carcinoma, which is an extremely rare entity with less than hundred cases described in the English literature [19, 23–25].

Mucoepidermoid carcinoma does not exhibit a gender predilection and may occur at any age (range, 6–78 years) with a median age at diagnosis of approximately 40 years [20, 22, 24]. Adenoid cystic carcinoma seems to have a slight predilection for women and is more likely to occur in older patients than mucoepidermoid carcinoma [19, 20, 24]. In patients with adenoid cystic carcinoma, the median age at diagnosis is 54 years (range, 21–76 years) [24, 25]. Epithelial-myoepithelial carcinoma affects men and women equally with a median age at diagnosis of approximately 60 years (range, 36–75 years) [19, 20, 23, 25].

Unlike other NSCLCs, smoking is not a risk factor for PSGCs [20, 24]. The clinical signs and

symptoms of PSGCs are not specific and are usually related to the involvement of the tracheo-bronchial tree. The most common presenting signs and symptoms include cough, hemoptysis, dyspnea, fever, and chest pain [19, 20, 24, 25]. However, PSGCs may remain asymptomatic in approximately 20% of cases (especially peripheral tumors) [20, 25].

PSGCs are usually considered slow-growing, low-grade malignancies with a significantly better prognosis than that of other NSCLCs [19, 24]. The literature reports that more than 50% of patients with PSGC survive for a long time [19]. Among the PSGCs, adenoid cystic carcinoma appears to have a worse prognosis than that of mucoepidermoid carcinoma and epithelial-myoeplithelial carcinoma [24]. However, some authors have shown that older age (>58 years), larger lesions, poor differentiation, intrathoracic invasion, and metastases are associated with prognosis, hampering any association with the histological subtypes [19, 25]. Therefore, early diagnosis and treatment are crucial for improving the prognosis in PSGCs, regardless of their histological subtypes.

From a prognostic point of view, the preferred method for curative treatment is surgical resection [19, 25]. In particular, a complete surgical resection with negative margins is associated with better long-term outcomes [25]. Radiation therapy and chemotherapy should be addressed in case of positive resection margins or inoperable tumors [19, 25].

4.2.2.2 Pathology

The definitive diagnosis and the differentiation grade of PSGCs are made by pathological analysis of the surgical specimens [19, 22].

The histology of mucoepidermoid carcinoma of the lung typically exhibits a mixture of mucus-secreting cells, squamous cells, and intermediate cells [22, 25]. Low-grade mucoepidermoid carcinoma is characterized by cystic areas lined with mucinous cells mixed with intermediate cells and few mitoses (■ Fig. 4.3) [22, 25]. High-grade mucoepidermoid carcinoma has few cysts, more intermediate, cellular pleomorphism, atypical squamous cells, and frequent mitosis [25].

Adenoid cystic carcinomas typically exhibit a cribriform pattern with nests of basaloid cells with low mitotic activity (■ Fig. 4.4) [26].

Epithelial-myoeplithelial carcinoma exhibits biphasic differentiation of epithelial cells and myoeplithelial cells. Some authors report that the myoeplithelial component may play a prognostic role [23, 25].

4.2.2.3 Imaging

Early detection of PSGCs is uncommon because the early stage of disease is mostly asymptomatic or paucisymptomatic. Therefore, the diagnosis is often delayed due to the nonspecific signs and symptoms and the slow growth of these malignant tumors.

In clinical practice, chest radiography plays a limited role in the assessment of the tracheo-bronchial tree [20, 22]. This radiological technique may be helpful for detecting indirect signs of bronchial obstruction, such as distal atelectasis or pneumonia; however, it is not accurate for direct detection of the neoplasm [20, 22]. Therefore, CT is currently regarded as the preferred noninvasive imaging modality used for the detection and characterization of such airway lesions [20].

Most PSGCs present as a solitary nodule or mass with smooth or lobulated margins located in the central airways (■ Figs. 4.3 and 4.5) [14, 20, 22].

Although mucoepidermoid carcinoma and adenoid cystic carcinoma of the lung are both PSGCs, they have some distinctive features on CT imaging (■ Table 4.2). Mucoepidermoid carcinomas are more frequently found in the lobar or segmental bronchi and usually exhibit well-defined margins with a round or oval shape (■ Fig. 4.3) [20]. Less commonly, mucoepidermoid carcinoma is found in the trachea and main bronchi, displaying a polypoid shape (■ Fig. 4.5) [20, 27]. Conversely, adenoid cystic carcinomas have a predilection for the trachea and main or lobar bronchi and more commonly exhibit poorly defined margins with polypoid shape or circumferential thickening (■ Fig. 4.4) [20, 27].

PSGCs may demonstrate punctate calcifications and enhancement after injection of contrast agent;

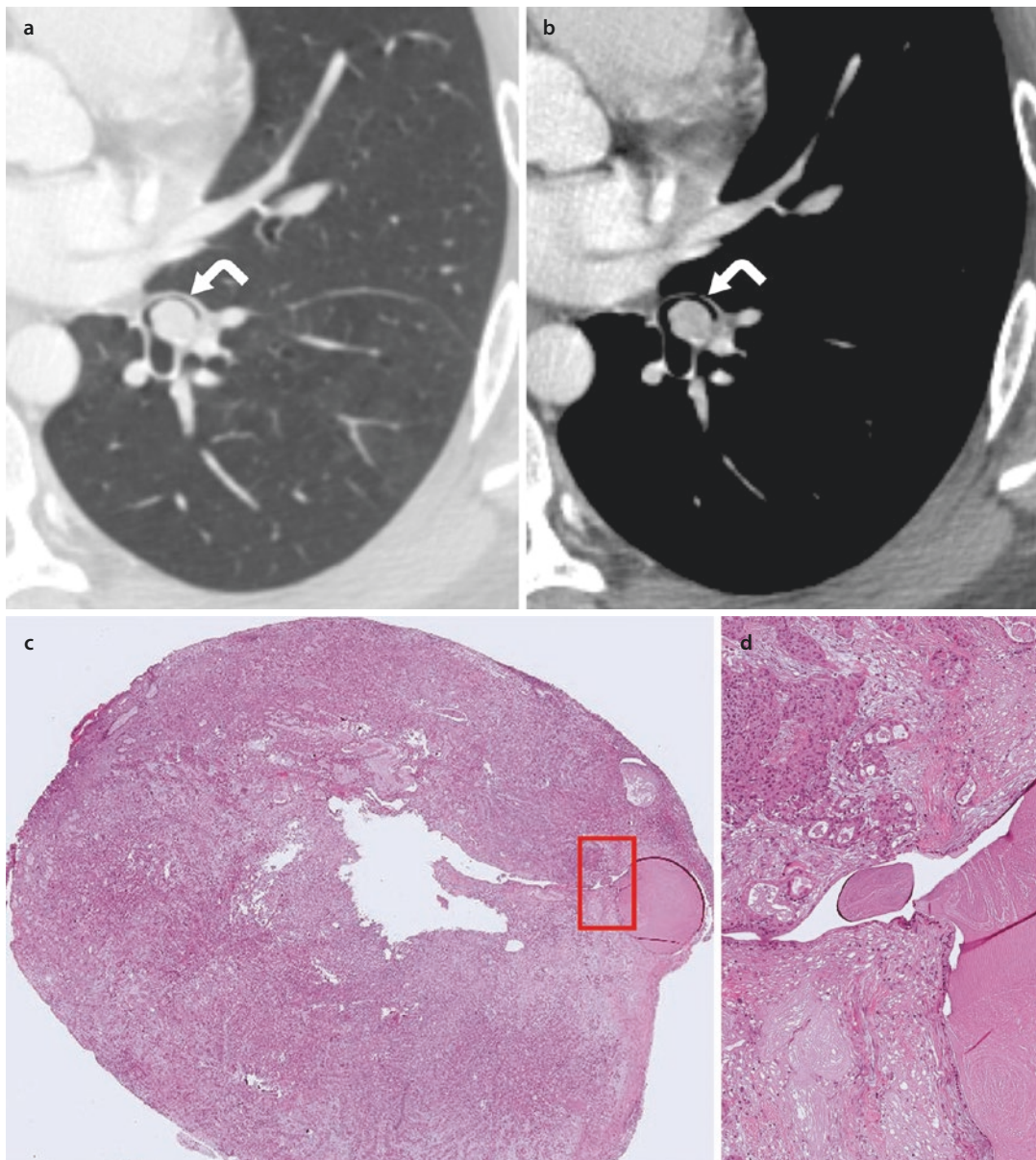


Fig. 4.3 Mucoepidermoid carcinoma in a 29-year-old man. **a, b** Axial CT images with lung and mediastinal window settings show a round lesion with smooth margins and contrast enhancement within the left inferior lobar bronchus (*curved arrows*). **c, d** Histological hematoxylin and

eosin images of the lesion at actual size **c** and at middle power $10\times$ **d**. The red square in **c** indicates the area of magnification displayed in **d**. The magnification in **d** shows a double neoplastic component that includes the cystic glandular component and nests of intermediate cells

these imaging features are more frequently observed in mucoepidermoid than adenoid cystic carcinomas [20, 27]. The literature also reports that PSGCs usually exhibit heterogeneous ^{18}F FDG uptake on PET/CT imaging (median SUVmax ranging from 2.8 to 5.8) with greater uptake in high-grade tumors and adenoid cystic carcinomas [20, 25, 28].

4.2.2.4 Local Spread and Metastatic Dissemination

The local spread of PSGCs depends on their histological subtype and location within the tracheobronchial tree. Mucoepidermoid carcinoma typically grows as intraluminal nodule within the

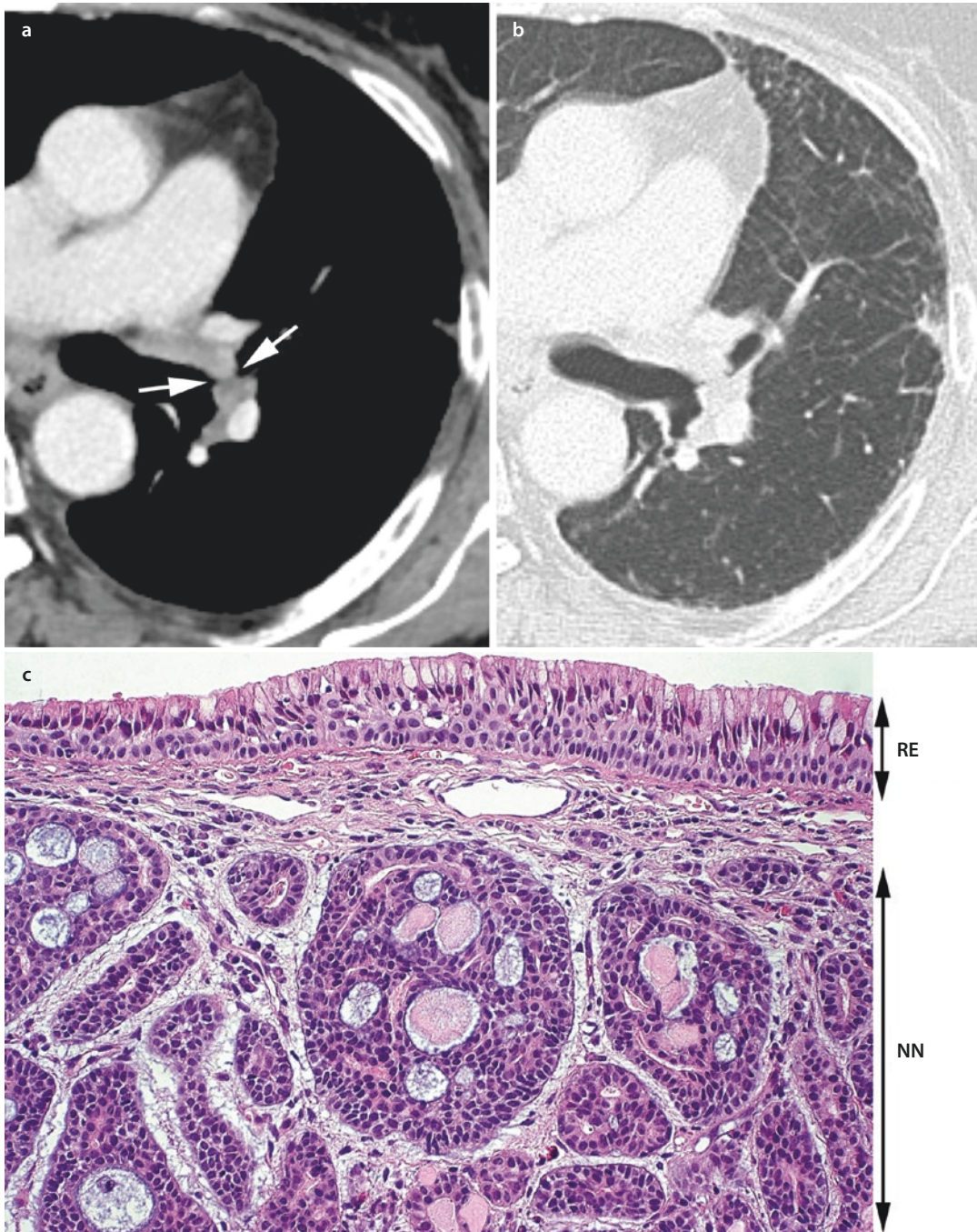


Fig. 4.4 Adenoid cystic carcinoma in a 59-year-old woman. **a, b** Axial CT images with mediastinal and lung window settings show an exophytic lesion with circumferential wall thickening of the left upper bronchus (*arrows*)

with associated bronchial stenosis and volume reduction of the left upper lobe. **c** Bronchial mucosa lined by respiratory epithelium (*RE*) and infiltrated by neoplastic nests (*NN*) with a typical cribriform appearance

lobar and segmental bronchi. Therefore, mucocylindroid carcinoma is oftentimes associated with atelectasis and postobstructive pneumonia.

Interestingly, oligemia with air trapping is also seen as a consequence of tumor-induced valve mechanism.

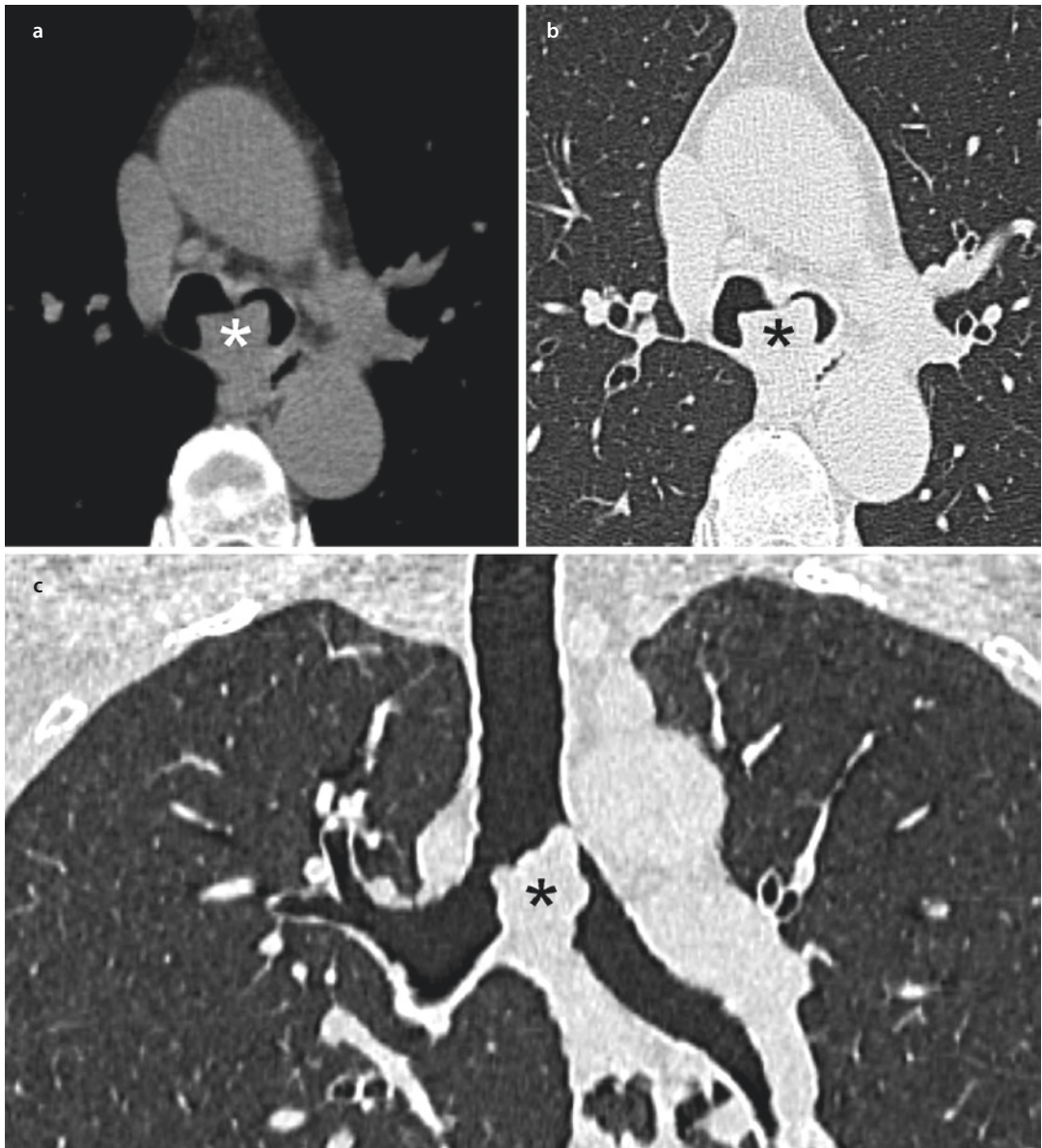


Fig. 4.5 Mucoepidermoid carcinoma in a 63-year-old woman. **a, b** Axial CT images with mediastinal and lung window settings demonstrate an exophytic lesion at the

level of the tracheal carina (*asterisk*). **c** Coronal CT image displays the polypoid shape of the lesion (*asterisks*)

In contrast, adenoid cystic carcinoma may occur within the more proximal airways (from the trachea to lobar bronchi) and have a predilection for submucosal spread with infiltrative growth. This peculiar pattern of growth is responsible for circumferential thickening and extraluminal extension, which are observed in approximately 20% of cases [20]. Therefore, in cases of adenoid cystic carcinoma, the description of intra- and extraluminal extension of the

tumor is paramount for optimal treatment planning [27]. From this point of view, magnetic resonance imaging (MRI) is regarded as the imaging reference standard for preoperative assessment of intraluminal and extraluminal components of adenoid cystic carcinomas. MRI is also considered useful in the follow-up because it is superior to CT in distinguishing between sign of recurrence and posttreatment fibrosis [20].

Generally, lymph node and distant metastases are uncommon in PSGCs, as expected by their nonaggressive behavior [20]. However, the literature reports that distant metastases (e.g., lung, brain, bones, chest wall, diaphragm, and liver) may be observed in up to one-third of patients and are more frequently found in adenoid cystic carcinomas [24].

4.3 Mesenchymal Malignant Lung Tumors

In addition to uncommon epithelial lung cancer, pulmonary lesions of mesenchymal origin may display a range of malignancy with clinical and radiological interest. Thereafter, the most interesting histotypes in this group are as follows:

- Epithelioid hemangioendothelioma (EHE)
- Pulmonary synovial sarcoma (SS)
- Pulmonary artery intimal sarcoma (PAIS)

4.3.1 Epithelioid Hemangioendothelioma

4.3.1.1 Overview

Epithelioid hemangioendothelioma (EHE) is a rare malignant vascular tumor of endothelial origin, accounting for less than 1% of all vascular tumors [1, 29–32]. EHE is a low- to intermediate-grade malignancy with clinical behavior and morphological features intermediate between hemangioma and angiosarcoma [1, 29–32]. EHE may develop in different tissues, and the most frequent sites are soft tissue, bone, liver, and lung [29]. The literature reports that only 12% of EHEs show a pulmonary origin [30]. The first case of pulmonary EHE was described in 1975 by Dail and Liebow [33].

This type of vascular tumor is more frequent in women, with a female-to-male ratio of 4:1 [30, 32, 34]. Pulmonary EHE may occur at any age (range, 7–83 years) with a peak of incidence around the fourth and fifth decades of life [30, 35].

Smoking and exposure to other carcinogenic agents are not considered risk factors for pulmonary EHE. However, certain authors suggest a possible association between *Bartonella* infection and the development of this malignancy. This

hypothesis is based on the peculiar activity of *Bartonella species* in determining epithelial proliferation, allegedly inducing an aberrant angiogenetic signal similar to the angiogenetic mechanism involved in the development of cancer [30, 36, 37].

The signs and symptoms of pulmonary EHEs are not specific, usually related to the involvement of adjacent structures such as the bronchial system, pleura, mediastinum, and chest wall [30]. Presenting signs and symptoms may include chest pain, cough, dyspnea, and hemoptysis [30, 32, 35]. However, approximately 50% of patients with pulmonary EHE have no signs or symptoms related to the disease [30, 35].

Pulmonary EHE is a cancer with borderline biological behavior and metastatic potential [1]. The 5-year survival rate ranges from 47% to 71% (median, 60%) [30, 38]. The prognosis is related to the differentiation grade of the tumor (low vs intermediate) and the presence of signs and symptoms [1, 30, 35]. Other negative prognostic factors include extensive intrapulmonary involvement, pleural effusion, and alveolar/pleural hemorrhage [1, 30, 35, 38].

No treatment guidelines have yet been established for pulmonary EHE [30, 32]. The currently available treatment options include surgical resection, radiation therapy, and systemic therapies, such as chemotherapy, immunotherapy, and targeted therapy.

Surgical resection is recommended in cases of limited and unilateral disease. In these cases, lymph node sampling or dissection should be performed even if their prognostic role is unclear due to the limited incidence of lymph node metastasis. The nonaggressive behavior and the radiobiological characteristics of pulmonary EHE are not suitable for radiation therapy [30]. Therefore, this treatment option may be considered only to control the residual disease after surgical resection.

Systemic therapies may be considered in case of widespread disease; however, their effectiveness is still debated [30, 39].

Finally, in case of multiple and bilateral nodules with little or no growth on serial imaging, the “wait-and-see” approach may be proposed as a valid alternative to conventional treatments, especially if we consider the potential spontaneous regression reported in EHE [30, 39].

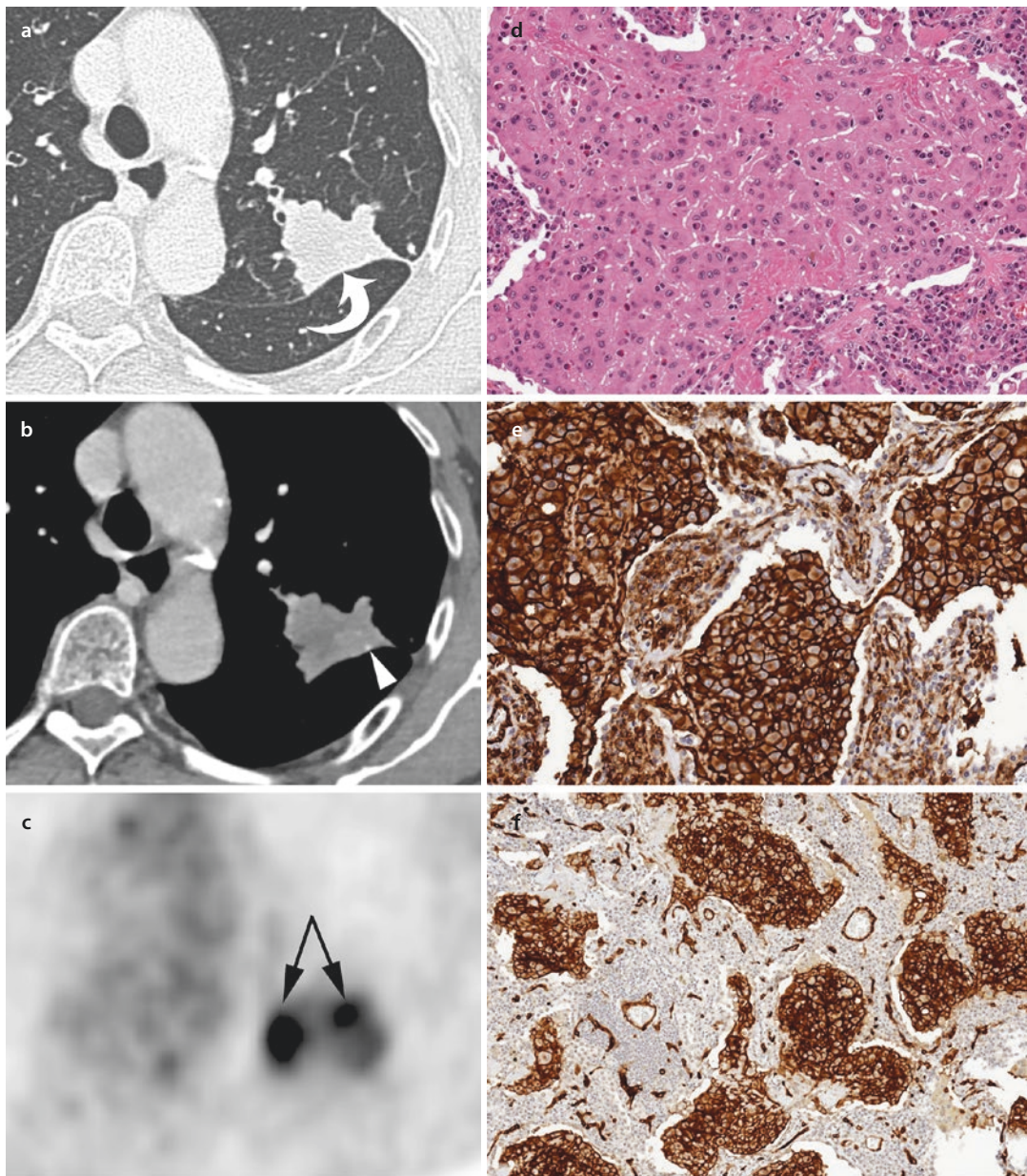


Fig. 4.6 Epithelioid hemangioendothelioma in a 70-year-old woman. **a** Axial CT image with lung window setting shows an irregular solitary mass with pleural indentation and pleural thickening (*curved arrow*) in the left upper lobe. **b** Axial CT image with mediastinal window setting demonstrates the heterogeneous enhancement of the mass and a punctate calcification

(*arrowhead*) at the periphery of the lesion. **c** Axial PET image displays the heterogeneous ^{18}F FDG uptake within the lesion (*arrows*). **d** Histological hematoxylin and eosin image of the lesion at 20 \times showing an intra-alveolar nest of epithelioid cells. **e, f** Anti-CD31 **e** and anti-CD34 **f** immunostaining showing strong reactivity of the epithelioid cells

4.3.1.2 Pathology

The diagnosis of pulmonary EHE is usually confirmed by pathological examination of open-lung or thoracoscopic biopsy [39]. Histologically, pulmonary EHE is composed of nests and short

corde of epithelioid endothelial cells (■ Figs. 4.6 and 4.7), frequently incorporated in a myxohyaline stroma. The histological diagnosis requires confirmation by immunohistochemical analysis, where EHE reveals strong reactivity to

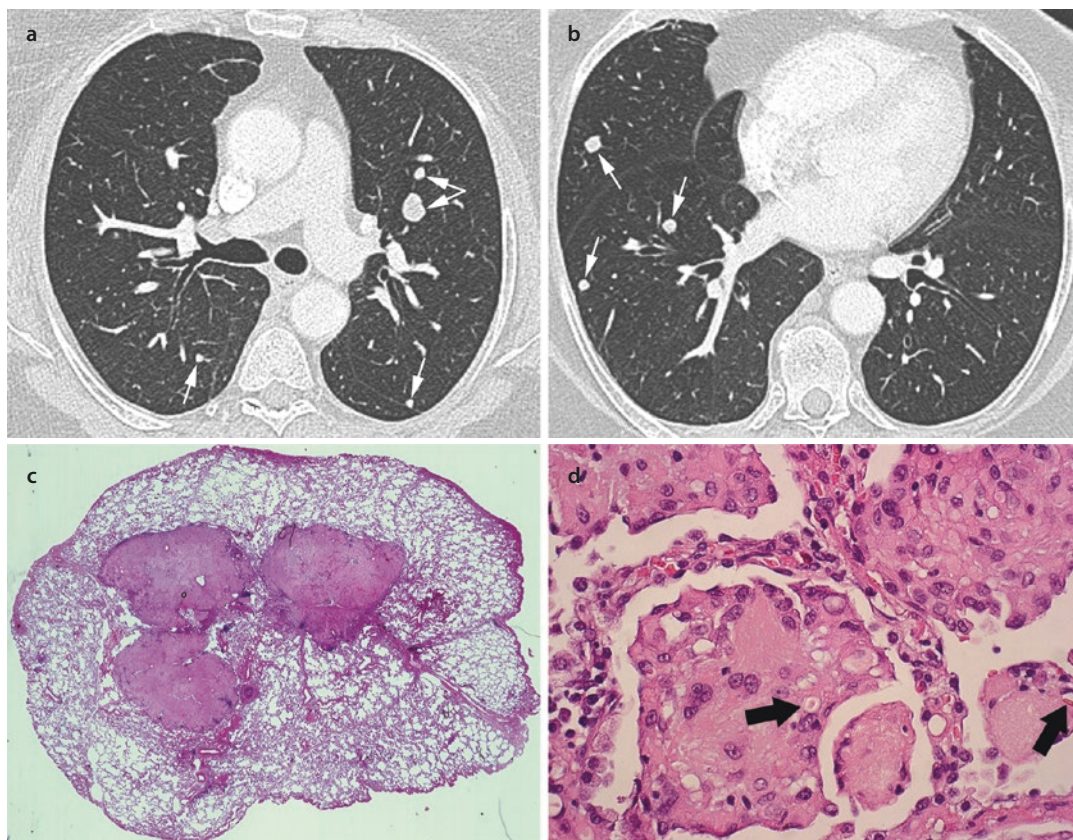


Fig. 4.7 Epithelioid hemangioendothelioma in a 66-year-old woman. **a, b** Axial CT images with lung window setting demonstrate multiple pulmonary nodules (*thin arrows*). **c** Histological hematoxylin and eosin (H-E) image

(actual size) of the wedge resection containing three nodules of epithelioid hemangioendothelioma. **d** Note that some epithelioid cells have cytoplasmic vacuoles containing red blood cells (*large arrows*) (H-E 40×)

vascular-specific markers (CD31 and CD34) (Fig. 4.6) [1].

In addition, cytogenetic studies have demonstrated that t(1;3)(p36.3;q25) chromosomal translocation is characteristic of EHE [1, 32].

4.3.1.3 Imaging

The radiological diagnosis of pulmonary EHEs is quite challenging, mainly because of their low incidence and their extremely slow growth rate. However, these tumors have some specific imaging features that might prompt the early brilliant diagnosis of pulmonary EHE by CT (Table 4.3).

On CT imaging, pulmonary EHE shows three main patterns of parenchymal involvement:

- Multinodular
- Solitary mass
- Reticulonodular

The most common pattern of pulmonary involvement is multinodular, followed by solitary mass and the reticulonodular pattern [35].

The multinodular pattern appears as multiple well-defined nodules less than 1 cm and potentially up to 2 cm in diameter (Fig. 4.7) [14, 27, 30, 32, 35]. The nodules are perivascular with smooth or lobulated margins and are more frequently located at the peripheral region of the lungs [14, 27, 30, 32, 35]. Sometimes, pulmonary EHE occurs as a large solitary pulmonary mass with lobulated or spiculated margins, resembling a common NSCLC (Fig. 4.6) [30, 35]. The reticulonodular pattern is rarely observed. This pattern exhibits multiple poorly defined nodules associated with irregular thickening of the peribronchovascular interstitium [35].

Pleural indentation may occur in subpleural nodules in the multinodular pattern, whereas it is

Table 4.3 Mesenchymal malignant lung tumors: key imaging features and main differential diagnoses

Tumor type	Key features on CT and PET/CT	Main differential diagnoses
Epithelioid hemangioendothelioma	Multinodular pattern Multiple perivascular nodules (≤ 2 cm) Peripheral region of the lung Smooth or lobulated margins	Pulmonary metastases Granulomatous diseases Benign metastasizing leiomyoma
	Solitary mass pattern Large mass with pleural indentation or pleural thickening Heterogeneous contrast enhancement Heterogeneous ^{18}F FDG uptake	Other NSCLCs
Synovial sarcoma	Solitary pleural-based mass Large (>5 cm) with well-defined margins Intratumoral vessels Heterogeneous contrast enhancement Pleural effusion	Pulmonary metastases from extrathoracic sarcoma Other high-grade NSCLCs
Pulmonary artery intimal sarcoma	Intraluminal filling defects occupying the entire lumen of pulmonary artery Surface nodularity of filling defects Wall eclipse sign Extravascular spreading Heterogeneous and delayed contrast enhancement ^{18}F FDG uptake	Pulmonary thromboembolism

FDG 18-fluorodeoxyglucose, NSCLC non-small-cell lung cancer

frequently observed in solitary masses along with pleural thickening (■ Fig. 4.6). Punctate calcification may occur within nodules or masses (■ Fig. 4.6) [27, 30], while necrosis and cavitation are unusual in pulmonary EHE [32].

On contrast-enhanced CT, pulmonary EHE exhibits mild heterogeneous enhancement [32].

The literature also reports that pulmonary EHEs measuring more than 2 cm in diameter may exhibit heterogeneous ^{18}F FDG uptake on PET/CT imaging (■ Fig. 4.6) [40]. In these cases, the increase in ^{18}F FDG uptake is probably related to the more aggressive behavior of the lesion. Therefore, PET/CT could be useful in the management of patients with multiple nodules, as it may help in selecting the surgical target [40].

4.3.1.4 Local Spread and Metastatic Dissemination

Pulmonary EHE is considered a locally aggressive neoplasm, yet with intermediate potential to systemic metastases. Local spread and metastatic dissemination of such rare vascular neoplasm depend on its pattern of distribution within the

lung (multinodular, solitary mass, or reticulonodular).

In the multinodular pattern, nodules exhibit predominant subpleural locations with pleural indentations [32]. From the subpleural regions, the nodule could extend deeper into the pleura and cause pleural thickening and subsequently pleural effusion. However, pleural effusion is an uncommon finding in the multinodular pattern [35]. A similar local spread can be observed when pulmonary EHE occurs as a large solitary pulmonary mass. In this pattern, pleural involvement with or without effusion is frequently observed (■ Fig. 4.6).

In the reticulonodular pattern, the local spread of EHE occurs predominantly into the peribronchovascular interstitium with infiltrative tumoral proliferation within the lumen of adjacent vessels [35, 41]. This pattern of growth suggests a more aggressive clinical course with early metastasis and, consequently, worse prognosis [35].

Metastatic dissemination of pulmonary EHE may occur through the blood and lymphatic vessels, as well as the pleural cavity. While distant

organ metastases are observed in 20–30% of cases, less than 10% shows hilar and/or mediastinal lymph nodes [42]. Distant hematogenous metastases occur mainly to the liver and bone; however, metastases in other sites (such as the skin, serosa, spleen, tonsils, retroperitoneum, kidneys, and colon) have been described [30].

4.3.2 Synovial Sarcoma

4.3.2.1 Overview

Synovial sarcoma (SS) is a malignant tumor that mainly occurs within the soft tissue of the extremities [43]. Primary involvement of the thorax is rare and includes different sites of origin, such as lung, mediastinum, pleura, and chest wall [43, 44]. Although the name of this lung cancer suggests a synovial origin, pulmonary SS develops from immature mesenchymal elements [45]. Pulmonary SS is extremely rare, accounting for less than 0.5% of all lung cancer cases [45, 46], the first of such case was described in 1995 by Zeren et al. [47]. As per its singularity, the diagnosis of pulmonary SS can only be confirmed after excluding metastatic extrathoracic sarcoma and other sarcoma-like lung malignancies.

Pulmonary SS shows neither gender nor age predilection (range, 9–77 years), with some peak of incidence around the second and the third decades of life [43, 45, 48]. Cigarette smoking is not a risk factor for pulmonary SS; in fact, most patients with pulmonary SS are never smokers.

The signs and symptoms of pulmonary SS are not specific. The most common signs and symptoms include chest pain, dyspnea, cough, and hemoptysis [45, 48, 49]. However, the literature reports that approximately 40% of patients with pulmonary SS are asymptomatic [48].

Pulmonary SS is a cancer with aggressive behavior, a high local recurrence rate, and a high metastatic potential [49, 50]. The 2-year disease-free survival rate is approximately 36% [43, 45]. The prognosis is generally poor and mainly related to the primary tumor size, treatment method, and the presence of local recurrence and/or distant metastases [45, 48]. Noteworthy, the incomplete resection is a major negative prognostic factor [43, 45, 48, 49]. Therefore, from a prognostic point of view, the best treatment

modality of pulmonary SS is complete surgical resection with free surgical margins [43, 44, 48, 49]. Adjuvant chemotherapy and/or radiation therapy may prolong disease-free survival [43, 44, 48, 49]. Chemotherapy with or without radiation therapy may be used in the treatment of non-resectable advanced disease.

4.3.2.2 Pathology

SS is a mesenchymal tumor characterized by variable epithelial differentiation [48]. Histologically, SS may be monophasic (only spindle cell or only epithelial cell) or biphasic (variable amount of both components) [43, 45, 48, 49]. The monophasic spindle cell subtype is the most common in the respiratory system (■ Fig. 4.8) [44, 45]. On immunohistochemistry, most pulmonary SSs reveal reactivity for cytokeratin, epithelial membrane antigen (EMA), Bcl-2, and vimentin [45].

The t(X;18)(p11;q11) chromosomal translocation, which can be demonstrated by fluorescence in situ hybridization (FISH) analysis, is the cytogenetic hallmark of SS (■ Fig. 4.8) [43, 45, 49].

4.3.2.3 Imaging

The imaging features of pulmonary SS may be similar to those of other lung cancers; however, some distinctive features may be observed (■ Table 4.3).

On CT images, most cases of pulmonary SS present as a solitary pleural-based mass (■ Fig. 4.8). The mass is usually well defined and large, with a diameter greater than 5 cm [43, 45, 48]. Punctate or amorphous calcifications are found in approximately 50% of cases [45]. Pulmonary SS shows heterogeneous enhancement after injection of iodinated contrast agent, typically with central low density that reflects intralesional necrosis, hemorrhage, or cystic changes (■ Fig. 4.8) [43, 45, 48]. Intratumoral vessels are frequently observed in pulmonary SS.

Although the data on metabolic activity are rather limited, some authors report that most pulmonary SS display ¹⁸F-FDG uptake on PET/CT imaging [45].

4.3.2.4 Local Spread and Metastatic Dissemination

Pulmonary SS is considered an aggressive mesenchymal tumor with high metastatic potential.

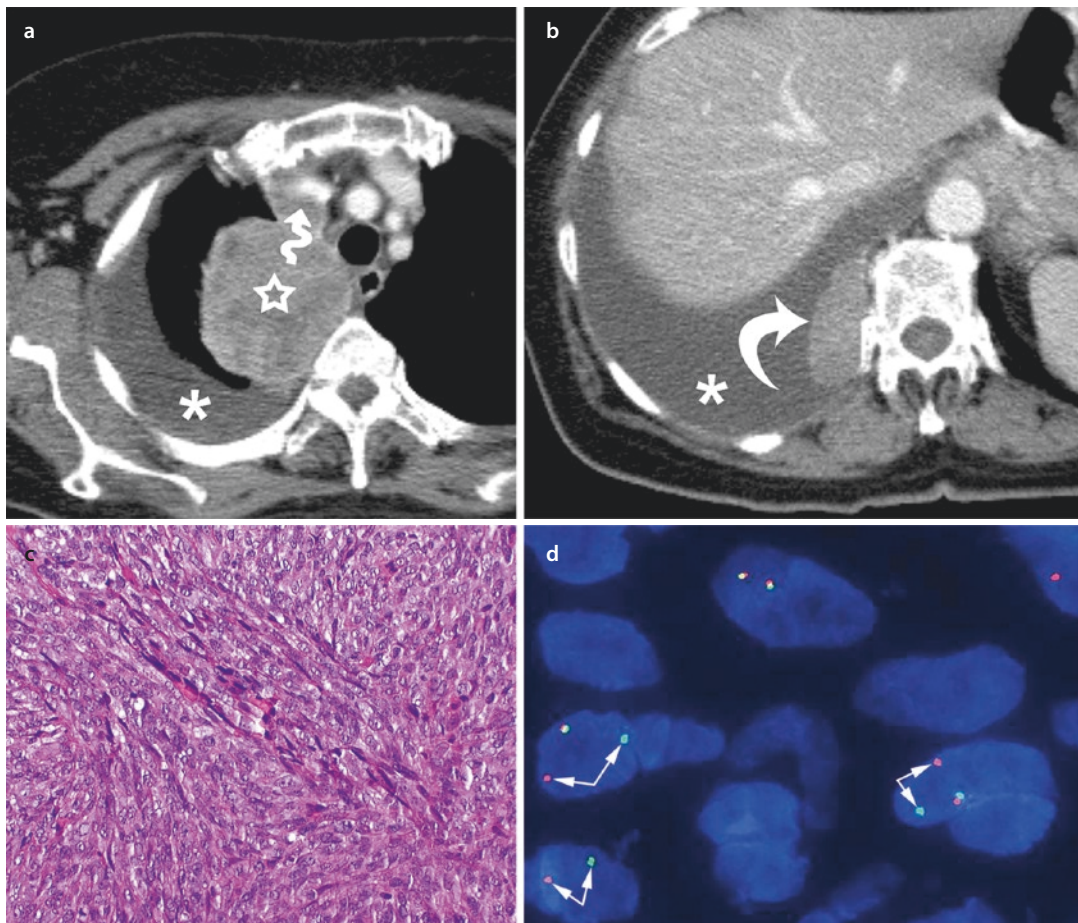


Fig. 4.8 Synovial sarcoma in a 74-year-old woman. **a, b** Axial CT images with mediastinal window setting show a pleural-based mass with heterogeneous enhancement in the right upper lobe (*star*). The mass infiltrates the mediastinum (*wavy arrow*). CT images with mediastinal window also demonstrate pleural localization (*curved arrow*) with associated pleural effusion (*asterisk*).

c Histological hematoxylin and eosin (H-E) image showing the monophasic spindle cell subtype of synovial sarcoma (H-E 20 \times). **d** FISH analysis with a break-apart probe demonstrates rearrangement of the SS18 (18q11) locus, shown as the splitting of red and green signals (*arrows*). (Courtesy of Dr. Piera Balzarini, Department of Molecular and Translational Medicine, University of Brescia, Italy)

The local spread of this uncommon cancer depends on its position within the lung. In its typical pleura-based location, pulmonary SS displays the peculiar characteristic of rupturing in the pleural space with hemothorax or pleural effusion (Fig. 4.8). This pattern of growth and evolution is observed in approximately 50% of cases [45], and it is frequently associated with metastatic dissemination throughout the pleural cavity (Fig. 4.8).

While the tumors in contact with the mediastinal pleura spread into the mediastinum or pericardium (Fig. 4.8), the tumors in contact with the costal pleura frequently spread into the extra-

pleural fat and/or chest wall, more often without bony involvement [45].

Metastatic dissemination of pulmonary SS may occur via the blood and lymphatic vessels. However, in contrast with other primary lung cancers, hilar and/or mediastinal adenopathy is very rare in pulmonary SS [45, 48]. Therefore, a well-defined large and pleura-based pulmonary mass without large adenopathy accompaniment may suggest a diagnosis of pulmonary SS rather than another lung cancer, notably in young adult patient [45, 48].

Distant hematogenous metastases occur mainly to the bone, liver, brain, and contralateral lung [50].

The literature also reports the exceptional possibility of spontaneous regression of pulmonary SS [46].

4.3.3 Pulmonary Artery Intimal Sarcoma

4.3.3.1 Overview

Pulmonary artery intimal sarcoma (PAIS) is an uncommon malignant tumor with a very low incidence. The reported incidence rate of this extremely rare malignancy is 0.001–0.030%, and only approximately 300 cases have been described in the literature [51, 52]. However, the incidence of PAIS might be underestimated because of potential misinterpretation as pulmonary thromboembolism [53].

The first case of PAIS was reported in 1923 by Mandelstamm [54]. This type of malignant tumor seems to have a predilection for women, with a female-to-male ratio of 2:1 [52, 53]. PAIS may occur at any age (range, 13–80 years), with a mean age at diagnosis of approximately 55 years [51, 53].

The signs and symptoms of PAIS are insidious and nonspecific and can simulate acute or chronic pulmonary thromboembolic disease [51–55]. Presenting signs and symptoms may include dyspnea (the most common), chest pain, cough, hemoptysis, and fatigue [51–53, 55].

PAIS is an aggressive malignant tumor with an extremely poor prognosis [52]. Therefore, early diagnosis and proper treatment are crucial for improving patient survival. From a prognostic point of view, many authors claim that complete surgical resection is the only effective therapy in patients with PAIS [51–53, 55, 56]. However, the 5-year survival rate is approximately 20% despite radical resection [51]. The role of adjuvant therapy has yet to be defined, although some studies have demonstrated its effectiveness [51, 55–57]. Likewise, the advantage of combination therapy by chemotherapy and radiation therapy is still unclear.

4.3.3.2 Pathology

PAIS is a poorly differentiated malignant mesenchymal tumor that originates from the intimal layer of the elastic pulmonary artery [52, 53, 55, 58]. PAIS may have features of low-grade spindle cell sarcoma or undifferentiated pleomorphic sar-

coma. It may also contain heterologous elements, mostly osteosarcoma and chondrosarcoma (■ Fig. 4.9) [52, 53, 58]. Immunohistochemical staining of PAIS reflects the specific differentiation of the tumor [58]. Undifferentiated sarcoma usually exhibits diffuse reactivity for vimentin [52, 58].

4.3.3.3 Imaging

PAIS is a proximal and diffuse tumor that occurs within the pulmonary artery, mainly with a tumoral impaction appearance [53]. This type of tumor represents a complex diagnostic challenge, as it may be mistaken for acute or chronic pulmonary thromboembolism [51, 53, 55].

Imaging by CT grants the injection of contrast agent for comprehensive characterization of the mass within the inner vascular aspect and the bloodstream. The main CT features suggestive of PAIS include intraluminal filling defects occupying the entire lumen of the pulmonary artery (tumoral impaction pattern), wall eclipse signs, bulging/lobulating contours, surface nodularity, intratumoral vessels, and heterogeneous and delayed contrast enhancement (■ Fig. 4.9) (■ Table 4.3) [53, 55, 59].

Despite their limitations, ¹⁸F-FDG PET/CT and MRI may be used as second-level imaging modalities in doubtful cases or to confirm the diagnostic hypothesis of PAIS [53, 55].

On PET/CT imaging, PAIS shows hypermetabolic ¹⁸F-FDG uptake [53, 55]. On MRI, PAIS typically displays intermediate to high signal intensity on T1-weighted sequences, diffusion restriction on diffusion-weighted images, and heterogeneous contrast enhancement [53].

4.3.3.4 Local Spread and Metastatic Dissemination

PAIS typically shows intraluminal growth pattern with a progressive reduction of the lumen of the pulmonary artery, as depicted by contrast-enhanced CT. From its site of origin, the tumor may spread along the intima, usually in the direction of blood flow [51, 52]. Sometimes, PAIS may also show a retrograde extension into the pulmonary valve or the right ventricle [51, 60].

At the time of diagnosis, the most commonly involved site is the main pulmonary artery (85%), followed by the right pulmonary artery (71%), the left pulmonary artery (65%), the pulmonary valve

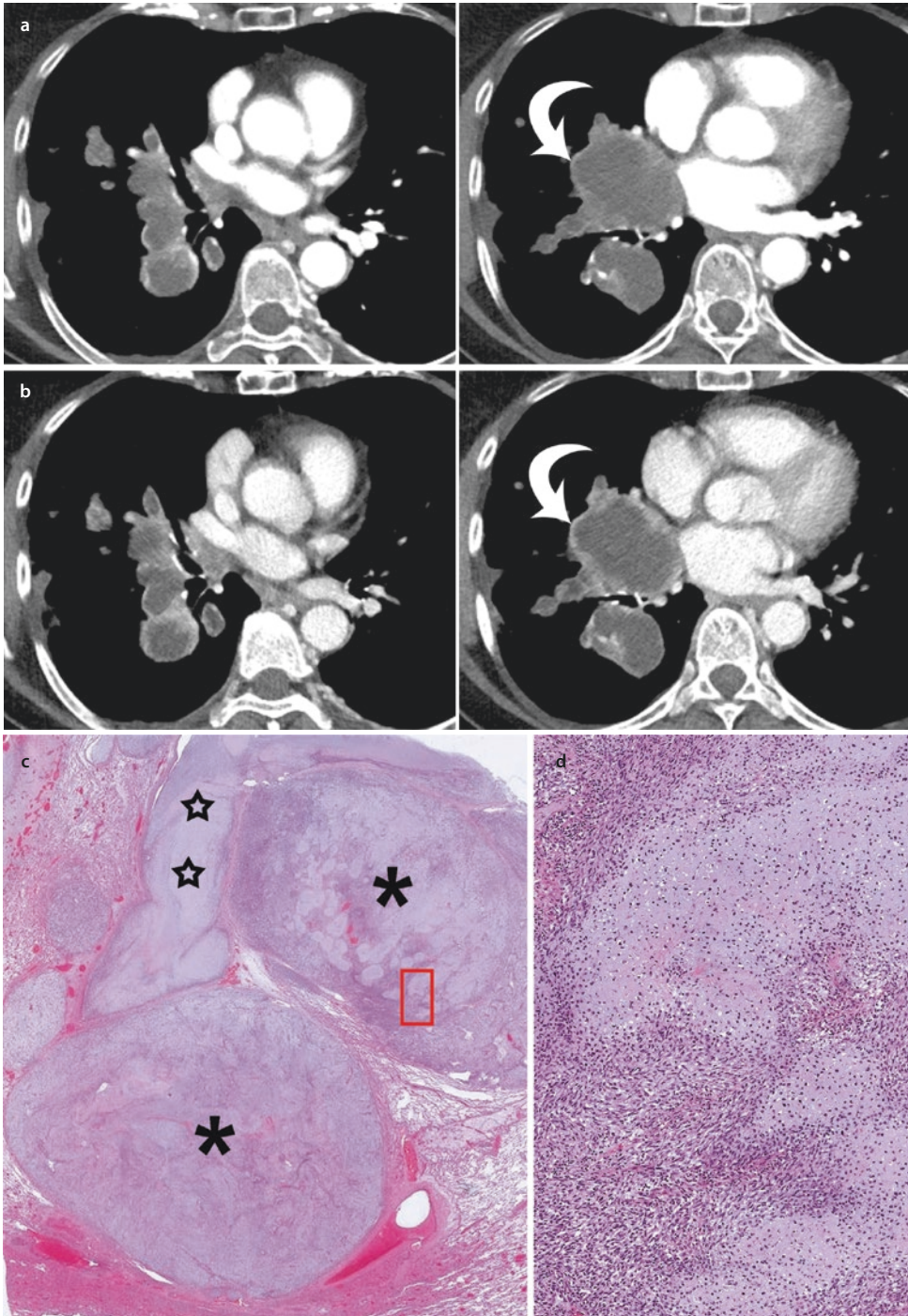


Fig. 4.9 Pulmonary artery intimal sarcoma in a 63-year-old woman. **a, b** Axial CT images obtained in arterial **a** and venous **b** phases demonstrate significant tumoral impaction within the branches of the right pulmonary artery. The lesion shows a peripheral enhancement on the venous phase and a prominent extravascular/intrapulmonary extension (*curved arrows*).

c, d Histological hematoxylin and eosin (H-E) images of the lesion at actual size **c** and at middle power $10\times$ **d**. The red square in **c** indicates the area of magnification displayed in **d**. At actual size, the endovascular (*stars*) and intrapulmonary nodules (*asterisks*) of intimal sarcoma are depicted. The magnification in **d** shows spindle cell neoplasia with cartilaginous differentiation

(32%), and the outflow tract of the right ventricle (10%) [52]. However, in most cases, two or more sites are involved [52]. Sometimes, extravascular spreading may be observed [51, 55]; this pattern of local dissemination is particularly useful in the differential diagnosis between PAIS and pulmonary embolism.

Lymph node and distant metastases are uncommon in PAIS, most likely due to the peculiar characteristics of the pulmonary artery and the pulmonary circulation (i.e., a low-pressure, low-resistance system carrying mixed venous blood to the lungs) [51].

Distant metastases occur mainly in the lung [51, 53, 55]; however, metastases in other sites (such as the brain, pleura, chest wall, bone, thyroid, and adrenal gland) have been reported [51, 53].

4.4 Lymphoid Malignant Lung Tumors

The pulmonary lymphoid system is complex and composed of lymphatics and bronchus-associated lymphoid tissue (BALT) [61]. According to the WHO classification of lung tumors [1], malignant pulmonary lymphoid lesions include the following:

- Extranodal marginal zone lymphoma of mucosa-associated lymphoid tissue (MALT lymphoma)
- Diffuse large cell lymphoma
- Intravascular large B-cell lymphoma

Among these malignant lesions, MALT lymphoma is the most common subtype.

4.4.1 MALT Lymphoma

4.4.1.1 Overview

Pulmonary MALT lymphoma is an extranodal low-grade lymphoma arising in the marginal zone from a B-cell progenitor within the BALT [61, 62]. The lymphoid aggregates of bronchial MALT are predominantly located in the peribronchial interstitium (divisions of the respiratory bronchioles) and to a lesser extent in the bronchial walls, interlobular septa, and subpleural interstitium. MALT lymphoma is the most common subtype of primary pulmonary lymphoma; it represents up

to 90% of pulmonary lymphoma [61, 62]. Still, MALT lymphoma remains a rare tumor accounting for less than 1% of all lung cancers [61, 63].

MALT lymphoma may develop in different tissues; the most frequent site is the stomach, while the lung is the most common non-gastrointestinal site [62, 63].

The first cases of pulmonary MALT lymphoma were described in 1984 by Herbert et al. [64]. This subtype of lymphoma does not follow a clear gender predilection and occurs mostly in the fifth and sixth decades of life. MALT lymphoma would seem to be related to chronic exposure to different antigen stimuli, such as smoking, autoimmune diseases, or infections [61, 62, 65].

The clinical signs and symptoms of MALT lymphoma are not specific and may include cough, dyspnea, chest pain, fever, weight loss, fatigue, and occasionally hemoptysis [66]. However, MALT lymphoma may remain asymptomatic in approximately 40–50% of cases and is often discovered as an incidental finding on imaging [61, 63, 65–67].

Pulmonary MALT lymphoma typically has indolent behavior and a good prognosis [61, 63, 65–67]. However, this tumor shows as high as 50% recurrence rate within 2 years after the initial diagnosis [61, 65]. Recurrent disease has a tendency to occur in areas containing MALT, such as the lung and gastrointestinal mucosa [61, 65]. The 5-year survival rate ranges from 84% to 94% [61, 63, 65, 67].

The main treatment modalities for MALT lymphoma include surgery, chemotherapy, and radiation therapy. Surgery and/or radiation therapy is preferred for localized tumors, whereas chemotherapy is favored in case of disseminated disease [61, 63, 65]. Nevertheless, the “wait-and-see” approach might represent an option according to the indolent course of the disease [66].

4.4.1.2 Pathology

The diagnosis of pulmonary MALT lymphoma requires adequate tissue sampling with immunohistochemical analysis [61].

Histologically, MALT lymphoma is characterized by small lymphocytes interspersed with a variable number of plasma cells [61, 65, 67], forming nodules and mass-like lesions. The disease spreads along the alveolar septa, the adjacent bronchovascular bundles, the interlobular septa,

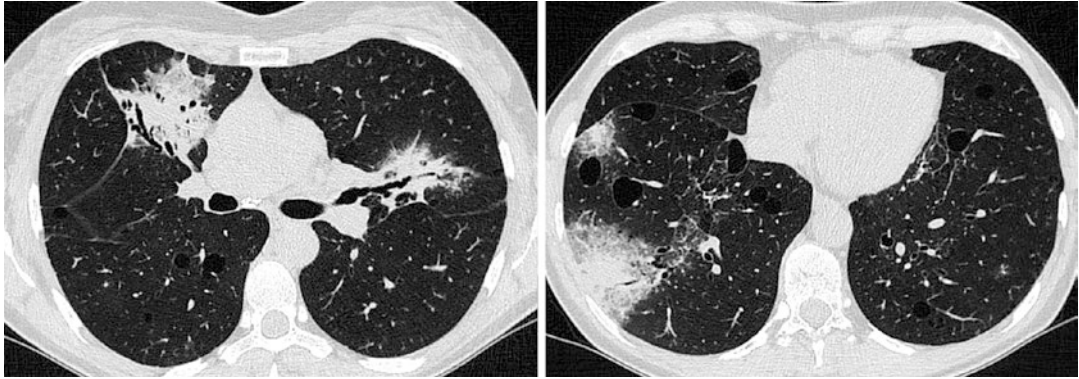


Fig. 4.10 Pulmonary MALT lymphoma in a 46-year-old woman. In both lungs, axial CT images show multiple consolidations, most with air bronchogram and some

degree of bronchial distortion. Multiple pulmonary cysts are also shown

Table 4.4 Pulmonary MALT lymphoma: key imaging features and main differential diagnoses

Tumor type	Key features on CT and PET/CT	Main differential diagnoses
MALT lymphoma	Consolidation (often with air bronchogram) Solid nodules or masses High ^{18}F FDG uptake	Invasive mucinous adenocarcinoma Other lymphoproliferative disorders Organizing pneumonia

MALT mucosa-associated lymphoid tissue, *FDG* 18-fluorodeoxyglucose, *NSCLC* non-small-cell lung cancer

and the visceral pleura (i.e., lymphangitic spread) [61, 65, 67].

Immunohistochemical analysis is pivotal for confirming the B-cell populations (such as positivity for CD19 and CD20) with the possible monoclonal expression of light chains by accompanying plasma cells.

4.4.1.3 Imaging

The CT findings of MALT lymphoma are heterogeneous and include single or multiple lesions, round or segmental consolidations, and nodules or masses with a predominant bronchovascular distribution [61, 62, 65]. Peribronchial consolidation, frequently associated with air bronchogram, is the most common CT feature (Fig. 4.10), followed by solid nodules and masses (Table 4.4)

[61, 62, 65–67]. Indeed, such consolidations might be limited in size or reach lobar extent. The bronchi within the lymphomatous consolidation are distorted (dilated, stretched, or narrowed), similar to the alterations seen in invasive mucinous adenocarcinoma (pneumonic-type) [68]. More rarely, MALT lymphoma manifests as interstitial disease or persistent subsolid nodules (Fig. 4.11) [62].

Parenchymal cysts are sometimes seen in association with MALT lymphoma, while intraleisional cavitation and calcifications are uncommon (Fig. 4.10) [62]. The CT angiogram sign may be observed on contrast-enhanced CT images, yet this feature is quite nonspecific [61].

On ^{18}F FDG PET/CT imaging, pulmonary MALT lymphomas exhibit an intense uptake in most cases (Fig. 4.11), and the ^{18}F FDG avidity is significantly related to lesion size [62].

4.4.1.4 Local Spread and Metastatic Dissemination

MALT lymphoma usually remains confined to the lung, although multiorgan involvement may occur in the late course of disease.

Locally, pulmonary MALT lymphoma shows a lymphangitic spread along the interstitium resulting in areas of ground-glass opacity and also interlobular reticulation [61, 65]. In addition, the tumor may spread along airways, occasionally determining a mosaic attenuation pattern that reflects small airway disease [61, 62].

While pleural effusion is uncommon, thoracic lymphadenopathies may occur in up to one-third of cases [61, 62, 67]. Likewise, the primary

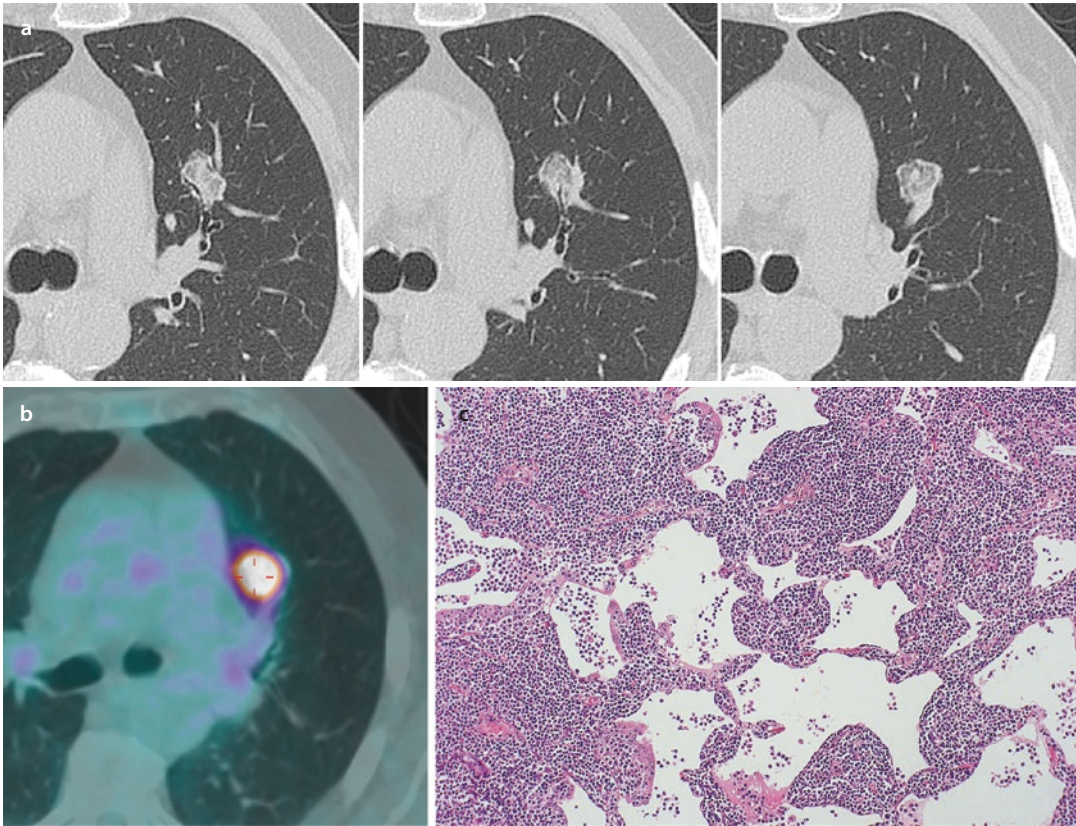


Fig. 4.11 Pulmonary MALT lymphoma in a 76-year-old man. **a** A series of axial CT images showing a single peribronchovascular subsolid nodule in the left upper lobe. **b** Axial fused PET/CT image demonstrates the intense ^{18}F FDG uptake of the nodule. **c** Histological hematoxylin and eosin

(H-E) image obtained after pulmonary segmentectomy displays a lymphoid interstitial infiltrate characterized by small monomorphic lymphocytes with only partial effacement of the alveolar architecture that reflects the subsolid appearance of the nodule on CT images (H-E 10 \times)

pulmonary lesion of MALT lymphoma, also its lymph node localization, exhibits high ^{18}F FDG uptake on PET/CT imaging [62].

Sometimes, extrapulmonary localizations of MALT lymphoma may be observed, especially in the stomach [62]. In these cases, ^{18}F FDG PET/CT imaging is particularly useful for adequate staging of the disease because it is more sensitive than CT for detecting extrapulmonary localizations.

References



1. Travis WD, Brambilla E, Nicholson AG, Yatabe Y, Austin JHM, Beasley MB, et al. The 2015 World Health Organization classification of lung tumors: impact of genetic, clinical and radiologic advances since the 2004 classification. *J Thorac Oncol.* 2015;10:1243–60.
2. Harms A, Herpel E, Pfarr N, Penzel R, Heussel CP, Herth FJ, et al. NUT carcinoma of the thorax: case report and review of the literature. *Lung Cancer.* 2015;90:484–91.
3. Liang Y, Wang L, Zhu Y, Lin Y, Liu H, Rao H, et al. Primary pulmonary lymphoepithelioma like carcinoma: fifty-two patients with long-term follow-up. *Cancer.* 2012;118:4748–58.
4. Hou J, Xing L, Yuan Y. A clinical analysis of 114 cases of sarcomatoid carcinoma of the lung. *Clin Exp Med.* 2018;18:555–62.
5. Pelosi G, Sonzogni A, De Pas T, Galetta D, Veronesi G, Spaggiari L, et al. Review article: pulmonary sarcomatoid carcinomas: a practical overview. *Int J Surg Pathol.* 2010;18:103–20.
6. Chen J, Xiao Y, Cai X, Liu J, Chen K, Zhang X. Overexpression of p53R2 is associated with poor prognosis in lung sarcomatoid carcinoma. *BMC Cancer.* 2017;17:855.
7. Park JS, Lee Y, Han J, Kim HK, Choi YS, Kim J, et al. Clinicopathologic outcomes of curative resection for sarcomatoid carcinoma of the lung. *Oncology.* 2011;81:206–13.
8. Huang SY, Shen SJ, Li XY. Pulmonary sarcomatoid carcinoma: a clinicopathologic study and prognostic analysis of 51 cases. *World J Surg Oncol.* 2013;11:252.
9. Mochizuki T, Ishii G, Nagai K, Yoshida J, Nishimura M, Mizuno T, et al. Pleomorphic carcinoma of the lung:

- clinicopathologic characteristics of 70 cases. *Am J Surg Pathol*. 2008;32:1727–35.
10. Gu L, Xu Y, Chen Z, Pan Y, Lu S. Clinical analysis of 95 cases of pulmonary sarcomatoid carcinoma. *Biomed Pharmacother*. 2015;76:134–40.
 11. Ito K, Oizumi S, Fukumoto S, Harada M, Ishida T, Fujita Y, et al. Clinical characteristics of pleomorphic carcinoma of the lung. *Lung Cancer*. 2010;68:204–10.
 12. Travis WD. Sarcomatoid neoplasms of the lung and pleura. *Arch Pathol Lab Med*. 2010;134:1645–58.
 13. Xu XL, Song W, Sui X, Song L, Wang X, Feng RE, et al. Computed tomographic and pathological features of primary pulmonary sarcomatoid carcinoma. *Zhongguo Yi Xue Ke Xue Yuan Xue Bao*. 2016;38:93–8.
 14. Landini N, Milanese G, Zambrini E, Ariozi I, Gnetti L, Carloni A, et al. Computed tomography – histology correlations of unusual lung tumors. *Pathologica*. 2016;108:110–9.
 15. Rapicetta C, Lococo F, Stefani A, Rossi G, Ricchetti T, Filice A, et al. Primary sarcomatoid carcinoma of the lung: radiometabolic ((18)F-FDG PET/CT) findings and correlation with clinico-pathological and survival results. *Lung*. 2016;194:653–7.
 16. Tournoy KG, Maddens S, Gosselin R, Van Maele G, van Meerbeeck JP, Kelles A. Integrated FDG PET/CT does not make invasive staging of the intrathoracic lymph nodes in non-small cell lung cancer redundant: a prospective study. *Thorax*. 2007;62:696–701.
 17. Roesel C, Terjung S, Weinreich G, Hager T, Chalvatzoulis E, Metznermacher M, et al. Sarcomatoid carcinoma of the lung: a rare histological subtype of non-small cell lung cancer with a poor prognosis even at earlier tumour stages. *Interact Cardiovasc Thorac Surg*. 2017;24:407–13.
 18. Romano A, Grassia M, Rossetti AR, Esposito G, Braccio B, Pezzella M, et al. Sarcomatoid carcinoma of the lung: a rare case of three small intestinal intussusceptions and literature review. *Int J Surg Case Rep*. 2015;13:48–50.
 19. Qin BD, Jiao XD, Liu K, Wu Y, He X, Liu J, et al. Clinical, pathological and treatment factors associated with the survival of patients with primary pulmonary salivary gland-type tumors. *Lung Cancer*. 2018;126:174–81.
 20. Han X, Zhang J, Fan J, Cao Y, Gu J, Shi H. Radiological and clinical features and outcomes of patients with primary pulmonary salivary gland-type tumors. *Can Respir J*. 2019;2019:1475024.
 21. Falk N, Weissferdt A, Kalhor N, Moran CA. Primary pulmonary salivary gland-type tumors: a review and update. *Adv Anat Pathol*. 2016;23:13–23.
 22. Chopra A, Shim C, Sharma N, Gordon D, Tibb A. Primary salivary type lung tumor: Mucoepidermoid carcinoma. *Respir Med Case Rep*. 2013;9:18–20.
 23. Song DH, Choi IH, Ha SY, Han KM, Han J, Kim TS, et al. Epithelial-myoepithelial carcinoma of the tracheo-bronchial tree: the prognostic role of myoepithelial cells. *Lung Cancer*. 2014;83:416–9.
 24. Molina JR, Aubry MC, Lewis JE, Wampfler JA, Williams BA, Midthun DE, et al. Primary salivary gland-type lung cancer: spectrum of clinical presentation, histopathologic and prognostic factors. *Cancer*. 2007;110:2253–9.
 25. Zhu F, Liu Z, Hou Y, He D, Ge X, Bai C, et al. Primary salivary gland-type lung cancer: clinicopathological analysis of 88 cases from China. *J Thorac Oncol*. 2013;8:1578–84.
 26. Roden AC, Greipp PT, Knutson DL, Kloft-Nelson SM, Jenkins SM, Marks RS, et al. Histopathologic and cytogenetic features of pulmonary adenoid cystic carcinoma. *J Thorac Oncol*. 2015;10:1570–5.
 27. Bhatia K, Ellis S. Unusual lung tumours: an illustrated review of CT features suggestive of this diagnosis. *Cancer Imaging*. 2006;6:72–82.
 28. Elnayal A, Moran CA, Fox PS, Mawlawi O, Swisher SG, Marom EM. Primary salivary gland-type lung cancer: imaging and clinical predictors of outcome. *AJR Am J Roentgenol*. 2013;201:W57–63.
 29. Anderson T, Zhang L, Hameed M, Rusch V, Travis WD, Antonescu CR. Thoracic epithelioid malignant vascular tumors: a clinicopathologic study of 52 cases with emphasis on pathologic grading and molecular studies of WWTR1-CAMTA1 fusions. *Am J Surg Pathol*. 2015;39:132–9.
 30. Sardaro A, Bardoscia L, Petruzzelli MF, Portaluri M. Epithelioid hemangioendothelioma: an overview and update on a rare vascular tumor. *Oncol Rev*. 2014;8:259.
 31. Lau K, Massad M, Pollak C, Rubin C, Yeh J, Wang J, et al. Clinical patterns and outcome in epithelioid hemangioendothelioma with or without pulmonary involvement: insights from an internet registry in the study of a rare cancer. *Chest*. 2011;140:1312–8.
 32. Liu K, Xie P, Peng W, Zhou Z. The computed tomographic findings of pulmonary epithelioid hemangioendothelioma. *Radiol Med*. 2014;119:705–13.
 33. Dail DH, Liebow AA. Intravascular bronchioloalveolar tumor. *Am J Pathol*. 1975;78:6a–7a.
 34. Cronin P, Arenberg D. Pulmonary epithelioid hemangioendothelioma: an unusual case and a review of the literature. *Chest*. 2004;125:789–93.
 35. Woo JH, Kim TJ, Lee KS, Kim TS, Kim BT. Epithelioid hemangioendothelioma in the thorax: Clinicopathologic, CT, PET, and prognostic features. *Medicine (Baltimore)*. 2016;95:e4348.
 36. Mascarelli PE, Iredell JR, Maggi RG, Weinberg G, Breitschwerdt EB. Bartonella species bacteremia in two patients with epithelioid hemangioendothelioma. *J Clin Microbiol*. 2011;49:4006–12.
 37. Dehio C. Recent progress in understanding Bartonella-induced vascular proliferation. *Curr Opin Microbiol*. 2003;6:61–5.
 38. Bagan P, Hassan M, Le Pimpec Barthes F, Peyrard S, Souilamas R, Danel C, et al. Prognostic factors and surgical indications of pulmonary epithelioid hemangioendothelioma: a review of the literature. *Ann Thorac Surg*. 2006;82:2010–3.
 39. Ye B, Li W, Feng J, Shi JX, Chen Y, Han BH. Treatment of pulmonary epithelioid hemangioendothelioma with combination chemotherapy: report of three cases and review of the literature. *Oncol Lett*. 2013;5:1491–6.
 40. Watanabe S, Yano F, Kita T, Soga S, Shinmoto H, Kosuda S, et al. 18F-FDG-PET/CT as an indicator for resection of pulmonary epithelioid hemangioendothelioma. *Ann Nucl Med*. 2008;22:521–4.

41. Mukundan G, Urban BA, Askin FB, Fishman EK. Pulmonary epithelioid hemangioendothelioma: atypical radiologic findings of a rare tumor with pathologic correlation. *J Comput Assist Tomogr.* 2000;24:719–20.
42. Tochigi N, Tsuta K, Maeshima AM, Shibuki Y, Asamura H, Hasegawa T, et al. Malignant pulmonary epithelioid hemangioendothelioma with hilar lymph node metastasis. *Ann Diagn Pathol.* 2011;15:207–12.
43. Duran-Mendicuti A, Costello P, Vargas SO. Primary synovial sarcoma of the chest: radiographic and clinicopathologic correlation. *J Thorac Imaging.* 2003;18:87–93.
44. Polverosi R, Muzzio PC, Panunzio A, Pasquotti G, Schiavon M, Rea F. Synovial sarcoma: CT imaging of a rare primary malignant tumour of the thorax. *Radiol Med.* 2011;116:868–75.
45. Kim GH, Kim MY, Koo HJ, Song JS, Choi CM. Primary pulmonary synovial sarcoma in a tertiary referral center: clinical characteristics, CT, and 18F-FDG PET findings, with pathologic correlations. *Medicine (Baltimore).* 2015;94:e1392.
46. Tsunozuka H, Miyata N, Furuya T, Konishi E, Inoue M. Spontaneous regression of primary pulmonary synovial sarcoma. *Ann Thorac Surg.* 2018;105:e129–31.
47. Zeren H, Moran CA, Suster S, Fishback NF, Koss MN. Primary pulmonary sarcomas with features of monophasic synovial sarcoma: a clinicopathological, immunohistochemical, and ultrastructural study of 25 cases. *Hum Pathol.* 1995;26:474–80.
48. Frazier AA, Franks TJ, Pugatch RD, Galvin JR. From the archives of the AFIP: Pleuropulmonary synovial sarcoma. *Radiographics.* 2006;26:923–40.
49. Falkenstern-Ge RF, Kimmich M, Grabner A, Horn H, Friedel G, Ott G, et al. Primary pulmonary synovial sarcoma: a rare primary pulmonary tumor. *Lung.* 2014;192:211–4.
50. Panigrahi MK, Pradhan G, Sahoo N, Mishra P, Patra S, Mohapatra PR. Primary pulmonary synovial sarcoma: a reappraisal. *J Cancer Res Ther.* 2018;14:481–9.
51. Mussot S, Ghigna MR, Mercier O, Fabre D, Fadel E, Le Cesne A, et al. Retrospective institutional study of 31 patients treated for pulmonary artery sarcoma. *Eur J Cardiothorac Surg.* 2013;43:787–93.
52. Chen D, Zhu G, Wang D, Zhang Z, Fang W, Qu Z. Clinicopathological and immunohistochemical features of pulmonary artery sarcoma: a report of three cases and review of the literature. *Oncol Lett.* 2016;11:2820–6.
53. Kim C, Kim MY, Kang JW, Song JS, Lee KY, Kim SS. Pulmonary artery intimal sarcoma versus pulmonary artery thromboembolism: CT and clinical findings. *Korean J Radiol.* 2018;19:792–802.
54. Mandelstamm M. Über primäre Neubildungen des Herzens. *Virchows Arch Pathol Anat.* 1923;245:43–54.
55. Attinà D, Niro F, Tchouanté P, Mineo G, Russo V, Palazzini M, et al. Pulmonary artery intimal sarcoma. Problems in the differential diagnosis. *Radiol Med.* 2013;118:1259–68.
56. Blackmon SH, Rice DC, Correa AM, Mehran R, Putnam JB, Smythe WR, et al. Management of primary pulmonary artery sarcomas. *Ann Thorac Surg.* 2009;87:977–84.
57. Secondino S, Grazioli V, Valentino F, Pin M, Pagani A, Sciortino A, et al. Multimodal approach of pulmonary artery intimal sarcoma: a single-institution experience. *Sarcoma.* 2017;2017:7941432.
58. Travis WD, Brambilla E, Burke AP, Marx A, Nicholson AG. WHO classification of tumours of the lung, pleura, thymus and heart. 4th ed. Lyon: World Health Organization; 2015.
59. Gan HL, Zhang JQ, Huang XY, Yu W. The wall eclipsing sign on pulmonary artery computed tomography angiography is pathognomonic for pulmonary artery sarcoma. *PLoS One.* 2013;8:e83200.
60. Vaideeswar P, Pillai R. Pulmonary arterial intimal sarcoma with retrograde extension: report of a case and review of literature. *Indian J Pathol Microbiol.* 2013;56:47–50.
61. Sirajuddin A, Raparia K, Lewis VA, Franks TJ, Dhand S, Galvin JR, et al. Primary pulmonary lymphoid lesions: radiologic and pathologic findings. *Radiographics.* 2016;36:53–70.
62. Albano D, Borghesi A, Bosio G, Bertoli M, Maroldi R, Giubbini R, et al. Pulmonary mucosa-associated lymphoid tissue lymphoma: (18)F FDG PET/CT and CT findings in 28 patients. *Br J Radiol.* 2017;90:20170311.
63. Li H, Wang T, Wei X, Dang X. Marginal zone B-cell lymphoma of the pulmonary mucosa-associated lymphoid tissue: a case report. *Oncol Lett.* 2015;10:1731–4.
64. Herbert A, Wright DH, Isaacson PG, Smith JL. Primary malignant lymphoma of the lung: histopathologic and immunologic evaluation of nine cases. *Hum Pathol.* 1984;15:415–22.
65. Restrepo CS, Carrillo J, Rosado de Christenson M, Ojeda Leon P, Lucia Rivera A, Koss MN. Lymphoproliferative lung disorders: a radiologic pathologic overview. Part II: neoplastic disorders. *Semin Ultrasound CT MR.* 2013;34:535–49.
66. Huang H, Lu ZW, Jiang CG, Li J, Xu K, Xu ZJ. Clinical and prognostic characteristics of pulmonary mucosa-associated lymphoid tissue lymphoma: a retrospective analysis of 23 cases in a Chinese population. *Chin Med J.* 2011;124:1026–30.
67. Hare SS, Souza CA, Bain G, Seely JM, Gomes MM, Quigley M. The radiological spectrum of pulmonary lymphoproliferative disease. *Br J Radiol.* 2012;85:848–64.
68. Patsios D, Roberts HC, Paul NS, Chung T, Herman SJ, Pereira A, Weisbrod G. Pictorial review of the many faces of bronchioloalveolar cell carcinoma. *Br J Radiol.* 2007;80:1015–23.



Pulmonary Neuroendocrine Neoplasms

Anna Rita Larici , *Giuseppe Cicchetti*, *Giulia D'Ambra*,
Rosa D'Abronzo, *Annemilia del Ciello*, *Lucio Calandriello*,
Alessandra Farchione, *Riccardo Manfredi*, and *Guido Rindi* 

5.1 Overview and Classification – 88

5.2 Carcinoid – 90

5.2.1 Epidemiology and Clinical Presentation – 90

5.2.2 Pathology – 91

5.2.3 Imaging – 91

5.2.4 Pathway of Diffusion: Local Spread – 92

5.2.5 Pathway of Diffusion: Lymph Node Involvement – 94

5.2.6 Pathway of Diffusion: Distant Metastatic Spread – 94

5.3 Large Cell Neuroendocrine Carcinoma – 95

5.3.1 Epidemiology and Clinical Presentation – 95

5.3.2 Pathology – 95

5.3.3 Imaging – 95

5.3.4 Pathway of Diffusion – 96

5.4 Small Cell Lung Carcinoma – 97

5.4.1 Epidemiology and Clinical Presentation – 97

5.4.2 Staging, Treatment, and Prognosis – 97

5.4.3 Pathology – 97

5.4.4 Imaging – 98

5.4.5 Pathway of Diffusion: Local Spread and Mediastinal Involvement – 99

5.4.6 Pathway of Diffusion: Distant Metastatic Spread – 101

5.5 Conclusions – 101

References – 102

5.1 Overview and Classification

Neuroendocrine neoplasms (NEN) are a heterogeneous group of malignancies, with different morphological, immunohistochemical, and molecular characteristics rendered into a noticeably different clinical and biological behavior [1]. The NENs are represented by cells with neuroendocrine phenotype similar to the normal cells of the diffuse neuroendocrine system [2]. Since this system is ubiquitous throughout the body, any organ can be involved by such category of malignancies. The respiratory system is the second most common site of NEN, after the gastrointestinal tract [3]. The global incidence of pulmonary NENs is about 0.2–2/1,000,000/year [4]. Despite rare, NENs showed an average frequency increase of 6% per year in the last 30 years [5, 6], namely, from 0.31 to 1.61/100,000 in the USA from 1973 to 2012 [5]. Particularly, the well-differentiated types of NENs seem to be on the rise, as opposed to the decrease in most aggressive type [6, 7]. This figure is probably due to the improvement in diagnostic tools and diffusion of lung cancer screening programs with computed tomography (CT) [4, 8]. Furthermore, the decrease in smoking rate, extended use of filtered cigarettes, and changes in the pathological diagnostic criteria could have played a role in the relative reduction of poorly differentiated types [9].

Pulmonary NENs arise in the bronchial and bronchiolar epithelium, likely from the pluripotent bronchial epithelial stem cells. They are composed of tumor cells similar in phenotype to the

endodermal pulmonary neuroendocrine cells, also known as Kulchitsky cells [10–12].

According to the 2015 *World Health Organization (WHO) classification*, there are four main types of pulmonary NEN: typical carcinoid (TC), atypical carcinoid (AC), large cell neuroendocrine carcinoma (LCNEC), and small cell lung carcinoma (SCLC) [13]. A correlation between smoking history and the onset of all these neoplasms has been clearly shown, with the exception of TC [1]. The major epidemiological aspects of lung NENs are summarized in **Table 5.1**. Pulmonary NENs account for approximately 25% of all invasive primary lung cancers [14], mostly consisting in SCLC (75%), followed by LCNEC (15%), TC (9%), and AT (1%) [4]. This classification was updated in 2015, and each of the aforesaid four histologic variants reflects a unique type of neuroendocrine cell proliferation, with different histological grades. The histological grade of NENs ranges from low-grade (TC), to intermediate-grade (AC) [15], to high-grade and poorly differentiated malignancies (LCNEC and SCLC) [16]. The prognosis and management are widely variable among NENs according to such heterogeneous histological features [13, 17]. Noteworthy, the 2018 consensus proposal of the *International Agency for Research on Cancer (IARC)* and *WHO* forwarded a uniform classification framework for NENs from any organ, with the aim of providing consistent taxonomy. Hierarchical classification of NEN is established into two families: *neuroendocrine tumor (NET)* and *neuroendocrine carcinoma (NEC)*. The term NET is intended to

Table 5.1 Comparison between major epidemiological factors of lung NENs

	Neuroendocrine tumor (NET)		Neuroendocrine carcinoma (NEC)	
	TC	AC	LCNEC	SCLC
Mean patient age	40–49	50–59	70–79	60–69
M:F ratio	>2.5:1	2:1	2.5:1	>2.5:1
Association with smoking	No	Yes	Yes	Yes
Paraneoplastic syndromes	↓	↓	↓↓	↑

NENs neuroendocrine neoplasms, *TC* typical carcinoid, *AC* atypical carcinoid, *LCNEC* large cell neuroendocrine carcinoma, *SCLC* small cell lung carcinoma, *M* male, *F* female, ↓ uncommon, ↓↓ very uncommon, ↑ frequent

Table 5.2 Lung NEN 2018 IARC-WHO proposed classification

Category	Family	Type	Grade	Current terminology
Neuroendocrine neoplasm (NEN)	Neuroendocrine tumor (NET)	Pulmonary neuroendocrine tumor (NET)	G1	Typical carcinoid (TC)
			G2	Atypical carcinoid (AC)
	Neuroendocrine carcinoma (NEC)	Pulmonary NEC, large cell type		Large cell neuroendocrine carcinoma (LCNEC)
				Small cell lung carcinoma (pulmonary NEC, small cell type)

IARC International Agency for Research on Cancer, WHO World Health Organization

Table 5.3 Lung NEN classification (WHO 2015)[13]

		Grade	Mitosis	Necrosis
Low grade ^a	Typical carcinoid (TC)	1	<2 mitosis/2 mm ²	Absent
Intermediate grade ^a	Atypical carcinoid (AC)	2	2–10 mitosis/2 mm ²	Present
High grade ^b	Large cell neuroendocrine carcinoma (LCNEC)	3	>10 mitosis/2 mm ²	Extensive
	Small cell carcinoma (SCLC)			High

NENs neuroendocrine neoplasms, WHO World Health Organization, TC typical carcinoid, AC atypical carcinoid, LCNEC large cell neuroendocrine carcinoma, SCLC small cell lung carcinoma

^aWell differentiated

^bPoorly differentiated

designate a family of well-differentiated neoplasms whose potential for dissemination depends on tumor site, type, and grade. Conversely, NEC is clearly indicative of high-grade malignant histology and biological behavior. In pulmonary NENs, the NET family encompasses the well-differentiated TC and AC. Otherwise, the poorly differentiated and high-grade LCNEC and SCLC are assigned in the NEC family (Table 5.2) [18].

According to the WHO classification [13], the diagnosis of NEN is based on two parameters: the mitotic index per 2 mm² of viable area and the presence/absence of necrosis (Table 5.3). The highest mitotic index and the most extensive areas of necrosis are typical of the high-grade poorly differentiated carcinomas, such as LCNEC and SCLC [13].

Furthermore, the last WHO classification mentions Ki-67 index for stratification of NENs [13, 19]. Interestingly, a new classification of lung NENs has been published [20], which combines mitosis count (≤ 2 , 3–47, >47), necrosis proportion (absent, <10%, or >10%), and Ki-67 cellular proliferation index (<4%, 4–24%, 25%). Such composite score correlated with prognosis and allowed stratification of AC and LCNEC.

Cytological (cell size and nuclear morphology) and architectural features are additional characteristics which can be particularly useful to distinguish between LCNEC and SCLC [16]. The typical immunohistochemical markers for identifying NENs are chromogranin A, CD56, and synaptophysin. Such immunohistochemical pattern is usually required for diagnosis of lung NEN [7], especially in case of LCNEC that

should be distinguished from undifferentiated large cell carcinoma, which is not classified as a NEN [16].

The staging system of NEN was quite heterogeneous in the past, while it is currently deemed within the standard of *AJCC/UICC* (American Joint Committee on Cancer/Union for International Cancer Control) *eighth edition of TNM system* for lung cancer [21].

5

5.2 Carcinoid

5.2.1 Epidemiology and Clinical Presentation

Lung carcinoid shows an annual incidence of 2.3–2.8 cases per million [22]; it accounts for almost 25% of all carcinoids throughout the body [6, 8] and 2.2% of all lung neoplasms [23].

From among all lung carcinoids, 80–90% are classified as TC and the remaining 10–20% as AC [23, 24].

The majority of carcinoids occurs as sporadic disease, while 5–10% of carcinoids are found in association with multiple endocrine neoplasia 1 (MEN 1) [25, 26]. Historically, TC occurs more frequently in women while AC in men. However, it seems that gender distribution is quite dynamic as it was recently observed that TC might be increasing in men [1]. The mean age at diagnosis is 45 years for TC and 55 years for AC (Table 5.1) [1, 27]. Carcinoid represents the most common primary pulmonary neoplasm in children and young adults [28]. Carcinoid was reported to occur more frequently in African-American subjects [5].

At the time of diagnosis, lung carcinoid might be asymptomatic or result in nonspecific respiratory symptoms; usually the clinical pattern follows the tumor location [15]. Central carcinoid presents with cough, hemoptysis, dyspnea, wheezing, recurrent infections, or obstructive pneumonia. Conversely, peripheral carcinoid usually appears as asymptomatic incidental imaging finding [29]. Most carcinoids are located centrally, in the main (10%) or lobar bronchi (75%). A centrally located tumor is more frequently a TC than an AC; therefore, TC tends to manifest about 10 years earlier because of signs and symptoms due to central airway obstruction.

Table 5.4 Carcinoids' differences in prognosis

	TC	AC
Metastases at presentation	Regional lymph node metastases: 5–15% Distant metastases: 3–5%	Regional lymph node metastases: 50% Distant metastases: 25%
Survival	5-year survival: 87–100% 10-year survival: 88–94%	5-year survival: 44–88% 10-year survival: 18–64%
Recurrence (median time: 4 years)	3.6%	33%

TC typical carcinoid, AC atypical carcinoid

Lung carcinoids are mostly nonfunctional (90%) [29]; hence, paraneoplastic syndrome is seldom reported [30].

TC has better prognosis than AC both because of their earlier symptoms and more indolent behavior. Indeed, both nodal involvement and distant metastatic spread are substantially lower in TC than AC at the time of diagnosis [31]. The 5-year survival of patients with TC ranges from 87% to 100%, while AT yields worse outcome ranging from 44% to 88% [28]. AC also shows a higher recurrence rate when compared to TC (33% vs. 3.6%) [32]. The major differences in the prognosis of carcinoids are reported in Table 5.4.

In a cohort of patients with metastatic disease (both TC and AC), the median survival is about 24 months, with a 5-year overall survival rate of 32% [33]. Negative prognostic factors for carcinoid are high grading and TNM stage, high tumor burden, peripheral location, higher age at diagnosis, poor performance status, and absence of uptake on somatostatin receptor scintigraphy [34, 35].

Surgical resection is the optimal treatment for localized lung carcinoid [28].

In the suspect of AC, the tumor resection should be completed with parenchymal resection associated with extended lymph node dissection. Furthermore, adjuvant chemotherapy should be considered. Although carcinoid tumors generally

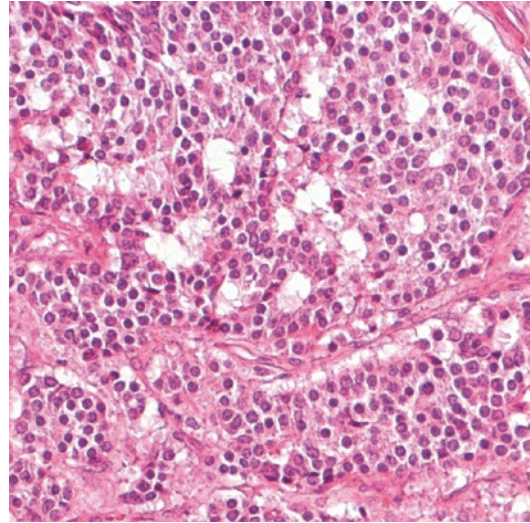
show indolent behavior, they could recur. Relapses in patients with TC and AC usually occur within 10 and 5 years, respectively. Therefore, surveillance is recommended for a minimum of 20 years [36]. Metastatic and unresectable tumors may be treated with chemotherapy, immunotherapy (particularly with everolimus), or radiolabeled agents such as somatostatin analogs [28, 34].

5.2.2 Pathology

Carcinoids are usually rounded tumors, with an average size of 2–3 cm. The definition of carcinoid relies on size: a carcinoid is intended to be ≥ 5 mm in diameter [13], whereas any proliferation of neuroendocrine cells < 5 mm is called *tumorlet*. The tumorlet pattern is typically an incidental finding in lung specimens showing various inflammatory or fibrotic conditions; nevertheless, it can also be found in the rare condition known as *diffuse idiopathic pulmonary neuroendocrine cell hyperplasia (DIPNECH)* [37]. Tumorlets show metastatic potential despite their limited size, especially when multiple in number and fused in larger size lesions in the context of DIPNECH [38, 39].

The nomenclature of TC and AC inherently reflects the grade, G1 and G2, respectively. Otherwise, the cytoarchitectural features are quite overlapping between TC and AC. Notably, they both display a moderate amount of eosinophilic cytoplasm and nuclei with finely granular chromatin, which may also display a coarse pattern in a minority of AC. Furthermore, inconspicuous nucleoli are seen in most TC, while they happen to be also more prominent in AC [37]. As opposed to TC (■ Fig. 5.1), AC displays possible focal or spotty (i.e., limited in size) necrosis and/or a mitotic index of 2–10 mitoses per 2 mm^2 (■ Table 5.3). In rare cases, AC morphology might be coupled with more than 10 mitoses per 2 mm^2 ; this scenario falls under the definition of LCNEC [13].

TC and AC are widely and strongly positive for the neuroendocrine markers chromogranin A, synaptophysin, and CD56 N-CAM (neural cell adhesion molecule) and usually for somatostatin receptors subtypes 2 and 5 (SSR_2 and SSR_5). Conversely, the expression of TTF1 (thyroid transcription factor 1) is limited to peripheral lesions only. The proliferation rate by Ki-67 staining is



■ Fig. 5.1 Typical carcinoid (TC). Image H&E×20 (hematoxylin and eosin) shows a trabecular/solid islet structure, void of necrosis and with very limited cell pleomorphism, abundant cytoplasm, and monomorphic nuclei; note the absence of mitosis. Overall, such features identify a well-differentiated neuroendocrine neoplasm

lower in TC (less than 5%) than in AC (usually 5–20%) [37].

5.2.3 Imaging

Typical and atypical lung carcinoids are indistinguishable from an imaging standpoint.

Chest X-ray is usually nonspecific, as it may show an isolated well-defined hilar or perihilar nodule/mass associated with parenchymal abnormalities, such as atelectasis or obstructive pneumonia. Isolated signs of endobronchial mucoid impaction might also be depicted into the “finger-in-glove” pattern [1].

CT is the main imaging technique for the detection, localization, and staging of these neoplasms. Size and location of the lesion might somehow suggest the differential between TC and AC, with the latter being relatively larger and more peripheral [28]. Three possible patterns are recognized for carcinoids: hilar or perihilar nodules/masses, endobronchial nodules, and peripheral nodules [40].

In case of hilar or perihilar nodules/masses ranging 2–5 cm in size, the tumor is usually a well-defined round or ovoid lesion, and it can

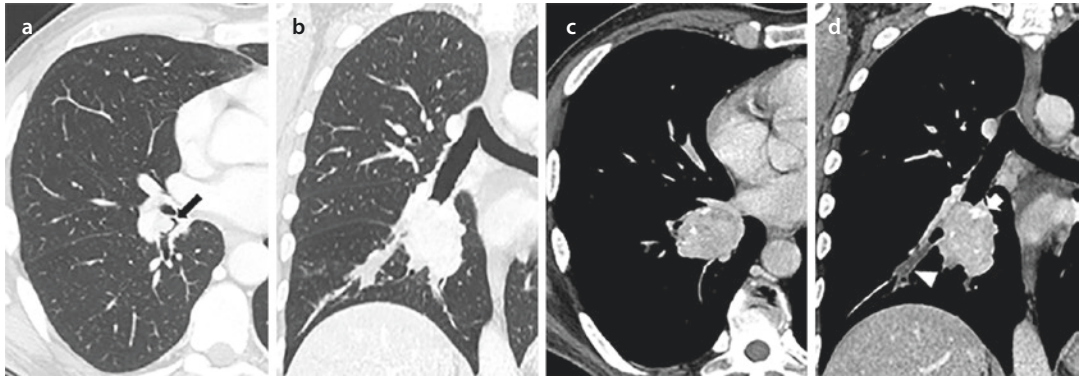


Fig. 5.2 Axial and coronal chest CT images at lung window setting **a, b** show an endoluminal lesion in the right lower lobe bronchus (*black arrow*) extending into the lung parenchyma. At mediastinal window setting **c, d**,

the solid lesion shows marked contrast enhancement and inner calcifications (*white arrow*), with distal endobronchial mucoid impaction (*arrowhead*). Histopathology demonstrated a typical carcinoid (TC)

appear with lobulated margins. Such lesions are typically located near the bifurcation of central bronchi [40].

Endobronchial lesion is often seen in central carcinoid. They frequently grow as primary endobronchial lesions with a subsequent extension to the adjacent lung parenchyma. Nonetheless, the endobronchial finding of carcinoid can also happen with opposite dissemination pathway, namely, a prominent extraluminal component can grow on the external aspect of the bronchus and subsequently trespass the bronchial wall into the bronchial lumen. Such scenario is known as “iceberg lesion” (Fig. 5.2) referring to the morphological parallelism between the tip of the iceberg (bronchoscopic vision) and its massive drowning portion (extrabronchial growth). Moreover, some small carcinoids can be entirely located within the bronchial lumen.

Carcinoid could also manifest as a solitary pulmonary nodule (SPN) in the lung periphery and may not show any bronchial relationship, usually measuring less than 3 cm in size [41].

Calcifications are seen in about 30% of carcinoids, notably with punctate or diffuse pattern [1, 40].

Both TC and AC show uniform intense contrast enhancement, commonly above 30 Hounsfield Unit (HU) (Fig. 5.2) [1]. However, some carcinoid may lack contrast enhancement and may have irregular contours, the majority of them being AC. Rarely, carcinoids can show cavitation and areas of central macroscopic necrosis; this pattern is expected for larger lesions [1].

Other imaging techniques can be useful in the diagnosis and staging of carcinoid. Scintigraphy with octreotide is helpful in the localization of occult tumors, for staging purpose and estimation of somatostatin receptor density, which is relevant information for treatment selection [15]. On positron emission tomography (PET) with Fluorine-¹⁸-fluorodeoxyglucose (¹⁸F-FDG), most carcinoid tumors do not show increased activity, with the exception of ACs, particularly in case of higher proliferation rate [42].

Recent analysis showed that 68-gallium-radiolabeled PET (⁶⁸Ga-DOTA-PET) displayed higher uptake in TC rather than in AC. Such pattern of uptake is attributed to the slow metabolism and the increased somatostatin receptor expression of TC. On the other hand, ⁶⁸Ga-DOTA uptake is decreased in AC due to its more aggressive behavior (Fig. 5.3) [43].

5.2.4 Pathway of Diffusion: Local Spread

Central carcinoids can have an endoluminal component with a focal or broad attachment to the bronchial wall. They usually do not infiltrate the bronchial mucosa, which may be substantially preserved above the lesion [30].

Although some carcinoids grow exclusively within the bronchial lumen, the invasion through the bronchial wall is common and can associate with infiltration of peribronchial soft tissue, cartilaginous rings, and adjacent lung parenchyma

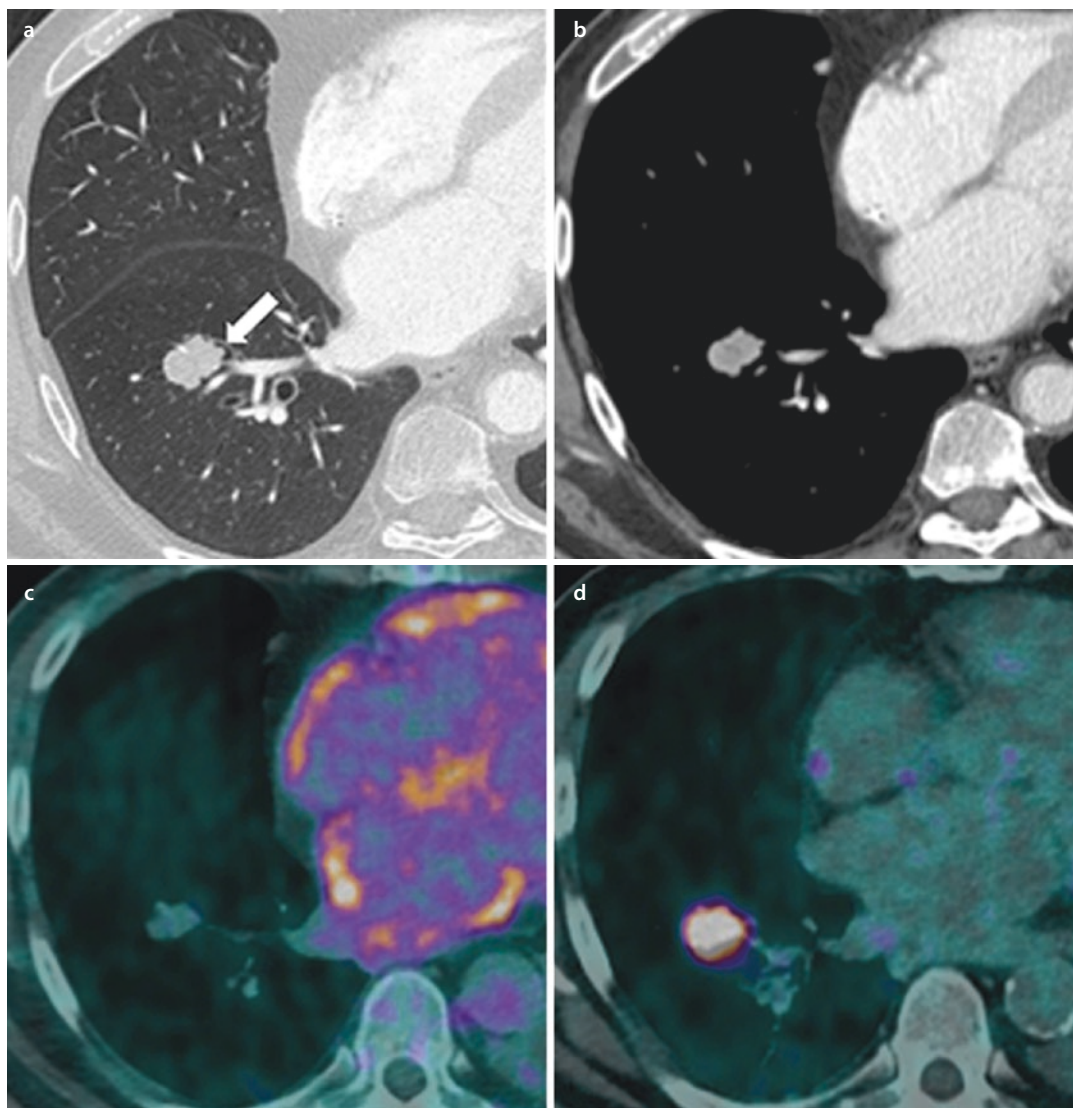


Fig. 5.3 Axial chest CT image in the lung window setting **a** of a solid nodule with lobulated margins in the anterior basal segment of the right lower lobe, showing both endobronchial (*arrow*) and extrabronchial intraparenchymal growth. Mediastinal window setting **b** demonstrates homogeneous contrast enhancement.

¹⁸F-FDG-PET/CT **c** does not show increased activity due to the low proliferation index. ⁶⁸Ga-DOTA-PET/CT **d** exhibits a high uptake due to major somatostatin receptor expression. (Courtesy of Prof. V. Rufini). The nodule was confirmed to be a typical carcinoid (TC) at histopathology

[30, 44]. This growth pattern gives a “dumbbell” appearance to the tumor, with variable proportion between the endobronchial and the extrabronchial component (■ Fig. 5.2) [45, 46].

Peripheral carcinoids usually grow without signs of infiltration despite being nonencapsulated tumors [44]. Infiltrating margins with extension into the adjacent lung parenchyma is reported with low frequency (22.2% of cases according to Ha and coworkers) [44].

AC is typically more aggressive than TC, and it is more likely to invade vascular or lymphatic structures (26.1% and 13%, respectively) [44], followed by increased likelihood of local recurrence and poor prognosis [9, 42, 44].

Direct pleural involvement is uncommon for lung carcinoids, as opposed to the frequent involvement by thymic carcinoid [47]; thus, pleural effusion is quite rare, and it is more likely associated with post-obstructive pneumonia [30].

The most aggressive lung carcinoids may show infiltration of the mediastinal fat, with eventually direct extension to the mediastinal structures (superior vena cava, pericardium, etc.) [40].

5.2.5 Pathway of Diffusion: Lymph Node Involvement

Carcinoids may exhibit lymphatic invasion [44]; they may be associated with hilar or mediastinal lymph node metastatic involvement [48]. Regional lymph node metastases can be found in 5–15% of patients with TC, whereas in AC they can be found in almost 50% of cases [49]. Dissemination to hilar and mediastinal stations is usually depicted by enlarged lymph nodes at imaging.

However, enlargement of thoracic lymph nodes in carcinoids may also represent hyperplasia from recurrent pneumonia or chronic peripheral infection [30]. This setting is more common in case of centrally located carcinoid determining bronchial obstruction.

According to Chong et al. [50], a metastatic involvement of N1 stations was found in 5% and 14% of TCs and ACs, respectively. Further dissemination to N2 stations was observed in 6% of TCs and 10% of ACs. Metastatic spread to distant intrathoracic lymph nodes is also possible, although it is rarely observed, namely about 7% of metastatic lung carcinoids [34]. The most frequent involvement of extrathoracic stations is found in the upper abdomen. According to the TNM staging system for lung cancer [21], these metastatic nodes have to be considered as distant metastasis because their prognostic yield overlaps metastatic disease [34].

5.2.6 Pathway of Diffusion: Distant Metastatic Spread

Carcinoids can evolve with distant metastases; notably, they are found in 25% of patients with AC, compared to 3–5% of TC [49].

The most frequent sites of metastasis from lung carcinoid are the liver, bone, central nervous system, and adrenal glands [24, 34]. More than 50% of patients with metastases from lung carcinoids show multiple sites of metastasis, with the liver affected in most cases [51]. It should be

underscored that liver involvement appears to be more common in metastatic lung carcinoids than in non-small-cell lung cancer (NSCLC) [51]. Metastatic disease from ACs is noted primarily in the bones, brain, and liver. Conversely, the rare metastases from TC preferably happen in the liver and bones [50]. For carcinoid tumors, a direct correlation between the size of the primary lesion and the probability of metastasis has been reported for hematogenous dissemination to the liver [52].

Among carcinoid tumors from any organ, lung carcinoids show a higher propensity to metastasize to the bone and to central nervous system. Bone metastases from lung carcinoid display solitary or multiple sclerotic bone lesions. Noteworthy, the lone detection of bone metastases from carcinoid tumors is a predictive factor for primary lung carcinoids, with a frequency of about 34% [52]. Likewise, primary lung carcinoids account for more than 50% of central nervous system metastases by all carcinoids, even in this case being the most common primary origin of metastatic carcinoid. Of note, the propensity of lung carcinoid to such metastatic targets might be also explained by anatomical reasoning: the departure of neoplastic cells from the lung can directly harbor to both bone and brain via the systemic circulation, whereas carcinoids from other regions (e.g., the midgut) are obligated to first pass through the liver and lungs.

Multiple synchronous bilateral lesions are reported, especially for TC. In these cases, it is unclear whether this represents true metastasis, enlarging tumorlets, or a tendency to form multiple primary pulmonary carcinoid tumors. Patients with multiple bilateral pulmonary TCs have been reported to have an excellent prognosis [50].

Unusual sites of metastatic spread can be occasionally seen toward pancreas, soft tissues, breasts, heart, skull, testis, and orbits [47].

The risk of recurrence is higher for resected ATs compared to TCs. Indeed, a smaller number of patients with TC (3.6%) than that with AC (33.3%) experience recurrences, with a median time to recurrence of 4 years, significantly longer than that for AC [32].

Most recurrences of carcinoid tumors of the lung are distant metastases, with local recurrences affecting only 2% of TC and 7% of AC [53, 54]. Metastatic lung carcinoid shows metachronous metastases in up to 50%, mostly in AC [34].

5.3 Large Cell Neuroendocrine Carcinoma

5.3.1 Epidemiology and Clinical Presentation

Pulmonary LCNECs are rare neoplasms representing about 2.1–3.5% of all lung tumors and about 15% of lung NENs. However, this frequency is potentially underestimated because of limitations in diagnosing LCNEC on cytological specimens [55, 56].

This neoplasm involves more frequently men than women (2.5:1), with a heavy smoking habit.

The average age at diagnosis is about 70 years [1, 55] (■ Table 5.1). This neoplasm shows peripheral location in 66–100% of cases. Centrally located LCNEC is associated with symptoms from bronchial obstruction and compression of vascular structures [57].

Slight predilection for upper lobe location has been reported, in about 63% of LCNEC [58].

LCNEC is rarely associated with paraneoplastic syndromes [29].

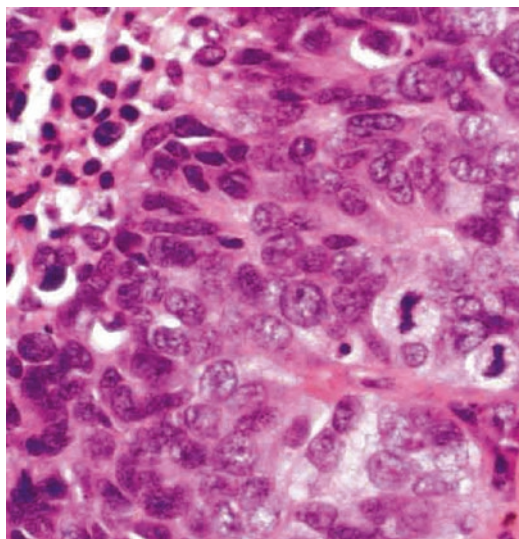
Surgical resection is recommended for all nonmetastatic stages, with subsequent adjuvant chemotherapy. Unfortunately, the majority of pulmonary LCNEC are not eligible for radical surgical treatment due to local or systemic spread [59]. The optimal therapeutic approach for systemic treatment is not established for LCNEC, yet [59].

It is increasingly understood that the pattern of response to chemotherapy is quite overlapping between LCNEC and SCLC, although with less chemo-responsivity, so they are frequently treated with the same chemotherapeutic regimens used for SCLC [55].

The prognosis of LCNEC is quite poor, with median overall survival of stages I–II, III, and IV about 32.4, 12.6, and 4.0 months, respectively. These figures are lower than survival rates in NSCLC [60]. Negative prognostic factors are advanced tumor stage, tumor size (greater than 3 cm), and male gender [61].

5.3.2 Pathology

LCNEC usually appears as a circumscribed mass of 3–4 cm, with central foci of hemorrhage and necrosis. LCNEC is by definition a poorly differ-



■ Fig. 5.4 Large cell neuroendocrine carcinoma (LCNEC). Image H&E×20b (hematoxylin and eosin) depicts a solid structure with evident necrosis (left upper corner) and is composed by large in size, severely atypical cells with abundant cytoplasm, often prominent nucleoli, and evident mitotic activity. Overall such features identify a poorly differentiated neuroendocrine neoplasm

entiated NEN, with high grading (G3). Diagnostic criteria for LCNEC are neuroendocrine morphology (organoid nesting, palisading, or rosette-like structures), high mitotic rate (greater than 10 mitoses per 2 mm²), and non-small-cell cytologic features (including large cell size and prominent nucleoli) (■ Fig. 5.4).

Diagnostic confirmation of neuroendocrine differentiation is required using immunohistochemical markers such as chromogranin A, synaptophysin, and CD56 or electron microscopy [13, 37]. In addition, TTF1 is usually strongly expressed, while SSR₂ and SSR₅ may also be present. Ki-67 usually shows a very high proliferation index (50–100% of tumor cells) [37].

LCNEC histology is not easily demonstrated on small biopsies or cytology; in most cases, the diagnosis of LCNEC requires a surgical lung biopsy [37]. Staining for Ki-67 may help in identifying the highly proliferative status of tumor cells.

5.3.3 Imaging

LCNECs share similar imaging characteristics with NSCLC; hence, there is no advantage in guessing the differential by imaging [29].

LCNEC typically manifests as a large peripheral pulmonary mass, with well-defined lobular margins, even though spiculated borders may be observed. Calcifications are uncommon, occurring in less than 9% of cases [28], and air bronchogram is extremely rare [58]. The tumor shows soft tissue density substantially similar to chest wall muscles. The contrast enhancement is quite variable: heterogeneous or peripheral, due to central necrosis in case of large lesions [58]. Extensive necrosis is also possible, but cavitation is rarely seen. Hilar and mediastinal nodal enlargement is frequent [28].

According to one series, pleural effusion has been described in almost a quarter of cases [62].

In case of centrally located lesion, post-obstructive signs can be observed such as mucus plugging, atelectasis, or pneumonia.

The comprehensive imaging of LCNEC includes ^{18}F -FDG-PET/CT, which is helpful for staging purpose. Furthermore, PET-CT yields prognostic information: SUV >13.7 has been related to worse prognosis [63].

Although LCNEC contains somatostatin receptors and can be octreoscan/ ^{68}Ga -DOTA-PET positive, this imaging modality is not suggested for the evaluation of this malignancy.

5.3.4 Pathway of Diffusion

LCNEC is a high-grade malignancy, with a high propensity to local and distant spread.

Tumor cells usually entirely fill pulmonary alveoli, or they can show a compressive growth pattern. This type of local growth into the lung parenchyma gives the tumor the appearance of a large lesion with well-defined margin. Still, lobulated margins observed on imaging may reflect the interruption of tumor growth by anatomic boundaries [58].

In centrally located lesions, tumors are usually adherent to the bronchial wall, with an associated endobronchial polypoid component that invades the surrounding lung parenchyma. In these cases, an endobronchial growth pattern can be seen, usually associated to invasion of lung parenchyma.

Tumor emboli in the adjacent lung parenchyma can be observed [64].

Vascular and lymphatic invasion are possible, and they can correspond to the radiological evidence of spiculations. Where observed, lymphatic permeation and vascular invasion were significantly associated with poorer outcome [64]. Other causes of spiculations are irregularly protuberant tumor nests or a diffuse desmoplastic response to tumor growth [58].

Lesions show multiple punctate necrosis. In large tumors, necrotic foci may become larger and prone to be confluent in extensive areas of necrosis, reflecting the CT appearance of inhomogeneous enhancement with peripheral rim within the lesion.

Direct pleural tumor seeding of LCNEC cells is uncommon [64]. This involvement may explain at least some of the pleural effusions not associated with pneumonia.

At diagnosis, LCNEC presents high rate of lymph node metastasis (60–80%) [55]. Metastatic involvement of lymph node is usually limited to hilar and mediastinal nodes. Metastatic lymph nodes have been associated with a poor outcome [65].

At diagnosis, distant metastasis can be found in about 40% of patients affected by LCNEC [55].

Most common metastatic sites are liver (47%), bone (32%), and brain (23%), similar to that seen in SCLC [60]. Another possible site of metastatic spread is adrenal gland. Moreover, multiple case reports have also described metastasis in atypical locations, including skin, scalp, and breast, substantially similar to other lung NENs.

Some patients may have oligometastatic disease (defined as ≤ 3 metastatic lesions) at the time of diagnosis. Despite radical treatment, recurrence is quite common; it is reported in almost 40% of patients, with over 90% of cases occurring within 2 years [61].

Local or regional recurrence has been reported in 27–35% of cases. Local recurrence usually affects bronchial stump in patients undergoing surgery, while lymph node recurrence mostly involves mediastinal and/or supraclavicular lymph nodes.

Distant recurrence is observed more frequently than local recurrence. This happens in about 56–60% of cases, with most cases involving brain and liver, followed by bone and lung [66, 67].

5.4 Small Cell Lung Carcinoma

5.4.1 Epidemiology and Clinical Presentation

Small cell lung carcinoma (SCLC) is the most common lung NEN; it represents 15% of any lung cancer [68]. It is strongly associated with cigarette smoking, with 95% of all patients having a history of heavy tobacco exposure. Other risk factors include exposures to agent including radon, halogenated ethers, arsenic, and asbestos.

SCLC typically affects patients between the ages of 60 and 70 years [69]. It has been more frequently observed in men than in women (ratio 2.6:1) (Table 5.1), even if women smokers are more likely to develop SCLC [70].

At the time of diagnosis, early-stage SCLC is very rare, representing only 5% of all cases [71]. The low incidence of early-stage SCLC is mainly attributable to its highly aggressive biological behavior, rapid tumor growth, and absence of early symptoms [71].

Patients typically present with a short duration of rapidly progressive symptoms.

Most patients present with advanced disease, and only 5% of cases of SCLC can display as a solitary lung nodule, usually incidentally discovered [37] or during CT lung cancer screening programs. The aggressive behavior of SCLC hampers early diagnosis and survival advantage of SCLC in lung cancer screening programs by low-dose CT [72].

Patients of any disease stage may present with a variety of paraneoplastic syndromes, such as endocrine ones: the syndrome of inappropriate antidiuretic hormone (SIADH) and Cushing's syndrome due to ectopic adrenocorticotroph hormone (ACTH) production. Furthermore, neurologic syndromes, as Lambert-Eaton syndrome, limbic encephalitis, and encephalomyelitis, can precede cancer diagnosis [9, 68].

5.4.2 Staging, Treatment, and Prognosis

According to the *Veterans Administration Lung Study Group (VALSG)* system, SCLC patients are classified as having limited-stage (LS) or extensive-stage (ES) disease [73]. The definition of LS disease

includes patients with disease limited to one hemithorax, with hilar and mediastinal nodes that can be encompassed within one tolerable radiotherapy portal, and possibly with ipsilateral supraclavicular lymph nodes. LS-SCLC is deemed a potentially curable disease. Conversely, ES disease is characterized by neoplastic invasion beyond the aforementioned boundaries.

The eighth *TNM staging* system replaces the VALSG [21]. According to TNM, stages I–III correspond to LS-SCLC, while stage IV corresponds to ES-SCLC.

Surgical resection with mediastinal lymph node dissection, followed by adjuvant chemotherapy, is indicated only for true stage I patients, which unfortunately are very rare (<5%). Most patients with LS receive a combination of cisplatin/carboplatin and etoposide plus thoracic radiation therapy (RT) [74].

Prophylactic cranial irradiation (PCI) is recommended for patients with good performance status who have responded to chemotherapy [75].

ES-SCLC is approached by chemotherapy with palliative purpose. Patients with a good response to therapy should be considered for PCI and/or thoracic RT [74].

SCLC is typically very responsive to chemotherapy; therefore, chemotherapy can prolong survival [76]. Unfortunately, relapse with chemoresistant disease is inevitable, with fewer than 10% of patients with ES alive after 2 years [74]. The overall survival rate is only about 5%: patients with ES-SCLC have a mean survival of about 8–10 months and a 2-year survival rate of 10%, against the 15–20 months in the LS disease, with 20–25% of long-term survival [77]. The 5-year survival rates of SCLC and LCNEC are reported in Table 5.5.

Negative prognostic factors include extensive disease, poor general conditions, weight loss, and markers such as lactic dehydrogenase. Conversely, positive prognostic factors include younger age, good general conditions, and single metastatic site in patients with extensive disease [78].

5.4.3 Pathology

SCLCs are by definition poorly differentiated NENs. Tumor cells are round to fusiform, with

Table 5.5 Survival according to stage, metastasis at presentation, and recurrence rate of high-grade NENs (NEC)

	LCNEC	SCLC
Metastasis at the presentation	40%	60–70%
5-year survival by stage	I: 33–62% II: 18–75% III: 8–45% IV: 0%	Ia 38% – Ib 21% IIa: 38% – IIb 18% IIIa: 13% – IIIb: 9% IV: 1%
Recurrence (median time: 2 years)	40%	74%

NENs neuroendocrine neoplasms, *NEC* neuroendocrine carcinoma, *LCNEC* large cell neuroendocrine carcinoma, *SCLC* small cell lung carcinoma

scant cytoplasm, and measure less than the diameter of three resting lymphocytes, with finely granular nuclear chromatin. Nucleoli are inconspicuous or absent. Tumor cells grow in sheets and nests with frequent necrosis, often extensive. Lesions exhibit a high mitotic rate (60–80 per 2 mm²) (Fig. 5.5). Unlike LCNEC, SCLC can readily be diagnosed in small specimens such as bronchosopic biopsies, fine-needle aspirates, or core biopsies [37].

Up to 90% of SCLCs are positive for at least one neuroendocrine marker such as CD56 N-CAM, chromogranin A, synaptophysin, and TTF1 [79]. SSR₂ and SSR₅ are usually negative or only focally positive in about 20% of investigated cases. Ki-67 is very helpful in distinguishing SCLC from carcinoids, because it shows a very high proliferation rate, of about 80–100% [37]. The main anatomic and histological features of SCLC with respect to those of other lung NENs are summarized in Table 5.6.

5.4.4 Imaging

About 90–95% of SCLC is centrally located, arising in lobar bronchi or main bronchus [80]. The most common appearance of SCLC is a large mass with central location, bulky hilar, and mediastinal

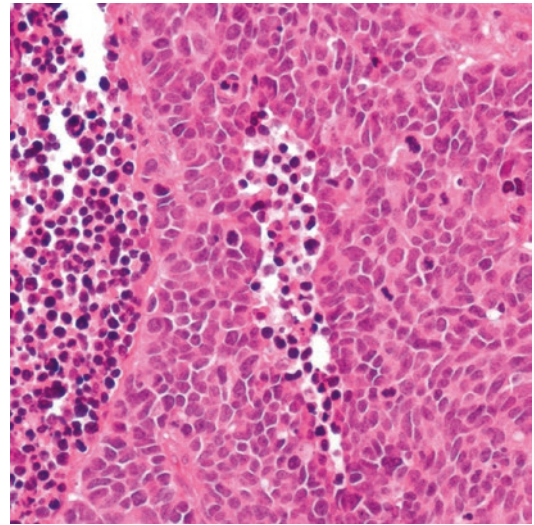


Fig. 5.5 Small cell lung carcinoma (SCLC). Image H&E×20 shows a solid structure with evident necrosis (left and center of the micrograph) and severely atypical cells with large nuclei and a thin rim of cytoplasm, overall resulting in small size; mitoses are evident often with atypical mitotic figures. As seen in LCNEC, such features identify a poorly differentiated neuroendocrine neoplasm

adenopathies invariably associated. Due to the close relationship with the tracheobronchial tree, SCLC can determine distal lung parenchyma atelectasis.

Chest X-ray usually shows an ill-defined hilar mass, with possible associated enlargement of the mediastinum and pulmonary volume loss due to obstruction and pleural effusion. Often the primary tumor is overshadowed by the mediastinal component, appearing as a poor-defined mediastinal mass involving at least one hilum [9, 29].

Among imaging techniques, CT allows an accurate assessment of intrathoracic involvement. Chest CT scan with contrast medium injection often shows the involvement of the major pulmonary vessels and mediastinal structure (including the superior vena cava), with common evidence of encasement of these structures by the tumor, as well as pleural effusion [9].

Rare manifestations include airspace opacities and consolidation. Thickening of the interlobular septa is reported as a sign of lymphangitic carcinomatosis [81]. Calcifications can be seen in up to 23% of the cases [1].

A peripheral primary tumor is rare. In approximately 5% of cases, SCLC may manifest as an solitary pulmonary nodule (SPN) [37], with well-defined lobulated margins or spiculated

Table 5.6 Comparison of the main anatomic and histological features of lung NENs

	TC	AC	LCNEC	SCLC
Central localization	+++	+++	+	++++
Calcifications	30%		<9%	23%
Cytology	Nuclei with finely granular chromatin Nucleoli inconspicuous	Chromatin may be coarse Nucleoli may be more prominent	Large cells Abundant cytoplasm Nuclear pleomorphism Prominent nucleoli	Small cells Scarce cytoplasm Nuclear pleomorphism No prominent nucleoli
Growth pattern	Organized growth pattern		Organoid, palisading	Diffuse sheets of cells
Ki-67	<5%	5–20%	>20%	>20%

NENs neuroendocrine neoplasms, *TC* typical carcinoid, *AC* atypical carcinoid, *LCNEC* large cell neuroendocrine carcinoma, *SCLC* small cell lung carcinoma, +++ frequent, + possible, ++++ extremely common

appearance. There are no imaging features that help to distinguish between SCLC and NSCLC when presenting as an SPN [1, 82].

The comprehensive clinical staging includes ¹⁸F-FDG-PET/CT. Otherwise, MRI is rarely used in the evaluation of SCLC, except when there are contraindications for the administration of intravenous iodine contrast material. To date, MRI of the brain for staging of SCLC shows better sensitivity than CT, particularly in neurologically asymptomatic patients [83]. MRI might be also useful for detecting and characterizing bone or liver metastases.

¹⁸F-FDG-PET/CT is extremely helpful in staging and restaging SCLC (with the exception of brain metastases). It turned out to be more sensitive and specific than other imaging techniques in the detection of metastatic disease, in prognosis evaluation – high standardized uptake seems to be significantly associated with poor survival – and, particularly, in the assessment of treatment response, due to the high metabolic activity degree of SCLC [29].

5.4.5 Pathway of Diffusion: Local Spread and Mediastinal Involvement

SCLC malignant cells exhibit heightened invasive properties and increased motility, resulting

in rapid tumor growth, high local invasiveness, and early metastatic spread to numerous organs.

The primary site is typically a submucosal endobronchial lesion of the proximal airways such as the lobar or main bronchi. The tumor itself is highly cellular and determines a limited fibrotic or inflammatory response. Consequently, it can rapidly spread through lymphatic and blood vessels even at an early stage of the disease, resulting in early nodal and distant metastatic deposits [84].

Kazawa et al. [81] have described eight different patterns of SCLC local diffusion according to the extension and spreading pattern recognized on CT scan. The most frequent patterns were the *central perihilar type*, when a central perihilar mass confined within the ipsilateral mediastinal tissue was seen; the *central plus mediastinal extension type*, with the mass extending to contralateral mediastinum (the most common pattern among their series, occurring in about 30% of cases); the *peripheral type*, in case of cancer located only in the peripheral lung parenchyma; and *peripheral plus mediastinal extension type*, in case of a peripheral tumor associated with a hilar/ipsilateral mediastinal lymph node metastasis (Fig. 5.6).

Peripheral SCLC typically appears on CT scan as a spiculated nodule, representing the vascular,

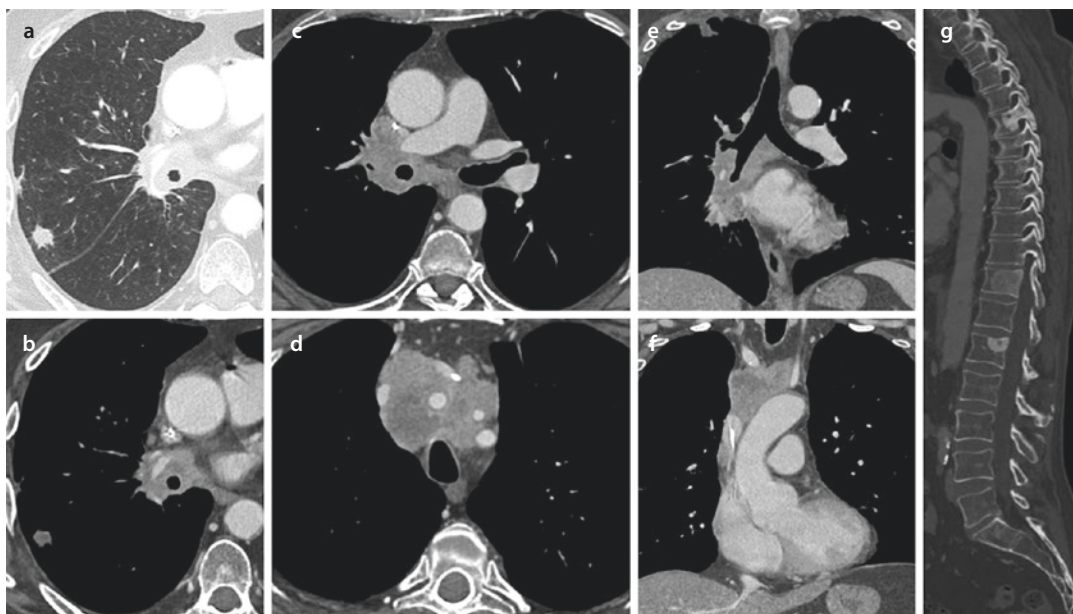


Fig. 5.6 Axial chest CT images at lung **a** and mediastinal **b** window settings depict a small (15 mm) nodule, with spiculated margins and necrotic appearance, in the posterior segment of the right upper lobe. Axial and coronal images at mediastinal window setting **c-f** show confluent and infiltrative adenopathies in the right

hilum, in the right paratracheal and subcarinal zones, and in the superior mediastinum, with encasement/infiltration of the vascular structures and the right bronchial tree. Sagittal reconstruction with bone window setting **g** shows multiple bone metastases of the spine. Histopathology revealed a small cell lung carcinoma

lymphatic, or intra-alveolar invasion by nest-forming tumor cells, with surrounding ground-glass opacity determined by edema, parenchymal hemorrhage, and intra-alveolar spread [85].

The centrilobular nodular or branching abnormalities – which usually represent bronchogenic diffusion of inflammation and disease – are usually not observed in SCLC.

Another possible identified pattern was the *lymphangitic-spread type*, with the presence of lymphangitic carcinomatosis, represented by thickening of the bronchovascular bundles and/or nodular or smooth thickening of the interlobular septa, usually associated with pleural effusion.

Other uncommon manifestations of SCLC local spread include the *lobar replacement type*, when tumor appears as a huge mass-like lesion that replaces an entire lobe, and the *airspace consolidation type*, in case of an ill-defined consolidation with cystic or tubular air bronchogram within the lesion [81].

Due to the easy spread via the lymphatic system, SCLC can also disseminate into the pleural space, appearing as multiple subpleural nodules

or, less commonly, masses associated with pleural thickening and malignant pleural effusion (*pleural dissemination type*) [9, 81].

SCLC diffusion often causes main airway stenosis, due to peribronchial extension of the disease, particularly in the submucosal tissue, with almost complete preservation of bronchial inner wall. Stenosis typically involves trachea and main bronchi (in about 50% of cases) and less likely lobar/segmental bronchi or subsegmental branches [81].

Mediastinum is by far the most common site of detected disease (up to 92% of cases), both for the presence of the primary malignancy and associated lymphadenopathies. Indeed, mediastinal and hilar lymph node metastases are detected in 92% and 84% of cases, respectively [1]. Mediastinal masses determine displacement, narrowing, and invasion of mediastinal structures, particularly great vessels, in about 68% of cases [9]. The superior vena cava, the pulmonary arteries, and the main pulmonary trunk are more frequently involved, followed by pulmonary veins and thoracic aorta, ranging from mild stenosis with wall irregularity to severe stenosis, luminal invasion

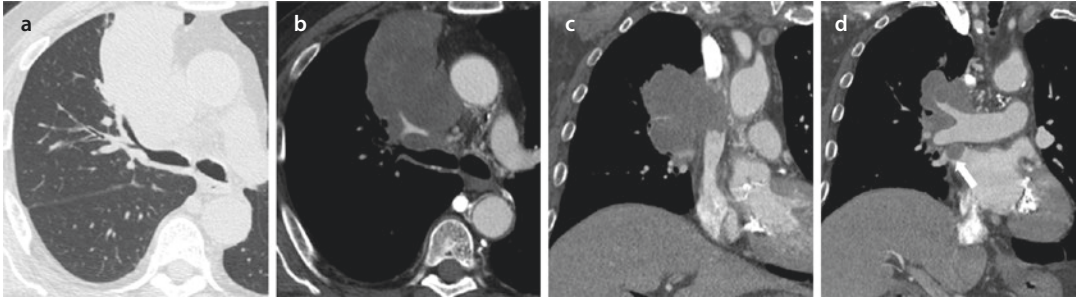


Fig. 5.7 Axial CT image at lung window setting **a** shows a mass in the anterior segment of the right upper lobe. Contrast-enhanced axial image **b** displays the extensive ipsilateral mediastinal involvement with encasement and infiltration of the right upper lobe artery and superior vena cava. Coronal images **c**, **d** better depict the longitudinal extension of the occlusion of superior vena cava, the encasement of the right main bronchus, the

distal right main pulmonary artery and the interlobar artery, which look patent, and the occlusion of the right superior pulmonary vein (*arrow*) close to the left atrium. Note the elevation of the right hemidiaphragm as a sign of the right phrenic nerve infiltration by the mass. Transbronchial biopsy through the anterior segmental bronchus of the right upper lobe revealed a small cell lung carcinoma

with tumor abutting into vessels, and complete encasement (**Fig. 5.7**) [81].

Also the azygos vein, the esophagus, the phrenic nerves, and the recurrent laryngeal nerve can be involved. Pericardial spread is relatively common, manifesting as pericardial effusion and/or irregular thickening of the pericardium. Even compression or direct extension to the heart may be seen, particularly to the left atrium [9, 81].

5.4.6 Pathway of Diffusion: Distant Metastatic Spread

Once the tumor reaches access to the mediastinum, there are pathways of spread downward into the abdomen via the aortic and esophageal hiatus, both through lymphatic vessels and direct diffusion. This can result in intra-abdominal lymphadenopathies primarily along the celiac vessels resulting in celiac, periportal, peripancreatic, and para-aortic lymph node metastases. Disease may also reach the gastrohepatic ligament either by spread along vascular planes or through the esophageal hiatus.

SCLC can also directly spread upward via the cervicothoracic hiatus, resulting in supraclavicular and, less commonly, lower neck adenopathies and possible involvement of the lower neck structure (cervical esophagus, hypopharynx, thyroid, etc.) [86].

Metastatic spread to distant organs is also frequent in SCLC. The most common metastatic

sites at diagnosis are bone (19–38%), liver (17–34%), adrenal glands (10–17%), and brain (up to 14%, whose 10–15% in neurologically asymptomatic patients) [9]. Particularly, SCLC has been associated with an increased metastatic potential to liver and brain with respect to NSCLC [87].

Nodules or masses in the contralateral lung can be also found as well as other uncommon metastatic sites, such as pancreas, prostate, spinal cord, and oropharynx [81]. Lastly, metastatic involvement of bone marrow has been detected in 10–15% of patients. However, less than 5% of these patients have bone marrow as isolate distant metastatic site [88].

5.5 Conclusions

Pulmonary neuroendocrine neoplasms (NENs) are a heterogeneous group of tumors, with different morphological, immunohistochemical, and molecular characteristics and noticeably different clinical and biological behavior, ranging from the indolent course of TC to the highly aggressive behavior of the SCLC. Also imaging characteristics of NENs are quite different among the two well-differentiated TC and AC, currently classified as NETs, and the two poorly differentiated LCNEC and SCLC, classified as NECs, reflecting the different pathways of diffusion of these neoplasms. Knowledge of the more common morphologic characteristics and diffusion pathways of these neoplasms might help in recognizing NENs.

CT and PET/CT are the most useful imaging modalities for diagnosing and staging these tumors, while MR has specific indication for brain, bone, and liver involvement, which is typical of the extensive stage of SCLC.

References

1. Chong S, Lee KS, Chung MJ, Han J, Kwon OJ, Kim TS. Neuroendocrine tumors of the lung: clinical, pathologic, and imaging findings. *Radiographics*. 2006;26(1):41–57.
2. Rossi G, Bisagni A, Cavazza G. High-grade neuroendocrine carcinoma. *Curr Opin Pulm Med*. 2014;20:332–9.
3. Gustafsson BI, Kidd M, Modlin IM. Neuroendocrine tumors of the diffuse neuroendocrine system. *Curr Opin Oncol*. 2008;20(1):1–12.
4. Filosso PL, Falcoz PE, Solidoro P, Pellicano D, Passani S, Guerrero F, et al. The European Society of Thoracic Surgeons (ESTS) lung neuroendocrine tumors (NETs) database. *J Thorac Dis*. 2018;10(Suppl 29):S3528–32.
5. Leoncini E, Boffetta P, Shafir M, Aleksovskaja K, Boccia S, Rindi G. Increased incidence trend of low-grade and high-grade neuroendocrine neoplasms. *Endocrine*. 2017;58(2):368–79.
6. Modlin IM, Lye KD, Kidd M. A 5-decade analysis of 13,715 carcinoid tumors. *Cancer*. 2003;97(4):934–59.
7. Caplin ME, Baudin E, Ferolla P, Filosso P, Garcia-Yuste M, Lim E, et al. Pulmonary neuroendocrine (carcinoid) tumors: European Neuroendocrine Tumor Society expert consensus and recommendations for best practice for typical and atypical pulmonary carcinoid. *Ann Oncol*. 2015;26(8):1604–20.
8. Yao JC, Hassan M, Phan A, Dagohoy C, Leary C, Mares JE, et al. One hundred years after “carcinoid”: epidemiology of and prognostic factors for neuroendocrine tumors in 35,825 cases in the United States. *J Clin Oncol*. 2008;26(18):3063–72.
9. Carter BW, Glisson BS, Truong MT, Erasmus JJ. Small cell lung carcinoma: staging, imaging, and treatment considerations. *Radiographics*. 2014;34(6):1707–21.
10. Paladugu RR, Benfield JR, Pak HY, Ross RK, Teplitz RL. Bronchopulmonary Kulchitzky cell carcinoma: a new classification scheme for typical and atypical carcinoids. *Cancer*. 1985;55:1303–11.
11. Travis WD, Brambilla E, Müller-Hermelink HK, Harris CC, editors. WHO classification of tumours. Pathology and genetics of tumours of the lung, pleura, thymus and heart. World Health Organization classification tumours. Lyon: IARC Press; 2004.
12. Ito T, Uda N, Okudela K, Yazawa T, Kitamura H. Mechanisms of neuroendocrine differentiation in pulmonary neuroendocrine cells and small cell carcinoma. *Endocr Pathol*. 2003;14(2):133–9.
13. Travis WD, Brambilla E, Burke AP, Marx A, Nicholson AG. WHO classification of tumours of the lung, pleura, thymus and heart. World Health Organization classification tumours. 4th ed. Lyon: IARC Press; 2015.
14. Yesner R. Small cell tumors of the lung. *Am J Surg Pathol*. 1983;7:775–85.
15. Hendifar AE, Marchevsky AM, Tuli R. Neuroendocrine tumors of the lung: current challenges and advances in the diagnosis and management of well-differentiated disease. *J Thorac Oncol*. 2017;12(3):425–36.
16. Righi L, Gatti G, Volante M, Papotti M. Lung neuroendocrine tumors: pathological characteristics. *J Thorac Dis*. 2017;9(Suppl 15):S1442–7.
17. Travis WD, Brambilla E, Nicholson AG, Yatabe Y, Austin JHM, Beasley MB, et al. The 2015 World Health Organization classification of lung tumors: impact of genetic, clinical and radiologic advances since the 2004 classification. *J Thorac Oncol*. 2015;10(9):1243–60.
18. Rindi G, Klimstra DS, Abedi-Ardekani B, Asa SL, Bosman FT, Brambilla E, et al. A common classification framework for neuroendocrine neoplasms: an International Agency for Research on Cancer (IARC) and World Health Organization (WHO) expert consensus proposal. *Mod Pathol*. 2018;31(12):1770–86.
19. Pelosi G, Rindi G, Travis WD, Papotti M. Ki-67 antigen in lung neuroendocrine tumors: unravelling a role in clinical practice. *J Thorac Oncol*. 2014;9(3):273–84.
20. Rindi G, Klersy C, Inzani F, Fellegara G, Ampollini L, Ardizzoni A, et al. Grading the neuroendocrine tumors of the lung: an evidence-based proposal. *Endocr Relat Cancer*. 2014;21(1):1–16.
21. Detterbeck FC, Boffa DJ, Kim AW, Tanoue LT. The eighth edition lung cancer stage classification. *Chest*. 2017;151(1):193–203.
22. Morandi U, Casali C, Rossi G. Bronchial typical carcinoid tumors. *Semin Thorac Cardiovasc Surg*. 2006;18(3):191–8.
23. Rekhtman N. Neuroendocrine tumors of the lung: an update. *Arch Pathol Lab Med*. 2010;134(11):1628–38.
24. Dincer HE, Podgaetz E, Andrade RS. Pulmonary neuroendocrine tumors. Part I. Spectrum and characteristics of tumors. *J Bronchology Interv Pulmonol*. 2015;22(3):267–73.
25. Wolin EM. Challenges in the diagnosis and management of well-differentiated neuroendocrine tumors of the lung (typical and atypical carcinoid): current status and future considerations. *Oncologist*. 2015;20(10):1123–31.
26. Phan AT, Oberg K, Choi J, Harrison LH Jr, Hassan MM, Strosberg JR, et al. NANETS consensus guideline for the diagnosis and management of neuroendocrine tumors: well-differentiated neuroendocrine tumors of the thorax (includes lung and thymus). *Pancreas*. 2010;39(6):784–98.
27. Gosain R, Mukherjee S, Yendamuri SS, Iyer R. Management of typical and atypical pulmonary carcinoids based on different established guidelines. *Cancers*. 2018;10(12):pii:E510.
28. Benson RE, Rosado-de-Christenson ML, Martínez-Jiménez S, Kunin JR, Pettavel PP. Spectrum of pulmonary neuroendocrine proliferations and neoplasms. *Radiographics*. 2013;33(6):1631–49.
29. Detterbeck FC. Clinical presentation and evaluation of neuroendocrine tumors of the lung. *Thorac Surg Clin*. 2014;24(3):267–76.

30. Rosado de Christenson ML, Abbott GF, Kirejczyk WM, Galvin JR, Travis WD. Thoracic carcinoids: radiologic-pathologic correlation. *Radiographics*. 1999;19(3):707–36.
31. Zagurovskaya M, Tran-Harding K, Gibbs R. Primary lung carcinoid metastatic to the breast. *Radiol Case Rep*. 2017;12(2):223–8.
32. Asamura H, Kameya T, Matsuno Y, Noguchi M, Tada H, Ishikawa Y, et al. Neuroendocrine neoplasms of the lung: a prognostic spectrum. *J Clin Oncol*. 2006;24(1):70–6.
33. Dasari A, Shen C, Halperin D, Zhao B, Zhou S, Xu Y, et al. Trends in the incidence, prevalence, and survival outcomes in patients with neuroendocrine tumors in the United States. *JAMA Oncol*. 2017;3(10):1335–42.
34. Robelin P, Hadoux J, Forestier J, Planchard D, Hervieu V, Berdelou A, et al. Characterization, prognosis, and treatment of patients with metastatic lung carcinoid tumors. *J Thorac Oncol*. 2019;13:S1556-0864(19)30103-0.
35. Huang Y, Yang X, Lu T, Li M, Zhao M, Yang X, et al. Assessment of the prognostic factors in patients with pulmonary carcinoid tumor: a population-based study. *Cancer Med*. 2018;7(6):2434–41.
36. Detterbeck FC. Management of carcinoid tumors. *Ann Thorac Surg*. 2010;89(3):998–1005.
37. Travis WD. Pathology and diagnosis of neuroendocrine tumors: lung neuroendocrine. *Thorac Surg Clin*. 2014;24:257–66.
38. Rossi G, Cavazza A, Spagnolo P, Sverzellati N, Longo L, Jukna A, et al. Diffuse idiopathic pulmonary neuroendocrine cell hyperplasia syndrome. *Eur Respir J*. 2016;47(6):1829–41.
39. Gorshtein A, Gross DJ, Barak D, Strenov Y, Refaeli Y, Shimon I, et al. Diffuse idiopathic pulmonary neuroendocrine cell hyperplasia and the associated lung neuroendocrine tumors: clinical experience with a rare entity. *Cancer*. 2012;118(3):612–9.
40. Jeung MY, Gasser B, Gangi A, Charneau D, Ducrocq X, Kessler R, et al. Bronchial carcinoid tumors of the thorax: spectrum of radiologic findings. *Radiographics*. 2002;22(2):351–65.
41. Baxi AJ, Chintapalli K, Katkar A, Restrepo CS, Betancourt SL, Sunnapwar A. Multimodality imaging findings in carcinoid tumors: a head-to-toe spectrum. *Radiographics*. 2017;37(2):516–36.
42. Erasmus JJ, McAdams HP, Patz EF Jr, Coleman RE, Ahuja V, Goodman PC. Evaluation of primary pulmonary carcinoid tumors using FDG PET. *AJR Am J Roentgenol*. 1998;170(5):1369–73.
43. Jiang Y, Hou G, Cheng W. The utility of 18F-FDG and 68Ga-DOTA-Peptide PET/CT in the evaluation of primary pulmonary carcinoid: a systematic review and meta-analysis. *Medicine (Baltimore)*. 2019;98(10):e14769.
44. Ha SY, Lee JJ, Cho J, Hyeon J, Han J, Kim HK. Lung parenchymal invasion in pulmonary carcinoid tumor: an important histologic feature suggesting the diagnosis of atypical carcinoid and poor prognosis. *Lung Cancer*. 2013;80(2):146–52.
45. Colby TV, Koss MN, Travis WD. Carcinoid and other neuroendocrine tumors. In: Colby TV, Koss MN, Travis WD, editors. *Atlas of tumor pathology: tumors of the lower respiratory tract, fasc. 13, ser. 3*. Washington, DC: Armed Forces Institute of Pathology; 1995. p. 287–317.
46. Salyer DC, Salyer WR, Eggleston JC. Bronchial carcinoid tumors. *Cancer*. 1975;36:1522–37.
47. Scarsbrook AF, Ganeshan A, Satham J, Thakker RV, Weaver A, Talbot D, et al. Anatomic and functional imaging of metastatic carcinoid tumors. *Radiographics*. 2007;27(2):455–77.
48. Naidich DP. CT/MR correlation in the evaluation of tracheobronchial neoplasia. *Radiol Clin N Am*. 1990;28:555–71.
49. Travis WD. Advances in neuroendocrine lung tumors. *Ann Oncol*. 2010;21(suppl 7):vii65–71.
50. Chong CR, Wirth LJ, Nishino M, Chen AB, Sholl LM, Kulke MH, et al. Chemotherapy for locally advanced and metastatic pulmonary carcinoid tumors. *Lung Cancer*. 2014;86(2):241–6.
51. Riihimäki M, Hemminki A, Sundquist K, Sundquist J, Hemminki K. The epidemiology of metastases in neuroendocrine tumors. *Int J Cancer*. 2016;139(12):2679–86.
52. Bhosale P, Shah A, Wei W, Varadhachary G, Johnson V, Shah V, et al. Carcinoid tumours: predicting the location of the primary neoplasm based on the sites of metastases. *Eur Radiol*. 2013;23(2):400–7.
53. Wolin EM. Advances in the diagnosis and management of well-differentiated and intermediate-differentiated neuroendocrine tumors of the lung. *Chest*. 2017;151(5):1141–6.
54. Lou F, Sarkaria I, Pietanza C, Travis W, Roh MS, Sica G, et al. Recurrence of pulmonary carcinoid tumors after resection: implications for postoperative surveillance. *Ann Thorac Surg*. 2013;96(4):1156–62.
55. Fasano M, Della Corte CM, Papaccio F, Ciardiello F, Morgillo F. Pulmonary large-cell neuroendocrine carcinoma: from epidemiology to therapy. *J Thorac Oncol*. 2015;10(8):1133–41.
56. Fernandez FG, Battafarano RJ. Large-cell neuroendocrine carcinoma of the lung: an aggressive neuroendocrine lung cancer. *Semin Thorac Cardiovasc Surg*. 2006;18(3):206–10.
57. Sulai NH, Kim ES, Ananthanarayanan V. Large cell carcinoma of the lung. In: Raghavan D, Ahluwalia MS, Blanke CD, Brown J, Kim ES, Reaman GH, Sekeres MA, editors. *Textbook of uncommon cancer*. Hoboken: Wiley; 2017. p. 293–304.
58. Oshiro Y, Kusumoto M, Matsuno Y, Asamura H, Tsuchiya R, Terasaki H, et al. CT findings of surgically resected large cell neuroendocrine carcinoma of the lung in 38 patients. *AJR Am J Roentgenol*. 2004;182(1):87–91.
59. Welter S, Aigner C, Roessel C. The role of surgery in high grade neuroendocrine tumours of the lung. *J Thorac Dis*. 2017;9(Suppl 15):1474–83.
60. Derks JL, Hendriks LE, Buikhuisen WA, Groen HJ, Thunnissen E, van Suylen RJ, et al. Clinical features of large cell neuroendocrine carcinoma: a population-based overview. *Eur Respir J*. 2016;47(2):615–24.
61. Naidoo J, Santos-Zabala ML, Iyriboz T, Woo KM, Sima CS, Fiore JJ, et al. Large cell neuroendocrine carcinoma of the lung: clinic-pathologic features, treatment, and outcomes. *Clin Lung Cancer*. 2016;17(5):121–9.

62. Shin AR, Shin BK, Choi JA, Oh YW, Kim HK, Kang EY. Large cell neuroendocrine carcinoma of the lung: radiologic and pathologic findings. *J Comput Assist Tomogr*. 2000;24(4):567–73.
63. Chong S, Lee KS, Kim BT, Choi JY, Yi CA, Chung MJ, et al. Integrated PET/CT of pulmonary neuroendocrine tumors: diagnostic and prognostic implications. *AJR Am J Roentgenol*. 2007;188(5):1223–31.
64. Jung KJ, Lee KS, Han J, Kwon OJ, Kim J, Shim YM, et al. Large cell neuroendocrine carcinoma of the lung: clinical, CT, and pathologic findings in 11 patients. *J Thorac Imaging*. 2001;16(3):156–62.
65. Kinoshita T, Yoshida J, Ishii G, Aokage K, Hishida T, Nagai K. The differences of biological behavior based on the clinicopathological data between resectable large-cell neuroendocrine carcinoma and small-cell lung carcinoma. *Clin Lung Cancer*. 2013;14(5):535–40.
66. Takei H, Asamura H, Maeshima A, Suzuki K, Kondo H, Niki T, et al. Large cell neuroendocrine carcinoma of the lung: a clinicopathologic study of eighty-seven cases. *J Thorac Cardiovasc Surg*. 2002;124(2):285–92.
67. Sarkaria IS, Iyoda A, Roh MS, Sica G, Kuk D, Sima CS, et al. Neoadjuvant and adjuvant chemotherapy in resected pulmonary large cell neuroendocrine carcinomas: a single institution experience. *Ann Thorac Surg*. 2011;92(4):1180–6.
68. Gazdar AF, Bunn PA, Minna JD. Small-cell lung cancer: what we know, what we need to know and the path forward. *Nat Rev Cancer*. 2017;17(12):725–37.
69. Gustafsson BI, Kidd M, Chan A, Malfertheiner MV, Modlin IM. Bronchopulmonary neuroendocrine tumors. *Cancer*. 2008;113(1):5–21.
70. Govindan R, Page N, Morgensztern D, Read W, Tierney R, Vlahiotis A, et al. Changing epidemiology of small-cell lung cancer in the United States over the last 30 years: analysis of the surveillance, epidemiologic, and end results database. *J Clin Oncol*. 2006;24(28):4539–44.
71. Käsmann L, Bolm L, Janssen S, Rades D. Prognostic factors and treatment of early-stage small-cell lung cancer. *Anticancer Res*. 2017;37(3):1535–7.
72. Silva M, Galeone C, Sverzellati N, Marchianò A, Calareso G, Sestini S, et al. Screening with low-dose computed tomography does not improve survival of small cell lung cancer. *J Thorac Oncol*. 2016;11(2):187–93.
73. Zelen M. Keynote address on biostatistics and data retrieval. *Cancer Chemother Rep* 3. 1973;4(2):31–42.
74. Kalemkerian GP, Schneider BJ. Advances in small cell lung cancer. *Hematol Oncol Clin North Am*. 2017;31(1):143–56.
75. Früh M, De Ruyscher D, Popat S, Crinò L, Peters S, Felip E, ESMO Guidelines Working Group. Small-cell lung cancer (SCLC): ESMO clinical practice guidelines for diagnosis, treatment and follow-up. *Ann Oncol*. 2013;24(Suppl 6):99–105.
76. Onn A, Vaporciyan A, Chang J, Komaki R, Roth J, Herbst R. Cancer of the lung. In: Kufe DW, Bast Jr RC, Hait WN, et al., editors. *Cancer medicine*. Hamilton: American Association for Cancer Research; 2006. p. 1179–24.
77. Lu HY, Wang XJ, Mao WM. Targeted therapies in small cell lung cancer. *Oncol Lett*. 2013;5(1):3–11.
78. Foster NR, Mandrekar SJ, Schild SE, Nelson GD, Rowland KM Jr, Deming RL, et al. Prognostic factors differ by tumor stage for small cell lung cancer: a pooled analysis of North Central Cancer Treatment Group trials. *Cancer*. 2009;115(12):2721–31.
79. Swartz DR, Ramaekers F, Speel E-JM. Molecular and cellular biology of neuroendocrine lung tumors: evidence for separate biological entities. *Biochim Biophys Acta (BBA) Rev Cancer*. 2012;1826(2):255–71.
80. Rosado-de-Christenson ML, Templeton PA, Moran CA. Bronchogenic carcinoma: radiologic-pathologic correlation. *Radiographics*. 1994;14(2):429–46.
81. Kazawa N, Kitaichi M, Hiraoka M, Togashi K, Mio N, Mishima M, et al. Small cell lung carcinoma: eight types of extension and spread on computed tomography. *J Comput Assist Tomogr*. 2006;30(4):653–61.
82. Kreisman H, Wolkove N, Quiox E. Small cell lung cancer presenting as a solitary pulmonary nodule. *Chest*. 1992;101(1):225–31.
83. Seute T, Leffers P, ten Velde GP, Twijnstra A. Detection of brain metastases from small cell lung cancer: consequences of changing imaging techniques (CT versus MRI). *Cancer*. 2008;112(8):1827–34.
84. Jackman DM, Johnson BE. Small-cell lung cancer. *Lancet*. 2005;366(9494):1385–96.
85. Yabuuchi H, Murayama S, Sakai S, Hashiguchi N, Murakami J, Muranaka T, et al. Resected peripheral small cell carcinoma of the lung: computed tomographic-histologic correlation. *J Thorac Imaging*. 1999;14(2):105–8.
86. Ravenel JG. Small cell carcinoma. In: Wheless L, James Brashears J, editors. *Lung cancer imaging*. New York: Humana Press; 2013. p. 79–88.
87. Riihimäki M, Hemminki A, Fallah M, Thomsen H, Sundquist K, Sundquist J, et al. Metastatic sites and survival in lung cancer. *Lung Cancer*. 2014;86(1):78–84.
88. Levitan N, Byrne RE, Bromer RH, Faling LJ, Caslowitz P, Pattern DH, et al. The value of the bone scan and bone marrow biopsy staging small cell lung cancer. *Cancer*. 1985;56(3):652–4.



Tumors of the Thymus

Carlotta Sartorio, Andrea Ciuni, and Gianluca Milanese

- 6.1 Introduction – 106**
 - 6.1.1 Embryology – 106
 - 6.1.2 Histology – 106
 - 6.1.3 Gross Anatomy and Normal Imaging Findings – 106
- 6.2 Thymic Epithelial Tumors – 109**
 - 6.2.1 Epidemiology – 109
 - 6.2.2 Local Growth – 110
 - 6.2.3 Metastatic Dissemination – 111
 - 6.2.4 Follow-Up – 113
- 6.3 Thymoma – 113**
 - 6.3.1 Epidemiology – 113
 - 6.3.2 Symptoms – 115
 - 6.3.3 Imaging – 115
 - 6.3.4 Local Spread and Metastatic Dissemination – 117
- 6.4 Thymic Carcinoma – 118**
 - 6.4.1 Epidemiology – 118
 - 6.4.2 Symptoms – 118
 - 6.4.3 Imaging – 118
 - 6.4.4 Local Spread and Metastatic Dissemination – 121
- 6.5 Carcinoid – 122**
 - 6.5.1 Epidemiology – 122
 - 6.5.2 Symptoms – 122
 - 6.5.3 Imaging – 122
 - 6.5.4 Local Spread and Metastatic Dissemination – 122
- 6.6 Thymoliposarcoma – 123**
 - References – 123**

6.1 Introduction

The thymus is a primary lymphoid organ of the immune system granting lymphocyte generation and maturation of T lymphocytes throughout life [1]. Neoplasms of the thymus show a wide range of histology and biological behaviour, potentially involving both adjacent and distant structures. Imaging is paramount for diagnosis, staging and management of thymic malignancies [1].

6.1.1 Embryology

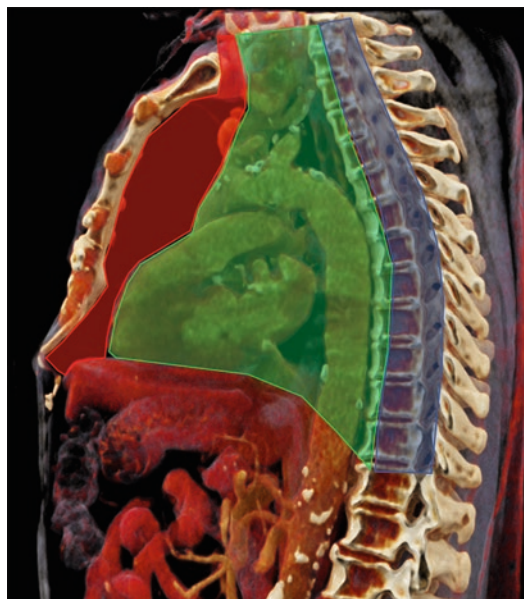
The thymus arises from the third and fourth branchial pouches, during the sixth gestational week. After the eighth gestational week, it migrates downwards to the anterosuperior mediastinum. The thymus is a purely epithelial organ until the ninth gestational week. Glandular lobulations develop since the tenth week when small lymphoid cells migrate from the foetal liver and bone marrow into the thymus.

6.1.2 Histology

The thymus displays a cortical and a medullar component. On the one hand, the cortex is mainly composed of lymphocytes (named thymocytes), with fewer epithelial and mesenchymal cells. On the other hand, the medulla features fewer thymocytes and a larger amount of epithelial cells. The interaction between the cortical and medullar component grants synergistic maturation of thymocytes under the paracrine action of epithelial cells, the latter also differentiating into macrophages and myoid cells. Moreover, epithelial cells also evolve into a peculiar structure of thymus: the “Hassall’s corpuscles” defined by round and keratinized formations of mature epithelial cells [1].

6.1.3 Gross Anatomy and Normal Imaging Findings

The thymus lies in the retrosternal region occupying the anterosuperior mediastinum (from sternal manubrium to the level of the fourth costal cartilage). Since 2017, a three-compartment



■ Fig. 6.1 ITMIG definition of mediastinal compartments. Cinematic CT image showing prevascular (red), visceral (green) and paravertebral (blue) compartments. (Carter et al. [14])

ment (prevascular, visceral and paravertebral) computed tomography (CT)-based classification of mediastinum is provided by the International Thymic Malignancy Interest Group (ITMIG) (■ Fig. 6.1). According to the ITMIG scheme, the thymus is located within the adipose tissue of prevascular compartment, along with lymph nodes and the left brachiocephalic vein. Macroscopic shape is determined by adjacent structures as thymus moulds against the trachea, left brachiocephalic vein, aortic arch and its branches, and pericardium [2]. Bilobate morphology is seen at complete maturation, each lobe is enclosed in its own thin fibrous capsule [2]. The right lobe shows quite simple and homogeneous shape and is located near the superior vena cava. Conversely, the left lobe features two components, namely, the main part (anterior to the ascending aorta) and the accessory limb (lateral to the pulmonary artery trunk, with variable size among individuals). Rarely, another small projection of the left lobe extends upwards behind the left brachiocephalic vein in front of the trachea; it is seen as a small tapering cranial extensions reaching the thyroid cartilage [3]. Such anatomic distribution reflects the most common spots of primary thymic

Table 6.1 Predictive features for anterior mediastinal mass diagnosis [4–6, 90–93]

	Thymic epithelial neoplasms	Lymphoma	Germ cell tumors	Benign lesions
Age	Thymoma: >35 years	<35 years	<35 years	Thymic hyperplasia: 20–30 years
	Thymic carcinoma: the portion tends to gradually increase as age increases			Thymic bed cyst: >50 years
Size	Thymoma: 5–10 cm	Bulky > 5 cm	Larger	Thymic cyst: 0.5–16 cm
	Thymic carcinoma: 5.00 ± 2.29 cm		(The largest ever mixed germ cell tumor of the mediastinum reported was 21 × 20 × 16 cm)	
Shape	Thymoma: round, oval, lobulated	Lobulated/amorphous	Lobulated/amorphous	Thymic hyperplasia: bipyramidal
Smooth contour CT	Only thymoma		Only mature teratoma	Thymic cyst: round, oval, saccular
Lobulated contour CT	++	++		+
Internal mammary lymphadenopathy	Rarely observed	+++	Not seen	Not seen
Mediastinal and supraclavicular lymphadenopathy	Rarely observed	+++	+	
Mediastinal encasement – lung invasion	Rarely observed	++	Rarely observed	
Marbled fat ^a	Occasionally seen	Occasionally seen		+
Globular fat			+	
Calcification	+	+	++	
Low CT attenuation (<40)				++
Midline location				+
Pleural effusion	+	++	+	Not seen

^aSeveral malignant lesions could contain interspersed intralesional fat that could simulate the marbled fat appearance; for this reason, radiologists should exercise caution and evaluate the characteristics of the lesion as a whole before concluding that it is benign
+++ very frequent; ++ frequent; + possible

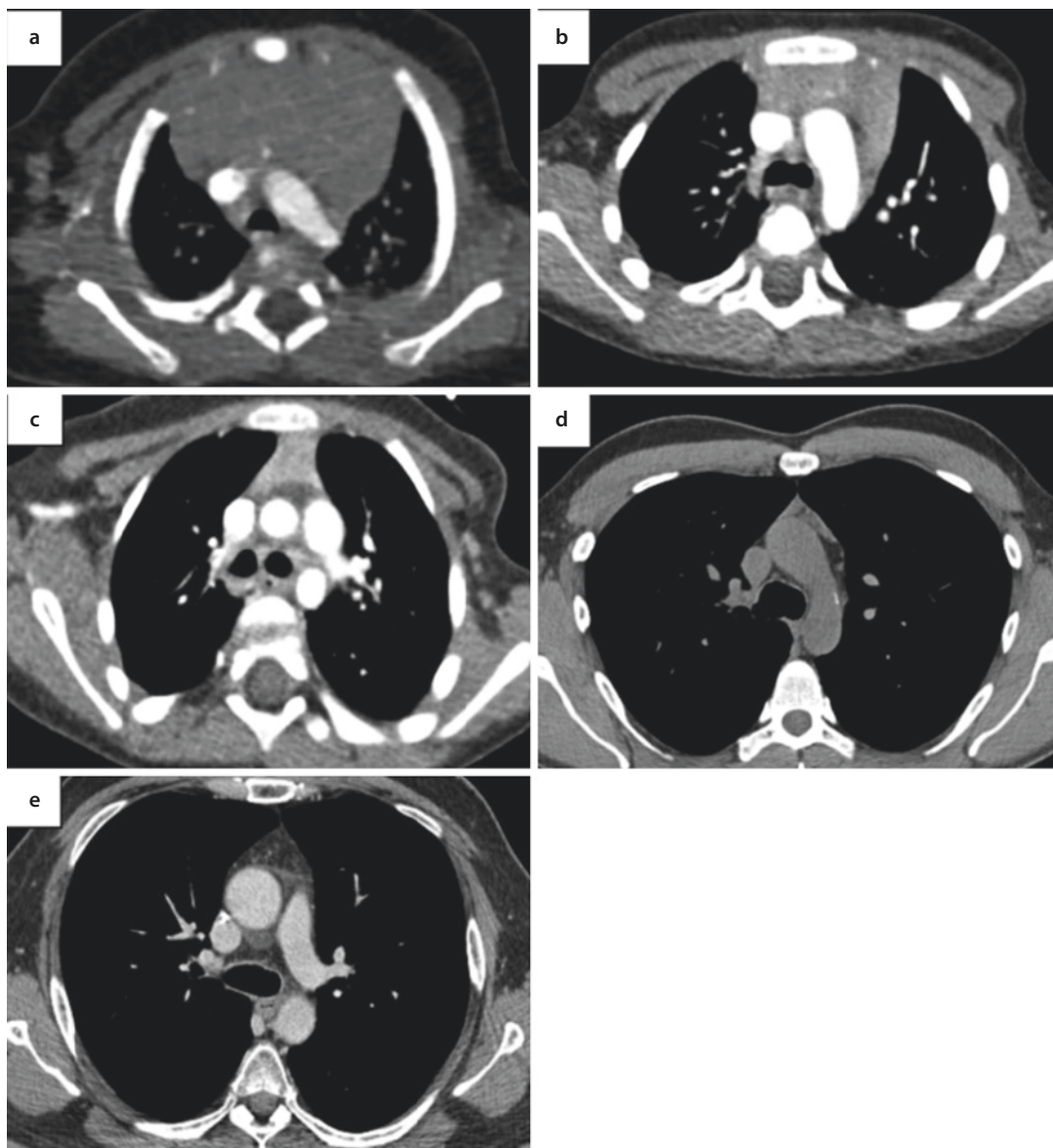


Fig. 6.2 Physiological modifications of thymic morphology throughout age. Chest CT in axial plane at the age of 2 months **a**, 3 years **b**, 4 years **c**, 39 years **d** and 48 years **e**. **a** The thymus appears as a bilobed homogeneous soft-tissue density structure, without compression

of vascular structures or airway. **b, c** The thymus shows a quadrangular shape in early childhood. **d, e** In adult age, the thymus displays a triangular shape, with progressive reduction of its volume and density (almost complete adipose tissue replacement in older individuals)

malignancy, exploited for systematic differential approach to imaging of mediastinal masses. Various neoplasms may arise from this anatomic region; still, the differential can be narrowed based on both clinical and radiological features [4–6] (Table 6.1). Thymic composition varies with age and so does its appearance

at imaging: at younger age, thymus density by computed tomography (CT) is similar to muscle, whilst in elderly it shows almost adipose density (Fig. 6.2). Homogeneous thymic density is the most common appearance on CT; nonetheless, lobular architecture with partial fatty replacement is occasionally seen [2].

Table 6.2 Diagnostic criteria of thymomas in the 2015 World Health Organization (WHO) classification

Thymoma subtype	Obligatory criteria	Optional criteria
Type A	Occurrence of bland, spindle-shaped epithelial cells (at least focally); paucity or absence of immature (TdT+) T cells throughout the tumor	Polygonal epithelial cells CD20+ epithelial cells
Atypical type A variant	Criteria of type A thymoma; in addition: comedo-type tumor necrosis; increased mitotic count (>4/2 mm ²); nuclear crowding	Polygonal epithelial cells CD20+ epithelial cells
Type AB	Occurrence of bland, spindle-shaped epithelial cells (at least focally); abundance of immature (TdT+) T cells focally or throughout tumor	Polygonal epithelial cells CD20+ epithelial cells
Type B1	Thymus-like architecture and cytology: abundance of immature T cells, areas of medullary differentiation (medullary islands); paucity of polygonal or dendritic epithelial cells without clustering (i.e. <3 contiguous epithelial cells)	Hassall's corpuscles; perivascular spaces
Type B2	Increased numbers of single or clustered polygonal or dendritic epithelial cells intermingled with abundant immature T cells	Medullary islands; Hassall's corpuscles; perivascular spaces
Type B3	Sheets of polygonal slightly to moderately atypical epithelial cells; absent or rare intercellular bridges; paucity or absence of intermingled TdT+ T cells	Hassall's corpuscles; perivascular spaces
Micronodular thymoma with lymphoid stroma	Nodules of bland spindle or oval epithelial cells surrounded by an epithelial cell-free lymphoid stroma	Lymphoid follicles; monoclonal B cells and/or plasma cells (rare)
Metaplastic thymoma	Biphasic tumor composed of solid areas of epithelial cells in a background of bland-looking spindle cells; absence of immature T cells	Pleomorphism of epithelial cells; actin-, keratin- or EMA-positive spindle cells

6.2 Thymic Epithelial Tumors

Thymic epithelial malignancies are rare entities (incidence 1.3 to 3.2/1.000.000 individuals in Europe) [7]. Various classifications of thymic malignancies have been proposed by variable perspectives.

Histological findings are accounted in the World Health Organization (WHO) classification system (last updated in 2015), which features both obligatory and optional diagnostic criteria (Table 6.2). Notably, WHO stratifies thymoma into five subtypes, as follows: A, AB, B1, B2 and B3 [8]. The latter two subtypes are described as “high-risk thymomas”, as opposed to the remainder “low-risk thymomas”. Besides the five subtypes of thymoma, a further category C is applied to thymic carcinoma [8].

Description of surgical findings is articulated within the Masaoka-Koga staging system

(Table 6.3), where the stratification of risk is obtained by signs of local invasion and presence of metastases [9]. A similar (yet different) approach is provided by the International Association for the Study of Lung Cancer (IASLC) and ITMIG. This system is endorsed by the eighth edition of the TNM classification of malignant tumors (Table 6.4a). Noteworthy, the similarities between the IASLC-ITMIG approach and the Masaoka-Koga system allow a detailed translation between each other (Table 6.4b).

6.2.1 Epidemiology

Thymic malignancies may affect all ages; nonetheless, mean age at diagnosis is around 50–60 years. Slight female predominance is seen in categories A, AB and B1; otherwise, thymoma

Table 6.3 Masaoka-Koga staging system for thymoma

Stage	Descriptor
I	Complete encapsulation of tumor
IIa	Microscopic tumor invasion through capsule
IIb	Macroscopic tumor invasion into surrounding fat
III	Invasion of the pericardium, great vessels or lung
IVa	Pleural or pericardial dissemination
IVb	Lymphatic/hematogenous metastasis

shows an overall balanced by-gender representation [10].

There is no confirmed evidence about environmental or infectious risk factors through the pathogenesis of thymic epithelial tumors. Rarely, thymoma was reported in subjects with solid-organ transplantation, HIV infection or after mediastinal radiation therapy [9]. Thymoma is found in association with cancer susceptibility syndromes (e.g. multiple endocrine neoplasia type I (MEN1)) as well as extra-thymic hematopoietic and solid cancers [11].

Five-year survival of thymic malignancies was 64% overall, with large variations across WHO subtypes ranging from 69% in malignant thymoma to 13% in undifferentiated thymic cancer [10].

6.2.2 Local Growth

Overall, it is estimated that 30% of patients diagnosed with thymic epithelial tumor present with locally advanced disease at time of diagnosis [12, 13]. The thin thymic own capsule is the only fence between thymic neoplasm and its progression to mediastinal fat where no anatomic boundary protects mediastinal compartments from local invasion. Several schemes were proposed to facilitate surgical planning of mediastinal masses [14].

Thymomas growing within prevascular compartment may be asymptomatic and incidentally discovered in about one-third of cases [15]. However, the majority of thymic tumors progressively enlarge until compression on adjacent structures and subsequent clinical manifestations.

Table 6.4a TNM staging

Stage		Descriptor
T1	T1a	Encapsulated or unencapsulated, with or without extension into the mediastinal fat
	T1b	Extension into the mediastinal pleura
T2		Direct invasion of the pericardium
T3		Direct invasion of the lung, brachiocephalic vein, superior vena cava, chest wall, phrenic nerve and/or hilar (extra pericardial) pulmonary vessels
T4		Direct invasion of the aorta, arch vessels, main pulmonary artery, myocardium, trachea or oesophagus
Node		
N0		No nodal involvement
N1		Anterior (peri-thymic) nodes (IASLC levels 1, 3a, 6 and/or supradiaphragmatic/inferior phrenic/pericardial)
N2		Deep intrathoracic or cervical nodes (IASLC levels 2, 4, 5, 7, 10 and/or internal mammary nodes)
Metastasis		
M0		No metastatic pleural, pericardial or distant sites
M1	M1a	Separate pleural or pericardial nodule(s)
	M1b	Pulmonary intraparenchymal nodule or distant organ metastasis

In case of predominantly posterior growth, the trachea and oesophagus can be compressed causing pain, cough, dyspnoea and dysphagia. Other clinical manifestations may be related to superior vena cava syndrome (arm or facial swelling) (Fig. 6.3) and to superior laryngeal (hoarseness) or phrenic (diaphragmatic palsy) nerve damage (Table 6.5) [16].

Tumor size is not included as a predictor of survival for thymic epithelial tumors [17], unlike many solid malignancies (e.g. breast, lung, renal

Table 6.4b TNM staging and corresponding Masaoka-Koga stage

Stage grouping	T	N	M	Corresponding Masaoka-Koga stage	Descriptors
I	T1	N0	M0	I	Grossly and microscopically completely encapsulated tumor
				IIA	Microscopic transcapsular invasion
				IIB	Macroscopic invasion into thymic or surrounding fatty tissue or grossly adherent to, but not breaking through, the mediastinal pleura or pericardium
II	T2	N0	M0	III	Macroscopic invasion into neighbouring organ (i.e. pericardium, great vessel or lung)
IIIA	T3	N0	M0		
IIIB	T4	N0	M0		
IVA	T any	N1	M0	IVA	Pleural or pericardial metastasis
	T any	N0, N1	M1a	IVB	Lymphatic or hematogenous metastasis
IVB	T any	N2	M0, M1a		
	T any	N any	M1b		

and pancreatic cancers). Nonetheless, a size greater than 40 mm represented an independent negative prognostic factor for recurrence-free survival in IASLC-ITMIG stage I disease ($T_1N_0M_0$) [18].

Malignant mediastinal tumors may directly extend in all directions, notably through the pleura and pericardium, or other mediastinal structures. A well-defined fat interface usually indicates absence of extensive local invasion; still, minimal invasion may be undetectable at imaging. On the other hand, infiltration of fat planes, irregular interfaces and encasement of mediastinal structures are highly suggestive of invasion.

Thickening, nodularity and effusion of either the pleura or pericardium are signs of infiltration and spread through the serous cavity [19].

Thymic lesions displaying lobulated or irregular contours, cystic or necrotic regions and multifocal calcifications are consistent with an underlying invasive thymoma, which can also associate with signs of fat infiltration, progression to lung parenchyma and great vessel invasion or encasement [20–23]. Endobronchial spread of thymic tumors has been occasionally reported as mass trespassing bronchial walls and further growth within the bronchial lumen [24].

6.2.3 Metastatic Dissemination

Independently from their histological grade, all thymic epithelial tumors may involve distant structures by *transcoelomic* (towards pleura and pericardium), *lymphatic* (towards thoracic and extra-thoracic lymph node) and *hematogenous* spread (towards any organ).

- The *transcoelomic* pathway is the most common modality of dissemination in thymic malignancies. It occurs when a locally aggressive neoplasm grows across the thymic capsule, invading the lungs, heart or great mediastinal vessels.

Subsequently, seeding phenomenon can take place in the pleural or pericardial cavity (■ Fig. 6.4) [25].

- The *lymphatic* pathway of dissemination is the second most common modality. It occurs when neoplastic cells are transported through lymphatics to regional lymph nodes. Of note, the thymus features only efferent lymphatics, which drain towards anterior mediastinal or parasternal lymph nodes [26].

Lymphatic involvement is seldom in early stage and low-grade thymic tumors as compared with

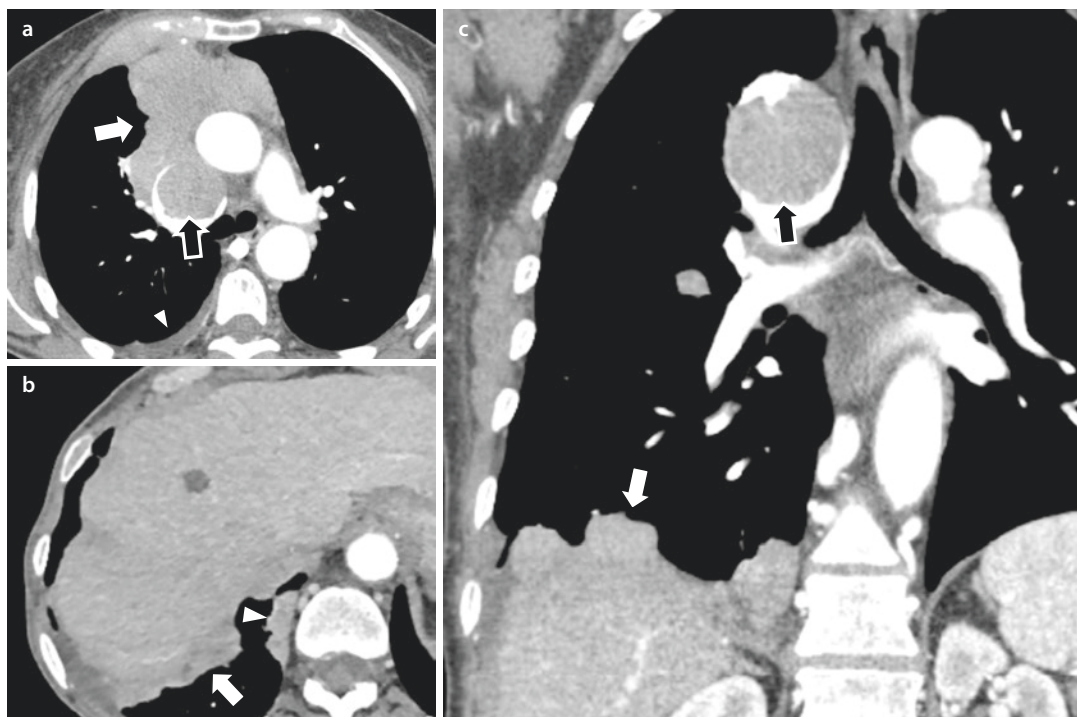


Fig. 6.3 a Axial CT image after intravenous administration of iodinated contrast media showing a large, lobulated and homogeneously enhancing mass (white arrow) located in the prevascular compartment. The superior vena cava is enlarged, and a soft-tissue lesion grows into its lumen (black arrow). A small right pleural effusion can be detected (white arrowhead). b Same patient of a, at a caudal level. Pleural nodules

with homogeneous contrast enhancement involve paravertebral space (white arrowhead) and diaphragmatic surface (white arrow), without an adipose fat plane with the hepatic parenchyma. The coronal reformatted image c shows both pleural nodules (white arrow) and the vascular invasion of the superior vena cava (black arrow). The patient was diagnosed with high-grade thymoma

Table 6.5 Local growth-related symptoms

Mediastinal structure	Related symptoms
Superior vena cava	Superior vena cava syndrome
Laryngeal recurrent nerve	Cough, dysphonia
Phrenic nerve	Diaphragm paralysis
Trachea	Dyspnoea, cough, haemoptysis
Oesophagus	Cough, dysphagia
Sympathetic cervical system	Claude-Bernard-Horner syndrome (ptosis, miosis, enophthalmos)

locally invasive and high-grade lesions such as thymic carcinoma where lymphatic involvement is reported in about 27% of cases [27, 61].

— *Hematogenous* spread occurs more frequently in high-grade thymoma, thymic carcinoma and thymic carcinoid [8]. Cancer cells access systemic circulation by trespassing into venous capillaries or indirectly via lymphatics [28]. The lung is the most common site of hematogenous metastatization, where metastases are displayed by solid and well-defined round nodules/masses randomly distributed [29]. Extra-thoracic organs are far less commonly involved, including the abdominopelvic organs (liver, pancreas, adrenal, spleen, kidney, small bowel and ovary), distant bone and brain. On *CT*, liver metastases are described as heterogeneous formations with central hypodense areas and peripheral enhancement (Fig. 6.5). On *magnetic resonance imaging (MRI)*, they appear as expansive well-defined heterogeneous formations showing T1 hypointensity, T2 hyperintensity and restricted diffusion on

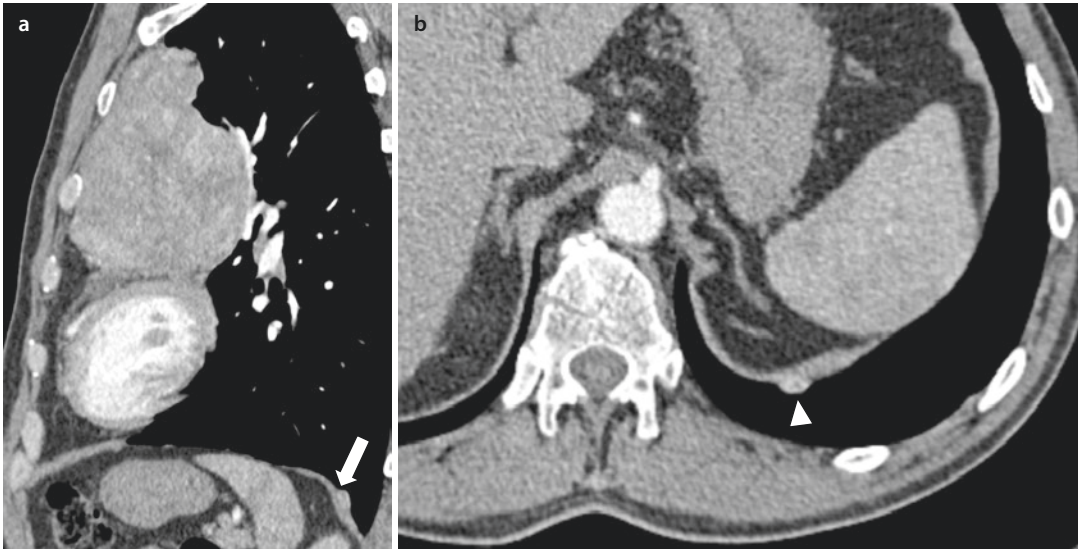


Fig. 6.4 **a** Magnification of a CT image (sagittal view) of a male patient suffering from chronic cough undergoing CT evaluation after chest radiograph detection of a mediastinal mass displaying a large and heterogeneously enhancing anterior mediastinal mass. A nodule showing contrast enhancement can be detected located at the

diaphragmatic surface of the left lung (white arrow). **b** Same patient of image **a** magnification of the enhancing pleural nodule (white arrowhead) showing intense contrast enhancement. The finding represents a drop metastasis in a patient with thymic carcinoma

diffusion-weighted image sequences [30].

Bone localizations can be lithic, sclerosing and mixed [31]. Spine metastases are rare, causing various neurological symptoms based on location (hoarseness, dysphagia, paraesthesia, sensory change, weakness, numbness, paraparesis/paralysis). Spine metastases might cause spinal instability in case of vertebral collapse [32]. Bone marrow metastases from thymic carcinoma are usually detected in late-stage diseases [33]. Brain metastases are very rare, being either solid or cystic, mostly located within the brain parenchyma (intra-axial location), although extradural extension invading the skull and mimicking meningiomas (extra-axial location) has been reported. Complications may include haemorrhage or extracranial extension. Notably, patients with brain metastases from thymic neoplasm show better prognosis compared to patients with brain metastases from other solid tumors [34].

6.2.4 Follow-Up

Median time to metastasis or recurrence happens to be longer than 5 years even after surgical

removal of high-risk thymomas, thus setting the role for long-term follow-up [8]. Intensity of surveillance procedures has been debated, as various approaches are possible, ranging from CT every 6 months for the first three years, followed by annual CT for 5 years and further 5 years of follow-up by alternating CXR and CT, to life-long annual CT (Table 6.6) [35].

6.3 Thymoma

6.3.1 Epidemiology

Thymoma is a rare malignancy (overall incidence: 0.13/100.000 person-years), involving more frequently middle-aged patients (peak in the seventh decade of life) with unknown aetiology. Thymoma patients may be at risk for development of other malignancies, such as soft-tissue sarcomas or B-cell non-Hodgkin lymphoma (NHL). The relationship between the latter and thymoma may be due to immune disturbance arising from thymoma itself or follow-up therapeutic treatment [36].

Most cases of thymoma develop from anterosuperior mediastinum, whilst only a small number involves either posterior mediastinum, cervical

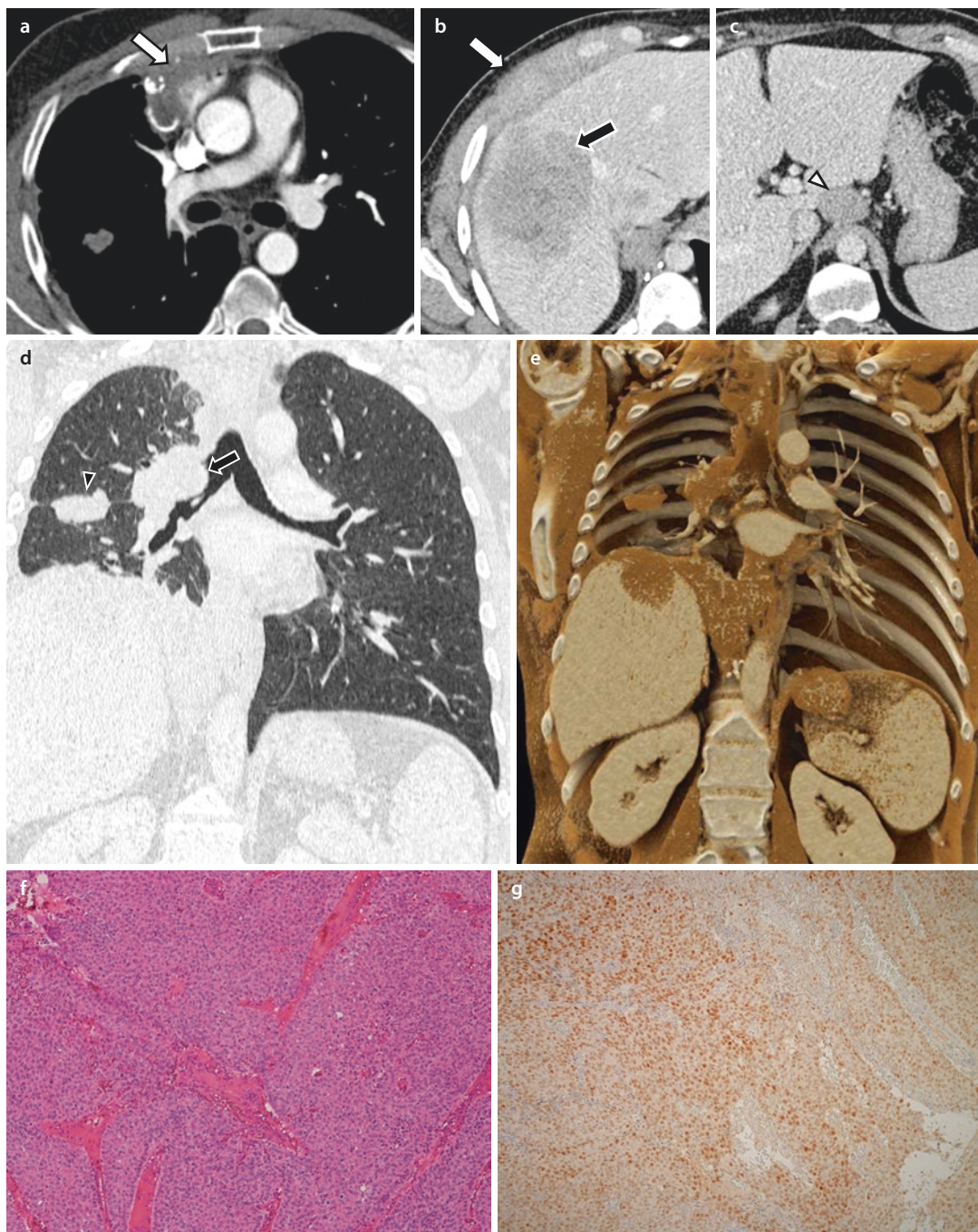


Fig. 6.5 a Follow-up CT scan of a 40-year-old male patients with previous resection of a B3 thymoma. Heterogeneous partly calcified mass within prevascular compartment that does not display an adipose fat plane with adjacent structures. Various localizations were detected, including a heterogeneous liver lesion in the right lobe (black arrow in b) and a diffuse thickening of anterior thoracic wall (white arrow in b), an enlarged coeliac lymph node (white arrowhead in c). The patient suffered from respiratory symptoms caused by bronchial invasion (black arrow in d, multiplanar reformatted

image). A large fissural nodule can be detected (black arrowhead). e Cinematic para-coronal reformatted image highlighting the different sites of metastization. f EE (20×) specimen derived from sampling obtained during bronchoscopy performed for bronchial disobstruction showing a solid neoplasm with thymic origin as demonstrated by positivity for PAX-8 g. PAX-8 20x. (The authors thank Letizia Gnetti, MD (Section of Pathology, Unit of Surgical Sciences, Diagnostic Department, University Hospital of Parma, Parma, Italy), for providing iconographic materials)

Table 6.6 Recommended follow-up protocols by ITMIG

After R0 surgical resection	Annual CT for 5 years
	Then annual CXR alternating with CT for 5 years
After curative intent treatment stage III, IVa	CT every 6 month for 3 years
	Then CT with contrast for 5 years
	Then CXR alternating with CT for 5 years

regions or other locations, following the presence of ectopic thymic tissue. Noteworthy, thymoma may involve various structures, including the trachea, thyroid, parathyroid, pericardium, heart, pleura and lung. Primary intrapulmonary thymomas are very rare and slow-growing lesions either located below the visceral pleura or entirely circumscribed by lung parenchyma. Beside the hypothesis of ectopic intrapulmonary tissue, another option postulated the presence of germinal cells capable of differentiating along a variety of cellular lines, including thymocytes [37]. Usually, they do not cause symptoms; however, local growth can develop into compression and invasion with chest pain, as well as bronchial obstruction or haemoptysis. Notably, intrapulmonary thymoma can be associated with paraneoplastic syndromes and late local recurrence [38, 39].

6.3.2 Symptoms

Because of the wide spectrum of appearance of thymoma, clinical manifestations might vary widely. Up to one-third of cases are asymptomatic thymomas incidentally detected on chest radiograph. In case of locally disseminated thymomas, patients may report symptoms related to airways, nerves or oesophageal involvement (i.e. cough, dyspnoea, respiratory infections, hoarseness, chest pain or dysphagia), whilst invasion of vascular or cardiac (e.g. right atrium) structures causes superior vena cava syndrome or sudden cardiac death, respectively [40].

Systemic symptoms (e.g. weight loss, fever and night sweats) are reported in about 30% of cases,

and here, the differential diagnosis with lymphoma is challenging. Furthermore, thymoma can be associated with autoimmune and paraneoplastic phenomena, including myasthenia gravis, pure red cell aplasia, hypogammaglobulinaemia, thymoma-associated multiorgan autoimmunity (TAMA) [41] and endocrine, cutaneous or connective tissue disorders [35, 36, 39, 40, 42, 43].

6.3.3 Imaging

Between 45% and 80% of thymomas are visible in chest radiograph (■ Fig. 6.6). In about one-third of cases, they appear as ovoid or lobulated soft-tissue masses located in the anterior mediastinum (median size ranging from 5 to 10 cm and extremely large ones over 30 cm) [40, 44, 45]. In such cases, lateral view usually depicts a soft-tissue mass in the retrosternal clear space. Thymomas more frequently are asymmetrical, although bilateral protrusion has been reported. CT can show also small thymoma few millimetres in diameter and a variety of locations such as the junction of the great vessels and the pericardium, the cardiophrenic angle, or the neck [38, 40].

CXR signs of local invasion are of difficult detection and evaluation. Irregular interface with pulmonary parenchyma may suggest intrapulmonary dissemination [40]. Pleural dissemination displays unilateral predominance, yet findings (pleural thickening/masses or diffuse/circumferential nodular thickening encasing pulmonary parenchyma) are usually non-specific, and differentiating thymoma from malignant mesothelioma or metastatic adenocarcinoma is utopian on CXR [40].

Individuals with strong clinical suspicion without detectable radiographic abnormalities are referred to CT for further investigation, which may confirm presence of anterior mediastinal masses and provide an overview on relationships with adjacent structures as well as signs of distant dissemination. On CT, thymomas are generally homogeneous, well-defined oval/rounded lobulated soft-tissue masses. Usually, thymoma shows homogeneous contrast enhancement, although hypodense areas reflecting cystic changes or haemorrhage and necrosis can be detected as well as punctuate, coarse, curvilinear calcifications. In up to 40% of cases, CT depicts large cystic lesions harbouring nodules on their inner wall; this is

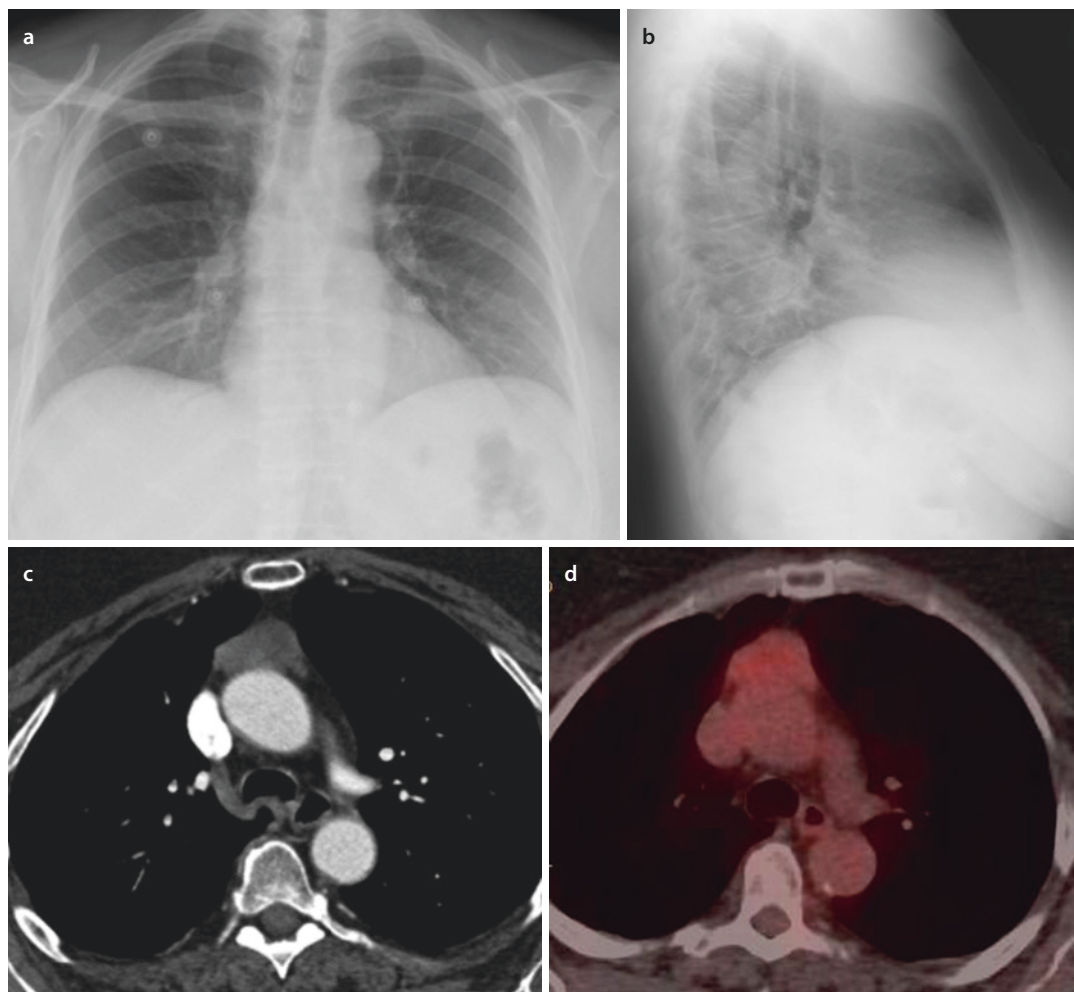


Fig. 6.6 a PA and b LL view of a chest radiograph in a female patient suffering from myasthenia gravis. The PA view appears regular, whilst on the LL view, an enlargement of the anterior mediastinal compartment can be detected. c The patient underwent contrast-enhanced CT, showing a

soft-tissue density mass, in the prevascular compartment. The lesion does not display a significant contrast enhancement. d A PET-CT scan was obtained, reporting an uptake of the radiotracer (SUVmax 3.6). The patient underwent surgery with a final diagnosis of thymoma

more frequently seen in larger lesions [46]. Thymomas can be partially or completely outlined by adipose tissue: local invasion may be reflected by absent fat planes between the lesion and mediastinal structures, yet this finding shows variable sensitivity. A mass showing irregular borders with pulmonary parenchyma is highly consistent for thymoma invading the lungs. CT allows detection of signs of local invasion and of encasement of vascular structures, for which intravenous administration of iodinated contrast media is demanded. Detecting areas of contrast enhancement within a mediastinal lesion as well as features consistent with local invasion and pleural or

pericardial implants allow for the differentiation between thymic lymphoid hyperplasia (TLH) and thymoma [40]. CT depicts pleural parietal dissemination (“drop metastases”), frequently found in posterior basilar pleural spaces and the diaphragm [35, 45].

MRI may be helpful to differentiate between thymoma and thymic cysts. Thymomas show signal intensity (SI) similar to muscular or normal thymic tissue on T1-weighted images and heterogeneous intensity on T2-weighted images. As previously mentioned, thymoma may show cystic, necrotic or haemorrhagic changes, and fibrous septa and nodules. These findings can be detailed on T2-weighted

Table 6.7 CT and MR findings of low-risk thymomas, high-risk thymomas and thymic carcinomas [94–97]

	Low risk (type A, AB, B1)	High-risk (type B2, B3)	Thymic carcinoma
CT – irregular margin	7%	22%	75%
CT – necrotic or cystic component	13%	28%	58%
CT – heterogeneous enhancement	33%	44%	92%
MR – complete or almost complete capsule ^a	27%	17%	0%
MR – partial capsule ^a	/	/	42%
MR – septum ^a	57%	44%	8%
MR – heterogeneous signal intensity	33%	56%	100%
MR – CT lymphadenopathy	3%	6%	58%
Surgical detection of great vessel invasion	0%	6%	42%
MR – smooth contours	A 100%	B2 64%	31%
	AB 64%	B3 33%	
	B1 42%		
MR – heterogeneous signal intensity T2W	A 20%	B2 64%	94%
	AB 45%		
	B1 58%		
MR – mean ADC value	1.82 ± 0.40 (x10 ⁻³ mm ² /s)	1.11 ± 0.40 (x10 ⁻³ mm ² /s)	1.11 ± 0.40 (x10 ⁻³ mm ² /s)
MR – intratumor low-signal foci T2W ^b	A 0%	B2 27%	56%
	AB 7%	B3 17%	
	B1 12%		
Calcification	B1 44%	B2 61%	6%
		B3 75%	

Gender, age and size have no statistical significance

^aMR is superior to CT in the depiction of capsule, septum and haemorrhage within the tumor

^bProbably due to abundant collagenous tissue

images, and post-contrast sequences may allow detection of solid components within cystic lesions, thus suggesting the presence of an underlying cystic thymoma [15, 17, 18].

PET with fluorine-18 (F-18) fluorodeoxyglucose (FDG-PET) helps in differentiating thymic carcinoma from other thymic neoplasms, as well as from thymic hyperplasia or normal physiological uptake. Notably, standardized uptake value (SUV) is expected to be greater in thymic carcinoma than either invasive or non-invasive thymomas [1, 35].

Imaging findings and their incidence are summarized in Table 6.7.

6.3.4 Local Spread and Metastatic Dissemination

Local spread of thymoma shows preferential mediastinal/pleural involvement, whilst distant metastases of thymoma most frequently occur within pulmonary parenchyma [20, 47]. Extrathoracic metastases are extremely rare (3–6% of

cases), and they are mainly reported in association with B subtypes of thymoma [21, 48].

Local spread beyond capsular invasion can happen with two prototypical pathways: infiltration of mediastinal and visceral pleural layers and eventually pulmonary parenchyma and progressive involvement of mediastinal adipose tissue until mediastinal structures such as the pericardium, heart and vessels [47, 48]. Endobronchial spread was reported as a rare pattern of presentation with few cases in the literature [49–51] (■ Figs. 6.5, 6.7, and 6.8).

Pleural dissemination is particularly frequent, and it may be present at time of diagnosis or it might occur even after tumor resection in up to 20% of cases. Prognosis is worse in case of many of pleural nodules (>11 nodules). Complete macroscopic resection of pleural lesions improves survival and reduces recurrence rate; nonetheless, life-long follow-up after surgical resection is recommended to promptly detect extra-thoracic recurrence [52, 53]. Pleural metastases from thymoma are seen as enhancing pleura-based nodules/masses, also called “drop metastasis”, they are variably associated with pleural effusion [19].

Distant metastases may involve pulmonary parenchyma and extra-thoracic organs, mainly the kidney, liver, brain and bones [40].

Liver metastases are the most frequent extra-thoracic localization, and indeed, exclusive liver involvement was reported in up to 40% of extra-thoracic metastatic thymoma [53]. Furthermore, liver metastases were found to occur also with a delay of more than 10 years after surgical resection of the thymoma [30].

Pancreatic and gastrointestinal metastases are particularly rare, and they were described in retroperitoneal space, stomach, transverse colon and mesentery [53, 54]. Cases of thymoma dissemination to ovary were described in autopsy series [55].

Hematogenous spread to bone may follow invasion of the superior vena cava [31]. Rarely, thymoma may metastasize to the spine. Likewise other dissemination target of thymoma, also spine involvement may be diagnosed ever lately after initial diagnosis. Symptoms include spinal cord/cauda equina compression [32].

6.4 Thymic Carcinoma

6.4.1 Epidemiology

Thymic carcinoma displays high malignant potential and aggressive behaviour related to its epithelial origin, resulting in poor prognosis. It represents about 1% of thymic malignancies, featuring male predominance and a mean age at diagnosis ranging from 47 to 60 years [26]. Interestingly, thymic carcinoma may arise de novo or follow transformation from pre-existing thymomas.

According to differences in cell morphology, the most common entity is squamous cell carcinoma, which can present as well-differentiated (keratinizing) squamous cell carcinoma, moderately differentiated squamous cell carcinoma and poorly differentiated (nonkeratinizing) squamous cell carcinoma, the latter also known as lymphoepithelioma-like carcinoma. Further subtypes are described that are extremely rare: basal cell, mucoepidermoid, sarcomatoid, adenosquamous, clear cell and undifferentiated carcinomas [56].

6.4.2 Symptoms

Thymic carcinoma may be either asymptomatic or cause various symptoms because of local invasiveness and/or metastatization. Cough, chest tightness and substernal pain, phrenic nerve palsy and superior vena cava syndrome can be associated with systemic and unspecific findings (e.g. fever, fatigue, anaemia, night sweats, weight loss and anorexia) [26]. Paraneoplastic syndromes (e.g. myasthenia gravis, pure red cell aplasia, hypercalcaemia) are reported with lower frequency compared with thymoma, and they are usually associated with thymic carcinoma arising from pre-existing thymomas [33].

6.4.3 Imaging

CXR may depict anterior mediastinal/hilar masses or subtle abnormalities including small mediastinal widening or paratracheal bulging. For such imaging manifestations, the differential

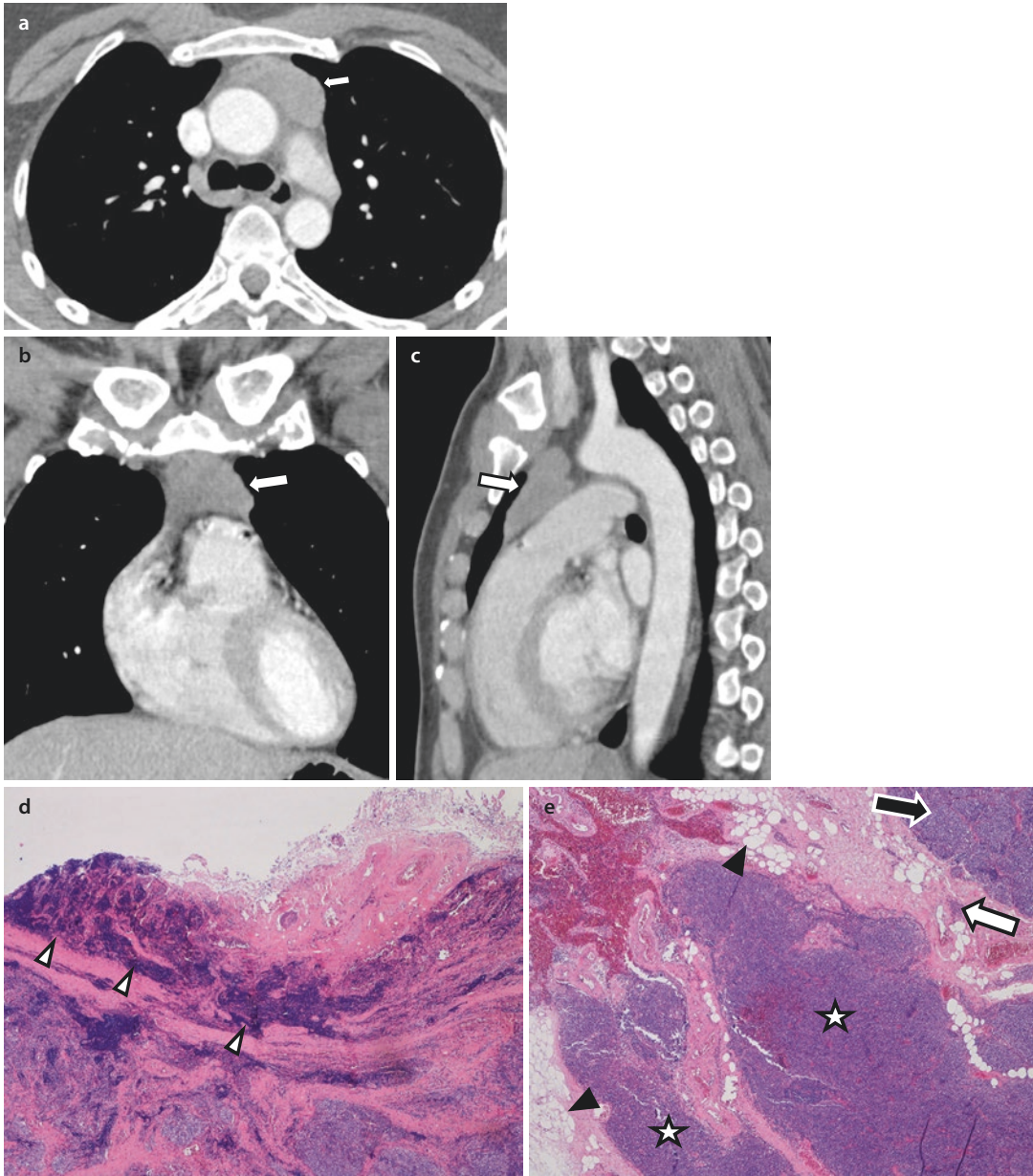


Fig. 6.7 CT scan (a, axial image; b, coronal reformatted image; c, sagittal reformatted image) of a 48-year-old female patient suffering from myasthenia gravis revealing a solid lesion in the prevascular compartment. The lesion shows smooth margins and homogeneous contrast enhancement. No clear signs of adjacent structures' invasion were reported. On histological evaluation performed after surgery, the lesion showed capsular invasion with growth mediastinal adipose tissue: (d, EE 10 \times) numerous neoplastic nodules (white arrowheads)

intermingled with fibrous tissue. At higher magnification (e, EE 20 \times), the nodule of greatest dimensions (black arrow) invades thymic fibrous capsule (white arrow) resulting in mediastinal adipose tissue (black arrowheads) infiltration from solid nodules (white stars) stemmed from the main nodule (black arrow). (The authors thank Letizia Gnetti, MD (Section of Pathology, Unit of Surgical Sciences, Diagnostic Department, University Hospital of Parma, Parma, Italy), for providing iconographic materials)

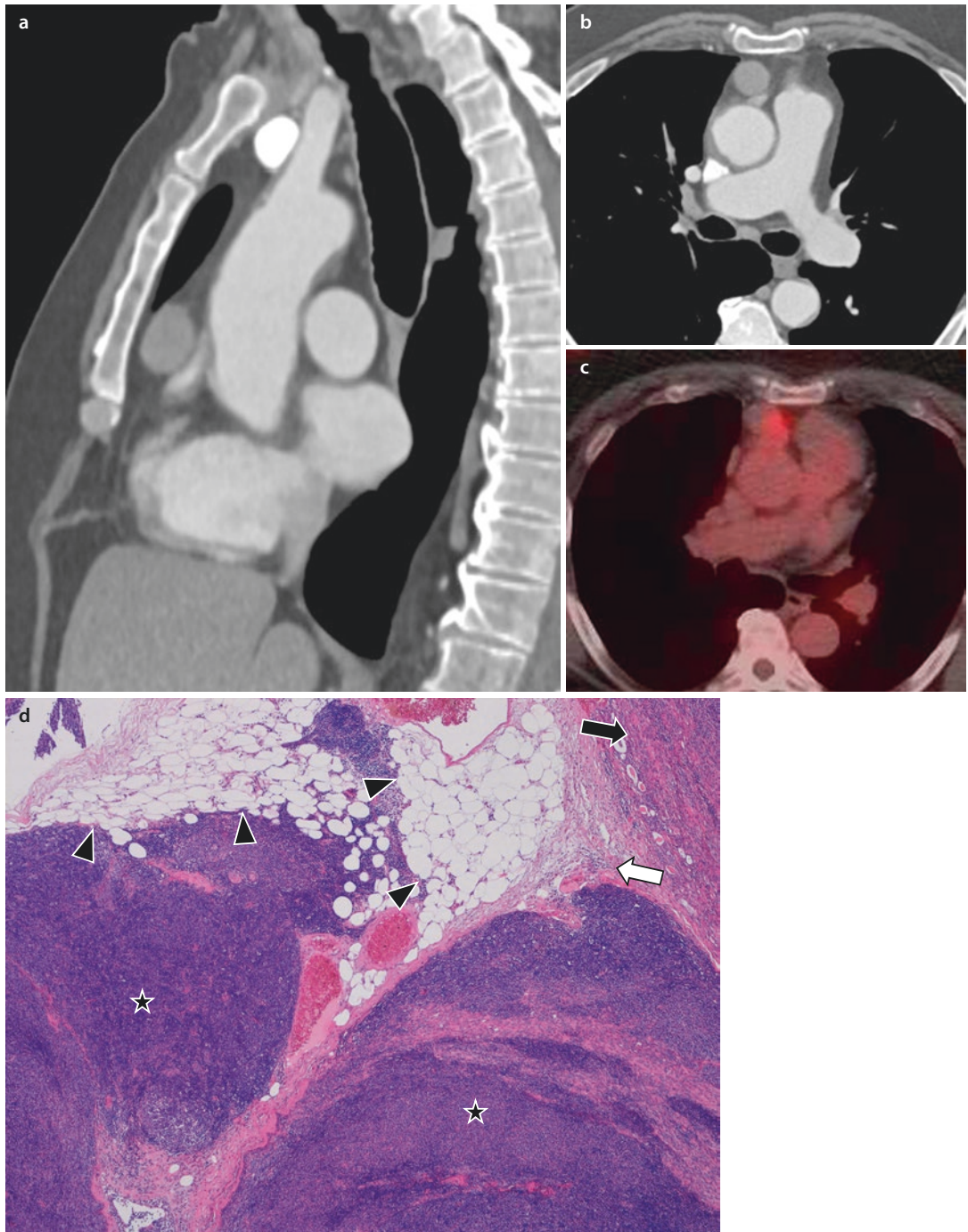


Fig. 6.8 Seventy-year-old male patient with a solid homogeneously enhancing nodule located in the prevascular compartment incidentally detected at a follow-up CT for melanoma. CT image (a, sagittal reformatted image; b, axial view) showing a soft-tissue density nodule with smooth margins located in the prevascular compartment. c FDG-PET scan showed uptake of the radiotracer. After surgery, histological evaluation (d, EE 20x) depicted the neoplastic nodule (black arrow,

AB thymoma) intermingled with fibrous tissue showing invasion of the thymic fibrous capsule (white arrow), resulting in mediastinal adipose tissue (black arrowhead) infiltration from solid nodules (black stars) stemming from the main nodule. (The authors thank Letizia Gnetti, MD - Section of Pathology, Unit of Surgical Sciences, Diagnostic Department, University Hospital of Parma, Parma, Italy, for providing iconographic materials)

diagnosis is wide; hence, further imaging evaluation is mandatory. On CT, thymic carcinomas appear as large masses with irregular margins and hypodense areas related to necrotic, haemorrhagic or cystic degenerations. The diagnosis of thymic carcinoma is also associated with heterogeneous contrast enhancement, lymphadenopathies and great vessel invasion assessed on CT (or MRI) [57].

CT after intravenous administration of contrast media is paramount for preoperative staging because it allows description of signs of local invasion, pleural seeding and metastatic disease. However, CT is hampered by various limitations, ranging from difficulty in differentiating between lymphoid/rebound hyperplasia and malignancy. Furthermore, detection of early local invasion or small pleural implants might be challenging by CT.

MRI is rarely performed, and nonetheless, it can provide valuable evaluation of fat planes between tumor and adjacent organs. It also allows mass characterization by description of necrotic, haemorrhagic or cystic degenerations [58–60].

6.4.4 Local Spread and Metastatic Dissemination

Thymic carcinoma invades adjacent mediastinal structures in up to 80% of cases at time of diagnosis. The most common sites of local invasion include brachiocephalic vein, pleura, lung, lymph nodes (supraclavicular, paraesophageal, retrocaval, pericardial and axillary nodes) and pericardium [8, 26, 61, 62]. Endobronchial dissemination is particularly rare, represented by polypoid lesions either mono- or bilateral (one case reported in the literature) [63, 64]. Intralesional calcifications, pleural nodules and adipose tissue infiltration were associated with increased risk of metastasis or recurrence [8]. Similarly, lymphatic involvement shows a positive correlation with tumor invasiveness [27]. Systematic surgical resection of lymph nodes is proposed in high-risk patients because thymic carcinoma shows high rates of recurrence (Table 6.8): 21% at 3 years, 27% at 5 years and 32% at 10 years [27, 48, 61, 65–67].

Table 6.8 Type of recurrence of thymic carcinoma

Recurrence	Regrowth after complete resection or radiographic complete response to curative intent therapy
Local recurrence	At site of original tumor or in thymic bed including adjacent nodes
Regional recurrence	Intrathoracic, but not contiguous with original tumor or thymus
Distant recurrence	Outside of the thorax or intraparenchymal nodules

Extra-thoracic metastases may involve multiple organs, including the bone, liver, adrenal gland, bone marrow, brain, ovary, spleen, pancreas, skin, breast and extra-thoracic lymph nodes [26, 48, 54, 68–72].

Bone marrow metastases are usually detected in late-stage diseases, although a case of a patient with bone marrow metastasis as first manifestation of otherwise occult thymic carcinoma has been reported [33].

Brain metastases are rare yet severely affecting prognosis. They can be located within frontal, parietal, cerebellar, temporal and occipital lobes, either being silent and incidentally discovered or causing headache and neurological manifestations including vision and mental status change, memory loss, speech difficulty and seizures. Lesions may appear solid or cystic and cause haemorrhage and extracranial extension [34, 73].

Spine metastases are rare, with neurological symptoms depending on location, such as hoarseness and dysphagia (C3–C4 location), paraesthesia, sensory change, weakness, numbness and paraparesis/paralysis. Furthermore, metastases may cause spinal instability because of vertebral collapse, as well as spinal cord compression [32].

Gastrointestinal tract invasion is extremely uncommon, with preferential involvement of small bowel tracts [54]. Similarly, splenic metastases are particularly rare [74].

Breast metastases are extremely rare, and they may develop by lymphatic (through intercostal lymphatics to parasternal lymph nodes) or haematogenous (intercostal perforators from internal thoracic artery) spread [72].

6.5 Carcinoid

6.5.1 Epidemiology

Thymic neuroendocrine tumors (NETs) are rare neoplasms composed of neuroendocrine cells (2–5% of epithelial tumors) with poor prognosis related to local invasion, recurrence or distant metastases [57]. Thymic carcinoids may arise at various ages (median age at presentation is 43 years) and usually show male predominance [1]. Thymic NETs are classified according to histopathological findings into typical carcinoid, atypical carcinoid (AC), large cell neuroendocrine carcinoma (LCNEC) and small cell neuroendocrine carcinoma (SCC) (Table 6.9). In the 2015 update of WHO classification of NETs, the term “well-differentiated neuroendocrine carcinoma” (referring to carcinoids) and “poorly differentiated neuroendocrine carcinoma” (referring to LCNEC and SCC) of the previous (third) edition were abandoned, because LCNECs and even SCC may be highly differentiated in terms of neuroendocrine features. Indeed, the fourth edition separates typical and atypical carcinoids as low-grade and intermediate-grade neuroendocrine tumors, respectively, from high-grade neuroendocrine carcinoma that comprise LCNEC and SCC [43].

6.5.2 Symptoms

Thymic carcinoids are often hormonally active and endocrine manifestations are mostly represented by Cushing’s syndrome (ectopic ACTH production), whilst non-active lesions may be associated with parathyroid adenoma, islet cell tumor of the pancreas and pituitary adenoma as component of multiple endocrine neoplasia (MEN) type I syndrome [26, 57, 75]. Furthermore, symptoms may follow compression or invasion of adjacent structures, such as the trachea, pleura, pulmonary parenchyma or blood vessels [57].

6.5.3 Imaging

Most typical carcinoid tumors are not encapsulated and can be grossly invasive, their size ranging from 2 to 20 cm. Of note, carcinoids causing Cushing’s syndrome tend to be smaller due to ear-

Table 6.9 Thymic neuroendocrine tumor classification

Typical carcinoid	< 2 mitoses/2mm ² ; no necrosis
Atypical carcinoid	< 2 mitoses/2mm ² ; with necrosis; or 2–10 mitoses/2mm ² ; + or – necrosis
LCNEC	> 10 mitoses/2mm ² ; no small-cell features
Combined LCNEC	LCNEC combined with any thymoma(s) or thymic carcinoma(s)
SCC	Typical SCC histology
Combined SCC	SCC combined with any thymoma(s) or thymic carcinoma(s)

lier detection. Calcifications are more frequently encountered in thymic than extra-thymic NETs, possibly because ACs are associated with necrosis and subsequent development of calcifications are more frequently encountered in the thymus [76].

CXR may be normal or equivocal in cases of small lesions and carcinoids may be more easily detected on CT [75]. Thymic carcinoids most frequently appear as large, lobulated and heterogeneous anterior mediastinal mass. Heterogeneity is due to intralesional calcifications and necrotic or cystic changes (as previously mentioned, more frequently appearing in ACs). Generally, thymic carcinoids display moderate-to-strong enhancement after intravenous administration of contrast media. CT scan can also highlight infiltration of surrounding structures and metastases [1, 77].

On MRI, thymic carcinoids manifest as T1-weighted hypointense and T2-weighted heterogeneous hyperintense masses with irregular contours and heterogeneous enhancement. ADC values in thymic carcinoids may be misleading because of cystic or necrotic changes that might interfere with ADC values [57, 60, 78].

6.5.4 Local Spread and Metastatic Dissemination

Thymic carcinoids display a more aggressive biological behaviour and have a higher propen-

sity to metastasize to distant sites as compared with other thymic epithelial tumors. Local invasion is reported in 50% of cases, notably involving the pericardium, mediastinal adipose tissue, blood vessels and lungs. Distant hematogenous metastatization is reported in 20–30% of cases [79–82] (metastatic spread ranges from 20% in carcinoids up to 80% in SCCs) [26, 83–85], most frequently reported in the bones, lungs, spleen, liver, brain and adrenal glands. Notably, local recurrence or distant metastases (usually abdominal lymph nodes and skeletal involvement) can occur after several years from diagnosis, despite surgical resection and perioperative chemotherapy [49].

Prognostic factors affecting long-term outcome include histological grade, mitotic activity, capsular invasion, incomplete resection, lymph node status and presence of metastasis at the time of diagnosis [80, 86]. In particular, prognosis of typical carcinoids (5-year survival rate ranges from 50% to 100%, median survival of about 10 years) is slightly better as compared to ACs and LCNEC (5-year survival rate ranges from 30% to 66%) [87]. About 75% of LCNEC infiltrates adjacent organs or shows distant metastases, usually to the spine and liver [87]. Most SCCs are diagnosed at advanced stage with signs of local invasion (to lung or pericardium) or with distant metastases to the lung, liver, bone or brain; commonly, prognosis is poor (5-year survival rate, 0%; median survival about 1 year) [76].

6.6 Thymoliposarcoma

Primary liposarcomas of the mediastinum are extremely rare lesions (<1% of mediastinal tumors, with about 150 cases reported), usually affecting adult individuals [88]. Malignant liposarcomas develop more commonly in the posterior mediastinum; still, thymoliposarcoma is the most common sarcoma of the anterior mediastinum. Noteworthy, a minority of cases of anterior mediastinum liposarcoma may exhibit extensive thymic tissue within the lesion, thus being considered as thymoliposarcomas [89].

Thymoliposarcomas grow mostly with an expansible pattern. No histologically proven metastases were reported except for local recurrence, similarly to biological behaviour of well-

differentiated liposarcoma [89]. Signs and symptoms are related to size and direct invasion of adjacent structures such as the pericardium or superior vena cava (i.e. dyspnoea, chest pain and tachypnoea), although incidental asymptomatic lesions have also been reported [88].

The predominant finding of mediastinal liposarcoma on CXR is a widened mediastinum. On CT, the appearance of mediastinal liposarcomas varies from a predominantly fat-containing mass to a solid mass. Low attenuation values between –50 and –150 Hounsfield unit are consistent with adipose tissue. Higher HU values are related to necrotic or soft-tissue intralesional components. MR is particularly useful: T1-weighted images show adipose tissue with a high SI, whereas SI diminishes in T2-weighted image [88].

References

1. Nishino M, Ashiku SK, Kocher ON, Thurer RL, Boiselle PM, Hatabu H. The thymus: a comprehensive review. *Radiographics*. 2006;26(2):335–48.
2. Baron RL, Lee JK, Sagel SS, Peterson RR. Computed tomography of the normal thymus. *Radiology*. 1982; 142(1):121–5.
3. Sone S, Higashihara T, Morimoto S, et al. Normal anatomy of thymus and anterior mediastinum by pneumomediastinography. *AJR Am J Roentgenol*. 1980; 134(1):81–9.
4. Hammer MM, Miskin N, Madan R, Hunsaker AR. Predictive features for anterior mediastinal mass diagnoses. *J Comput Assist Tomogr*. 2019;43(1):98–103.
5. Ackman JB, Verzosa S, Kovach AE, et al. High rate of unnecessary thymectomy and its cause. Can computed tomography distinguish thymoma, lymphoma, thymic hyperplasia, and thymic cysts? *Eur J Radiol*. 2015;84(3):524–33.
6. Tomiyama N, Honda O, Tsubamoto M, et al. Anterior mediastinal tumors: diagnostic accuracy of CT and MRI. *Eur J Radiol*. 2009;69(2):280–8.
7. de Jong WK, Blaauwgeers JL, Schaapveld M, Timens W, Klinkenberg TJ, Groen HJ. Thymic epithelial tumours: a population-based study of the incidence, diagnostic procedures and therapy. *Eur J Cancer*. 2008;44(1): 123–30.
8. Khandelwal A, Sholl LM, Araki T, Ramaiya NH, Hatabu H, Nishino M. Patterns of metastasis and recurrence in thymic epithelial tumours: longitudinal imaging review in correlation with histological subtypes. *Clin Radiol*. 2016;71(10):1010–7.
9. Girard N, Ruffini E, Marx A, Faivre-Finn C, Peters S, Committee EG. Thymic epithelial tumours: ESMO Clinical Practice Guidelines for diagnosis, treatment and follow-up. *Ann Oncol*. 2015;26(Suppl 5): v40–55.

10. Imbimbo M, Maury JM, Garassino M, Girard N, Group RAW. Mesothelioma and thymic tumors: treatment challenges in (outside) a network setting. *Eur J Surg Oncol*. 2019;45(1):75–80.
11. Kojima Y, Ito H, Hasegawa S, Sasaki T, Inui K. Resected invasive thymoma with multiple endocrine neoplasia type 1. *Jpn J Thorac Cardiovasc Surg*. 2006;54(4):171–3.
12. Drevet G. Optimal management of thymic malignancies: current perspectives. *Cancer Manag Res*. 2019; 22(11):6803–14. <https://doi.org/10.2147/CMAR.S171683>. ecollection 2019.
13. Ruffini E, Detterbeck F, Van Raemdonck D, et al. Tumours of the thymus: a cohort study of prognostic factors from the European Society of Thoracic Surgeons database. *Eur J Cardiothorac Surg*. 2014;46(3):361–8.
14. Carter BW, Benveniste MF, Madan R, et al. ITMIG classification of mediastinal compartments and multidisciplinary approach to mediastinal masses. *Radiographics*. 2017;37(2):413–36.
15. Detterbeck FC, Parsons AM. Thymic tumors. *Ann Thorac Surg*. 2004;77(5):1860–9.
16. Chung SR, Kim IS, Kim J. Thymoma of the middle mediastinum. *Korean J Thorac Cardiovasc Surg*. 2012; 45(4):267–8.
17. Van Raemdonck D, Ruffini E. Thymic malignancies: does size matter? *Eur J Cardiothorac Surg*. 2016;50(6):1075–6.
18. Fukui T, Fukumoto K, Okasaka T, et al. Prognostic impact of tumour size in completely resected thymic epithelial tumours. *Eur J Cardiothorac Surg*. 2016;50(6):1068–74.
19. Nasserri F, Eftekhari F. Clinical and radiologic review of the normal and abnormal thymus: pearls and pitfalls. *Radiographics*. 2010;30(2):413–28.
20. Priola AM, Priola SM, Di Franco M, Cataldi A, Durando S, Fava C. Computed tomography and thymoma: distinctive findings in invasive and noninvasive thymoma and predictive features of recurrence. *Radiol Med*. 2010;115(1):1–21.
21. Tomiyama N, Muller NL, Ellis SJ, et al. Invasive and non-invasive thymoma: distinctive CT features. *J Comput Assist Tomogr*. 2001;25(3):388–93.
22. Marom EM, Milito MA, Moran CA, et al. Computed tomography findings predicting invasiveness of thymoma. *J Thorac Oncol*. 2011;6(7):1274–81.
23. Zhao Y, Chen H, Shi J, Fan L, Hu D, Zhao H. The correlation of morphological features of chest computed tomographic scans with clinical characteristics of thymoma. *Eur J Cardiothorac Surg*. 2015;48(5):698–704.
24. Honda T, Hayasaka M, Hachiya T, Hirose Y, Kubo K, Katsuyama T. Invasive thymoma with hypogammaglobulinemia spreading within the bronchial lumen. *Respiration*. 1995;62(5):294–6.
25. Shepard J-AO. Thoracic imaging the requisites. Philadelphia: Elsevier Health Sciences; 2018.
26. Bushan K, Sharma S, Verma H. A review of thymic tumors. *Indian J Surg Oncol*. 2013;4(2):112–6.
27. Gu Z, Wei Y, Fu J, et al. Lymph node metastases in thymic malignancies: a Chinese Alliance for Research in Thymomas retrospective database analysis. *Interact Cardiovasc Thorac Surg*. 2017;25(3):455–61.
28. Wong SY, Hynes RO. Lymphatic or hematogenous dissemination: how does a metastatic tumor cell decide? *Cell Cycle*. 2006;5(8):812–7.
29. Mengoli MC, Longo L, Varini S, Rossi G, Lococo F. Invasive medullary type A thymoma with recurrent distant metastases. *Ann Thorac Surg*. 2017;103(5): e423–e5.
30. Speisky D, de Davila MT, Vigovich F, et al. Hepatic metastasis of thymoma: case report and immunohistochemical study. *Ecancermedicalscience*. 2016;10:693.
31. Montecalvo J, Chang J, Rektman N, et al. Type A thymoma presenting with bone metastasis. *Histopathology*. 2018;73(4):701–3.
32. Achey RL, Lee BS, Sundar S, Benzel EC, Krishnaney AA. Rare thymoma metastases to the spine: case reports and review of the literature. *World Neurosurg*. 2018;110:423–31.
33. Sharma S, Dawson L. A rare tumor with a very rare initial presentation: thymic carcinoma as bone marrow metastasis. *Case Rep Pathol*. 2017;2017:6497376.
34. Gharwan H, Kim C, Thomas A, et al. Thymic epithelial tumors and metastasis to the brain: a case series and systematic review. *Transl Lung Cancer Res*. 2017;6(5):588–99.
35. Scorsetti M, Leo F, Trama A, et al. Thymoma and thymic carcinomas. *Crit Rev Oncol Hematol*. 2016;99: 332–50.
36. Engels EA. Epidemiology of thymoma and associated malignancies. *J Thorac Oncol*. 2010;5(10 Suppl 4):S260–5.
37. Marchevsky AM. Lung tumors derived from ectopic tissues. *Semin Diagn Pathol*. 1995;12(2):172–84.
38. Wang Z, Li H, Cao H, Zheng J. Clinicopathological features of type AB thymoma with liver metastases. *Int J Clin Exp Pathol*. 2014;7(12):8700–5.
39. Myers PO, Kritikos N, Bongiovanni M, et al. Primary intrapulmonary thymoma: a systematic review. *Eur J Surg Oncol*. 2007;33(10):1137–41.
40. Santana L, Givica A, Camacho C, Armed Forces Institute of P. Best cases from the AFIP: thymoma. *Radiographics*. 2002;22 Spec No:S95–S102.
41. Wadhera A, Maverakis E, Mitsiades N, Lara PN, Fung MA, Lynch PJ. Thymoma-associated multiorgan autoimmunity: a graft-versus-host-like disease. *J Am Acad Dermatol*. 2007;57(4):683–9.
42. Agarwal S, Cunningham-Rundles C. Thymoma and immunodeficiency (Good syndrome): a report of 2 unusual cases and review of the literature. *Ann Allergy Asthma Immunol*. 2007;98(2):185–90.
43. Marx A, Chan JK, Coindre JM, et al. The 2015 World Health Organization classification of tumors of the thymus: continuity and changes. *J Thorac Oncol*. 2015;10(10):1383–95.
44. Restrepo CS, Pandit M, Rojas IC, et al. Imaging findings of expansile lesions of the thymus. *Curr Probl Diagn Radiol*. 2005;34(1):22–34.
45. Marom EM. Imaging thymoma. *J Thorac Oncol*. 2010;5(10 Suppl 4):S296–303.
46. Rieker RJ, Aulmann S, Schnabel PA, et al. Cystic thymoma. *Pathol Oncol Res*. 2005;11(1):57–60.

47. Kondo K, Monden Y. Lymphogenous and hematogenous metastasis of thymic epithelial tumors. *Ann Thorac Surg.* 2003;76(6):1859–64; discussion 64–5.
48. Vladislav T, Jain RK, Alvarez R, et al. Extrathoracic metastases of thymic origin: a review of 35 cases. *Mod Pathol.* 2012;25(3):370–7.
49. Asamura H, Morinaga S, Shimosato Y, Ono R, Naruke T. Thymoma displaying endobronchial polypoid growth. *Chest.* 1988;94(3):647–9.
50. Sakuraba M, Sagara Y, Tamura A, Park Z, Hebisawa A, Komatsu H. A case of invasive thymoma with endobronchial growth. *Ann Thorac Cardiovasc Surg.* 2005;11(2):114–6.
51. Benton SM Jr, Rogers RP 3rd, Reed CE. Invasive thymoma with endobronchial metastasis. *Ann Thorac Surg.* 2010;89(2):612–4.
52. Kimura K, Kanzaki R, Kimura T, et al. Long-term outcomes after surgical resection for pleural dissemination of thymoma. *Ann Surg Oncol.* 2019;26(7):2073–80.
53. Passuello N, Pozza G, Blandamura S, Valmasoni M, Sperti C. Thymoma metastatic to liver and pancreas: case report and review of the literature. *J Int Med Res.* 2017;45(2):868–74.
54. Kobrinsky B, Khaykys I, Hill D, et al. Case report: thymic carcinoma metastatic to small bowel. *Clin Med Oncol.* 2008;2:477–80.
55. Demirkiran F, Bese T, Arvas M, Yilmaz O, Ilvan S. Ovarian metastasis from malignant thymoma. *Int J Gynaecol Obstet.* 2009;105(2):176–7.
56. Moran CA, Suster S. Thymic carcinoma: current concepts and histologic features. *Hematol Oncol Clin North Am.* 2008;22(3):393–407.
57. Shimamoto A, Ashizawa K, Kido Y, et al. CT and MRI findings of thymic carcinoid. *Br J Radiol.* 2017; 90(1071):20150341.
58. Priola AM, Priola SM. Imaging of thymus in myasthenia gravis: from thymic hyperplasia to thymic tumor. *Clin Radiol.* 2014;69(5):e230–45.
59. Priola AM, Priola SM. Morphological assessment of thymic carcinoma through imaging: is computed tomography useful in selecting patients for surgery and in predicting incomplete resection? *J Thorac Dis.* 2018;10(Suppl 33):S3933–S7.
60. Broncano J, Alvarado-Benavides AM, Bhalla S, Alvarez-Kindelan A, Raptis CA, Luna A. Role of advanced magnetic resonance imaging in the assessment of malignancies of the mediastinum. *World J Radiol.* 2019;11(3):27–45.
61. Yamamoto Y, Kodama K, Maniwa T, Kishima H. Successful treatment of advanced thymic carcinoma with lymph node and pleural metastases: a case report. *Mol Clin Oncol.* 2016;5(5):550–2.
62. Kondo K, Monden Y. Therapy for thymic epithelial tumors: a clinical study of 1,320 patients from Japan. *Ann Thorac Surg.* 2003;76(3):878–84.. discussion 84–5
63. Kao HW, Yu CP, Tzao C, Lin WC, Hsu HH, Chen CY. An unusual case of thymic carcinoma with endobronchial metastases manifesting as centrilobular opacities. *J Thorac Imaging.* 2006;21(3):238–40.
64. Nagamata M, Okuma Y, Hosomi Y, Hishima T. Thymic carcinoma with endobronchial metastasis: a case report. *J Bronchology Interv Pulmonol.* 2017;24(2): 159–62.
65. Wright CD, Wain JC, Wong DR, et al. Predictors of recurrence in thymic tumors: importance of invasion, World Health Organization histology, and size. *J Thorac Cardiovasc Surg.* 2005;130(5):1413–21.
66. Ruffini E, Detterbeck F, Van Raemdonck D, et al. Thymic carcinoma: a cohort study of patients from the European society of thoracic surgeons database. *J Thorac Oncol.* 2014;9(4):541–8.
67. Yabuki H, Minowa M. Long survival and recurrence of thymic carcinoma 10 years after resection. *Asian Cardiovasc Thorac Ann.* 2019;218492319848958
68. Youk JH, Kim EK, Kim MJ, Oh KK, Park YN. Metastatic breast lesion from thymic carcinoma. *J Ultrasound Med.* 2006;25(10):1339–42.
69. Walid MS, Troup EC, Robinson JS Jr. Brain metastasis from thymic carcinoma in association with SIADH and pituitary enlargement: a case report. *South Med J.* 2008;101(7):764–6.
70. Bott-Kothari T, Aron BS, Bejarano P. Malignant thymoma with metastases to the gastrointestinal tract and ovary: a case report and literature review. *Am J Clin Oncol.* 2000;23(2):140–2.
71. Ahn JY, Kim NK, Oh D, Ahn HJ. Thymic carcinoma with brain metastasis mimicking meningioma. *J Neuro-Oncol.* 2002;58(3):193–9.
72. Deng YW, Li YW, Hao WJ, Lu D. A clinical observation of thymic epithelial tumor metastatic to breast. *Breast Care (Basel).* 2018;13(2):136–9.
73. Kouitcheu R, Appay R, Diallo M, Troude L, Melot A. A case of brain metastasis of a thymic carcinoma with a review of the literature. *Neurochirurgie.* 2019;65(1):43–8.
74. Guilan RA, Zelman S, Smalley RL, Iglesias PA. Malignant thymoma associated with myasthenia gravis, and evidence of extrathoracic metastases. An analysis of published cases and report of a case. *Cancer.* 1971;27(4):823–30.
75. Brown LR, Aughenbaugh GL. Masses of the anterior mediastinum: CT and MR imaging. *AJR Am J Roentgenol.* 1991;157(6):1171–80.
76. Bohnenberger H, Dinter H, Konig A, Strobel P. Neuroendocrine tumors of the thymus and mediastinum. *J Thorac Dis.* 2017;9(Suppl 15):S1448–S57.
77. Araki T, Sholl LM, Hatabu H, Nishino M. Radiological features and metastatic patterns of thymic neuroendocrine tumours. *Clin Radiol.* 2018;73(5):479–84.
78. Razek AA, Elmorsy A, Elshafey M, Elhadedy T, Hamza O. Assessment of mediastinal tumors with diffusion-weighted single-shot echo-planar MRI. *J Magn Reson Imaging.* 2009;30(3):535–40.
79. Fukai I, Masaoka A, Fujii Y, et al. Thymic neuroendocrine tumor (thymic carcinoid): a clinicopathologic study in 15 patients. *Ann Thorac Surg.* 1999;67(1):208–11.
80. de Montpreville VT, Macchiarini P, Dulmet E. Thymic neuroendocrine carcinoma (carcinoid): a clinicopathologic study of fourteen cases. *J Thorac Cardiovasc Surg.* 1996;111(1):134–41.
81. Du Y, Wang Y, Tang J, et al. Pancreatic metastasis resulting from thymic neuroendocrine carcinoma: a case report. *Oncol Lett.* 2016;11(3):1907–10.

82. Soga J, Yakuwa Y, Osaka M. Evaluation of 342 cases of mediastinal/thymic carcinoids collected from literature: a comparative study between typical carcinoids and atypical varieties. *Ann Thorac Cardiovasc Surg.* 1999;5(5):285–92.
83. Girard N. Neuroendocrine tumors of the thymus: the oncologist point of view. *J Thorac Dis.* 2017;9(Suppl 15):S1491–S500.
84. Klemm KM, Moran CA. Primary neuroendocrine carcinomas of the thymus. *Semin Diagn Pathol.* 1999;16(1):32–41.
85. Mei Z, Wang H, Ren S, Wei J, Gu Y. Metastatic thymic carcinoid responds to chemoradiation and octreotide: a case report. *Medicine (Baltimore).* 2018;97(47):e13286.
86. Gaude GS, Hattiholi V, Malur PR, Hattiholi J. Primary neuroendocrine carcinoma of the thymus. *Niger Med J.* 2013;54(1):68–71.
87. Boubacar E, Atsame-Ebang G, Rabiou S, et al. Thymic large cell neuroendocrine carcinoma – a rare and aggressive tumor: a case report. *J Med Case Rep.* 2017;11(1):155.
88. Barbetakis N, Samanidis G, Samanidou E, et al. Primary mediastinal liposarcoma: a case report. *J Med Case Rep.* 2007;1:161.
89. Sung MT, Ko SF, Hsieh MJ, Chen YJ, Chen WJ, Huang HY. Thymoliposarcoma. *Ann Thorac Surg.* 2003;76(6):2082–5.
90. Hayati F, Ali NM, Kesu Belani L, Azizan N, Zakaria AD, Rahman MR. Giant mediastinal germ cell tumour: an enigma of surgical consideration. *Case Rep Surg.* 2016;2016:7615029.
91. Nam JG, Goo JM, Park CM, Lee HJ, Lee CH, Yoon SH. Age- and gender-specific disease distribution and the diagnostic accuracy of CT for resected anterior mediastinal lesions. *Thorac Cancer.* 2019;10(6):1378–87.
92. Aggarwal R, Rao S, Dhawan S, Bhalla S, Kumar A, Chopra P. Primary mediastinal lymphomas, their morphological features and comparative evaluation. *Lung India.* 2017;34(1):19–24.
93. Fritzsche FR, Kristiansen G, Frauenfelder T, et al. Large mixed germ cell tumor in a young patient presenting as an intrapulmonary mass. *Pathol Res Pract.* 2009;205(8):572–8.
94. Sadohara J, Fujimoto K, Muller NL, et al. Thymic epithelial tumors: comparison of CT and MR imaging findings of low-risk thymomas, high-risk thymomas, and thymic carcinomas. *Eur J Radiol.* 2006;60(1):70–9.
95. Inoue A, Tomiyama N, Fujimoto K, et al. MR imaging of thymic epithelial tumors: correlation with World Health Organization classification. *Radiat Med.* 2006;24(3):171–81.
96. Tomiyama N, Johkoh T, Mihara N, et al. Using the World Health Organization Classification of thymic epithelial neoplasms to describe CT findings. *AJR Am J Roentgenol.* 2002;179(4):881–6.
97. Seki S, Koyama H, Ohno Y, et al. Diffusion-weighted MR imaging vs. multi-detector row CT: direct comparison of capability for assessment of management needs for anterior mediastinal solitary tumors. *Eur J Radiol.* 2014;83(5):835–42.



Other Mediastinal Tumors

*Francesca Milone, Gianluca Taronna, Letizia Gnetti,
and Mario Silva*

- 7.1 Introduction – 128**
- 7.2 Lymphoma – 128**
 - 7.2.1 Overview – 128
 - 7.2.2 Hodgkin's Lymphoma – 128
 - 7.2.3 Non-Hodgkin's Lymphoma – 129
- 7.3 Germ Cell Tumors – 135**
 - 7.3.1 Overview – 135
 - 7.3.2 Patterns of Local Spread and Implication to Treatment – 137
 - 7.3.3 Lymph Node Involvement and Distal Spread – 141
- 7.4 Soft-Tissue Tumors – 143**
 - 7.4.1 Overview – 143
 - 7.4.2 Adipocytic Tumors – 143
 - 7.4.3 Other Mesenchymal Tumors – 145
- 7.5 Neurogenic Tumors – 148**
 - 7.5.1 Overview – 148
 - 7.5.2 Patterns of Local Spread and Implication to Treatment – 153
 - 7.5.3 Lymph Node Involvement and Distal Spread – 154
- References – 155**

7.1 Introduction

There is a variety of primary mediastinal tumors that include malignancies with heterogeneous histopathology. Each histology follows representative anatomical distribution according to compartments from the International Thymic Malignancy Interest Group (ITMIG) as follows: prevascular (anterior), visceral (middle), and paravertebral (posterior). Thereof, the anatomical location is a major determinant for differentiating mediastinal masses on cross-sectional imaging [1]. More than half of all mediastinal masses occur in the anterior compartment, with the thymus being the most common site of origin. Topics of this chapter are non-thymic mediastinal tumors, namely, neoplasms arising from lymphatic, germinal, mesenchymal, and neurogenic tissue.

7.2 Lymphoma

7.2.1 Overview

Lymphomas represent a heterogeneous group of lymphoid malignancies with a broad spectrum of clinical behavior and response to treatment. They are classified into two major groups: Hodgkin (HL) and non-Hodgkin's lymphoma (NHL). Lymphomas represent nearly 20% of all mediastinal neoplasms in adults and 50% in children [2]. Primary mediastinal lymphoma is relatively rare (10%), whereas the mediastinal involvement is most commonly encountered within systemic disease [3]. Notably, mediastinal involvement is seen in 80% HL and up to 45% NHLs. Lymphoma can involve any mediastinal compartment, though a notable preference is reported for the anterior mediastinum and middle mediastinum (especially with predominant paratracheal distribution).

7.2.2 Hodgkin's Lymphoma

Hodgkin's lymphoma (HL) has an incidence of approximately 2.5 cases per 100,000 persons/year, with a bimodal distribution of incidence (young adulthood and after the age of 50 years) [4].

HL arises from B cells, and it is characterized by a limited proportion of neoplastic cells (Reed-Sternberg cells) within a predominant component of inflammatory background. Two distinctive types of HL are described, namely, the classical Hodgkin's

lymphoma (>95% of the cases) and the nodular lymphocyte-predominant Hodgkin's lymphoma (NLPHL). There are two common subtypes of classical Hodgkin's lymphoma, "nodular sclerosis" and "mixed cellularity," and two uncommon subtypes, "lymphocyte rich" and "lymphocyte depleted" [5]. Mediastinal involvement from lymphoma accounts classical Hodgkin's lymphoma in approximately 50–70% of cases, usually as part of disease with predominant extra-mediastinal dissemination [3].

The majority of HL presents lymphadenopathy at the time of diagnosis, with obvious multi-site presentation according to the diffuse distribution of lymphatic network. Therefore, mediastinal involvement is oftentimes accompanied by cervical, supraclavicular, and axillary lymph node enlargement. Otherwise, lymph node stations below the diaphragm are rather sporadic.

Primary mediastinal classical HL is by definition stage I (single lymph node area or thymus involvement) or stage II (≥ 2 lymph node areas involved on the same side of the diaphragm; the number of lymph node regions involved may be indicated by a subscript, such as II₃ in case of three lymph nodes involved) disease, according to Ann Arbor classification [6] (■ Table 7.1). Staging of HL is helped by PET scan, which is expected to upstage stage I–II disease. Clinical subclassification remarks "A" for absence of symptoms or "B" for presence of fever (greater than 101 °F or 38.3 °C), weight loss, and night sweats, which are reported in some 30% of cases. Symptoms may include compartmental stiffness in case of lymphatic bulks (e.g., vessel compression, tracheal compression).

Primary mediastinal classical HL without bulky disease is routinely treated with combined chemotherapy ABVD (adriamycin, bleomycin, vinblastine, and dacarbazine), Stanford V regimen (doxorubicin, vinblastine, mechlorethamine, etoposide, vincristine, bleomycin, and prednisone), or escalated BEACOPP (bleomycin, etoposide, adriamycin, cyclophosphamide, oncovin, procarbazine, and prednisone). Radiation therapy can also be applied in specific sites of disease. The same medical approach is applied to bulky primary mediastinal classical HL and followed by ABVD and RT.

7.2.2.1 Imaging Features and Patterns of Disease Spread

Primary mediastinal HL is rare and mostly represented by the *nodular sclerosis* subtype. Mediastinal

Table 7.1 Ann Arbor classification of lymphoma

Stage	Definition
Stage I	Involvement of a single lymph node region (I) or of a single extralymphatic organ or site (IE) without nodal involvement. A single lymph node region can include one node or a group of adjacent nodes
Stage II	Involvement of two or more lymph node regions on the same side of the diaphragm alone (II) or with involvement of limited, contiguous extralymphatic organ or tissue (IIE)
Stage III	Involvement of lymph node regions or lymphoid structures on both sides of the diaphragm
Stage IV	Additional noncontiguous extralymphatic involvement, with or without associated lymphatic involvement
Annotations	Definition
A	No B symptoms
B	On or more of the following three systemic symptoms: Unexplained fever (more than 38.3 °C), drenching night sweat, or unexplained weight loss (exceeding 10% of the body weight during the 6 months prior to diagnosis)
X	Bulky disease: Mediastinal mass \geq 10 cm or greater than one-third of the internal transverse diameter of the thorax
E	Extranodal contiguous extension

HL usually occurs as a solid mass in the anterior mediastinum (up to 10 cm) (■ Fig. 7.1a, b), followed by pre-tracheal and paratracheal lymph nodes, and is seldom reported in the posterior mediastinum [7]. Primary mediastinal HL may involve the thymus, with gland enlargement and preserved organ shape (see ► Chap. 6). The involvement and coalescence of multiple nodes is rendered by lobulated mass with mild to moderate contrast enhancement and irregular contours (■ Fig. 7.1c, d). Cystic and necrotic changes can be identified (■ Fig. 7.1c, d). On MRI, homogeneous high signal intensity is seen on T2-weighted sequences (greater than muscle and similar to fat), though heterogeneous pattern is also reported [2].

Local growth of primary mediastinal HL results in compression of mediastinal structures [8], notably the most subtle lymphatic network. Lymphatic compression is the most common cause of pleural effusion (15%, either unilateral or bilateral) and/or pericardial effusion (20%, more common in case of nodular sclerosis histology), whereas pleuropericardial effusion from hematogenous dissemination is rare [9]. Both pleural and pericardial effusions might also be a consequence of therapy (e.g., idiopathic, drug-induced, or radiation-induced pericarditis). Pericardial effusion mostly resolves along with HL mass shrinkage; nonetheless, pericardial tamponade risk rises in case of rapid onset (\geq 250 ml). Such acute complication prompts subxiphoid pericardial windowing [10].

Bulky primary mediastinal HL can compress great mediastinal vessels; yet superior vena cava syndrome is quite rare.

Direct infiltration of adjacent structures is rare, allegedly as a consequence of the minor proliferation and motility potential of Reed-Sternberg cells, which are substantially unable to spread through the neighboring epithelium [11]. Direct invasion is more likely for extensive mediastinal disease. Pulmonary involvement is seen in less than 10% of cases, either as direct invasion from mediastinal mass (■ Fig. 7.2a–c) or hematogenous dissemination with peripheral nodules (cavitation can happen) [12]. Chest wall invasion by bulk growth of mediastinal mass is reported in about 5% of cases at diagnosis.

The spread of disease is commonly seen along contiguous lymph node stations, while skip involvement to the second next node station is quite unusual [13]. The most commonly involved extranodal sites are the spleen, lungs, liver, and bone marrow [11]. Hematogenous spread was reported in only 5–10% of all HL cases, notably suggested by Reed–Sternberg cells emboli within blood vessels in autopsy and biopsy findings. Intriguingly, these cells were described as being frequent in HL with perivascular location, potentially reflecting a favorable condition for neoplastic cells passing through vessels into the bloodstream [14].

7.2.3 Non-Hodgkin's Lymphoma

Non-Hodgkin's lymphoma (NHL) represents a spectrum of diseases that range from relatively indolent to most aggressive malignancies. About

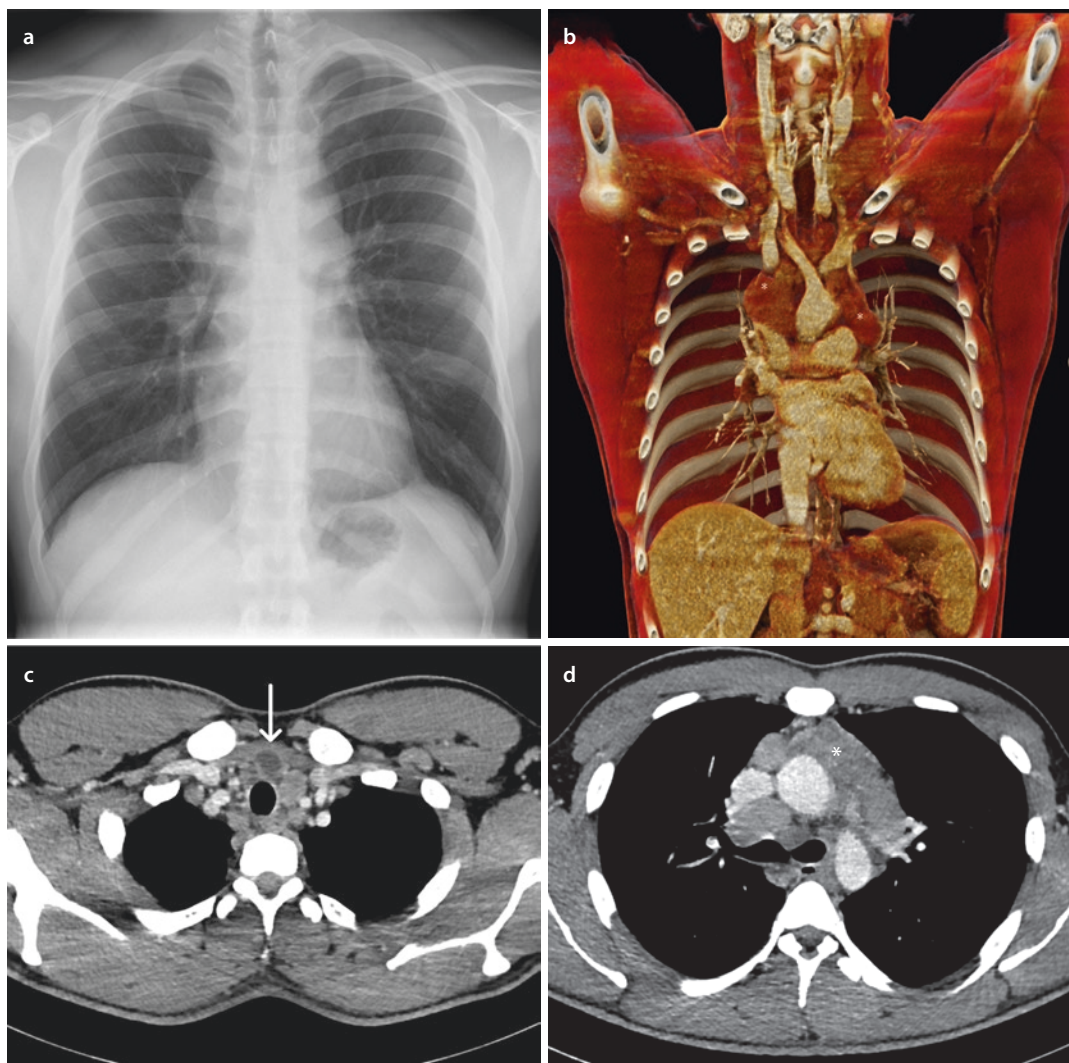


Fig. 7.1 a–d *Primary mediastinal HL*. **a** Posteroanterior chest radiography shows middle-anterior mediastinal mass with superior extent beyond the thoracic inlet. Encasement of tracheobronchial stripe is seen with signs of minor compression. **b** Volume rendering reconstruction of contrast-enhanced CT (venous phase) depicts the mass (red

structure amongst vessels) and its relation with adjacent structures. **c, d** Axial contrast-enhanced CT (venous phase) shows polylobulated mass composed of coalescent lymphadenomegalies (asterisk) in the anterior and middle mediastinum, with signs of lymph node necrosis and cystic degeneration (arrow)

85–90% of NHLs are derived from B cells, while the remainders derive from T cells or NK cells. NHL has an incidence of 19.4 cases per 100,000 persons/year in the USA [15]. Primary mediastinal large B-cell lymphoma and lymphoblastic leukemia/lymphoma are the two most common subtypes of mediastinal NHL, which will be discussed in the following paragraphs. Further, mediastinal NHL is extranodal marginal zone lymphoma of mucosa-associated lymphoid tissue (MALT lymphoma), anaplastic large-cell lymphoma (T-cell lymphoma involving lymph nodes or skin; medias-

tinal location is anecdotal), and B-cell lymphoma unclassifiable (with intermediate features between diffuse large B-cell and classical HL) [16].

Primary mediastinal large B-cell lymphoma (PMBL) arises from thymic B cells, and its clinical and biological features are different from other types of diffuse large B-cell lymphoma (DLBCL). It represents 2–3% of all NHL and 6–10% of all DLBCL, and it mostly occurs in young to middle-aged patients [17].

Chemo-immunotherapy by chemotherapy and the monoclonal antibody rituximab is the first medical option in both limited and advanced dis-

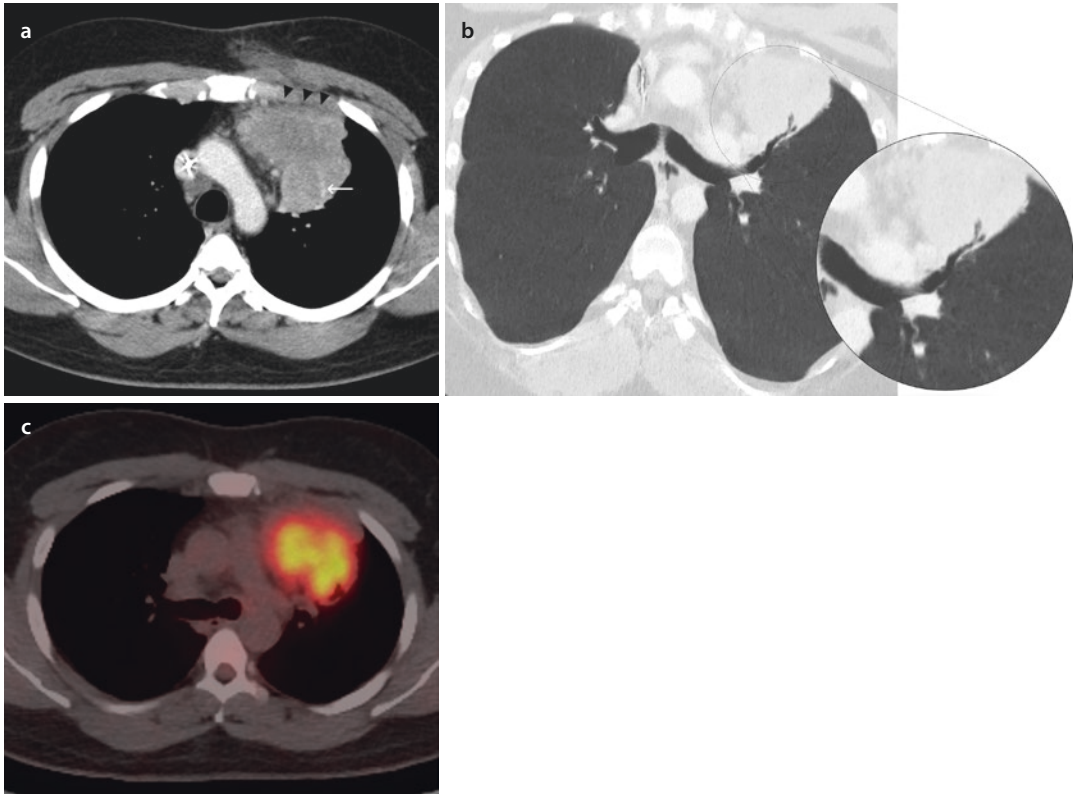


Fig. 7.2 a–c *Primary mediastinal HL.* **a** Axial contrast-enhanced CT (venous phase) shows a bulky HL in the anterior mediastinum abutting the mediastinal aspect of the left lung, with signs of direct pulmonary infiltration. Encasement of a subsegmental branch of pulmonary artery (arrow). The mass displays large contact surface with the anterior chest wall, still with some residual fat interposition (low likelihood of infiltration – arrowheads); effusion of the subcutaneous adipose tissue is seen as a consequence of transthoracic biopsy. **b** Oblique axial CT image with minimum intensity projection reformatting

shows bronchial invasion from the solid mass growing from the anterior mediastinum through pleural sheets and into pulmonary parenchyma. The obstruction of bronchial lumen from solid mass is seen at the level of subsegmental branch (vignette) in the anterior segment of the left upper lobe. **c** Axial fusion PET-CT image shows interruption of the bronchial tree from invasion by the bulky HL with high and heterogeneous metabolic activity, suggesting a rapidly growing neoplasm with extremely aggressive biological behavior

ease [18]. Limited disease is defined by treatment achievable within one irradiation field. In such case, the use of radiation therapy depends on the medical treatment by chemo-immunotherapy. Otherwise, radiation therapy is rather controversial in case of advanced disease. Disease relapse or refractory PMBL can be treated with alternative chemo-immunotherapy or stem cell transplantation [17].

Lymphoblastic lymphoma accounts for about 8% of all lymphoid malignancies. Lymphoblastic neoplasms are divided into two categories according to cell lineage, either precursor B cells or precursor T cells, the latter being the most typical of mediastinal involvement. Another classification of lymphoblastic neoplasm is established by the proportion of blasts in bone marrow

(independently from mediastinal mass), namely, “lymphoblastic lymphoma” (<25% blasts in bone marrow – aka T-LBL and B-LBL) or “lymphoblastic leukemia” (>25% blasts in bone marrow – aka T-ALL and B-ALL) [19]. T-LBL is far more common than T-ALL and it displays as mediastinal mass in 91% of cases [20] (■ Fig. 7.3a–c).

Standard therapeutic option for LBL was formerly represented by conventional chemotherapy regimens for NHL; however, it is now set according to leukemia chemotherapy regimens, which include intensive intrathecal chemotherapy prophylaxis (or cranial RT) and mediastinal irradiation. Noteworthy, mediastinal RT is not administered in most pediatric LBL protocols because of short- and long-term morbidities.

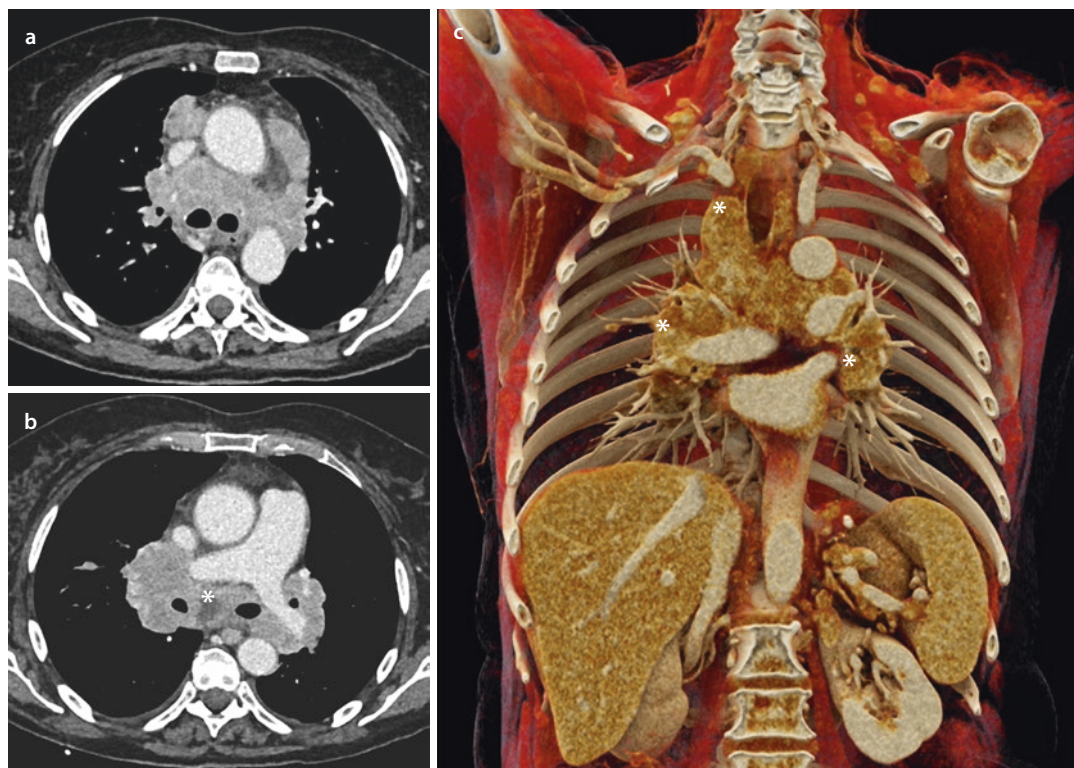


Fig. 7.3 a–c Primary mediastinal NHL (angioimmunoblastic T-cell lymphoma). a, b Axial contrast-enhanced CT (venous phase) shows large mass in the anterior and middle mediastinum with encasement of major airways and vessels, displaying heterogeneous enhancement from lymph node necrosis (asterisk). c Volume rendering

reconstruction of contrast-enhanced CT (venous phase) shows the extensive mass that grows with encasement of major airways and vessels, throughout the mediastinum and down to hilar and lobar-segmental region (asterisk)

Patients with adverse prognostic features should be considered for high-dose chemotherapy and stem cell transplantation. The management of residual mediastinal masses in LBL is also controversial: the options include local RT, surgical resection of the residual mass or close observation in patients receiving maintenance chemotherapy, or undergoing stem cell transplantation [20].

7.2.3.1 Imaging Features and Patterns of Disease Spread

NHL of the mediastinum usually occurs as a large anterior mediastinal mass, representing thymic and lymph node enlargement. On CT, such neoplasms may show low attenuation areas due to hemorrhage, necrosis, or cystic degeneration (Fig. 7.4a–d). Anterior mediastinum and para-

tracheal lymph node stations are typically involved; subcarinal, hilar, internal mammary, pericardial, and posterior mediastinal nodes may also be involved [13].

Local invasion of NHL is quite frequent towards several adjacent mediastinal structures. Pleural and/or pericardial effusion is seen in 30% of patients with NHL, with potential evolution into cardiac tamponade (Fig. 7.5a–f). Unlike classical HL, the NHL mass does not present surface lobulation but rather ill-defined borders with progressive mass growth towards compression, encasement, and infiltration of great vessels, oftentimes resulting in superior vena cava syndrome. Airway infiltration is also seen with variable association with symptoms (e.g., cough, wheezing, shortness of breath, orotracheal obstruction). The growth within the

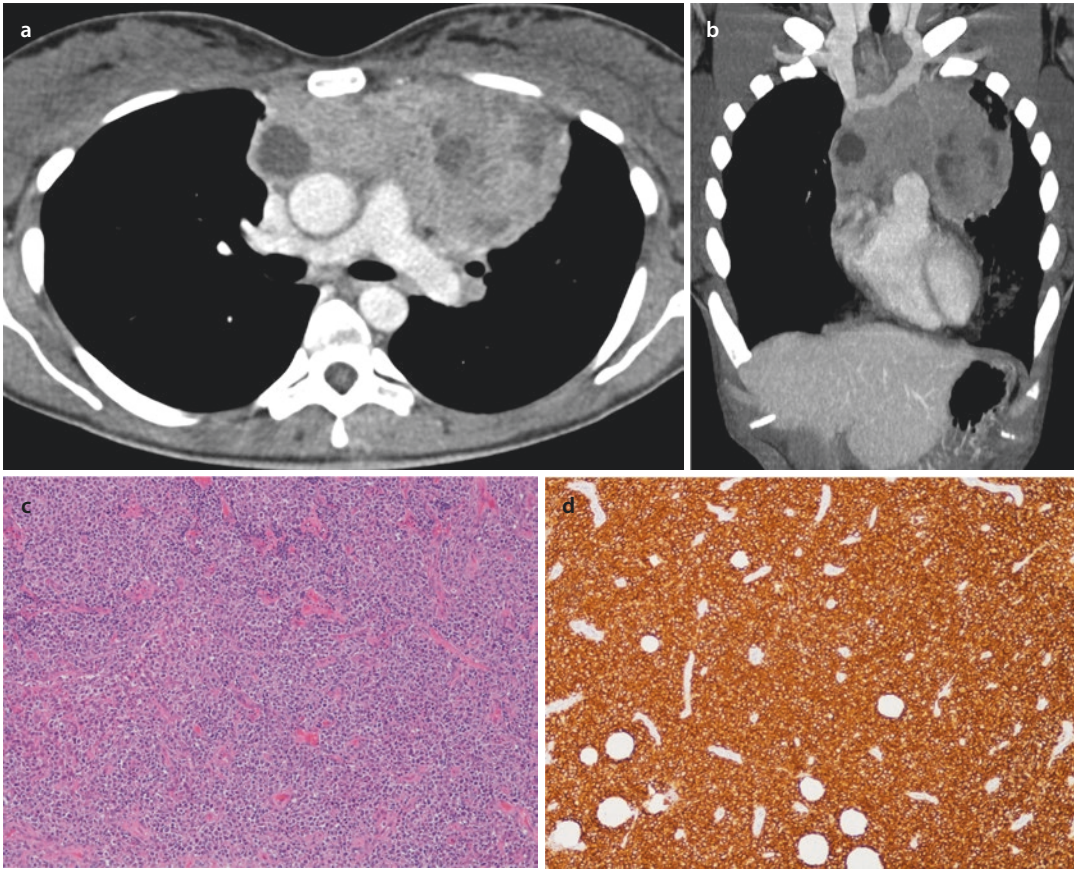


Fig. 7.4 a–d Primary mediastinal NHL (primary mediastinal large B-cell lymphoma, PMBL). a, b Axial a and oblique coronal b contrast-enhanced CT (venous phase) show large mass in the anterior mediastinum with heterogeneous contrast enhancement from necrotic evolution and cystic degeneration. c, d Hematoxylin-eosin

staining of the histologic specimen (c – 20×) shows many large atypical lymphoid cells with clear cytoplasm and irregular nuclei. CD20 immunohistochemical staining (d – 20×) is diffusely positive, indicating elements derived from B lineage lymphomas

middle-posterior mediastinum happens to involve also the nervous system, notably with phrenic nerve palsy.

Primary mediastinal B-cell lymphoma This neoplasm more frequently displays bulky mass (over 10 cm) originating in the thymus, with propensity to infiltration of the lung, chest wall (Fig. 7.6a–e), pleura, and pericardium (70–80%). Also, symptoms and signs of superior vena cava syndrome are depicted in as high as 50% of cases (e.g., thoracic and neck vein swelling, facial edema, conjunctival swelling, and arm edema) (Fig. 7.7a–c). Hoarseness may occur in case of recurrent laryngeal nerve infiltration. Despite the blunt local invasiveness, the involvement of extrathoracic structures is less common at presentation of PMBL than for

lymphoblastic lymphoma. Extranodal sites may, however, occur during disease progression or at recurrence, including the kidneys, adrenal glands, liver, and ovaries and the central nervous system (Fig. 7.8a–e). Otherwise, spread to bone marrow or cerebrospinal fluid involvement is unusual [17].

Lymphoblastic lymphoma This neoplasm shows tendency to the extrathoracic lymph nodes (Fig. 7.9a–e), bone marrow, central nervous system, and gonads. Such diffusion pathways are akin in the first diagnosis of extensive disease and disease relapse [13]. Abdominal dissemination is not common, with the liver and spleen being primary sites of involvement following morphological appearance of splenomegaly and hepatomegaly [21].

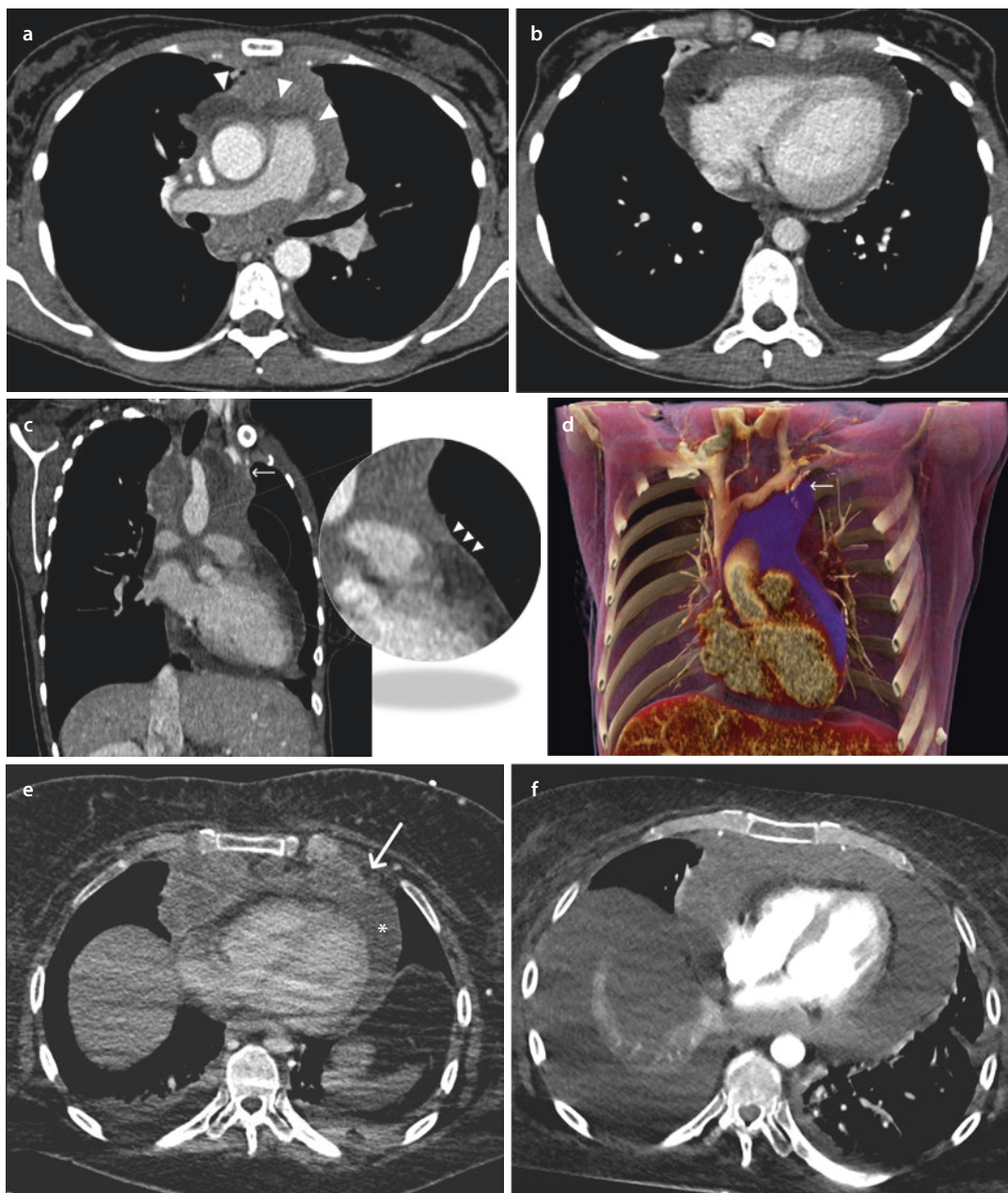


Fig. 7.5 a–f Primary mediastinal NHL (primary mediastinal large B-cell lymphoma, PMBL). a–c Axial a, b and oblique coronal c contrast-enhanced CT (arterial phase) show pericardial invasion (arrowheads) with sheet thickening (vignette) and circumferential pericardial effusion. The anterior mediastinal mass abuts the upper pericardial portion with direct infiltration (arrowheads). Infiltration of the left anomalous trunk (arrow) with onset of collateral venous circles. d Volume rendering reconstruction of contrast-enhanced CT (venous phase) shows

the extensive mass (purple area) spreading from left anomalous trunk (arrow – anatomical site of systemic lymphatic drainage from thoracic duct into the venous system) down to pericardial surface. e–f Axial contrast-enhanced CT at time of staging (e – venous phase) shows the mediastinal mass with pericardial infiltration (arrow) and effusion (asterisk), rapidly evolving 3 months later (f – arterial phase) towards pericardial tamponade and right-sided massive pleural effusion

7.3 Germ Cell Tumors

7.3.1 Overview

Germ cell tumors (GCT) are a heterogeneous group of malignancies with different histopathological, clinical, and prognostic features. They usually occur in the gonads, while less than 5% has a different origin. The mediastinum represents the most common extragonadal site. A diagnosis of primary mediastinal germ cell tumor (PMGCT) always requires the absence of

a gonadal mass on physical exam and imaging evaluation [22]. Most PMGCTs arise from the anterior/prevascular mediastinum, and they are histologically classified in teratomas, seminomatous, and non-seminomatous tumors, likewise their gonadal counterpart [23]. Klinefelter syndrome is the recognized risk factor for PMGCT, notably associated with non-seminomatous tumors. PMGCT develops overwhelmingly among males, and its clinical presentation depends largely on tumor size. Symptoms include chest pain, respiratory distress, cough,

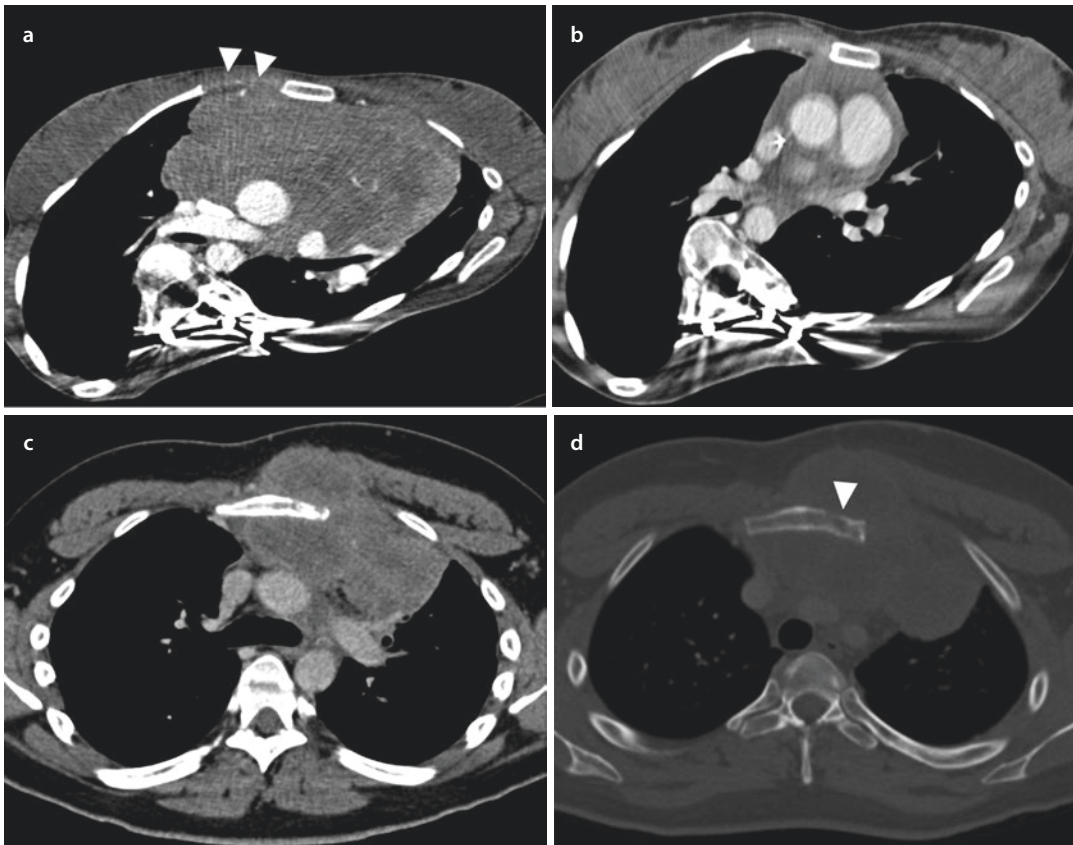


Fig. 7.6 a–e Primary mediastinal NHL (primary mediastinal large B-cell lymphoma, PMBL). **a, b** Axial contrast-enhanced CT (**a** – arterial phase) shows anterior mediastinal mass with direct invasion of the chest wall in the right parasternal region of the second intercostal space (arrowheads). The bulk shrinks and its invasion of chest wall rapidly regresses at 4 months after initiation of chemotherapy (**b** – venous phase). **c, d** Axial contrast-enhanced CT (**c** – mediastinal window) shows anterior

mediastinal mass with direct invasion of the chest wall in the left parasternal region of the first intercostal space and cortical bone erosion (**d** – bone window) in the anterior aspect of the sternal manubrium (arrowhead). **e** Volume rendering reconstruction of contrast-enhanced CT (venous phase) shows the extensive necrotic mass (purple area) with direct infiltration of the anterior chest wall at the level of first and second intercostal space

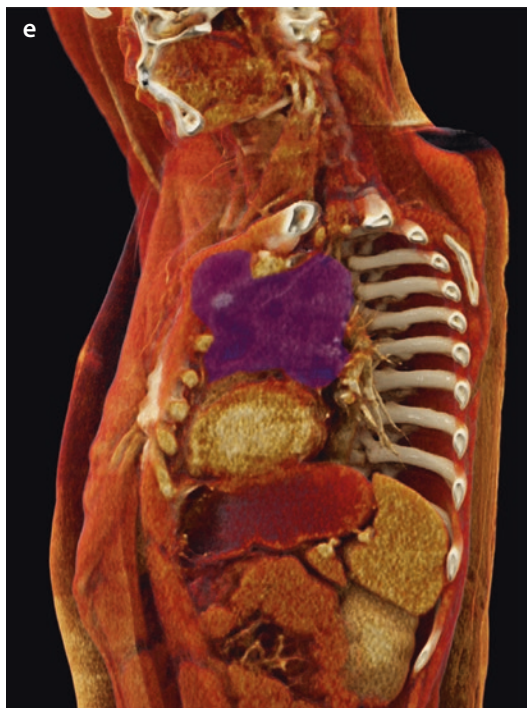


Fig. 7.6 (continued)

hoarseness, and superior vena cava syndrome [24, 25] (Fig. 7.10a–f).

A clinical staging system has been proposed by Moran et al. in 1997, based on 322 cases [26]; however, an officially recognized staging protocol does not exist. The WHO recommends using a modification of the AJCC TNM staging [16]. Beyond staging approach, ultimately, the prognosis of PMGCT depends on its histology, but in general, the outcome is worse than for gonadal GCT.

7.3.1.1 Teratomas

Mediastinal teratoma shows variable composition by assemblage of histologic tissues from all germinal layers. Unlike other PMGCTs, teratoma occurs in all age groups without gender predilection. The main histologic classification describes mature and immature teratoma and teratoma with other malignant components [26].

Mature teratoma displays benign behavior with evolution into either large central cystic cavity or multiple and confluent cystic spaces [27]. On CT, it usually appears as encapsulated and well-circumscribed masses containing fluid, soft-

tissue, and fat attenuation; on MRI, heterogeneous signal intensity is quite typical. The presence of intralesional fat-fluid levels is pathognomonic of teratoma [2].

Otherwise, immature teratoma commonly appears as a large and solid mass composed by incompletely differentiated elements of embryonic tissues, typically arising from the neuroectoderm [24]. The percentage of immature elements is routinely reported from pathological specimen; however, grading of immature teratoma does not have an established prognostic value for such mediastinal neoplasm.

Mediastinal teratoma with other malignant components appears as poorly circumscribed and may be solid or cystic with hemorrhagic and necrotic areas [26]. It can originate as a sporadic spontaneous disease or it can be induced by chemotherapy and radiation [28]. Such subtype of teratoma can be classified into two histologic variants: (a) teratoma with other germ cell components (so-called mixed MGCT) and (b) teratoma with somatic malignancy.

7.3.1.2 Non-seminomatous Tumors

Mediastinal non-seminomatous GCT is a rare entity including three major subtypes: (a) yolk sac tumor (YST) (Fig. 7.11a–d), (b) embryonal carcinoma (EC), and (c) choriocarcinoma. YST and EC occur either in the pure form or as component of mixed GCTs [29]. The pure form of mediastinal choriocarcinoma is extremely rare. They all appear as large tumors with extensive areas of hemorrhage and necrosis.

7.3.1.3 Seminomatous Tumors

Mediastinal seminomas are malignant GCTs almost always occurring in men in postpubertal age, with a predilection for the third and fourth decade. They form a large, soft, and solid mass with a lobulated contour. Despite their hypothetical bulky growth, on CT imaging, these tumors show homogeneous appearance with minimal contrast enhancement [2]. Punctate foci of hemorrhage or necrosis may be seen. Their size can vary from 1 to 20 cm at the time of diagnosis; however, they typically appear as localized mass in the anterior mediastinum [30]. Mediastinal seminoma occurs either in the pure form or as component of mixed GCTs.

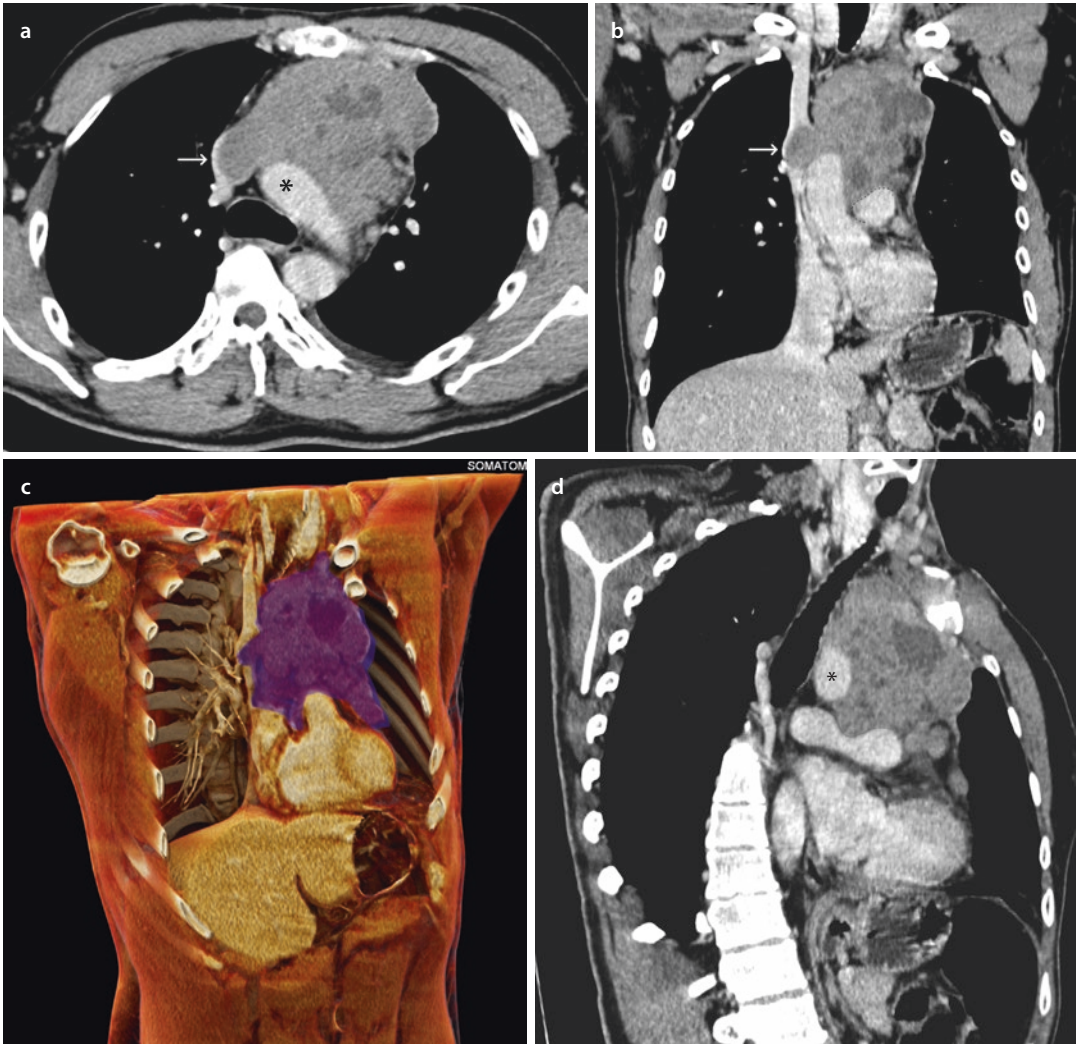


Fig. 7.7 a–d Primary mediastinal NHL (primary mediastinal large B-cell lymphoma, PMBL). **a** Axial contrast-enhanced CT (venous phase) shows invasion of the upper vena cava (arrow) and compression of the aortic arch (asterisk). **b** Coronal reformatting of contrast-enhanced CT (venous phase) shows invasion of the upper vena cava (arrow). **c** Volume rendering reconstruction of

contrast-enhanced CT (venous phase) shows the extensive necrotic mass (purple area) with direct infiltration of the upper vena cava. **d** Oblique sagittal reformatting of contrast-enhanced CT (venous phase) shows compression of the aortic isthmus (asterisk) and the main left pulmonary artery (dashed line)

7.3.2 Patterns of Local Spread and Implication to Treatment

Primary mediastinal GCT often appears as a large incidental finding on chest X-ray because it can grow asymptomatic in the relatively large area of the anterior mediastinum. Both CT and MRI are mandatory for accurate characterization of the lesion, namely, for defining exact tumor location

and for description of pathognomonic signs and patterns: density, calcification, cystic spaces, and hemorrhagic or necrotic areas. The dissemination pathway of PMGCT depends on the histologic subtype, and the specific growth pattern defines the characteristics of local invasion.

Mature teratoma displays benign behavior; however, large size can result in compression and obstruction of lymphatic collectors, mediastinal

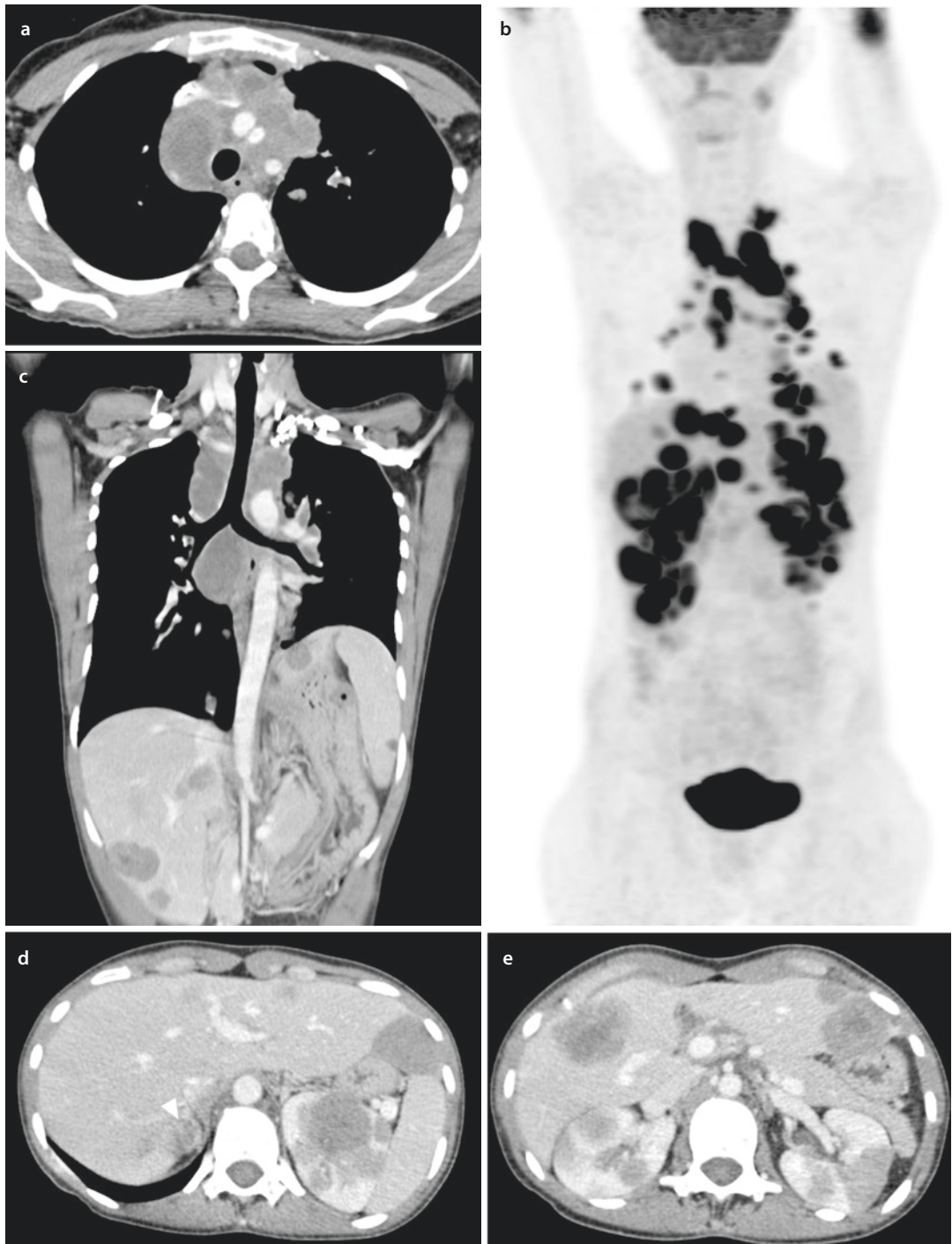


Fig. 7.8 a–e Primary mediastinal NHL (primary mediastinal large B-cell lymphoma, PMBL). a–c Axial a and curved coronal reformatting b of contrast-enhanced CT (venous phase) shows mediastinal mass and extranodal dissemination as confirmed by high metabolic activity

spots at 18-FDG-PET c, at the time of disease progression. d, e Axial contrast-enhanced CT (venous phase) shows multiple-site extranodal metastases involving the adrenals (arrowhead), kidney, and liver

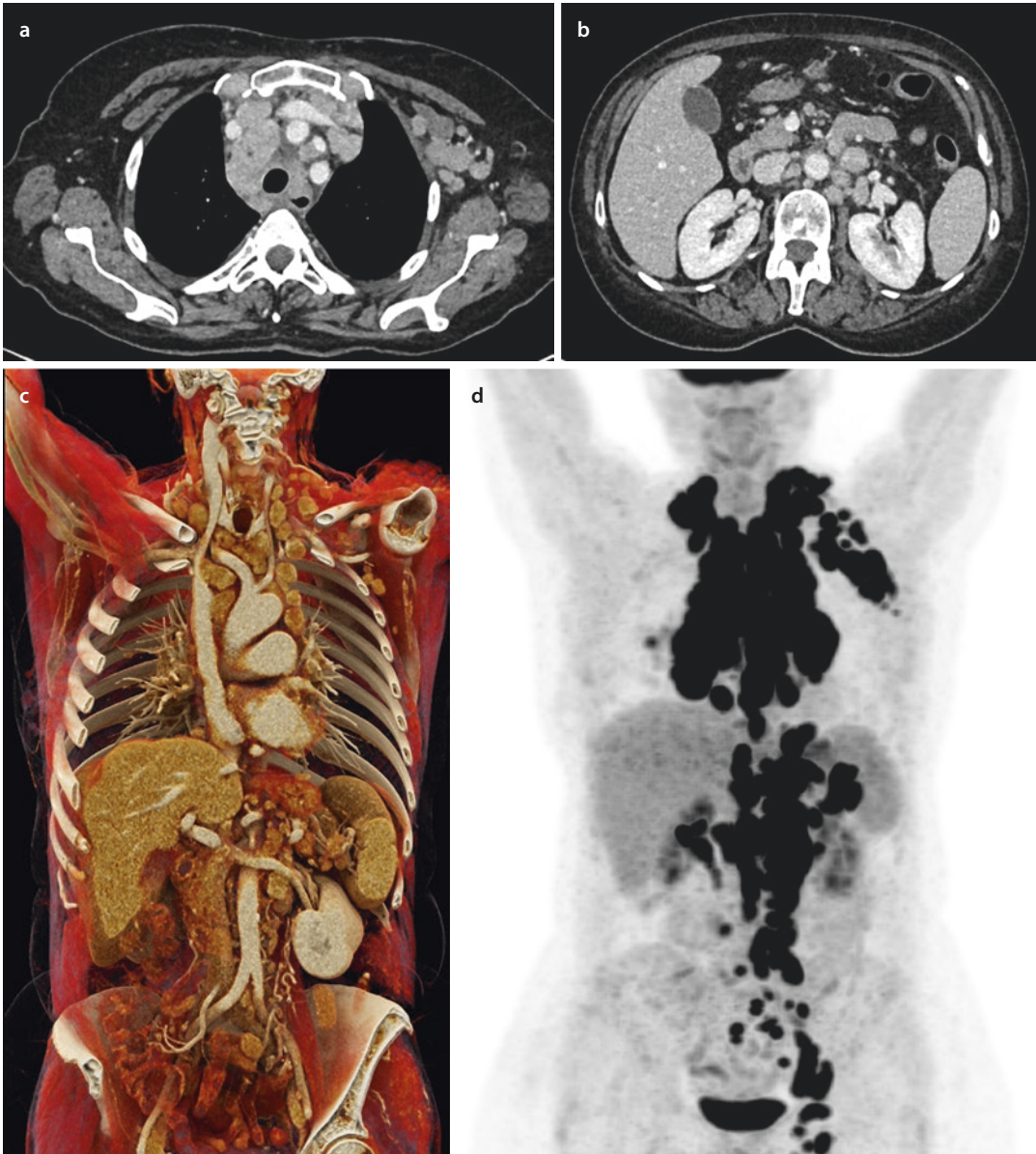


Fig. 7.9 a–d Primary mediastinal NHL (angioimmunoblastic T-cell lymphoma). a, b Axial contrast-enhanced CT (venous phase) shows the involvement of the mediastinal, left axillary, and retroperitoneal lymph nodes, at the time of disease relapse. c, d Volume rendering reconstruction

of contrast-enhanced CT (venous phase) shows the involvement of intrathoracic and extrathoracic lymph nodes, as witnessed by the high metabolic activity spots at 18-FDG-PET d, at the time of disease relapse

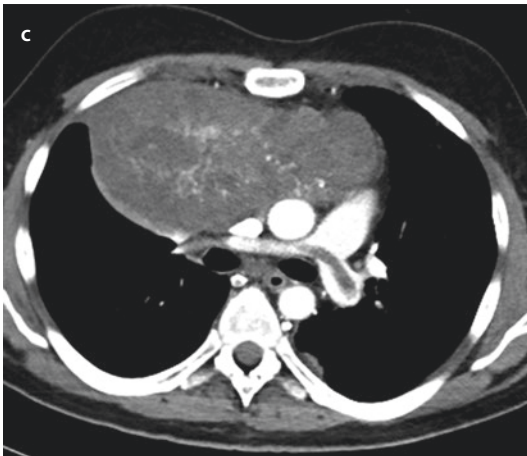
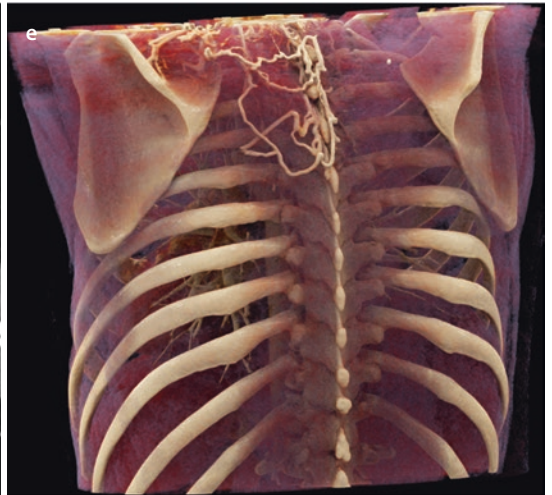
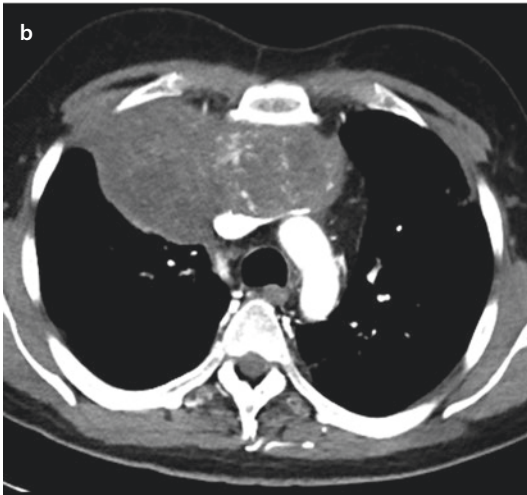
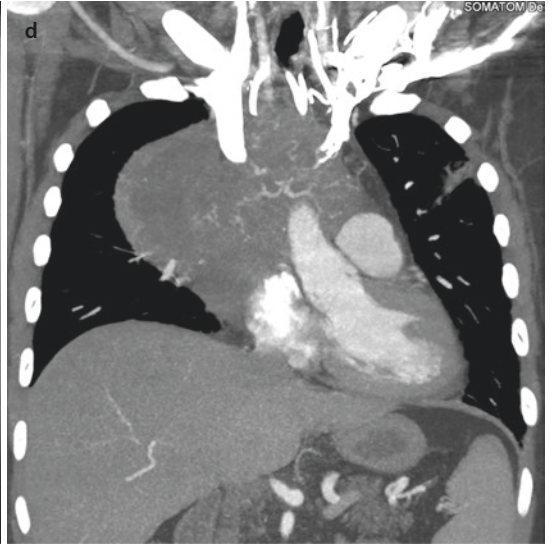
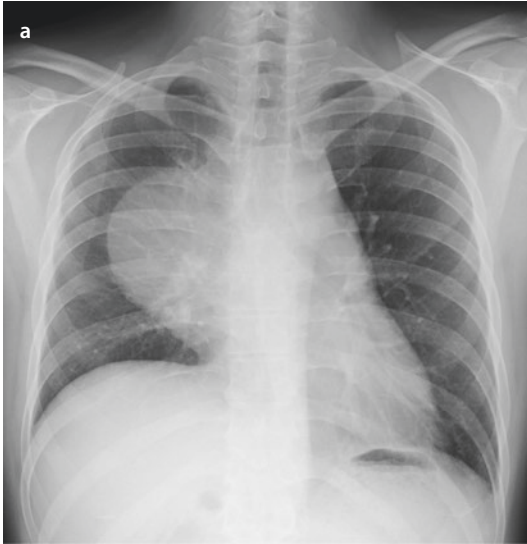
vessels, and airway until mediastinal shift (Fig. 7.12a–e). Nonetheless, surgical treatment is almost always feasible and results in radical resection of disease [31].

Immature teratoma is usually confined to the mediastinum and variably associated with signs of local invasion, which are associated with the presence of malignant component. Imaging is

paramount in depicting local invasion, which prevents surgical resection [32] (Fig. 7.13a, b).

The heterogeneity of mixed MGCTs is associated with quite a range of patterns of local spread, which mostly displays extensive local infiltration into mediastinal structures.

Non-seminomatous PMGCT is frankly aggressive; therefore, infiltration of all mediasti-



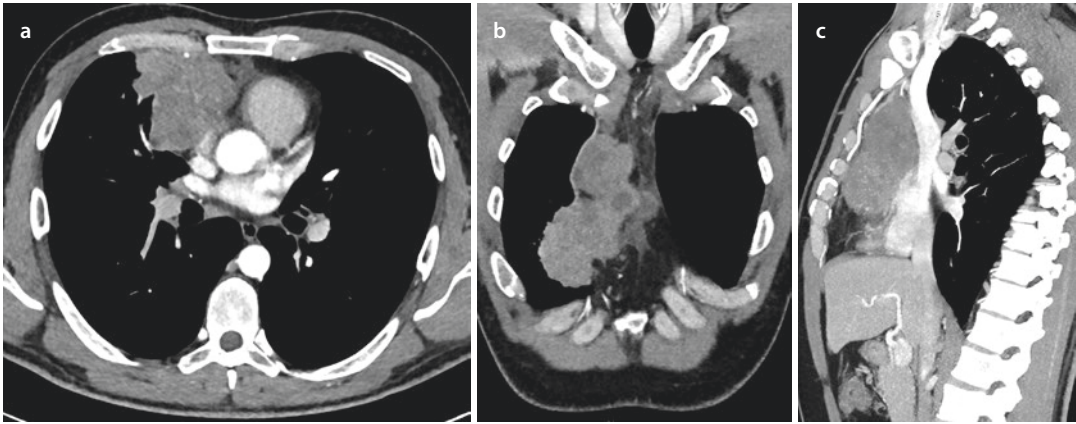


Fig. 7.11 a–c Primary mediastinal germ cell tumor (yolk sac tumor). a–c Axial a, coronal b, and sagittal maximum intensity projection formatting c contrast-enhanced CT

(arterial phase) show the mass with early heterogeneous contrast enhancement and heterogeneous density from areas of hypodense necrosis and cystic degeneration

nal compartments and lung invasion are common even at clinical presentation [31]. The rapid and bulky growth of non-seminomatous PMGCT oftentimes results in heterogeneous appearance at imaging evaluation [2]. Pleural and pericardial effusions are common. Signs of local infiltration drive the management towards neoadjuvant therapy with the aim of surgical resection of the residual mass [29, 33].

Seminoma mostly presents with large mass with bulky growth and limited invasion [32]. Occasionally, at primary diagnosis, the mass may involve thoracic structures with obliteration of the fatty planes [31]. Chemotherapy is the treatment of choice because of its relatively good out-

come, while radiotherapy represents a second-line treatment due to the higher toxicity on the mediastinum. Typically, surgical resection is not possible in the initial management because of the presence of bulky disease [34].

7.3.3 Lymph Node Involvement and Distal Spread

The histologic subtype of PMGCT is strictly related to the presence of metastatic disease. In general, prognosis is unfavorable for non-seminomatous types, including teratomas and non-teratomatous tumors [34].

Fig. 7.10 a–f Primary mediastinal germ cell tumor (immature teratoma). a Posteroanterior chest radiography a shows anterior mediastinal mass with lateral extent and without signs of airway compression, despite the large size. b–c Axial contrast-enhanced CT (arterial phase) shows bulky mass in the anterior mediastinum with compression of anonymous trunks and upper vena cava. The upper venous system compression is associated with venous shunting into recruitment of collateral veins in the posterior chest wall that drain in the azygos and hemiazygos veins. Compression of the main pulmonary artery is also seen c; massive clot is depicted in the main

pulmonary artery, right and left main. Thrombosis of the azygos vein is depicted c. d Coronal maximum intensity projection reformatting of contrast-enhanced CT (arterial phase) shows bulky mass in the anterior mediastinum with compression of both anonymous branches. e, f Volume rendering reconstruction of contrast-enhanced CT (arterial phase) shows dorsal collateral circles (e – left posterior paraspinal space) and their connection to the azygos vein (f – the vignette shows the collateral vein shunting from right paravertebral space into the azygos arch). The mediastinal mass is displayed in purple

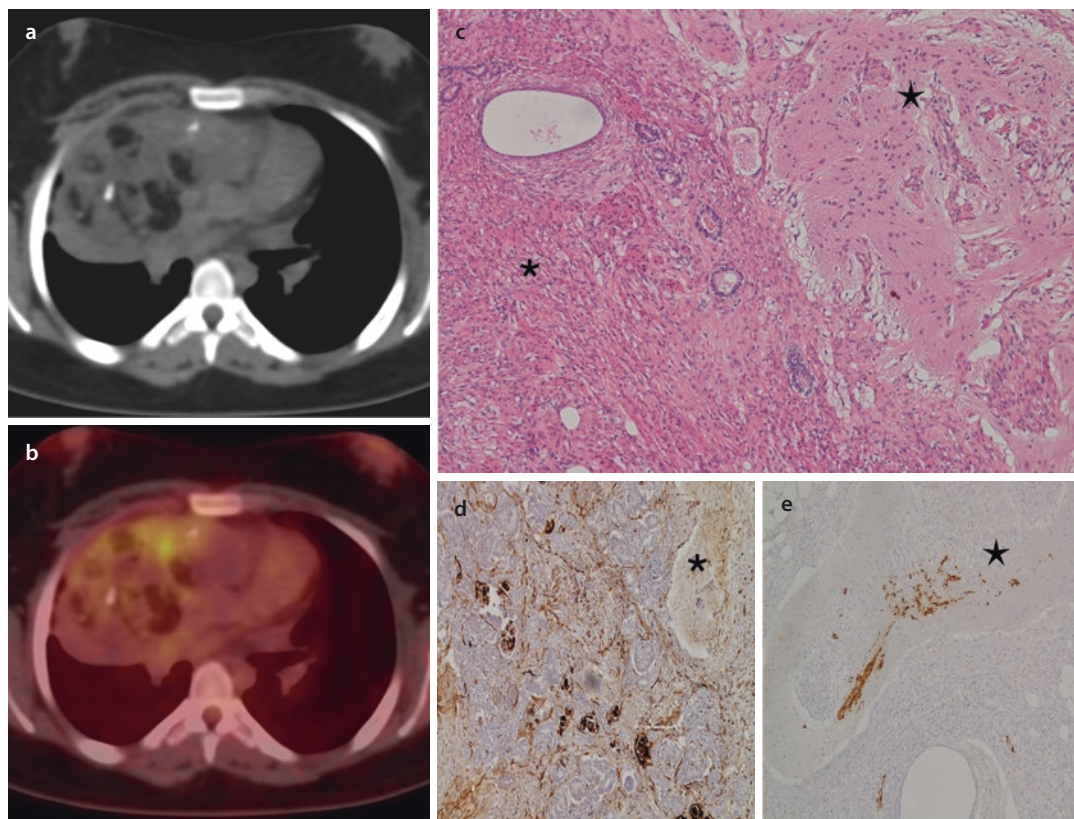


Fig. 7.12 a–e Primary mediastinal germ cell tumor (teratoma with immature elements < 10% – grade I). a, b Axial non-enhanced CT a and 18-FDG-PET b show a bulky capsulated mass in the anterior mediastinum with mild compression on the major mediastinal vessels. The mass shows heterogeneous density (fat component, soft tissue, and calcification) and moderate metabolic activity.

c–e Hematoxylin-eosin staining of the histologic specimen (c – 20x) shows mature element deriving from mesonephric tissue (asterisk) and immature elements deriving from neuroectodermal layer (star). WT-1 staining d confirms the presence of mesonephric tissue (asterisk), and positivity of synaptophysin staining e confirms the presence of immature neuroectodermal elements (star)

Despite their potentially malignant nature, immature teratomas happen to show very low risk of distant metastasis, while teratoma with other malignant components has a more aggressive behavior. Both mixed GCTs and teratomas with somatic malignancy are metastatic at presentation: the lung, pleura, lymph node, liver, bone, and brain are the most involved sites [26]. Conversely, tumors with sarcomatous component infrequently cause hematogenous spread, especially if compared to gonadal counterpart, whereas local invasion into mediastinal structures represents the most frequent cause of morbidity and mortality [35].

In non-seminomatous PMGCT, hematogenous dissemination prevails over lymphatic pattern. Single or multiple metastases are seen in the majority of non-seminomatous PMGCTs at the

time of diagnosis. Choriocarcinoma is probably the most aggressive PMGCT. Hot spots for hematogenous metastases of this tumor are seen in the lung, liver, kidney, and spleen; it can seldom diffuse into the brain, heart, adrenals, and bone [32].

Pure seminomas are associated with a positive prognosis as compared to other malignant PMGCTs. Lymph node involvement is much more common than in non-seminomatous malignancies, and particular attention should be paid in the setting of imaging protocol because cervical nodes are oftentimes affected by tumor dissemination [32, 34]. Preferential sites of local spread are the chest wall and pleura. The lung can be involved either by local invasion or hematogenous spread, and further common targets of hematogenous spread are the brain, liver, adrenal gland, and bone. Noteworthy, visceral metastases

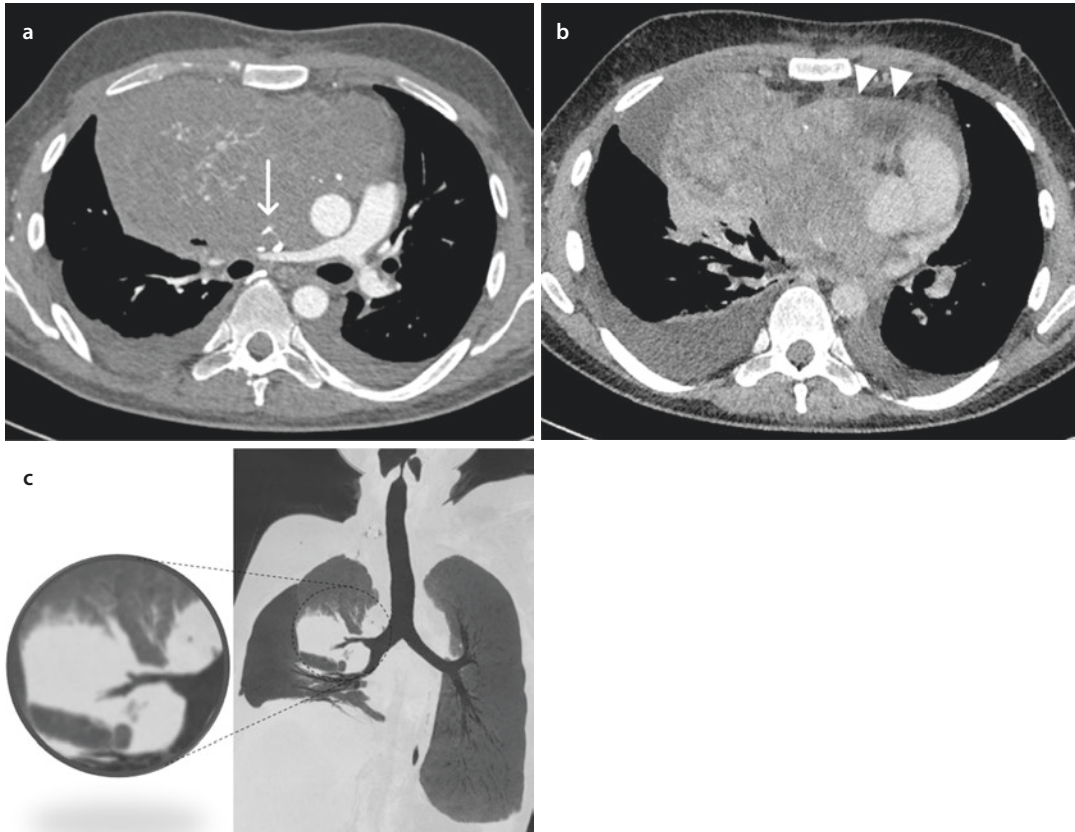


Fig. 7.13 a–c Primary mediastinal germ cell tumor (immature teratoma). a–b Axial contrast-enhanced CT in arterial phase a and venous phase b shows the high potential of dissemination by local invasion from bulky mass in the anterior mediastinum: infiltration of the upper vena cava (arrow), direct invasion of pericardial (arrow-

heads) as well as invasion through the pleura and right lung. c Oblique coronal minimum intensity projection reformatting shows bronchial interruption in the right middle lobe from the mediastinal mass that invades the right lung

correlate with a poorer outcome, liver involvement being the most significant negative prognostic factor [34].

7.4 Soft-Tissue Tumors

7.4.1 Overview

Soft-tissue tumors of the mediastinum are rare, with an estimated incidence of 2–6% of all mediastinal neoplasms [36]. Almost all types of mesenchymal neoplasms have been described in this location, with the exception of peculiar site-specific neoplasms (such as gastrointestinal stromal tumors, aka GIST). Mediastinal sarcomas may occur de novo or, more rarely, as sarcomatous component in mediastinal germ cell tumor

(GCT) [35]. Sarcomatous areas in thymic sarcomatoid carcinoma or as pseudosarcomatous stroma in a thymoma have been also reported [37–39].

Because of their singularity, most mesenchymal tumors in the mediastinum have been reported as case reports or small series. Among soft-tissue tumors of the mediastinum, adipocytes are by far the most represented cell line [40].

7.4.2 Adipocytic Tumors

Adipocytic tumors are one of the most common soft-tissue neoplasms in the mediastinum. Mediastinal lipomatous tumors may be located in any mediastinal compartment as they arise from connective tissues throughout the mediastinum.

In case of lipomatous tumor appearing as distinct component of thymic tissue, it is considered a site-specific tumor (*thymolipoma* – see ► Chap. 6).

Liposarcoma is a malignant adipocytic tumor with a range of subtypes; it is the most common primary malignant mesenchymal tumor of the mediastinum, variably seen as adipose component with the thymus (*thymoliposarcoma*). Mediastinal liposarcoma has been estimated to account for 1–2% of all liposarcomas and <1% of all mediastinal tumors [41]. Liposarcomas may occur in all mediastinal compartments and typically show well-circumscribed multinodular mass, the size of which can range from few centimeters up to even more 60 cm [42] (► Fig. 7.14a, b). Liposarcoma can show several histologic subtypes with variable representation according to the tumor location; noteworthy, mediastinal liposarcoma shows different frequency of subtypes as compared to other anatomical primary sites. Well-differentiated/dedifferentiated liposarcoma is the most prevalent mediastinal subtype (57%, versus 65% in overall distribution), followed by pleomorphic liposarcoma (23%, versus 5% in overall distribution) and myxoid liposarcoma (20%, versus 30% in overall distribution) [43]. Well-differentiated liposarcomas are similar to lipomas as per their large fat component (even more than 75% of their volume), and fibrous septa may be observed; this is the most represented histologic subtype of liposarcoma. Conversely, myxoid liposarcomas have limited adipose proportion

(usually 10–25% of the tumor volume); therefore, they display overall higher density with further radiological differential. Furthermore, pleomorphic and dedifferentiated liposarcomas are very similar on CT imaging, since they contain little or no fat and it is often impossible to differentiate them from other soft-tissue tumors of the mediastinum [44].

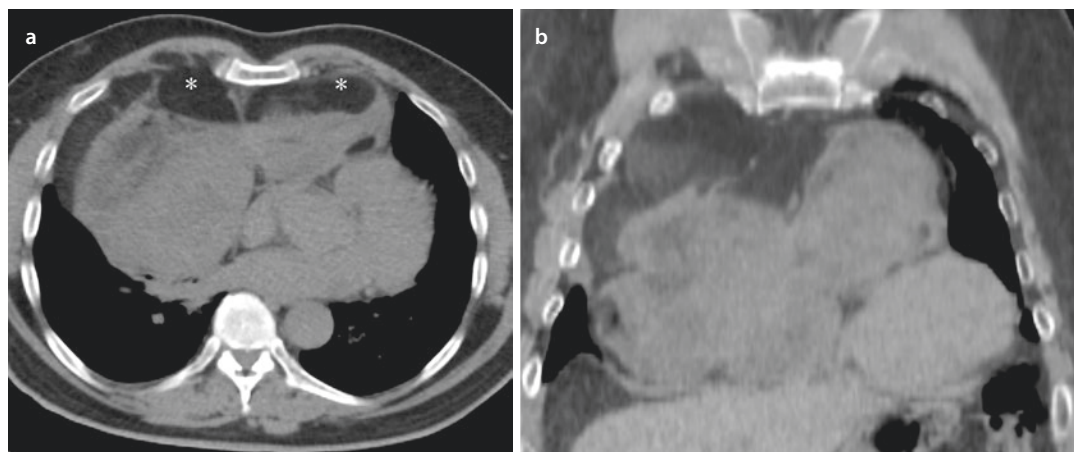
Liposarcomas are usually found in adults, except for a rare morphological variant of pleomorphic liposarcoma with myxoid features, named as “pleomorphic myxoid liposarcoma” that was mostly reported in teenager and young adults. Pleomorphic myxoid liposarcoma is associated with a particularly poor prognosis [43].

Recently, a new subtype named “giant mediastinal liposarcoma” has been proposed. It refers to an abnormally large and rapidly growing mediastinal mass associated with symptoms due to compression of mediastinal structures; surgical approach is preferred when achievable [45, 46].

7.4.2.1 Patterns of Local Spread and Implication to Treatment

The histologic subtype defines prognosis: 70% survival for patients with well-differentiated and dedifferentiated liposarcomas, <50% for myxoid liposarcomas, and about 30% for pleomorphic liposarcomas [43]. The prognosis readably follows the potential of diffusion.

Well-differentiated liposarcoma is quite common with local compression and invasion [47].



► Fig. 7.14 a–b *Liposarcoma of the mediastinum*. a–b Axial a and coronal b non-enhanced CT show well-circumscribed multinodular mass in the anterior

mediastinum, with both adipose (asterisk) and solid component; mediastinal structures are compressed and displaced rather than infiltrated

Tumor size is not a unique determinant of resectability [44], since expansive rather than infiltrative pattern is expected for this neoplasm [42]. Recurrence is rare after complete surgical excision, whereas it is quite common if otherwise clear-margin resection is not achievable [42]. Thereof, tumor location is a prominent prognostic factor of liposarcoma because its close proximity to vital organs favors tumor dissemination by contiguity. The invasion of tumors into adjacent vital structures frequently prevents surgery [44]. Radiology can describe the absence of infiltration (in case of preserved cleavage plane) but is quite weak in defining presence of infiltration because the direct contact between the mass and mediastinal structures (absence of cleavage planes) might be ambiguous [48]. MRI has high accuracy in preoperative planning due to its utmost contrast resolution, which allows definition of the tumor invasion into vessels in the mediastinum and the thoracic inlet [44].

A possible reason for non-radical resection is reported to be the presence of lobules of tumor wrapping around great vessels and main stem bronchi. These lobules can grossly simulate normal adipose tissue and result in substantial challenge in obtaining negative margins [44, 47] (■ Fig. 7.15a–g). Likewise, it might be challenging to assess relapse of liposarcoma after surgical resection with residual disease because quantification of adipose volume around viscera is indeed everything but intuitive by imaging.

Radiation therapy was proposed as an alternative to surgery for controlling local recurrence [42], whereas chemotherapy has limited potential in the primary or secondary treatment of such tumor [49, 50].

7.4.2.2 Lymph Node Involvement and Distal Spread

Dedifferentiated liposarcoma, pleomorphic, and myxoid liposarcoma report a high rate of mortality from metastatic disease. The disease recurrence is more rapid in patients with pleomorphic than dedifferentiated subtype [42].

Even though cytogenetic and molecular genetic alterations overlap between well-differentiated liposarcoma and dedifferentiated liposarcoma [43], the latter shows local recurrences in 40% of cases and distant metastases in up to 20% of cases [51], still less aggressive than pleomorphic subtype.

Nodal metastases are not reported, probably because liposarcoma (like almost all sarcomas) metastasizes through blood vessels rather than lymph node [44]. Indeed, metastasis to the lung, pleura, liver, kidneys, and bone is described.

7.4.3 Other Mesenchymal Tumors

7.4.3.1 Vascular Tumors

Vascular tumors can arise in almost any location, with broad histologic range. Hemangioma is the most common benign vascular neoplasm. Mediastinal hemangioma may occur in the mediastinal soft tissue (frequently in the anterior mediastinum) or in the thymus; both capillary and cavernous hemangioma subtypes have been reported [52]. Signs of compression of vital structures may occur, such as Horner's syndrome, neurological signs, and superior vena cava syndrome. Local recurrence seldom occurs after radical resection [52].

Vascular endothelial tumors of intermediate malignancy may display local invasion, while hematogenous metastases are rare; these include kaposiform hemangioendothelioma (KHE) and composite hemangioendothelioma [53].

Malignant vascular tumors of the mediastinum include epithelioid hemangioendothelioma (EHE) and angiosarcoma (AS). The former is typically resident in the anterior mediastinum where it develops from mediastinal large veins (superior vena cava and anonymous trunk). Major mediastinal veins are also a common site of local invasion. Radical surgical resection grants good survival, depending on the histologic grade [54]. In contrast, AS is mostly symptomatic at the time of diagnosis because it appears with masses up to 10 cm in size and with infiltrative growth pattern. The survival of patients with mediastinal AS is extremely low, likewise AS in other anatomical regions [51].

7.4.3.2 Myogenic Tumors

Leiomyoma arises from the somatic soft tissue of the mediastinum. It is mostly represented in the retroperitoneum, while mediastinal leiomyosarcoma is very rare and occurs in adulthood. Mediastinal onset of leiomyoma is more represented in the posterior mediastinum. Mediastinal leiomyosarcoma usually presents as a nonencapsulated, circumscribed mass. It can spread locally

into the heart, lungs, thoracic vertebrae, and until spinal canal [55–57]. The elective treatment depends on the infiltration of mediastinal structures and can include different combinations of surgical resection, chemotherapy, and/or radiation therapy; still, local recurrence and hematogenous metastasis are very common.

Mediastinal mesenchymal tumors with skeletal muscle differentiation include rhabdomyoma and rhabdomyosarcoma (RMS). Furthermore, rhabdomyosarcoma component can be seen in malignant peripheral nerve sheath tumor (PNST) (Triton tumor) or as a somatic-type malignancy in germ cell tumor.

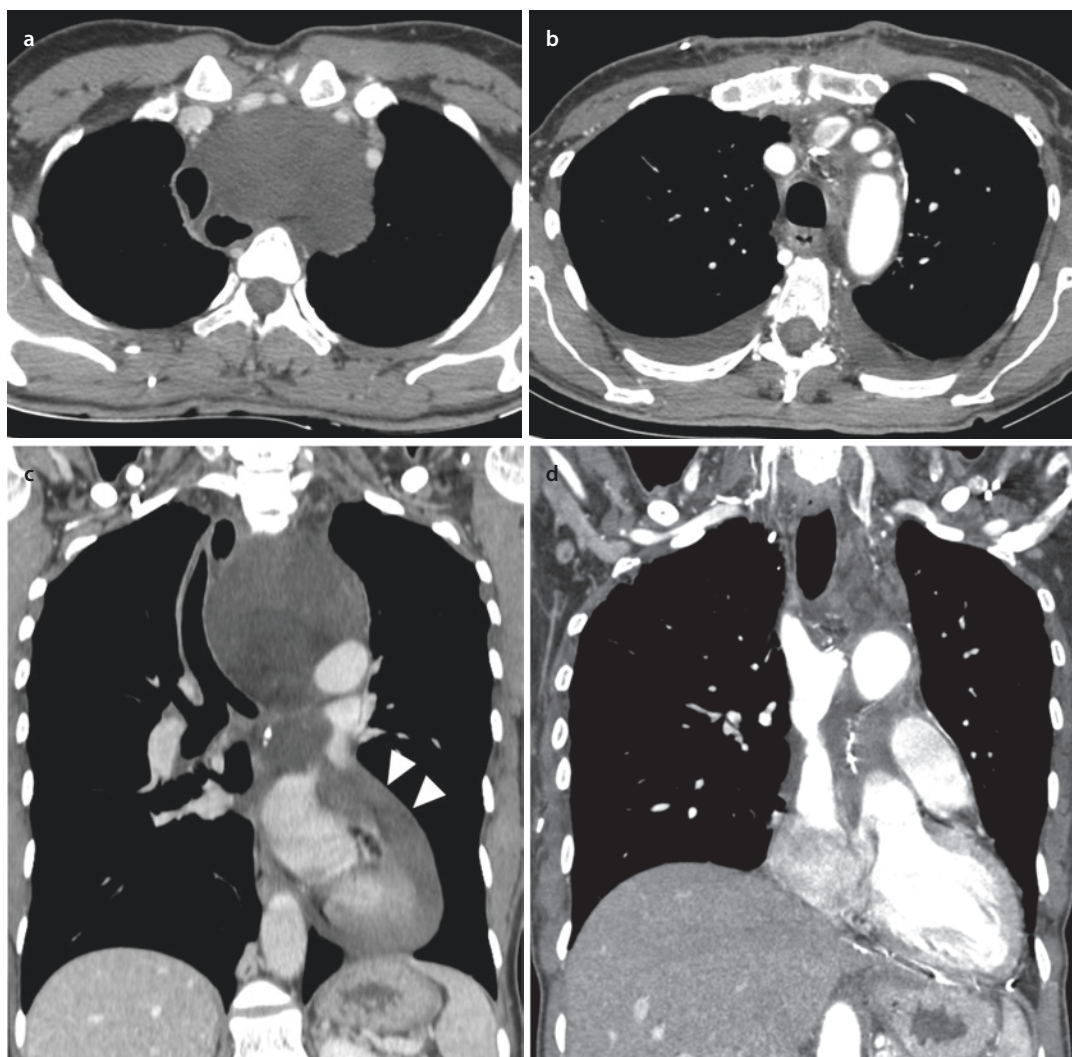
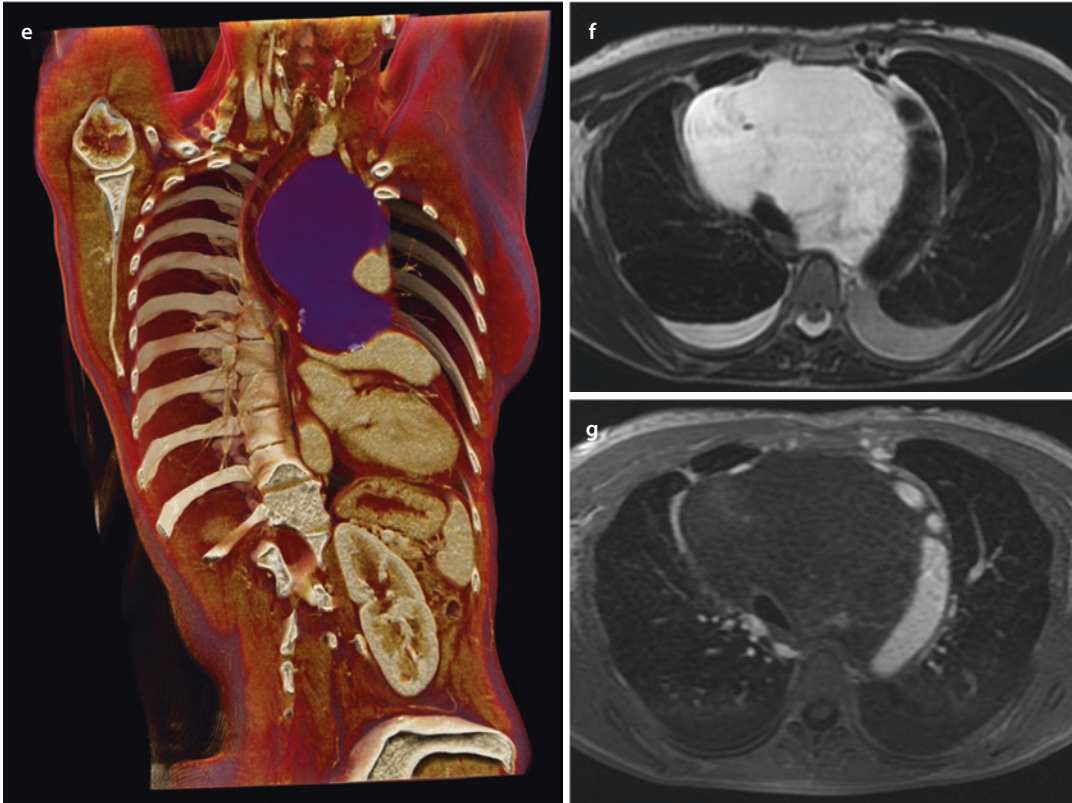


Fig. 7.15 a–g *Liposarcoma of the mediastinum*. a–d Axial a and coronal c contrast-enhanced CT (venous phase) show well-circumscribed mass in the anterior and middle mediastinum, with severe compression (complete leftward displacement of the trachea, anterior displacement of epiaortic trunks, and major veins); sign of pericardial invasion is seen (arrowheads). Axial b and coronal d contrast-enhanced CT (arterial phase) show maintained mediastinal anatomy after surgical resection of the bulky mass and a proportion of residual disease in the site of pericardial infiltration. e Volume rendering

reconstruction of contrast-enhanced CT (venous phase) shows the mass (purple) and its compression onto the trachea with rightward shift. Compression on the pulmonary trunk is noted in the site of pericardial infiltration (see Fig. 7.15b). f–g Axial MRI images in T2-weighted sequence e and T1-weighted high-resolution isotropic volume examination (THRIVE) sequence after contrast agent f show the anterior-middle mediastinum mass with predominantly fat component and without contrast enhancement



■ Fig. 7.15 (continued)

Rhabdomyosarcoma (RMS) is the most common soft-tissue tumor of childhood; indeed, it represents about 50% of pediatric soft-tissue sarcomas; slight male predominance and age less than 6 years represent the most common setting. Mediastinal RMS is seen in the anterior mediastinum; however, primary mediastinal rhabdomyosarcoma is very rare because it is mostly related to germ cell or teratomatous tumors. Subtypes of RMS include embryonal RMS, alveolar RMS, spindle cell/sclerosing RMS, and pleomorphic RMS. Alveolar rhabdomyosarcoma is the most frequently reported subtype in the mediastinum [58, 59]. Mediastinal rhabdomyosarcoma tends to be larger and more locally invasive than RMS in other regions. Thereof, mediastinal RMS is associated with poor prognosis, notably by early local and distant recurrence post resection.

7.4.3.3 Fibroblastic/Myofibroblastic Tumors

Fibroblastic/myofibroblastic tumors typically originate in the skin and superficial soft tissues, while only few cases were reported in the mediastinum.

Solitary fibrous tumor (SFT) is an intrathoracic fibroblastic tumor. It often shows pleural origin/connection; nonetheless, it can also happen without pleural involvement. It may arise in any compartment of the mediastinum. Mediastinal SFT may show more aggressive behavior compared with non-mediastinal SFTs [60]; indeed, it may reach large size and extend to the chest wall and lung by direct invasion [61].

Aggressive fibromatosis (AF) is a rare fibroblastic/myofibroblastic proliferation with local aggressive behavior and without metastatic potential. Mediastinal AF occurs mainly in young patients (median 38 years), and it can be seen in association with surgical scars [62, 63].

Inflammatory myofibroblastic tumor (IMT) is composed of fibroblastic/myofibroblastic cells and a non-neoplastic inflammatory component. Similar to IMTs that occur in other body sites, mediastinal IMT is predominantly a tumor of children and young adults [64]. Variable biological behavior is reported, with common local recurrence.

7.4.3.4 Bone and Cartilaginous Tumors

Primary mediastinal osteosarcoma or chondrosarcoma can originate from bone structures, chest wall soft-tissue, and tracheobronchial structures.

About 10 cases of primary extraskeletal mediastinal osteosarcoma and 10 cases of chondrosarcoma have been reported, occurring in all compartments of the mediastinum. Masses were up to 15 cm in size and were variably well-encapsulated. Ewing sarcoma (ES) may occur in 20% of cases as extraskeletal tumor, and it can locate in various soft-tissue sites as well as in parenchymal organs. Less than 20 cases of extraskeletal ES have been reported in the mediastinum, occurring in all mediastinal compartments [65].

7.4.3.5 Synovial Sarcoma

Synovial sarcoma (SS) represents about 5–10% of all soft-tissue sarcomas, mainly arising in the extremities of young adults. It is not related to normal synovium, and a derivation from pluripotent mesenchymal cells with epithelial differentiation has been proposed [66–70]. In fact, any site can be involved with SS and 10–20% of SS arise out of limbs [71]. A total of 55 cases of mediastinal SS were reported by two series [72, 73].

Mediastinal SS, in contrast to other sites, tends to present with larger size within all the mediastinum compartment. Pericardial invasion is relatively common and variably associated with effusions on imaging [72].

Histologic subtypes of SS encompass monophasic (spindle cells only or occasionally epithelial component only) and biphasic subtypes (spindle-shaped cells and epithelial differentiation) and a poorly differentiated variant of synovial sarcoma [74, 75]. All mediastinal compartments can be involved by SS.

On imaging, SS may display well-circumscribed mass or even ill-defined tumor mass with infiltrative growth pattern (■ Fig. 7.16a–d). Invasion of hilar structures, great vessels, and the esophagus, pleura, lung, heart, and chest wall is seen (■ Fig. 7.16e–g) with accompaniment from signs of necrotic, hemorrhagic, or cystic evolution within the primary mass and its components. Focal calcifications may be observed. SS in the posterior mediastinum can display local infiltration of ribs and vertebrae. Tumor up to 20 cm in size is reported [73], in contrast to 5–7 cm median size in studies of

SS in the extremities [76–78]: this is probably related to mediastinal location that allows tumors to grow before the symptom onset (e.g., chest pain, shortness of breath, dyspnea). In fact, a significant proportion of reported cases presented with advanced and unresectable disease.

Size of SS (in any site) is reported as the most important factor of survival. Patients with SS <5 cm had a survival at 10 years of 88%, which dropped to 38% for 5–10 cm and 8% for >10 cm [79]. A complete resection of these tumors is the only identified prognostic factor of improved survival. Location within the mediastinum, pericardial effusion, and histologic subtype showed no influence on survival [72]. Resection is the main therapeutic strategy, sometimes as a part of multimodality treatment including adjuvant radiotherapy. SS is frequently high responsive to radiation therapy and chemotherapy. Adequate adjuvant response may improve outcome after resection with positive histologic margins [80]. In addition, neoadjuvant chemotherapy has been used to reduce tumor size and reach surgical feasibility and the rate of radical resection [81].

Lymphatic and hematogenous dissemination was demonstrated by histology in the hilar lymph node, lung, liver, and epidural space [73].

7.5 Neurogenic Tumors

7.5.1 Overview

Neurogenic tumors arise from tissues of the neural crest, including cells of the peripheral, autonomic, and paraganglionic nervous systems. Neurogenic tumors are classified among soft-tissue tumors of the mediastinum in the fourth edition of the *WHO Classification of Tumors of the Lung, Pleura, Thymus and Heart* (a summary of the main neurogenic tumors is provided in ■ Table 7.2). They are among the most common masses in the posterior/paravertebral compartment. Neurogenic tumors account for 20% of mediastinal tumors in adulthood and 35% in pediatric patients [16, 82]. According to their origin, they have highly variable behavior, either regressing spontaneously or proliferating towards malignant disease.

Nerve sheath tumors usually occur in adults and are benign in most cases. Otherwise, sympathetic ganglia tumors are much more common in children and often show an aggressive behavior

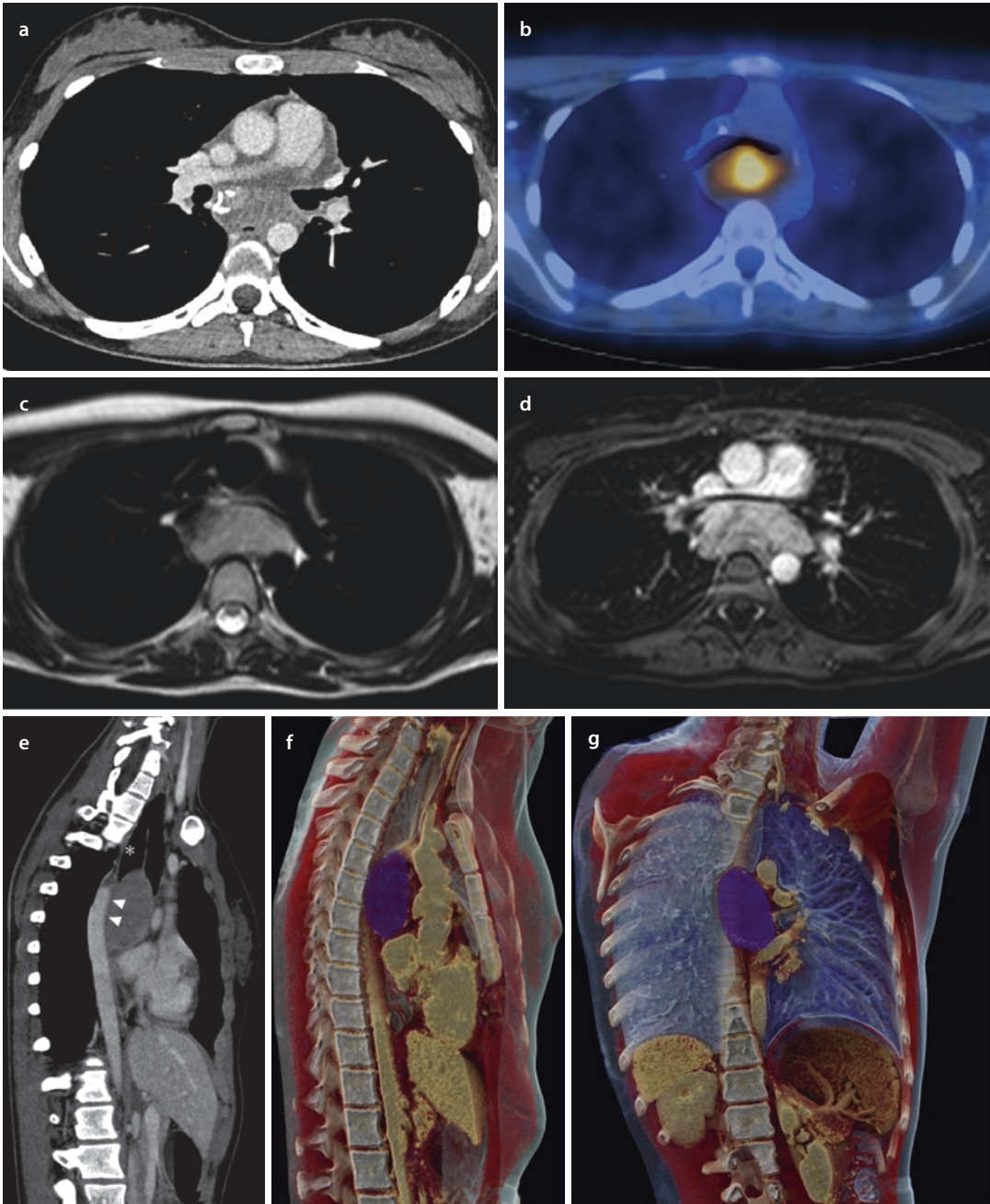


Fig. 7.16 a–f *Synovial sarcoma of the mediastinum.* a–d Axial contrast-enhanced CT (a – venous phase), axial 18-FDG-PET b, axial MRI images in T2-weighted sequence c, and T1-weighted high-resolution isotropic volume examination (THRIVE) sequence after contrast agent d show a solid well-circumscribed mass in the posterior mediastinum with coarse calcification, high metabolic activity, and contrast enhancement. e–g Oblique reformatted of contrast-enhanced CT

(c – venous phase) shows signs of esophageal infiltration as depicted by dilation of the proximal esophagus (asterisk) and abrupt interruption of its lumen; signs of compression of the descending aorta are seen (arrowheads) with thickening of the vessel wall suggesting some degree of aortic infiltration by direct invasion. Volume rendering reconstruction of contrast-enhanced CT (venous phase)

[83]. Most neurogenic mediastinal tumors are asymptomatic, and indeed, they happen to be diagnosed incidentally during radiological examinations. Occasionally, they can present with chest

pain, cough, and hoarseness from compression of mediastinal structures. Neurological symptoms are also described in association with the tumor origin [3]. Prognosis and treatment depend on the specific subtype. Surgery is the overall preferred treatment for localized mass.

Table 7.2 Mediastinal neurogenic tumors

Derivation	Type
Peripheral nerve sheath tumors	Schwannoma
	Cellular schwannoma
	Melanotic schwannoma
	Plexiform schwannoma
	Neurofibroma
	Malignant peripheral nerve sheath tumors
Sympathetic ganglia tumors	Ganglioneuroma
	Ganglioneuroblastoma
	Neuroblastoma
Parasympathetic ganglia tumors	Chemodectoma
	Paraganglioma

7.5.1.1 Peripheral Nerve Sheath Tumors

Peripheral nerve sheath tumors (PNSTs) are a heterogeneous group of benign and malignant neoplasms; they mostly arise from spinal or proximal intercostal nerves. Unusual locations of primary PNSTs are the vagus, recurrent laryngeal, and phrenic nerves [82].

Neurofibromas and schwannomas originate from the Schwann cell. The presence of intratumor nerve fibers is hallmark of neurofibromas in the differential. They are usually asymptomatic and affect patients of young and middle ages (20–50 years of age) [84]. Schwannoma is the most common subtype among PNSTs of the posterior mediastinum, and it is classified into conventional, cellular, melanotic, and plexiform subtypes. They are mostly solid, lobulated, and encapsulated masses (■ Fig. 7.17a–e). Solitary lesions are often sporadic

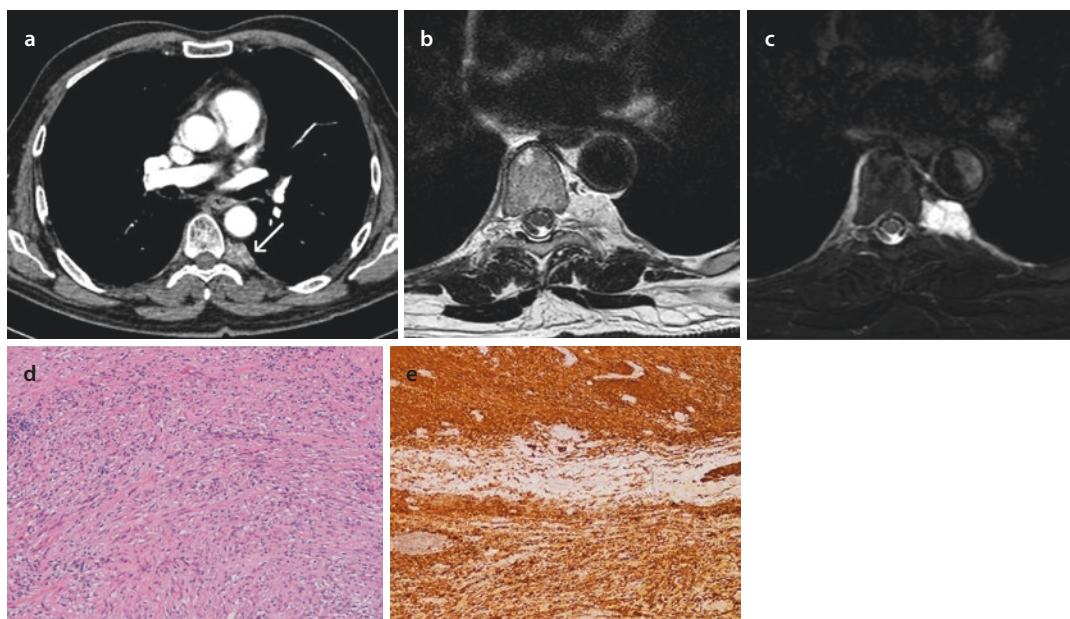


Fig. 7.17 a–e Schwannoma. a–c Axial contrast-enhanced CT (a – arterial phase) shows left paraspinal oval finding with early and intense contrast enhancement after injection iodinated contrast agent. Axial MRI images in T2-weighted sequence b and short tau inversion

recovery (STIR) sequence c show the hyperintense signal and the tight contact with the nerve root. d, e Hematoxylin-eosin staining of the histologic specimen (d – 20x) shows a large number of well-differentiated spindle cells with strongly positivity for S-100 protein e

and infrequently become malignant. The other variants, especially if in multiple forms, may be associated with neurofibromatosis (NF) and carry a higher risk of malignancy [85].

Malignant peripheral nerve sheath tumors (MPNSTs) are spindle cell sarcomas with a recurrent origin from a precursor neurofibroma. Almost half of MPNSTs is associated with NF1, which is one of the most common cancer genetic predisposition syndromes [82]. They mostly occur in middle-aged patients. Symptoms as pain and neurological deficit are usually caused by nerve compression [3]. Some variants may show divergent epithelioid, glandular, or mesenchymal differentiation. Components of skeletal muscle cell (rhabdomyosarcoma) are also reported into the so-called Triton tumor [85]. Likewise the other mediastinal PNSTs, the malignant ones are typically located in the posterior mediastinum, although they may be seen also in the anterior mediastinum [65]. MPNSTs are usually large masses that often show hemorrhage and necrosis [82]. Unlike their benign counterpart, they are clinically aggressive and yield poor prognosis, mostly due to large tumor size and consequent incomplete resection, as well as to the frequent association with NF [41].

7.5.1.2 Sympathetic Ganglia Tumors

Tumors arising from sympathetic ganglia of the posterior mediastinum encompass benign ganglioneuroma (GN), malignant ganglioneuroblastoma (GNB), and aggressive malignant neuroblastoma (NB), and they mainly occur in pediatric population [41].

GN is fully differentiated tumors with own capsule, usually composed of one or multiple large ganglion cells without immature neuroblastic component [3]. It may arise as sporadic neoplasm; nonetheless, they are also reported after chemotherapy. These tumors are usually asymptomatic at presentation, unless local compression or intraspinal growth. Occasionally, flashing or palpitations may occur due to tumoral secretion of catecholamines. The outcome is generally excellent [86].

GNB is composed by ganglion cells with intermediate degree of maturation and may show histologic features of both the other sympathetic ganglia tumors. These lesions frequently occur in infants, while the presentation in adults is seldom. Although they can be asymptomatic at diagnosis, clinical manifestation associated with large tumor size is quite common [3]. GNB often

produces catecholamine, although symptoms derived from their excess are rare. Staging of the disease is similar to that for NB. The outcome mostly depends on the location as well as the age at presentation; confined disease and very young age at the time of diagnosis are indeed positive prognostic factors [86].

NB represents the most common extracranial solid malignancy in pediatric patients. It is composed by immature, undifferentiated sympathetic cells and appears as a nonencapsulated mass with varying degree of necrosis, hemorrhage, and cystic degeneration [86]. After the abdomen, the posterior mediastinum is the most common site of disease. Noteworthy, primary mediastinal NBs show a low grade of malignancy compared with all the other sites [87]. Clinical features range from systemic symptoms (e.g., malaise and weight loss) to symptoms associated with local invasion (e.g., chest pain, cough, dysphagia). The compression of tumor upon mediastinal structures can result in the Horner's syndrome. More specific manifestations are neurological deficiency, paralysis, and ataxia. Hypertension, flushing, and diarrhea can happen in association with vasoactive amine secretion [3]. Metastatic symptoms as osseous pain or Hutchinson syndrome are seen in more than 50% of patients at the time of diagnosis. There are multiple staging systems for NB, among which the International Neuroblastoma Staging System (INSS) is largely the most used. The INSS is based on clinical, radiological, and surgical features (■ Table 7.3). Because the INSS is not suitable for the pretreatment risk classification in cases of localized disease, in 2009, the International Neuroblastoma Risk Group (INRG) Project proposed a new staging system for tumor staging before any treatment (■ Tables 7.4 and 7.5) [88]. The disease stage is the main predictor of prognosis; further, negative prognostic factors are poor differentiation and older age at presentation [86].

7.5.1.3 Parasympathetic Ganglia Tumors

Mediastinal paraganglionic tumors include non-secreting chemodectoma in the anterior mediastinum and functioning paraganglioma in the posterior mediastinum.

Chemodectoma arises from the aortopulmonary paraganglia in the prevascular mediastinum, and they selectively occur in adults. Chemodectoma is often asymptomatic; still, large mass is associated

Table 7.3 International Neuroblastoma Staging System

1	Localized tumor with complete gross excision, with or without microscopic residual disease; representative ipsilateral lymph nodes negative for tumor microscopically. Nodes attached to and removed with the primary tumor may be positive
2A	Localized tumor with incomplete gross excision; representative ipsilateral non-adherent lymph nodes negative for tumor microscopically
2B	Localized tumor with or without complete gross excision, with ipsilateral non-adherent lymph nodes positive for tumor; enlarged contralateral lymph nodes negative microscopically
3	Unresectable unilateral tumor infiltrating across the midline (beyond the opposite side of the vertebral column) with or without regional lymph node involvement or midline tumor with bilateral extension via infiltration (unresectable) or lymph node involvement
4	Any primary tumor with dissemination to distant lymph nodes, bone, bone marrow, liver, skin, and/or other organs (except for stage 4S)
4S	Localized primary tumor (stages 1, 2A, 2B) with dissemination limited to the skin, liver and /or bone marrow (limited to infants younger than 1 year, marrow involvement of less 10% of total nucleated cells, and MIBG scan findings negative in the marrow)

Table 7.4 International Neuroblastoma Risk Group tumor stage [88]

L1	Localized tumor not involving vital structures (defined by the list of IDRFs) and confined to one body compartment
L2	Local-regional tumor with one or more IDRFs
M	Distant metastatic disease (except stage MS)
MS	Metastatic disease confined to the skin, liver and/or bone marrow in children younger than 18 months

IDRFs image-defined risk factors (see [Table 7.4](#))

Table 7.5 Image-defined risk factors

Multiple body compartments	Ipsilateral tumor extension within two body compartments
Neck	Tumor encasing the carotid artery, vertebral artery, and/or internal jugular vein Tumor extending to the skull base Tumor compressing the trachea
Cervicothoracic junction	Tumor encasing brachial plexus roots Tumor encasing the subclavian vessels, vertebral artery, and/or carotid artery Tumor compressing the trachea
Thorax	Tumor encasing the aorta and/or major branches Tumor compressing the trachea and/or principal bronchi Lower mediastinal tumor infiltrating costovertebral junction between T9 and T12 vertebral levels
Thoracoabdominal junction	Tumor encasing the aorta and/or vena cava
Abdominal and pelvis	Tumor infiltrating the porta hepatis and/or hepatoduodenal ligament Tumor encasing branches of the superior mesenteric artery at the mesenteric root Tumor encasing origin of the celiac axis and/or origin of the superior mesenteric artery Tumor invading one or both renal pedicles Tumor encasing the aorta and/or vena cava Tumor encasing iliac vessels Pelvic tumor crossing the sciatic notch
Intraspinal tumor extension	Intraspinal tumor extension (whatever the location) provided that more than one-third of the spinal canal in axial plane is invaded, the perimedullary leptomeningeal spaces are not visible, or the spinal cord signal intensity is abnormal
Infiltration of adjacent organs and structures	The pericardium, diaphragm, kidney, liver, duodenopancreatic block, and mesentery

with symptoms determined by compression of mediastinal structures [65].

Paraganglioma (aka extra-adrenal pheochromocytoma) originates along the sympathetic chain in the posterior mediastinum [82]. They occur in younger patients and may be associated with multiple endocrine neoplasia (MEN), Carney's triad, or von Hippel-Lindau disease. As biologically active tumors, they can cause signs and symptoms related to catecholaminergic activity: flushing, headache, anxiety, and hypertension [87]. Paraganglion tumors are solid and partially encapsulated masses that may have internal necrosis and hemorrhage. The outcome is mostly related to the tumor site and is worse for neoplasm located in the anterior mediastinum because invasion of vital organs is more likely [41].

7.5.2 Patterns of Local Spread and Implication to Treatment

7.5.2.1 Peripheral Nerve Sheath Tumors

Neurofibroma and schwannoma are slow-growing masses with a benign behavior. Despite some pathological differences between these entities, both tumors appear as sharply outlined lesions of soft-tissue density with possible split fat sign [85]. Schwannoma has a fusiform shape and an eccentric location close to the involved nerve. Conversely, neurofibroma tends to grow with infiltration between the nerve fascicles; still, it mostly maintains discrete margins. When presenting as single lesion, they frequently do not show signs of invasion; nonetheless, they may cause compression over bony structures with consequent erosion of adjacent ribs or vertebrae [87]. Complete resection of the mass is often curative; noteworthy, combined approach by thoracic surgeon and neurosurgeon can be required for the best surgical outcome, including radical resection and averting neurological damage.

MPNSTs are aggressive tumors characterized by rapid growth, developing along the nerve. They grow from the nerve bundle into ellipsoid mass with ill-defined borders. Their rugged growth can cause destruction of nearby mediastinal structures as well as invasion of pleural sheets, up to invasion of extra-mediastinal compartments [87]. MPNSTs are usually low attenuating on CT and typically hyperintense on T2-weighted images, although

the MRI appearance can be heterogeneous depending on the proportion of cystic component, hemorrhage, and necrosis [89]. Furthermore, peripheral enhanced pattern and perilesional edema-like zone are more specific MRI features pointing at diagnosis of MPNSTs. The patient management depends on the possibility to obtain a complete resection. Neoadjuvant therapy is proposed in case of unresectable mass [87].

7.5.2.2 Sympathetic Ganglia Tumors

From a radiological point of view, the characterization of primary neuroblastic tumors is obtained by complementary contribution of both CT and MRI. First, the CT is useful to define the origin, morphology, and extent of tumor, while MRI is preferred to estimate intraspinal extension of the mass [3]. CT is not specific, and the appearance of the tumor can vary from solid homogeneous to more heterogeneous mass for the presence of necrosis and hemorrhage. Nonetheless, CT is pivotal for detection of intralesional calcification. Furthermore, MRI by diffusion-weighted imaging (DWI) shows lower ADC values in poorly differentiated and undifferentiated neuroblastic tumors compared with mature and differentiated subtypes [90].

The benign pattern of growth of GN displays slow-growing and relatively homogeneous mass without signs of invasion, compared with GNB and NB. Despite its benign biological behavior, the mass compression onto adjacent structures may cause rib or vertebral (notably foraminal) erosion [86]. The lesion is hypodense relative to muscle on unenhanced CT, with mild enhancement on contrast-enhanced CT; a heterogeneous intermediate signal on all MRI sequences is generally seen [87].

Conversely, the potential range of malignancy of GNB renders either homogeneous and circumscribed mass or poorly marginated mass largely composed of immature cells with necrotic or hemorrhagic foci [87]. When neuroblastic tissue predominates in the composition of the tumor, GNB shows imaging features comparable to NB, the utmost malignant variety of sympathetic ganglia tumor (■ Fig. 7.18). Indeed, GNB and NB can share diffusion pathway and imaging features as well as implication to treatment. They may display mass effect on mediastinal structures as well as show signs of local invasion. Invasion of the bony structures of the posterior mediastinal compartment and pedicles erosion are quite common features deriv-

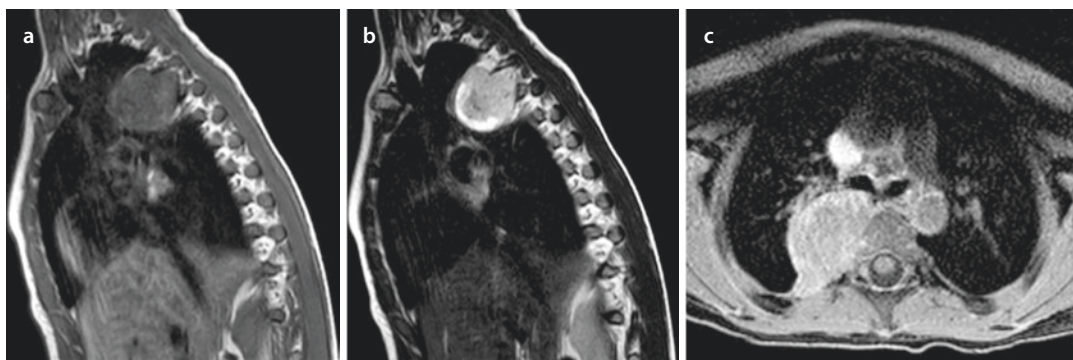


Fig. 7.18 a–c Neuroblastoma with borderline pattern like Ganglioneuroblastoma “intermixed” type. a–c Sagittal T1-weighted sequence a, sagittal T2-weighted sequence b, and axial T1-weighted high-resolution isotropic volume

examination (THRIVE) sequence after contrast agent c show right paraspinal mass with relatively hypointense signal in T2-weighted sequence suggesting high cellularity of the lesion; high contrast enhancement is noted

ing from intraspinal growth of both GNB and NB [86]. A lower mediastinal tumor can easily infiltrate also the costovertebral junctions, in particular between the T9 and T12 vertebral level. Moreover, encasement of the great mediastinal vessels, both the descending aorta and pulmonary pedicles, and compression of trachea and major bronchi are life-threatening findings in the natural evolution of such neoplasms [88]. Treatment is related to the stage of disease and ranges from surgery alone to combination of surgery and chemotherapy.

7.5.2.3 Parasympathetic Ganglia Tumors

Paraganglionic tumors can arise from any of the three mediastinal compartments and may be associated to an aggressive behavior in up to 15% of cases [91]. They show rich vascularization which is reflected by contrast enhancement on both CT and MRI. Moreover, low attenuation areas on CT scan can be seen in case of necrosis and hemorrhage [87]. Paraganglionic tumors usually display indolent development; hence, complete resection is the treatment of choice. Noteworthy, catecholamine blockage is needed before surgical resection of functioning tumors.

7.5.3 Lymph Node Involvement and Distal Spread

Peripheral nerve sheath tumors – MPNSTs have a high metastatic potential. Likewise high-grade sarcomas, hematogenous dissemination of MPNSTs commonly harbors in the lung and bone [92].

Although adjuvant radiation therapy and chemotherapy do not improve survival rates, they are usually performed in case of metastatic disease [41].

Sympathetic ganglia tumors – Few case reports of metastatic GN have been described in the literature; still, it has been hypothesized that they might be referred to metastases of NB, or GNB eventually matured to GN [86].

GNB has metastatic potential, however no standard diffusion pathway because it strongly depends on the histologic grading and mitosis index.

NB seldom disseminates via lymph node chain. When lymph node involvement is seen in NB, it is usually limited to local lymphatic stations [88]. Primary site of hematogenous metastasis from NB are the bone marrow and bone [93]. When NB comes to bone marrow involvement, two different patterns of invasion are described: the nodular and the diffuse one. The latter is often-times associated with cortical metastases, and a consequent worse prognosis follows. Furthermore, liver and skin metastases are common findings of hematogenous dissemination in NB, especially in infants. Liver involvement may be nodular or diffuse; in particular, massive liver neoplastic involvement with hepatomegaly is referred to as “Pepper syndrome” [86]. Lung and pleural metastases are rare, without distinctive pattern on CT. Similarly, metastatic diffusion to the brain and meninges is very unusual; indeed, such location is not routinely screened at diagnosis but rather evaluated in case of specific symptoms [88]. Nonetheless, hematogenous spread of NB can involve any organ, although extremely rare.

References

- Carter BW, Tomiyama N, Bhora FY, Rosado de Christenson ML, Nakajima J, Boiselle PM, Detterbeck FC, Marom EM. A modern definition of mediastinal compartments. *J Thorac Oncol*. 2014;9:S97–101.
- Juanpere S, Cañete N, Ortuño P, Martínez S, Sanchez G, Bernado L. A diagnostic approach to the mediastinal masses. *Insights Imaging*. 2013;4:29–32.
- Duwe BV, Sterman DH, Musani AI. Tumors of the mediastinum. *Chest*. 2005;128:2893–909.
- Hodgkin Lymphoma – Cancer Stat Facts. In: SEER. <https://seer.cancer.gov/statfacts/html/hodg.html>. Accessed 29 Mar 2019.
- Campo E, Swerdlow SH, Harris NL, Pileri S, Stein H, Jaffe ES. The 2008 WHO classification of lymphoid neoplasms and beyond: evolving concepts and practical applications. *Blood*. 2011;117:5019–32.
- Lister TA, Crowther D, Sutcliffe SB, Glatstein E, Canellos GP, Young RC, Rosenberg SA, Coltman CA, Tubiana M. Report of a committee convened to discuss the evaluation and staging of patients with Hodgkin's disease: Cotswolds meeting. *J Clin Oncol*. 1989;7:1630–6.
- Piña-Oviedo S, Moran CA. Primary mediastinal classical Hodgkin lymphoma. *Adv Anat Pathol*. 2016;23:285–309.
- Kumar A, Burger IA, Zhang Z, et al. Definition of bulky disease in early stage Hodgkin lymphoma in computed tomography era: prognostic significance of measurements in the coronal and transverse planes. *Haematologica*. 2016;101:1237–43.
- Marks LJ, McCarten KM, Pei Q, Friedman DL, Schwartz CL, Kelly KM. Pericardial effusion in Hodgkin lymphoma: a report from the Children's Oncology Group AHOD0031 protocol. *Blood*. 2018;132:1208–11.
- Chiles C, Woodard PK, Gutierrez FR, Link KM. Metastatic involvement of the heart and pericardium: CT and MR imaging. *Radiographics*. 2001;21:439–49.
- Gharbaran R, Park J, Kim C, Goy A, Suh KS. Circulating tumor cells in Hodgkin's lymphoma – a review of the spread of HL tumor cells or their putative precursors by lymphatic and hematogenous means, and their prognostic significance. *Crit Rev Oncol Hematol*. 2014;89:404–17.
- Castellino RA, Blank N, Hoppe RT, Cho C. Hodgkin disease: contributions of chest CT in the initial staging evaluation. *Radiology*. 1986;160:603–5.
- Takahashi K, Al-Janabi NJ. Computed tomography and magnetic resonance imaging of mediastinal tumors. *J Magn Reson Imaging*. 2010;32:1325–39.
- Bouroncle BA. Sternberg-Reed cells in the peripheral blood of patients with Hodgkin's disease. *Blood*. 1966;27:544–56.
- Non-Hodgkin Lymphoma – Cancer Stat Facts. In: SEER. <https://seer.cancer.gov/statfacts/html/nhl.html>. Accessed 29 Mar 2019.
- Marx A, Chan JKC, Coindre J-M, et al. The 2015 World Health Organization classification of tumors of the thymus: continuity and changes. *J Thorac Oncol*. 2015;10:1383–95.
- Martelli M, Ferreri A, Di Rocco A, Ansuinelli M, Johnson PWM. Primary mediastinal large B-cell lymphoma. *Crit Rev Oncol Hematol*. 2017;113:318–27.
- Pfreundschuh M, Kuhnt E, Trümper L, et al. CHOP-like chemotherapy with or without rituximab in young patients with good-prognosis diffuse large-B-cell lymphoma: 6-year results of an open-label randomised study of the MabThera International Trial (MInT) Group. *Lancet Oncol*. 2011;12:1013–22.
- You MJ, Medeiros LJ, Hsi ED. T-lymphoblastic leukemia/lymphoma. *Am J Clin Pathol*. 2015;144:411–22.
- Cortelazzo S, Ferreri A, Hoelzer D, Ponzoni M. Lymphoblastic lymphoma. *Crit Rev Oncol Hematol*. 2017;113:304–17.
- Tateishi U, Müller NL, Johkoh T, Onishi Y, Arai Y, Satake M, Matsuno Y, Tobinai K. Primary mediastinal lymphoma: characteristic features of the various histological subtypes on CT. *J Comput Assist Tomogr*. 2004;28:782–9.
- Albany C, Einhorn LH. Extragenital germ cell tumors. *Curr Opin Oncol*. 2013;1.
- Stang A, Trabert B, Wentzensen N, Cook MB, Rusner C, Oosterhuis JW, McGlynn KA. Gonadal and extragonadal germ cell tumours in the United States, 1973–2007. *Int J Androl*. 2012;35:616–25.
- McKenney JK, Heerema-McKenney A, Rouse RV. Extragenital germ cell tumors: a review with emphasis on pathologic features, clinical prognostic variables, and differential diagnostic considerations. *Adv Anat Pathol*. 2007;14:69–92.
- Takeda S-I, Miyoshi S, Akashi A, Ohta M, Minami M, Okumura M, Masaoka A, Matsuda H. Clinical spectrum of primary mediastinal tumors: a comparison of adult and pediatric populations at a single Japanese institution. *J Surg Oncol*. 2003;83:24–30.
- Moran CA, Suster S. Primary germ cell tumors of the mediastinum: I. analysis of 322 cases with special emphasis on teratomatous lesions and a proposal for histopathologic classification and clinical staging. *Cancer*. 1997;80:681–90.
- Williamson SR, Ulbright TM. Germ cell tumors of the mediastinum. In: *Marchevsky AM, Wick MR, Marchevsky AM, Wick MR, editors. Pathology of the mediastinum*. Cambridge: Cambridge University Press; 2014. p. 146–68.
- Kim HJ, Kim HR. Naturally occurring mediastinal teratoma with malignant transformation in an adult male. *Korean J Thorac Cardiovasc Surg*. 2013;46:305–8.
- Moran CA, Suster S, Koss MN. Primary germ cell tumors of the mediastinum: III. Yolk sac tumor, embryonal carcinoma, choriocarcinoma, and combined nonteratomatous germ cell tumors of the mediastinum – a clinicopathologic and immunohistochemical study of 64 cases. *Cancer*. 1997;80:699–707.
- Moran CA, Suster S, Przygodzki RM, Koss MN. Primary germ cell tumors of the mediastinum: II. Mediastinal seminomas – a clinicopathologic and immunohistochemical study of 120 cases. *Cancer*. 1997;80:691–8.
- Takeda S-I, Miyoshi S, Ohta M, Minami M, Masaoka A, Matsuda H. Primary germ cell tumors in the mediastinum: a 50-year experience at a single Japanese institution. *Cancer*. 2003;97:367–76.

32. World Health Organization, International Agency for Research on Cancer, International Academy of Pathology. Pathology and genetics of tumours of the lung, pleura, thymus and heart. IARC Press; 2004. [https://www.jto.org/article/S1556-0864\(15\)33571-1/fulltext](https://www.jto.org/article/S1556-0864(15)33571-1/fulltext).
33. Fizazi K, Culine S, Droz JP, Kramar A, Théodore C, Ruffié P, Le Chevalier T. Primary mediastinal nonseminomatous germ cell tumors: results of modern therapy including cisplatin-based chemotherapy. *J Clin Oncol*. 1998;16:725–32.
34. Bokemeyer C, Nichols CR, Droz J-P, et al. Extragonadal germ cell tumors of the mediastinum and retroperitoneum: results from an international analysis. *J Clin Oncol*. 2002;20:1864–73.
35. Malagón HD, Valdez AMC, Moran CA, Suster S. Germ cell tumors with sarcomatous components: a clinicopathologic and immunohistochemical study of 46 cases. *Am J Surg Pathol*. 2007;31:1356–62.
36. Dubashi B, Cyriac S, Tenali SG. Clinicopathological analysis and outcome of primary mediastinal malignancies – a report of 91 cases from a single institute. *Ann Thorac Med*. 2009;4:140–2.
37. Eimoto T, Kitaoka M, Ogawa H, Niwa H, Murase T, Tateyama H, Inagaki H, Soji T, Wang HJ. Thymic sarcomatoid carcinoma with skeletal muscle differentiation: report of two cases, one with cytogenetic analysis. *Histopathology*. 2002;40:46–57.
38. Okudela K, Nakamura N, Sano J, Ito T, Kitamura H. Thymic carcinosarcoma consisting of squamous cell carcinomatous and embryonal rhabdomyosarcomatous components. Report of a case and review of the literature. *Pathol Res Pract*. 2001;197:205–10.
39. Suster S, Moran CA, Chan JKC. Thymoma with pseudo-sarcomatous stroma: report of an unusual histologic variant of thymic epithelial neoplasm that may simulate carcinosarcoma. *Am J Surg Pathol*. 1997;21:1316–23.
40. den Bakker MA, Marx A, Mukai K, Ströbel P. Mesenchymal tumours of the mediastinum – part I. *Virchows Arch*. 2015;467:487–500.
41. Macchiarini P, Ostertag H. Uncommon primary mediastinal tumours. *Lancet Oncol*. 2004;5:107–18.
42. Hahn HP, Fletcher CDM. Primary mediastinal liposarcoma: clinicopathologic analysis of 24 cases. *Am J Surg Pathol*. 2007;31:1868–74.
43. Boland JM, Colby TV, Folpe AL. Liposarcomas of the mediastinum and thorax: a clinicopathologic and molecular cytogenetic study of 24 cases, emphasizing unusual and diverse histologic features. *Am J Surg Pathol*. 2012;36:1395–403.
44. Chen M, Yang J, Zhu L, Zhou C, Zhao H. Primary intrathoracic liposarcoma: a clinicopathologic study and prognostic analysis of 23 cases. *J Cardiothorac Surg*. 2014;9:119.
45. Nguyen DC, Olatubosun O, Yu W, Loor G, Burt BM. Giant mediastinal liposarcoma: a rare yet distinct clinical entity. *Ann Thorac Surg*. 2018;106:e117–9.
46. Galli A, Giordano L, Muriana P, Bandiera A, Negri G, Zannini P, Bussi M. Multidisciplinary management of a giant cervico-mediastinal liposarcoma: a case report and literature review. *Ear Nose Throat J*. 2017;96:E10–3.
47. Ortega P, Suster D, Falconieri G, Zambrano E, Moran CA, Morrison C, Suster S. Liposarcomas of the posterior mediastinum: clinicopathologic study of 18 cases. *Mod Pathol*. 2015;28:721–31.
48. Eisenhuber E, Herold C. Imaging of diseases of the chest, 3rd Edn. By P. Armstrong, A. G. Wilson, P. Dee and D. M. Hansell. Mosby, London, 2000. Price: £50. *Clin Radiol*. 2002;57:A1.
49. Mikkilineni RS, Bhat S, Cheng AW, Prevosti LG. Liposarcoma of the posterior mediastinum in a child. *Chest*. 1994;106:1288–9.
50. Hirai S, Hamanaka Y, Mitsui N, Uegami S, Matsuura Y. Surgical resection of primary liposarcoma of the anterior mediastinum. *Ann Thorac Cardiovasc Surg*. 2008;14:38–41.
51. Fletcher CDM. WHO classification of tumours of soft tissue and bone. World Health Organization; 2013. <https://apps.who.int/bookorders/anglais/detart1.jsp?codlan=1&codcol=70&codcch=4005>.
52. Cohen AJ, Sbaschnig RJ, Hochholzer L, Lough FC, Albus RA. Mediastinal hemangiomas. *Ann Thorac Surg*. 1987;43:656–9.
53. Cakir E, Demirag F, Gulhan E, Oz G, Tastepez I. Mediastinal composite hemangioendothelioma. A rare tumor at an unusual location. *Tumori*. 2009;95:98–100.
54. Anderson T, Zhang L, Hameed M, Rusch V, Travis WD, Antonescu CR. Thoracic epithelioid malignant vascular tumors: a clinicopathologic study of 52 cases with emphasis on pathologic grading and molecular studies of WWTR1-CAMTA1 fusions. *Am J Surg Pathol*. 2015;39:132–9.
55. D'Aiuto M, Veronesi G, Pompilio G, Gasparri R, Presicci F, Galetta D, Biglioli P, Spaggiari L. Extended right pneumonectomy with partial left atrial resection for primary leiomyosarcoma of the mediastinum. *J Thorac Cardiovasc Surg*. 2005;129:694–5.
56. Lee DH, Park C-K, Keum D-Y, Kim J-B, Hwang I. Leiomyosarcoma of the posterior mediastinum extending into the adjacent spinal canal. *Korean J Thorac Cardiovasc Surg*. 2012;45:192–5.
57. Moran CA, Suster S, Perino G, Kaneko M, Koss MN. Malignant smooth muscle tumors presenting as mediastinal soft tissue masses. A clinicopathologic study of 10 cases. *Cancer*. 1994;74:2251–60.
58. Chu WP, Department of Radiology, Princess Margaret Hospital, Laichikok, Hong Kong (currently at the Department of Radiology, Tseung Kwan O Hospital, O TK, Kong H) Anterior mediastinal alveolar rhabdomyosarcoma in an infant: rare site for a common paediatric tumour. *Hong Kong Med J*. 2013;19:458–9.
59. Sartelet S, Lantuejoul S, Armari-Alla C, Pin I, Delattre O, Brambilla E. Solid alveolar rhabdomyosarcoma of the thorax in a child. *Histopathology*. 1998;32:165–71.
60. Weidner N. Solitary fibrous tumor of the mediastinum. *Ultrastruct Pathol*. 1991;15:489–92.
61. Xue X, Chen J, Ma W, Zhu D, Zhang W, Chen G, Wei S, Zhou Q. Mediastinal solitary fibrous tumor with right diaphragm invasion: report of a case. *Surg Today*. 2009;39:332–4.
62. Bouchikh M, Arame A, Riquet M, Le Pimpec-Barthes F. Cardiac failure due to a giant desmoid tumour of the posterior mediastinum. *Eur J Cardiothorac Surg*. 2013;44:1137–9.

63. Nakagiri T, Koseki M, Nakamoto K, Taniyama K. Paraesophageal mediastinal desmoid tumor: case report. *Gen Thorac Cardiovasc Surg*. 2007;55:125–9.
64. Warraich I, Dunn DM, Oliver JW. Solitary fibrous tumor of the orbit with epithelioid features. *Arch Pathol Lab Med*. 2006;130:1039–41.
65. den Bakker MA, Marx A, Mukai K, Ströbel P. Mesenchymal tumours of the mediastinum – part II. *Virchows Arch*. 2015;467:501–17.
66. Corson JM, Weiss LM, Banks-Schlegel SP, Pinkus GS. Keratin proteins and carcinoembryonic antigen in synovial sarcomas: an immunohistochemical study of 24 cases. *Hum Pathol*. 1984;15:615–21.
67. Dickersin GR, Richard Dickersin G. Synovial sarcoma: a review and update, with emphasis on the ultrastructural characterization of the nonglandular component. *Ultrastruct Pathol*. 1991;15:379–402.
68. Fisher C. Synovial sarcoma: ultrastructural and immunohistochemical features of epithelial differentiation in monophasic and biphasic tumors. *Hum Pathol*. 1986;17:996–1008.
69. Krall RA, Kostianovsky M, Patchefsky AS. Synovial sarcoma. *Am J Surg Pathol*. 1981;5:137–51.
70. Salisbury JR, Isaacson PG. Synovial sarcoma: an immunohistochemical study. *J Pathol*. 1985;147:49–57.
71. Salter DM. Pulmonary and thoracic sarcomas. *Curr Diagn Pathol*. 2006;12:409–17.
72. Salah S, Salem A. Primary synovial sarcomas of the mediastinum: a systematic review and pooled analysis of the published literature. *ISRN Oncol*. 2014;2014:412527.
73. Suster S, Moran CA. Primary synovial sarcomas of the mediastinum: a clinicopathologic, immunohistochemical, and ultrastructural study of 15 cases. *Am J Surg Pathol*. 2005;29:569–78.
74. Eilber FC, Dry SM. Diagnosis and management of synovial sarcoma. *J Surg Oncol*. 2008;97:314–20.
75. Rossi S, Nascimento AG, Canal F, Tos APD. Small round-cell neoplasms of soft tissues: an integrated diagnostic approach. *Curr Diagn Pathol*. 2007;13:150–63.
76. Stanelle EJ, Christison-Lagay ER, Healey JH, Singer S, Meyers PA, La Quaglia MP. Pediatric and adolescent synovial sarcoma: multivariate analysis of prognostic factors and survival outcomes. *Ann Surg Oncol*. 2013;20:73–9.
77. Wisanuyotin T, Radapat K, Sirichativapee W, Paholpak P, Kosuwon W, Sumnanoont C, Jeeravipoolvarn P. Prognostic factors and clinical outcomes in synovial sarcoma of the extremities. *Asia Pac J Clin Oncol*. 2013;9:80–5.
78. Eilber FC, Brennan MF, Eilber FR, Eckardt JJ, Grobmyer SR, Riedel E, Forscher C, Maki RG, Singer S. Chemotherapy is associated with improved survival in adult patients with primary extremity synovial sarcoma. *Ann Surg*. 2007;246:105–13.
79. Deshmukh R, Mankin HJ, Singer S. Synovial sarcoma: the importance of size and location for survival. *Clin Orthop Relat Res*. 2004;419:155–61.
80. Balieiro MA, Lopes AJ, Costa BP, Veras GPM, Perelson PS, Acatauassú Nunes R, Saito EH. The surprising outcome of a giant primary mediastinal synovial sarcoma treated with neoadjuvant chemotherapy. *J Thorac Dis*. 2013;5:94–6.
81. Zhou Y, Dong W, Zou F, Zhou D-A, Ma J-A. Primary giant mediastinal synovial sarcoma of the neck: a case report and review of the literature. *Oncol Lett*. 2014;7:140–4.
82. Nakazono T, White CS, Yamasaki F, Yamaguchi K, Egashira R, Irie H, Kudo S. MRI findings of mediastinal neurogenic tumors. *AJR Am J Roentgenol*. 2011;197:W643–52.
83. Tanaka O, Kiryu T, Hirose Y, Iwata H, Hoshi H. Neurogenic tumors of the mediastinum and chest wall: MR imaging appearance. *J Thorac Imaging*. 2005;20:316–20.
84. Pilavaki M, Chourmouzi D, Kiziridou A, Skordalaki A, Zarampoukas T, Drevlengas A. Imaging of peripheral nerve sheath tumors with pathologic correlation: pictorial review. *Eur J Radiol*. 2004;52:229–39.
85. Skovronsky DM, Oberholtzer JC. Pathologic classification of peripheral nerve tumors. *Neurosurg Clin N Am*. 2004;15:157–66.
86. Lonergan GJ, Schwab CM, Suarez ES, Carlson CL. From the archives of the AFIP. *Radiographics*. 2002;22:911–34.
87. Pavlus JD, Carter BW, Tolley MD, Keung ES, Khorashadi L, Lichtenberger JP 3rd. Imaging of thoracic neurogenic tumors. *AJR Am J Roentgenol*. 2016;207:552–61.
88. Brisse HJ, McCarville MB, Granata C, et al. Guidelines for imaging and staging of neuroblastic tumors: consensus report from the International Neuroblastoma Risk Group Project. *Radiology*. 2011;261:243–57.
89. Kamran SC, Shinagare AB, Howard SAH, Nishino M, Hornick JL, Krajewski KM, Ramaiya NH. Intrathoracic malignant peripheral nerve sheath tumors: imaging features and implications for management. *Radiol Oncol*. 2013;47:230–8.
90. Wen Y, Peng Y, Duan XM, Zhang N. Role of diffusion-weighted imaging in distinguishing thoracoabdominal neuroblastic tumours of various histological types and differentiation grades. *J Med Imaging Radiat Oncol*. 2017;61:718–24.
91. Suster S, Moran CA. Neuroendocrine neoplasms of the mediastinum. *Am J Clin Pathol*. 2001;115(Suppl):S17–27.
92. Baldassarre RL, Nakanote KA, Hughes TH. Imaging of peripheral neurogenic tumors. In: *Handbook of neuro-oncology neuroimaging*; Herbert Newton; 2016. p. 777–96.
93. He W-G, Yan Y, Tang W, Cai R, Ren G. Clinical and biological features of neuroblastic tumors: a comparison of neuroblastoma and ganglioneuroblastoma. *Oncotarget*. 2017;8:37730–9.



Primary Tumors of the Pleura

*Roberta Eufrasia Ledda, Claudia Commisso,
Luciano Cardinale, and Nicola Sverzellati*

- 8.1 Malignant Pleural Mesothelioma – 161**
 - 8.1.1 Epidemiology and Risk Factors – 161
 - 8.1.2 Pathology – 161
 - 8.1.3 Imaging – 162
 - 8.1.4 Staging – 164
 - 8.1.5 Treatment and Prognosis – 164

- 8.2 Malignant Pleural Mesothelioma:
Patterns of Local Spread – 166**
 - 8.2.1 Mediastinum – 166
 - 8.2.2 Diaphragm – 166
 - 8.2.3 Chest Wall – 166
 - 8.2.4 Lung – 167

- 8.3 Malignant Pleural Mesothelioma:
Lymph Node Involvement – 168**

- 8.4 Malignant Pleural Mesothelioma:
Distant Metastatic Spread – 169**

- 8.5 Solitary Fibrous Tumor – 169**
 - 8.5.1 Overview – 169
 - 8.5.2 Pathology – 169
 - 8.5.3 Imaging – 169
 - 8.5.4 Local Recurrence and Distant Spread – 172

8.6 Primary Pleural Lymphoma – 172

8.6.1 Overview – 172

8.6.2 Pathology – 173

8.6.3 Imaging – 173

8.6.4 Lymph Node Involvement – 173

8.7 Other Primary Pleural Tumors – 173

8.7.1 Overview – 173

8.7.2 Patterns of Metastatic Dissemination – 175

References – 175

8.1 Malignant Pleural Mesothelioma

8.1.1 Epidemiology and Risk Factors

Malignant pleural mesothelioma (MPM) is a rare and highly aggressive neoplasm that arises from the mesothelial cells of the pleural surface [1–3]. Dyspnea and chest wall pain represent the two main symptoms [4–6]. Other symptoms include fatigue, malaise, anorexia, weight loss, and sweats [5]. Malignant mesothelioma is strongly associated with long-term mineral fiber exposure, mostly asbestos, with a latency period of approximately 40 years between fiber inhalation and disease occurrence [5, 7, 8]. The carcinogenicity of asbestos fibers is related to the fiber aspect ratio (the ratio of fiber length to width): the higher the aspect ratios, the higher their tumorigenicity [3]. Although the use of asbestos has been limited or banned in several industrialized countries, the incidence of this uncommon neoplasm has been increasing over the last 30 years due to its long latency period and is predicted to peak in the next few years [5, 9, 10]. The association between mesothelioma and occupational exposure to asbestos has been largely investigated and well-established. Relatively less attention has been paid to the impact of the environmental exposure, as follows: (i) exposure to naturally occurring asbestos; (ii) neighborhood exposure, based on residence adjacent to industrial sources of asbestos; (iii) household exposure, for family members of occupationally exposed subjects (also named *familial exposure*); and (iv) other nonoccupational exposures, including home-related or domestic exposure [7, 8]. Regardless of the source of asbestos inhalation, the environmental exposure accounts for a small portion of the total number of MPM (from approximately 4% in Japan to 9% in France, according to large population-based studies) [7, 11]. Occurrence of MPM has been also observed in patients treated with external radiotherapy for other malignancies, including lymphoma and testicular cancer [12]. A large retrospective study enrolling nearly 300,000 lymphoma patients demonstrated that the risk of mesothelioma was increased after radiotherapy among patients with both non-Hodgkin's lymphoma (NHL) and Hodgkin's lymphoma (HL). Of note, their findings showed that the risk of second

primary mesothelioma was greater among those subjects diagnosed before 1995, when either radiation volumes or radiation dose was higher [13].

Some evidence also suggests that simian virus 40, an oncogenic virus that blocks tumor-suppressor genes, may act as a cofactor in the development of MPM as well as other cancers, including NHL, ependymoma, and osteosarcoma [8, 12].

The incidence of MPM is higher in men than in women, with a male/female ratio of 4:1 [3, 5, 6]. The vast majority of epidemiological studies, however, has been conducted in occupational settings, where male subjects represent the wider proportion of MPM cases [7]. Female patients, conversely, are more subject to environmental exposure compared to men [7, 14, 15].

8.1.2 Pathology

In 2015, pleural mesotheliomas were classified by the World Health Organization (WHO) into diffuse malignant mesothelioma (DMM), localized malignant mesothelioma (LMM), and well-differentiated papillary mesothelioma (WDPM), which represents a distinct rare entity with an epithelioid architecture and a tendency to spread superficially without invasion [2].

Macroscopically, DMM typically encases the lung as a thick rind that grows along the interlobular fissures, sparing the underlying lung parenchyma [16]. The diffuse pleural thickening is usually of firm consistency and gray/white in color [17]. The parietal pleura is often more extensively involved [3]. There are three main histological subtypes: epithelioid (accounting for about 70% of all cases), sarcomatoid (10%), and biphasic or mixed, which accounts for the remainder [6, 18, 19].

Microscopically, epithelioid MPM is commonly composed of polygonal or cuboidal cells with abundant pink cytoplasm and uniform round nuclei that resemble nonneoplastic reactive mesothelial cells [16]. This subtype is associated with a better prognosis and can be confused with metastatic lung adenocarcinoma, which can mimic MPM when predominantly involves the pleura [19–21]. Sarcomatoid DMM consists of spindle cells of variable plumpness, cellularity, and pleomorphism, organized in either sheets or fascicles. Mixed DMM contains both epithelial

and sarcomatous components in a proportion of at least 10% each [16]. Heterologous differentiation, including osseous or chondroid, is a rare feature that is observed more frequently in sarcomatoid subtypes, but it can also be seen with biphasic and epithelioid patterns [22].

LMM presents a localized growth and shares similar morphologic and immunohistochemical features to their diffuse counterpart, though a better overall survival (OS) rate after surgical resection has been reported [19, 23, 24]. There are two histological subtypes of LMM: epithelioid and sarcomatoid type [23]. These neoplasms are extremely rare with only 50 cases reported in the literature [25]. The differential diagnosis of the LMM from other pleural tumors, such as solitary fibrous tumor of the pleura (SFTP), can be challenging even pathologically [25, 26].



■ **Fig. 8.1** CXR of a 69-year-old woman with an epithelioid malignant pleural mesothelioma. Posteroanterior view shows diffuse pleural thickening and unilateral pleural effusion, associated with ipsilateral mediastinal shift and hemidiaphragm elevation

8.1.3 Imaging

8.1.3.1 Chest Radiography

The diagnosis of MPM is often suggested by the chest radiography (CXR), which may show unilateral pleural effusion (in up to 80% of cases), diffuse pleural thickening (in approximately 60% of cases), or pleural nodularity or masses (in 45–60% of cases) [3]. Unlike other malignancies, there is not a concentrically enlarging primary tumor, but multiple nodules that might merge and spread along the pleural surfaces [27], causing encasement of the lung with consequent volume loss. The recognition of CXR signs of volume loss, such as elevation of the ipsilateral hemidiaphragm, ipsilateral mediastinal shift, and narrowing of the intercostal spaces, is important to suggest pleural malignancy [3] (■ Fig. 8.1).

8.1.3.2 Transthoracic Ultrasound

Transthoracic ultrasound (TUS) may promptly help distinguish benign from malignant pleural effusions. TUS features suggestive for malignant effusion include pleural thickening >1 cm, pleural-based mass lesions, nodular pleural thickening, and diaphragmatic nodularity [28]. These features are highly specific, though not much sensitive. Therefore, if MPM or other pleural malignancy is suspected, further investigations are mandatory.

8.1.3.3 Computed Tomography

Contrast-enhanced computed tomography (CT) scan is the primary imaging modality used for both diagnosis and staging of the disease [4, 18]. CT features of MPM overlap those of other primary or metastatic pleural disorders. CT features of DMM include circumferential and nodular pleural thickening (up to 92% of cases), ipsilateral volume loss, pleural effusion (74%), mediastinal and pericardial infiltration, chest wall involvement, lymphadenopathy, and distant metastases [3, 29–31] (■ Fig. 8.2).

LMM, conversely, appears as a single pleural mass with heterogeneous contrast uptake that reflects the degree of intralesional necrosis and/or degeneration [25]. In case of osseous or chondroid differentiation, large or punctate foci of mineralization might be depicted within the pleural thickening or masses, resembling an osteosarcoma or a chondrosarcoma [6, 32]. Calcified pleural plaques, representing asbestos-related pleural disease, are observed in up to 20% of MPM patients and should not be mistaken for heterologous differentiation [33]. In the latter case, calcifications appear linear rather than punctate and localized along the plaques' margins. Of note, calcified or noncalcified pleural plaques, secondary to asbestos exposure, may be encased by the tumor, and up to 20% of patients

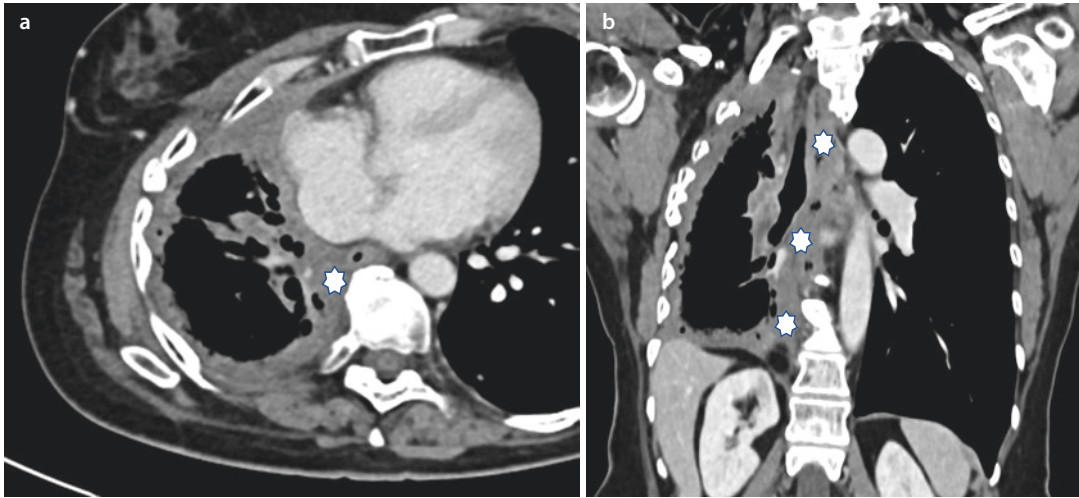


Fig. 8.2 Encasement of the right lung by a malignant pleural mesothelioma in a 74-year-old woman. Both axial **a** and coronal **b** images from contrast CT scan show

circumferential pleural thickening, ipsilateral volume loss, and ipsilateral hemidiaphragm elevation, along with mediastinal invasion (asterisks)

with MPM show signs of parenchymal asbestosis [3, 6, 33]. A recent retrospective study on 125 patients showed that pleural plaques are more common in non-epithelioid subtypes [18].

On CT, the differentiation between MPM and metastatic pleural disease (MPD) may be difficult if not impossible, given their similar features [6, 31, 33]. Indeed, MPD usually manifests as pleural nodules or masses, pleural thickening, and pleural effusion, which is the most frequent manifestation of metastatic pleural involvement [34].

The presence of systemic metastases is more in keeping with MPD as distant metastases are relatively uncommon in MPM. Conversely, the presence of pleural plaques is more often observed in MPM, as well as ipsilateral volume loss and chest wall invasion. Circumferential pleural thickening with mediastinal pleural involvement, fissural pleural thickening, diaphragmatic pleural thickening, pericardial involvement, and the presence of a pleural mass are significantly more frequent CT findings in MPM. Conversely, nodular pleural thickening with hilar or mediastinal lymph node (LN) enlargement are more frequently observed in MPD [34, 35].

8.1.3.4 Magnetic Resonance Imaging

At magnetic resonance imaging (MRI), unilateral pleural effusion has high signal intensity on T_2 -weighted images, whereas pleural thickening is typically isointense or mildly hyperintense to

muscle on T_1 -weighted images and moderately hyperintense on T_2 -weighted and proton density-weighted images and enhances gadolinium-based contrast [6, 36]. Although MRI is not routinely used to evaluate MPM, it is still regarded superior to CT in the assessment of adjacent structure involvement [6, 37, 38]. Indeed, MRI may help refine disease staging, with respect to involvement of the chest wall, mediastinum, and diaphragm [4, 30, 32, 36]. MRI may also help to discriminate malignant from benign pleural disease [37]. In 2009, Coolen et al. reported significant differences in apparent diffusion coefficient (ADC) values between malignant and benign pleural entities, with ADC values lower in malignant neoplasms, most likely due to their hypercellularity and hypervascularity. Conversely, in case of necrosis or inflammation, the diffusion restriction is low and the ADC high [39]. Diffusion-weighted imaging (DWI) sequences suggest the histological subtype, as ADC values of epithelioid MPM are higher than those of sarcomatoid mesothelioma [36, 40].

MRI might contribute to distinguish MPM from MPD, which typically demonstrates high signal intensity compared to intercostal muscles on T_2 -weighted images and tissue uptake following the administration of intravenous (IV) contrast [6]. The MRI signal, however, is strongly related to the characteristics of the primary neoplasm, which vary according to the primary

tumor nature. If the ADC of the primary tumor is known, this value can be used as a potential marker to characterize pleural metastases [36].

It was suggested that the time delay between IV gadolinium injection and the initiation of image acquisition can be too short for optimal assessment of mesothelioma. The standard time delay for optimal tissues enhancement and opacification of arterial and venous structures is typically 40–60 seconds, and protocols usually do not include delayed phase imaging beyond 2 minutes after the administration of IV contrast [41]. It was estimated that the optimal time delay between contrast injection and image acquisition should be within the range of 230–300 seconds [41]. Likewise, Patel et al. observed that the optimal time delay for maximal MPM tumor enhancement is between 150 and 300 seconds following IV contrast injection [42]. Optimizing tumor enhancement may allow for increased accuracy in both staging and treatment response assessment. Further studies on the impact of delayed phase enhancement on radiologic staging accuracy and therapy response assessment are warranted [43].

The potential application of quantitative imaging in the evaluation of therapy response in MPM has been also investigated [44]. It was shown that either dynamic contrast-enhanced CT (DCE-CT) or MRI (DCE-MRI) predict early response to chemotherapy and might suggest alternative therapy strategies in case of poor response [44, 45]. Despite the development and implementation of the modified response evaluation criteria in solid tumors (RECIST) for measurement of mesothelioma, some questions on their applicability in clinical practice still need to be answered, limiting a broad and effective use [41]. In this setting, quantitative imaging might be a valuable adjunctive tool for the assessment of the response to treatment [46].

With respect to quantitative imaging, Pena et al. have already observed that a radiomics-based approach, applied on both CT and MRI images, may improve the radiologists' accuracy in discriminating benign from malignant pleural lesions [38].

8.1.3.5 Positron Emission Tomography

Positron emission tomography (PET)/CT has been proposed as a valid imaging technique to allow differentiation between benign and malignant pleural entities. In this respect, various small

prospective and retrospective studies reported differing values of sensitivity, from 88% to 100%, and specificity, from 35% to 100% [33].

Undoubtedly, PET/CT with fluorodeoxyglucose (FDG) is an important additional examination for both diagnosis and staging of MPM [3, 30]. The ability to accurately estimate LN involvement and to detect distant metastases represents the main strength of FDG-PET/CT [47]. Moreover, it provides functional information, such as metabolic activity or metabolic tumor volume, which has a prognostic relevance. However, its contribution to local T staging is limited, compared to contrast-enhanced CT [47, 48], and its sensitivity for small pleural lesions remains low [39]. PET/MRI, on the other hand, seems to perform better than PET/CT in T staging, which often represents the main factor of whether a patient is a candidate for surgery [47].

PET/CT might have a potential in the evaluation of treatment response. PET/CT can help differentiate between scar tissue from disease recurrence (sensitivity 94% and specificity 100%). However, the uptake of FDG can be increased in the early time frame after surgery or radiotherapy [49].

8.1.4 Staging

The recommended staging system for clinical use, which is based on TNM, has been updated in 2018 by the International Mesothelioma Interest Group and the International Association for the Study of Lung Cancer (■ Tables 8.1 and 8.2) [27]. In this latest TNM staging edition, previous N1 (intrapleural LNs) and N2 (extrapleural LNs) categories have been grouped into one single category – N1 – and previous N3 nodes shifted into N2 category, since no significant differences in survival rate were observed between previous N1 and N2 category [50].

8.1.5 Treatment and Prognosis

There is no curative treatment for MPM. Surgery is reserved to patients with early stage of disease and good functional status [3, 5, 51]. Lung-sparing procedures, such as pleurectomy/decortication (P/D), are largely used as proven to be comparable to extrapleural pneumonectomy (EPP) in terms of

Table 8.1 The eighth edition of the TNM staging system for malignant pleural mesothelioma

<i>T category</i>	
Tx	Primary tumor not assessable
T0	No evidence of primary tumor
T1	Tumor involving the ipsilateral parietal pleura (including mediastinal and diaphragmatic pleura) with or without involvement of the visceral pleura
T2	Tumor involving each of the ipsilateral pleural surfaces (parietal, mediastinal, diaphragmatic, and visceral pleura) with at least one of the following features: <ul style="list-style-type: none"> – Confluent visceral pleural tumor (including the fissures) – Involvement of diaphragmatic muscle – Invasion of the lung parenchyma
T3	Tumor involving all of the ipsilateral pleural surfaces (parietal, mediastinal, diaphragmatic, and visceral pleura) with at least one of the following features: <ul style="list-style-type: none"> – Invasion of the endothoracic fascia – Extension into the mediastinal fat – Solitary, completely resectable focus invading soft tissues of the chest wall – Nontransmural involvement of the pericardium
T4	Tumor involving all of the ipsilateral pleural surfaces with at least one of the following features: <ul style="list-style-type: none"> – Diffuse or multifocal invasion of soft tissues of the chest wall – Any rib involvement – Invasion of the peritoneum through the diaphragm – Invasion of any mediastinal organ – Direct extension to the contralateral pleura – Invasion of the spine or brachial plexus – Transmural invasion of the pericardium (with or without pericardial effusion) or myocardium invasion
<i>N category</i>	
Nx	Regional lymph nodes not assessable
N0	No regional lymph node metastases
N1	Metastases in the ipsilateral bronchopulmonary, hilar, or mediastinal lymph nodes (including the internal mammary, peridiaphragmatic, pericardial fat pad, or intercostal lymph nodes)
N2	Metastases in the contralateral bronchopulmonary, hilar, or mediastinal lymph nodes or ipsilateral or contralateral supraclavicular lymph nodes

Table 8.1 (continued)

<i>M category</i>	
Mx	Presence of distant metastases not assessable
M0	No evidence of distant metastases
M1	Evidence of distant metastases

Table 8.2 Stage grouping for malignant pleural mesothelioma from the eighth edition of the TNM classification

Stage	T	N	M
IA	T1	N0	M0
IB	T2,3	N0	M0
II	T1,2	N1	M0
IIIA	T3	N1	M0
IIIB	T1–3	N2	M0
IV	T4	N0–2	M0
	Any T	Any N	M1

macroscopic complete resection, OS, perioperative mortality, and readmission rates [52, 53]. Although P/D is generally thought to be associated with a better quality of life, the 14th International Conference of the International Mesothelioma Interest Group emphasized that longer-term prospective studies are necessary to confirm this observation beyond the first year after surgery [9]. The choice between EPP and P/D is still a matter of debate [8, 54]. Treatment strategies also include radiotherapy and polychemotherapy (CHOP) as no single treatment modality has been shown to be fully effective [3, 5, 51]. Novel therapies, such as intrapleural immunotherapy, have shown promising preliminary results [55]. However, the patient prognosis remains poor, with a median survival ranging from 6 to 14 months from the time of diagnosis [3, 8, 30, 56]. Histological pattern represents a strong prognostic factor: epithelioid subtype has the longest survival, sarcomatoid the worst, and biphasic an intermediate survival [18]. Females tend to have a more favorable prognosis [15, 57]. A large

study including over 16,000 MPM patients has recently shown that female patients survive significantly longer than males, with an OS of 26.5% vs 16.6% at 2 years and of 9.4% vs 4.2% at 5 years. Their results have also suggested that estrogen receptor beta (ER β) expression, present on epithelial-type MPM, and circulating estrogens might act as favorable prognostic factors in women, especially young ones [58].

8.2 Malignant Pleural Mesothelioma: Patterns of Local Spread

8.2.1 Mediastinum

CT signs of mediastinal invasion include obliteration of surrounding fat planes and tumoral encasement of more than 50% of the circumference of a mediastinal structure, including the trachea, the esophagus, and mediastinal vessels [3] (■ Figs. 8.3 and 8.4). Direct extension into mediastinal structures is more commonly observed in MPM rather than MPD (mediastinal pleura involvement 85% vs 33%, pericardial involvement 25% vs 15%, mediastinal structures 22% vs 10%) [35].

The involvement of the pericardium has been reported in nearly 45% of cases in postmortem study [59]; it may be either nontransmural or transmural and result in pericardial effusion, pericardial thickening, and/or pericardial nodules or masses [30]. The presence of epicardial fat suggests nontransmural invasion, whereas trans-



■ Fig. 8.3 Postcontrast CT image shows infiltration of both right pulmonary trunk (asterisk) and superior vena cava (arrow) in a 74-year-old woman with malignant pleural mesothelioma



■ Fig. 8.4 Diffuse chest wall and mediastinal infiltration in a 74-year-old man with malignant pleural mesothelioma. Axial CT image shows chest wall (arrows) and mediastinal infiltration (asterisks), with contralateral shift of the heart

mural disease is demonstrated by the extension of the tumor into the internal surface of the pericardium or into the myocardium [3]. Myocardium involvement was reported in 13.1% of cases by Finn et al. [59]. Although pericardial effusion is usually due to direct pericardial invasion, it could be also secondary to pericardial lymphatic obstruction [60].

8.2.2 Diaphragm

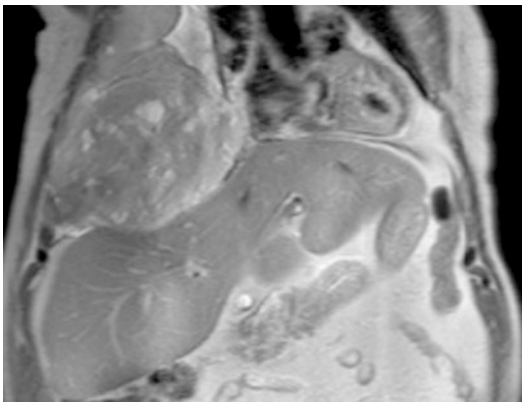
MRI is considered superior to CT for identifying transdiaphragmatic extension of pleural mesothelioma [36, 61] (■ Fig. 8.5). Gill et al. estimated that the sensitivity of CT imaging for evaluating the resectability of MPM along the diaphragm and the chest wall was 94% and 93%, respectively, whereas the sensitivity of MRI was 100% for both structures [37]. Usually, when diaphragmatic infiltration occurs, a soft tissue mass encases the hemidiaphragm [61]. The presence of a distinct fat plane between the inferior surface of the diaphragm and the underlying abdominal structures is the most reliable sign that MPM is limited to the thorax [3].

8.2.3 Chest Wall

MPM invades adjacent chest wall structures in up to 18% of cases [62]. The most accurate CT and MRI signs of chest wall invasion include loss of normal extrapleural fat planes, invasion of inter-

costal muscles, rib displacement, and/or osseous destruction [32] (■ Figs. 8.4 and 8.6). On MRI, MPM shows intermediate to slightly higher signal intensity on T₁-weighted images and moderately high signal intensity on T₂-weighted images compared with adjacent chest wall musculature [36, 37] (■ Fig. 8.7).

MPM has a propensity to spread along needle or transthoracic trocar procedure tracts to skin puncture or incision sites, with tumor cell seeding leading to symptomatic subcutaneous metastases in up to 51% of patients [63]. The use of prophylactic radiotherapy to prevent procedure-tract metastases in malignant pleural mesothelioma remains controversial [63, 64].

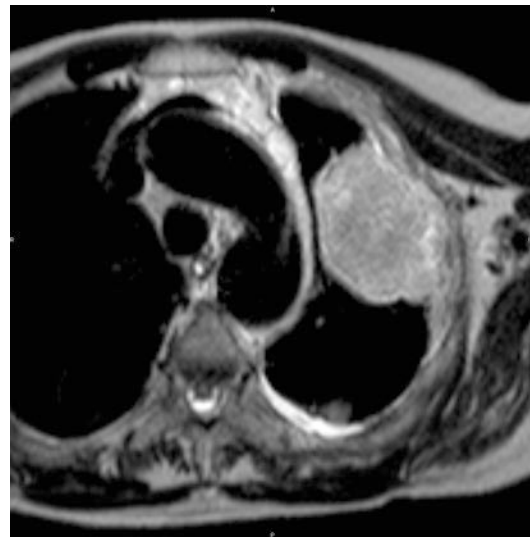


■ **Fig. 8.5** Coronal T₂-weighted fast spin-echo MR image: solid and liquid components have different signal intensity and can be easily differentiated, thanks to the excellent contrast resolution showing hyperintense effusion and hypointense pleural masses. The image clearly depicts the tumor infiltration of the right diaphragm in a 67-year-old man with a history of malignant pleural mesothelioma

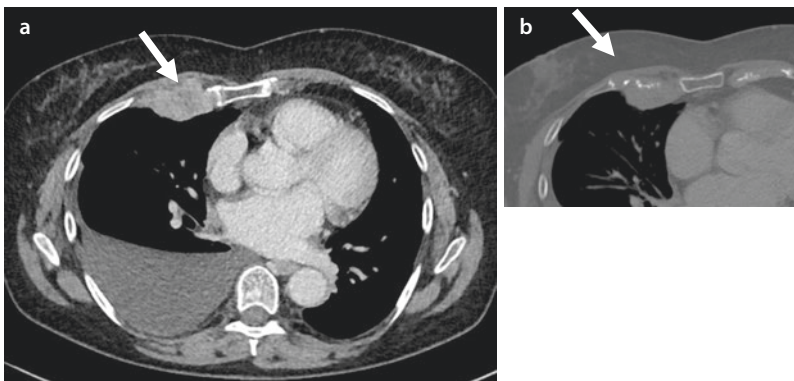
8.2.4 Lung

The two principal patterns of intraparenchymal lung involvement by MPM are represented by direct subpleural lung infiltration and lymphangitic spread [65]. The latter is rarer and associated to a poorer prognosis [66]. In case of lung parenchyma involvement, pleural-based nodular masses extending into the lung or round and sharply demarcated masses within the lung can be observed [67].

Other patterns of spread through the lung parenchyma were also described, as follows: an intra-alveolar growth pattern in 1.5% of cases, a



■ **Fig. 8.7** Local invasion of malignant pleural mesothelioma at MRI. Chest wall invasion in a 65-year-old woman is clearly depicted on axial T₂-MRI image



■ **Fig. 8.6** Chest wall invasion in a 72-year-old woman with a history of malignant pleural mesothelioma. Axial CT images show chest wall infiltration a and ribs destruction b

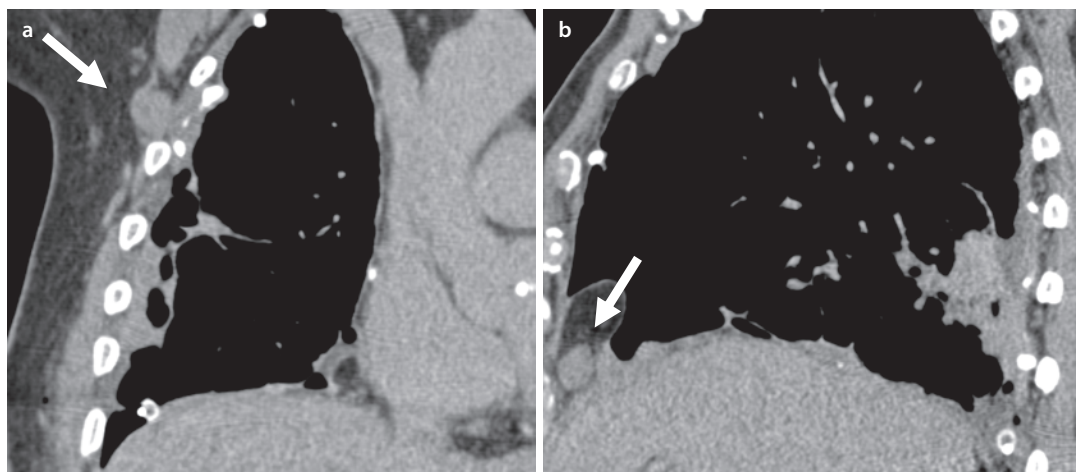


Fig. 8.8 Lymph node involvement in malignant pleural mesothelioma. Coronal **a** and sagittal **b** CT images show axillary and diaphragmatic metastatic lymph nodes in a 71-year-old man

8

bronchioalveolar carcinoma-like pattern (0.5%), and a desquamative interstitial pneumonia-like pattern (0.5%) [17]. These uncommon patterns of local spread are difficult to interpret and could be misdiagnosed. Lepidic intrapulmonary growth represents another rare pattern of spread [68].

8.3 Malignant Pleural Mesothelioma: Lymph Node Involvement

LN involvement is frequent in MPM, being reported in 35–50% of patients undergoing cytoreductive surgery [69] and in 76% of autopsies, according to some postmortem series [59]. LN metastases are one of the most important prognostic factors. Subjects with LN involvement at the time of diagnosis have a poorer prognosis [27].

Internal mammary, pericardial, and diaphragmatic nodes [70] are more frequently involved (e.g., compared to intrapleural ones) given their direct drainage pathway from the parietal pleura [69] (■ Figs. 8.8, 8.9, and 8.10). Internal mammary LN metastases usually occur when the primary lesion arises either from the upper or middle portion of the anterior pleura, while peridiaphragmatic LN metastases are more likely seen in association with lower lesions. Hilar LN metastases are usually seen when MPM involves either the visceral pleura or the lung parenchyma. Subcarinal, paraesophageal, or para-aortic nodes of ≥ 10 mm

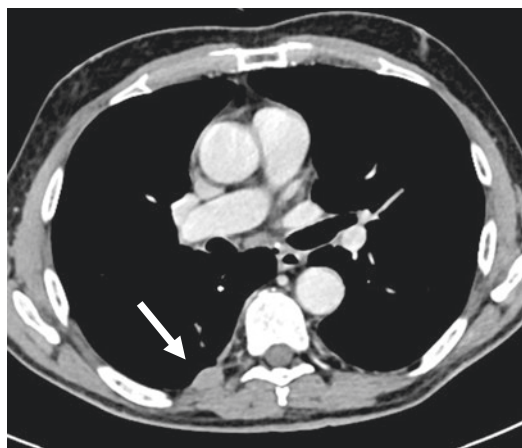


Fig. 8.9 Axial CT image shows paravertebral lymph node metastasis in a 75-year-old man with recurrent malignant pleural mesothelioma

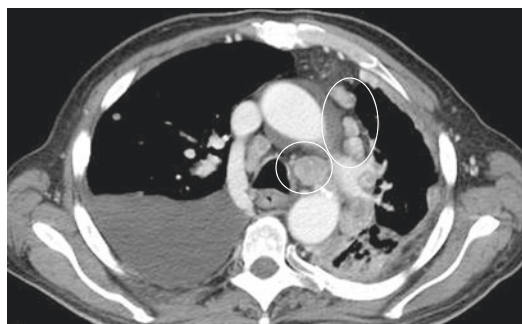


Fig. 8.10 Axial CT image shows mediastinal lymphadenopathies (circles) with right irregular circumferential left pleural thickening and contralateral pleural effusion in a 67-year-old man with malignant pleural mesothelioma

in short axis diameter should be considered abnormal, whereas any enlargement of internal mammary, retrocrural, or extrapleural locations are suspicious for tumor involvement on CT [32].

CT is the most commonly used modality to assess LNs, but its accuracy remains less than optimal, with a sensitivity and specificity of 60% and 71%, respectively [61]. Thus, LN biopsy is recommended for a definitive diagnosis [71].

MRI has not been proven to be superior to CT in the assessment of LN involvement [61, 71]. In a recent retrospective study, whole-body MRI, along with FDG-PET/MRI (with and without signal intensity assessment) and FDG-PET/CT, have shown greater diagnostic accuracy compared to CT alone (87%, 87%, 73.9%, and 73.9%, respectively, vs 56.5%) with respect to LN involvement [72].

8.4 Malignant Pleural Mesothelioma: Distant Metastatic Spread

Distant metastases are relatively uncommon and represent a late manifestation of MPM [59]. However, biphasic and sarcomatoid subtypes can present with distant metastases in early stages of disease given their aggressive behavior [37]. The contralateral lung, liver (31.9%), and peritoneum are the most common sites of distant spread [6]. Secondary involvement of adrenal glands and spleen (10.8%) has also been reported [59]. Bones (7.3%), thyroid (6.9%), and brain (3%) are less frequently involved [59, 73, 74] (■ Figs. 8.11 and 8.12).

Perineural tumor dissemination, which is associated with a poor prognosis, has been described in eight cases only [75]. Such an insidious occurrence may lead to spinal cord metastases and should be suspected when neurological symptoms are present. Neurological symptoms include sphincter dysfunction, extremities motor and sensory disturbances, and Horner's syndrome [75].

8.5 Solitary Fibrous Tumor

8.5.1 Overview

SFTP accounts for less than 5% of pleural tumors. It occurs more frequently in middle-aged adults with no sex preponderance, though a slightly higher frequency has been reported in women

[76]. Little is known about etiologic agents and no link with tobacco or asbestos exposure has been demonstrated [77]. A complete surgical resection with sublobar resection, lobectomy, or pneumonectomy is the mainstay of treatment for all SFTPs, for both benign and malignant lesions [76]. Recent series demonstrated excellent local control rate and distant metastatic-free survival using combined surgery and radiotherapy [78]. At present, the benefit of adjuvant chemotherapy is still debated [79].

SFTP is asymptomatic in approximately 50% of cases [80] and has usually a good prognosis, but it can be malignant in 10–20% of the cases [81]. The 5-year OS rate of malignant SFTP is about 70%. However, recurrence may occur more than 15 years after the initial resection [82].

8.5.2 Pathology

A poor prognosis is related to several macroscopic and microscopic features, such as the absence of a pedicle, tumor size greater than >10 cm, mitotic index, tumor necrosis, hypercellularity, pleomorphism, and high p53 expression [83]. Unlike MPM, the majority of SFTP arises from the visceral pleural [6, 31]. Macroscopically, it appears as a well-circumscribed, partially encapsulated firm yellow or white mass, often larger than 10 cm in diameter [5, 19] (■ Fig. 8.13). Giant SFTPs of up to 30 cm in diameter have been described [84]. The most common histological pattern, called *patternless pattern*, is represented by spindle or ovoid cells usually not arranged in a specific pattern but in a heterogeneous architecture of collagen, reticulum fibers, and branching hemangiopericytoma-like vasculature [19].

8.5.3 Imaging

On CXR, SFTP usually appears as a solitary, homogeneous round/oval mass or nodule, with smooth and well-defined margins [31]. It typically abuts the pleural surface or is located within a fissure (■ Fig. 8.14). SFTP affects mostly the middle and inferior hemithorax [85], while a fissural location is seen in 30% of cases [81].

On CT imaging, SFTP generally demonstrates a broad attachment to the pleura, forming an obtuse angle [31, 33]. It often shows a heterogeneous attenu-

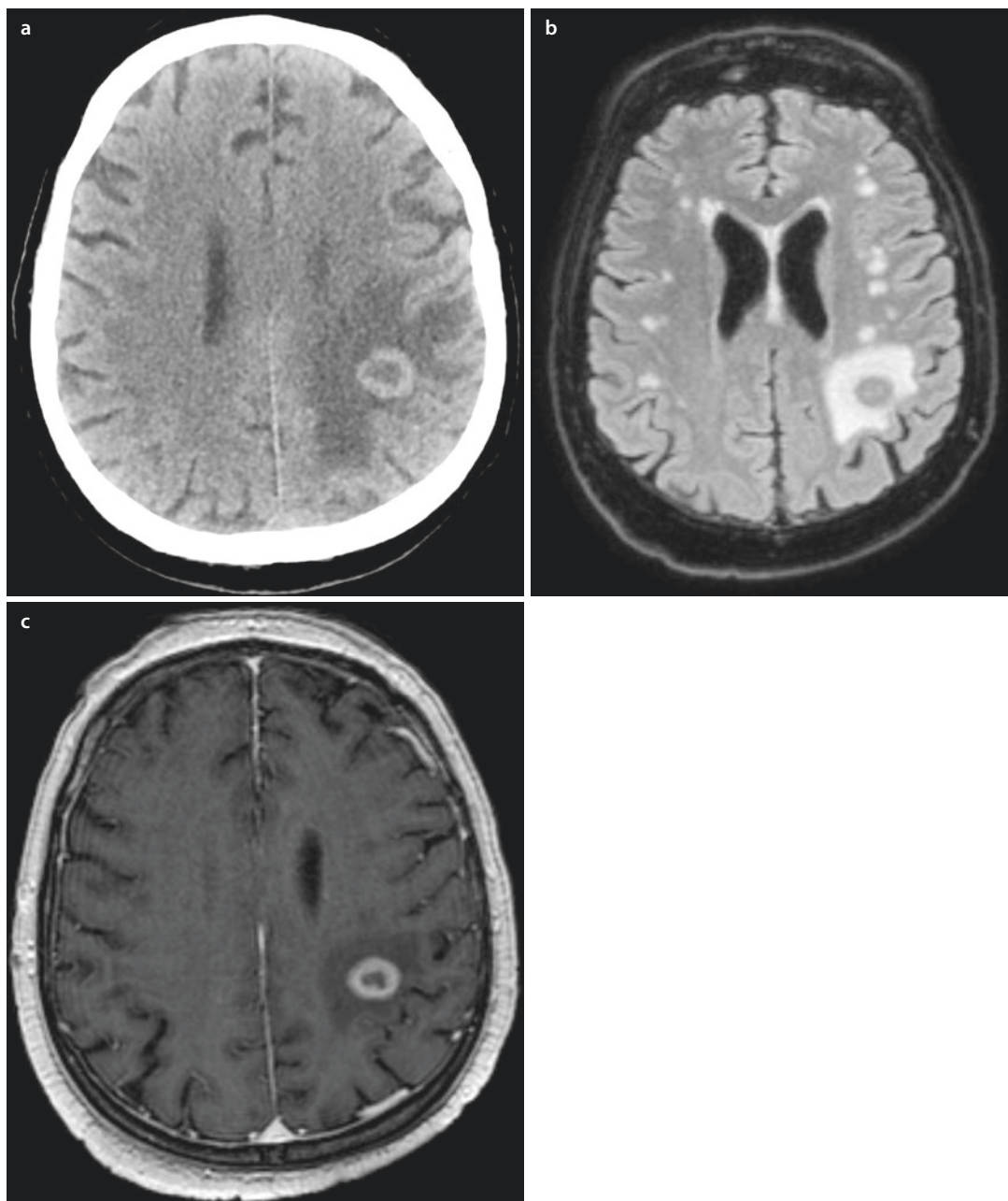


Fig. 8.11 Single brain metastasis in a 64-year-old man with malignant pleural mesothelioma. Contrast-enhanced CT **a** and MRI (FLAIR, **b**, and contrast-enhanced

T₁-weighted, **c**) images show a left-sided parietal mass with ring enhancement and surrounding edema

ation that becomes more obvious following contrast IV administration. Indeed, it may be characterized by central areas of low attenuation reflecting internal hemorrhage or necrosis [31] (Fig. 8.15). Punctate, linear, or coarse calcifications within the lesion may be also observed. Pleural effusion can occasionally coexist (6–17%) [85]. Lymphadenopathy is infre-

quent, as opposed to localized malignant pleural mesothelioma (LMPM) [86].

On MRI, SFTP shows low to intermediate signal intensity on T₁-weighted and T₂-weighted images given its predominant fibrous tissue-based content. High heterogeneous signal intensity on T₂-weighted images is observed in case of necro-

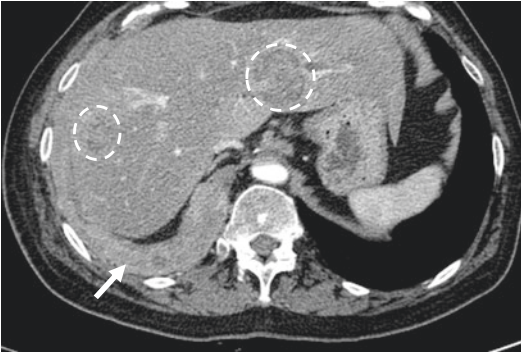


Fig. 8.12 Hepatic metastases in a 71-year-old man with malignant pleural mesothelioma. Axial contrast-enhanced CT image shows two liver metastases (circles) and a right pleural thickening consistent with malignant pleural mesothelioma (arrow)

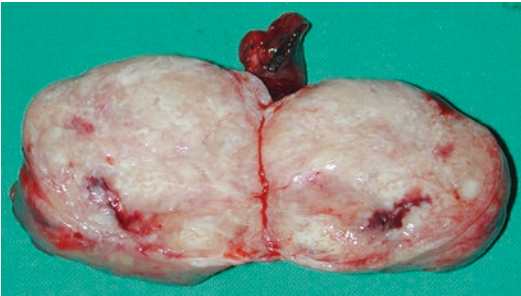


Fig. 8.13 Photograph of a surgical specimen showing a pedunculated and capsulated solitary fibrous tumor of the pleura

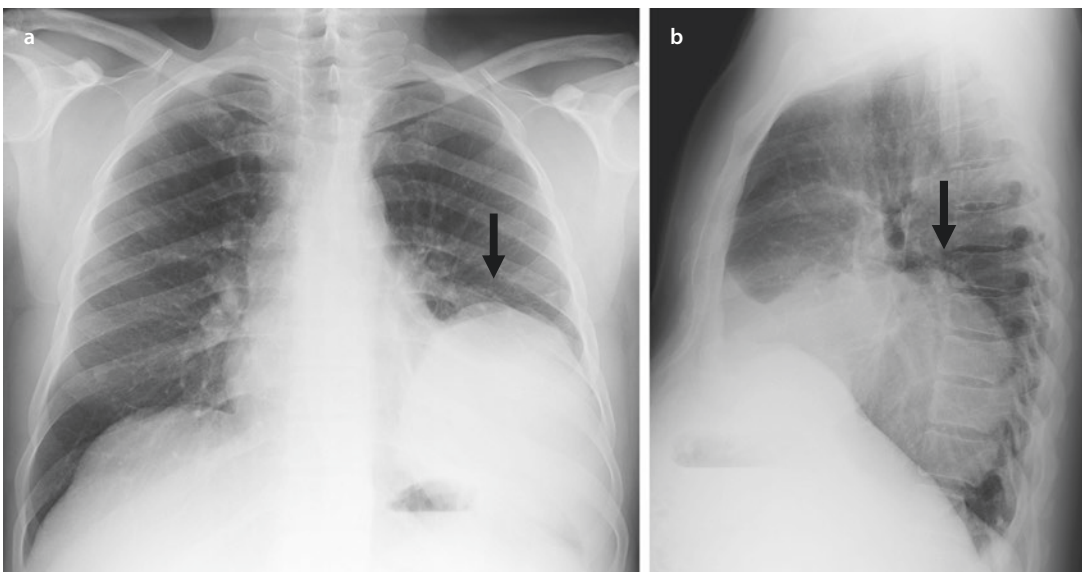


Fig. 8.14 CXR of a 63-year-old man with a history of malignant solitary fibrous tumor of the pleura. Posteroanterior **a** and lateral **b** views show a round, well-defined pleural mass in the inferior left hemithorax (arrows)

sis and cystic or myxoid degeneration, with prominent vascular structures and areas of high cellularity [36]. Usually, there is intense heterogeneous enhancement after the administration of IV gadolinium contrast medium (■ Fig. 8.16).

MRI helps to better define the relationship of large SFTP with adjacent mediastinal structures and diaphragm [6], while DWI sequences can be used to initially differentiate benign from malignant lesions [87]. However, this differential diagnosis is only reliable at histological examination.

The role of FDG-PET/CT in SFTP is controversial [79, 88]. Kohler et al. observed FDG-PET positivity in all malignant SFTPs [89], whereas others reported no FDG uptake in benign lesions [90, 91]. Other Authors observed low-grade metabolic activity in benign SFTPs and homogeneously high-grade activity in malignant lesions [92, 93]. Tazeler et al., who assessed the utility of FDG-PET/CT for the differentiation of benign and malignant SFTPs prior to surgery, observed that malignant SFTPs tend to exhibit a slightly higher uptake than benign tumors [94]. However, more recent evidence seems to demonstrate that high cellularity might be the cause of increased FDG uptake, regardless of the malignancy [95]. Chick et al. stated that larger tumors may show heterogeneously low uptake with a relatively lower uptake in areas of necrosis, cystic degeneration, myxoid change, hemorrhage, and calcification [96].

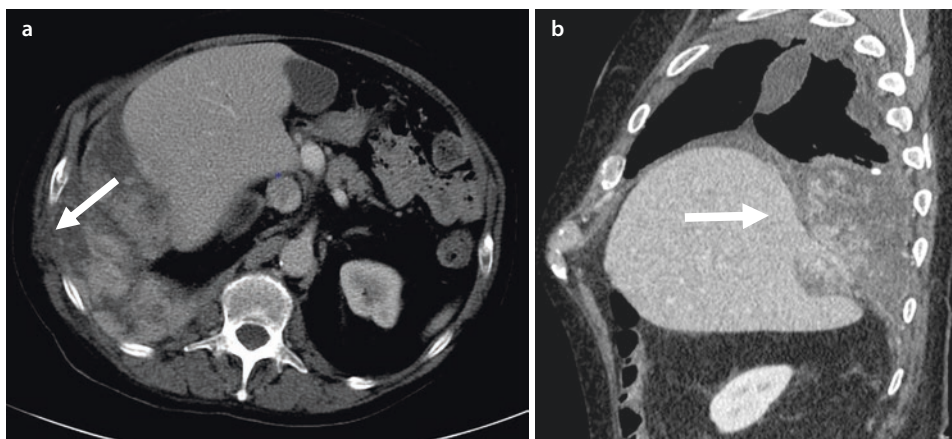


Fig. 8.15 Chest wall invasion and diaphragmatic infiltration in a 67-year-old man with a history of malignant solitary fibrous tumor of the pleura. Both axial **a** and sagittal **b** CT images show an ill-defined, right-sided

pleural mass with heterogeneous contrast enhancement. This mass infiltrates the chest wall **a**, the diaphragm, and the liver **b**

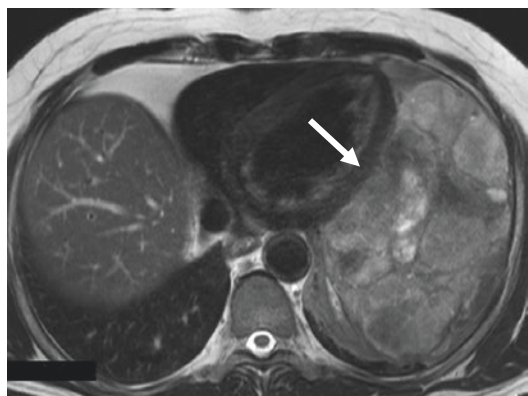


Fig. 8.16 Giant malignant solitary fibrous tumor of the pleura in a 65-year-old man. T₂-weighted MRI image shows a heterogeneous basal pleural mass with cystic and necrotic areas (arrow)

FDG-PET/CTs might be suitable for the detection of local recurrence and distant metastases after surgery in patients with malignant SFTP [89, 94].

8.5.4 Local Recurrence and Distant Spread

Malignant SFTPs can either locally recur or metastasize after surgical resection (63%) [80, 97]. The risk of recurrence is fairly high after resection of malignant sessile SFTPs [85]. Disease recurrence usually occurs in the same hemithorax. Chest wall involvement, manifest-

ing as sclerosis or erosion of adjacent ribs, is a rare manifestation of disease recurrence. Either mediastinal compression or vena cava obstruction secondary to disease recurrence is associated with a poor prognosis and may lead patients to death before distant dissemination [98]. Distant metastases have been reported in the liver, central nervous system, spleen, peritoneum, adrenal gland, gastrointestinal tract, kidney, and bone [85].

8.6 Primary Pleural Lymphoma

8.6.1 Overview

Primary pleural lymphoma is a rare entity, representing about 7% of all primary lymphomas [6, 99, 100].

Primary effusion lymphoma (PEL) is an aggressive and uncommon NHL that grows exclusively or predominantly in the serous body cavities, including the pleural cavity. It usually presents with unilateral pleural effusion (frequently exudative and bloody) without lymphadenopathy or any recognizable solid masses [6, 16, 100] (Fig. 8.17). Splenomegaly and hepatomegaly might be present [101]. PEL is strongly associated with human herpesvirus 8 (HHV-8) infection and occurs in immunocompromised subjects, more commonly human immunodeficiency virus (HIV)-positive ones, accounting for approximately 4% of all HIV-related NHL [102].

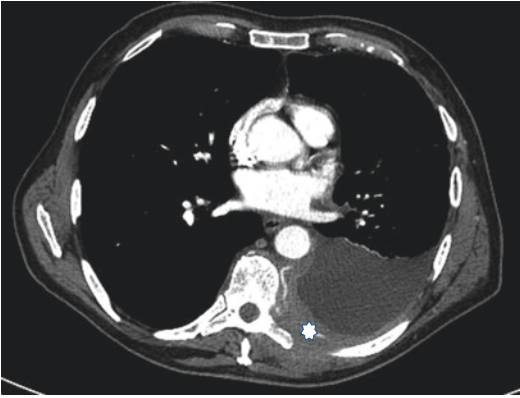


Fig. 8.17 Pleural effusion lymphoma in a 53-year-old man. Axial CT image shows a left pleural effusion associated with a soft tissue component that seems to infiltrate both pleura and chest wall (asterisk)

Diffuse large B-cell lymphoma associated with chronic inflammation (DLBCL-CI) is an extremely rare Epstein-Barr (EBV)-associated NHL that usually affects male adults (median age of 65 years) in the context of long-standing inflammation [77]. More often, DLBCL-CI develops in subjects with a history of pyothorax due to either artificial pneumothorax for the treatment of tuberculosis or chronic tuberculous pleuritis [16, 100].

Given the rarity of PEL, no therapeutic guidelines are currently available. Although CHOP remains the first therapeutic option, the combination of chemotherapy with antiviral therapies seems to improve the prognosis [102]. According to recent evidences, EBV-positive DLBCL benefit from a combination of CHOP with immunotherapy, even if a higher response is observed in EBV-negative DLBCL [103].

Median survival after diagnosis is <1 year in both cases, whereas the 5-year overall survival is approximately 20% [101, 102, 104].

8.6.2 Pathology

PEL cells are immunoblastic, plasmablastic, or anaplastic in origin. Immunohistochemistry and viral analyses are both required to make the definitive diagnosis. Pleural biopsies might show malignant cells embedded in fibrin attached to the pleural surface [102]. Macroscopically, DLBCL-CI shows firm and tan-colored pleural thickening, whereas microscopically, it consists of rich aggregations of centroblastic or immunoblas-

tic cells. Exuberant apoptosis may be observed within areas of extensive necrosis [77].

8.6.3 Imaging

PEL presents with pleural effusion, often associated with pleural and/or pericardial thickening on both CXR and CT. DLBCL-CI is more commonly characterized by pleural soft tissue masses without effusion [100]. When DLBCL is due to chronic pyothorax, CT might show pleural masses adjacent to a coexistent empyema cavity and pleural calcifications [105]. Enhanced MRI scan may be helpful to distinguish DLBCL-CI from empyema, as the latter does not have the same degree of contrast enhancement [6]. Other MRI features include significant restriction of water diffusion in functional analysis [36].

Up to date, no studies have investigated the applicability of TUS in the management of pleural lymphoma. Nonetheless, few studies have demonstrated the ability of expert radiologists to predict malignancy in a controlled population with pleural effusion by means of TUS [106]. These evidences could lead to a larger applicability of TUS in the diagnosis of PEL. Pleural lymphoma, however, does not show peculiar imaging features, being often indistinguishable from other malignancies and benign pleural diseases [100].

8.6.4 Lymph Node Involvement

In NHL, thoracic LN involvement is observed in up to 45% of cases [107]. Generally, the paratracheal and anterior mediastinal nodes are the most common sites of involvement, followed by the subcarinal, hilar, posterior mediastinal (para-aortic, paravertebral, and retrocrural), and pericardial ones. Primary pleural disease, however, is more likely to involve posterior mediastinal nodes [107]. Pericardial and internal mammary LNs are common sites of recurrence, as usually excluded from the radiation field [107].

8.7 Other Primary Pleural Tumors

8.7.1 Overview

According to the newest WHO classification, primary pleural neoplasms include also *well-differentiated papillary mesothelioma* and *ade-*

nomatoid tumor, both mesothelial in origin, and *epithelioid hemangioendothelioma*, *angiosarcoma*, *synovial sarcoma*, *desmoid-type fibromatosis*, *calcifying fibrous tumor*, and *desmoplastic round cell tumor*, which are of mesenchymal nature [2]. Some of these tumors are extremely rare [31]. Their main features are summarized in Table 8.3.

Table 8.3 Summary of the rarest primary pleural neoplasms, as per 2015 WHO classification

Tumor	Epidemiology	Pathology	Imaging	Prognosis
<i>Well-differentiated papillary mesothelioma</i> Low malignant potential	Mean age of 60 years No sex predilection	Broad papillae with fibrovascular cores, lined by a single layer of flat to cuboidal mesothelial cells	Diffuse nodular lesions (from few mm to some cm in size)	Good (especially for small lesion and in case of complete excision)
<i>Adenomatoid tumor</i> Benign	Usually involves the genital tract	Vacuolated epithelioid mesothelial cells, organized in tubular spaces	Small, solitary, and well-defined pleural lesion	Good
<i>Epithelioid hemangioendothelioma</i> Malignant (vascular differentiation)	Males from 30 to 50 years	Cords, strands, and nests of epithelioid cells in a myxohyaline or sclerotic stroma	Diffuse pleural involvement similar to diffuse MPM	Local progression and distant metastases (lung, liver, and regional LNs)
<i>Angiosarcoma</i> Malignant (vascular differentiation)	Males from 20 to 80 years	Sheets of large anaplastic epithelioid cells, with abundant eosinophilic cytoplasm	Pneumothorax or hemothorax, with or without pleural thickening	Poor Rapid progression
<i>Synovial sarcoma</i> Malignant	Median age of 40 years with no sex predilection	Sheets or vague fascicles of spindle cells. Staghorn vasculature is frequently observed. Infiltrating mast cells can be abundant. Stromal calcifications can be seen	Localized and large solid masses, often pedunculated (rarely diffuse pleural lesions) Common lung involvement	Poor (median survival of 2 years)
<i>Desmoid-type fibromatosis</i> Low malignant potential	Adults with no sex predilection	Bland and uniform spindle cells arranged in fascicles. Myxoid stromal changes can occur	Large and ill-defined masses that infiltrate the soft tissue of the chest wall	Local recurrence, but no metastatic potential
<i>Calcifying fibrous tumor</i> Benign	Usually adult women (mean age of 34 years)	Abundant collagenous stroma and scant fibroblasts, lymphocytic aggregates, and focal dystrophic or psammomatous calcification	Single or multiple well-defined pleural lesions with calcifications	Good
<i>Desmoplastic round cell tumor</i> Malignant	Adolescents and young men	Well-defined nests of small round hyperchromatic cells with vascularized stromal desmoplasia. Mitosis and central necrosis are common	Pleural effusion	Poor (median survival of 2 years)

8.7.2 Patterns of Metastatic Dissemination

Pleural epithelioid hemangioendothelioma (PEH) and *pleural angiosarcoma* are rare malignant vascular neoplasms, with a tendency for local recurrence and metastatic spread. PEH distant metastases have been reported in the lungs, liver, LNs, bone, and skin. PEH lacks distinctive imaging features, and diagnosis entirely relies on histology [108]. PEH-related diffuse pleural involvement mimics diffuse MPM, whereas pleural angiosarcoma usually manifests with pneumothorax or hemothorax, with or without pleural thickening [16, 108].

Synovial sarcoma is an aggressive tumor of uncertain histogenesis [16]. A concurrent involvement of the underlying lung parenchyma is common, whereas LN metastases are rare. The tumor can recur and metastasizes to the liver, bone, lung, and brain in approximately 20% of cases [109].

Desmoplastic round cell tumor, which usually arises from abdominal tissues such as retroperitoneum, mesentery, omentum, pelvis, and paratesticular regions, is an extremely rare and aggressive tumor [31]. Only a handful of cases have been described. Distant metastases are already present at the time of the diagnosis in the vast majority of the cases. Unlike the aforementioned neoplasms, *desmoid-type fibromatosis* is locally aggressive without a metastatic potential. Local recurrence occurs in approximately 25% of patients [16, 109].

References

- Mossman BT, Shukla A, Heintz NH, Verschraegen CF, Thomas A, Hassan R. New insights into understanding the mechanisms, pathogenesis, and management of malignant mesotheliomas. *Am J Pathol.* 2013;182:1065–77.
- Galateau-Salle F, Churg A, Roggli V, Travis WD. World Health Organization Committee for Tumors of the Pleura. The 2015 World Health Organization Classification of Tumors of the Pleura: Advances since the 2004 Classification. *J Thorac Oncol.* 2016;11:142–54.
- Nickell LT Jr, Lichtenberger JP 3rd, Khorashadi L, Abbott GF, Carter BW. Multimodality imaging for characterization, classification, and staging of malignant pleural mesothelioma. *Radiographics.* 2014;34:1692–706.
- Opitz I. Management of malignant pleural mesothelioma-The European experience. *J Thorac Dis.* 2014;6 Suppl 2:S238–52.
- Bibby AC, Tsim S, Kanellakis N, Ball H, Talbot DC, Blyth KG, Maskell NA, Psallidas I. Malignant pleural mesothelioma: an update on investigation, diagnosis and treatment. *Eur Respir Rev.* 2016;25:472–86.
- Carter BW, Betancourt SL, Shroff GS, Lichtenberger JP 3rd. MR imaging of pleural neoplasms. *Top Magn Reson Imaging.* 2018;27:73–82.
- Liu B, van Gerwen M, Bonassi S, Taioli E. Epidemiology of environmental exposure and malignant mesothelioma. *J Thorac Oncol.* 2017;12:1031–45.
- Rossini M, Rizzo P, Bononi I, Clementz A, Ferrari R, Martini F, Tognon MG. New perspectives on diagnosis and therapy of malignant pleural mesothelioma. *Front Oncol.* 2018;8:91.
- Wu L, Dell'Anno I, Lapidot M, Sekido Y, Chan M-L, Kohno M, Serre-Beinier V, Felley-Bosco E, de Perrot M. Progress of malignant mesothelioma research in basic science: a review of the 14th international conference of the international mesothelioma interest group (iMig2018). *Lung Cancer.* 2019;127:138–45.
- Kato K, Gemba K, Fujimoto N, Aoe K, Takeshima Y, Inai K, Kishimoto T. Pleural irregularities and mediastinal pleural involvement in early stages of malignant pleural mesothelioma and benign asbestos pleural effusion. *Eur J Radiol.* 2016;85:1594–600.
- Gemba K, Fujimoto N, Kato K, Aoe K, Takeshima Y, Inai K, Kishimoto T. National survey of malignant mesothelioma and asbestos exposure in Japan. *Cancer Sci.* 2012;103:483–90.
- Røe OD, Stella GM. Malignant pleural mesothelioma: history, controversy and future of a manmade epidemic. *Eur Respir Rev.* 2015;24:115–31.
- Chang ET, Lau EC, Mowat FS, Teta MJ. Therapeutic radiation for lymphoma and risk of second primary malignant mesothelioma. *Cancer Causes Control.* 2017;28:971–9.
- Marinaccio A, Corfiati M, Binazzi A, Di Marzio D, Scarselli A, Ferrante P, Bonafede M, Verardo M, Mirabelli D, Gennaro V, Mensi C, Schallemborg G, Mazzoleni G, Merler E, Girardi P, Negro C, D'Agostin F, Romanelli A, Chellini E, Silvestri S, Pascucci C, Calisti R, Stracci F, Romeo E, Ascoli V, Trafficante L, Carrozza F, Angelillo IF, Cavone D, Cauzillo G, Tallarigo F, Tumino R, Melis M, Iavicoli S, ReNaM Working Group. The epidemiology of malignant mesothelioma in women: gender differences and modalities of asbestos exposure. *Occup Environ Med.* 2018;75:254–62.
- De Rienzo A, Archer MA, Yeap BY, Dao N, Sciaranghella D, Sideris AC, Zheng Y, Holman AG, Wang YE, Dal Cin PS, Fletcher JA, Rubio R, Croft L, Quackenbush J, Sugarbaker PE, Munir KJ, Battilana JR, Gustafson CE, Chirieac LR, Ching SM, Wong J, Tay LC, Rudd S, Hercus R, Sugarbaker DJ, Richards WG, Bueno R. Gender-specific molecular and clinical features underlie malignant pleural mesothelioma. *Cancer Res.* 2016;76:319–28.

16. Ali G, Bruno R, Fontanini G. The pathological and molecular diagnosis of malignant pleural mesothelioma: a literature review. *J Thorac Dis.* 2018;10: S276–84.
17. Nind NR, Attanoos RL, Gibbs AR. Unusual intraparenchymal growth patterns of malignant pleural mesothelioma. *Histopathology.* 2003;42:150–5.
18. Escalon JG, Harrington KA, Plodkowski AJ, Zheng J, Capanu M, Zauderer MG, Rusch VW, Ginsberg MS. Malignant pleural mesothelioma: are there imaging characteristics associated with different histologic subtypes on computed tomography? *J Comput Assist Tomogr.* 2018;42:601–6.
19. Karpathiou G, Stefanou D, Froudarakis ME. Pleural neoplastic pathology. *Respir Med.* 2015;109:931–43.
20. Parker C, Neville E. Lung cancer * 8: management of malignant mesothelioma. *Thorax.* 2003;58:809–13.
21. Sahin N, Akatli AN, Celik MR, Ulutas H, Samdanci ET, Colak C. The role of CD90 in the differential diagnosis of pleural malignant mesothelioma, pulmonary carcinoma and comparison with calretinin. *Pathol Oncol Res.* 2017;23:487–91.
22. Husain AN, Colby T, Ordonez N, Krausz T, Attanoos R, Beasley MB, Borczuk AC, Butnor K, Cagle PT, Chirieac LR, Churg A, Dacic S, Fraire A, Galateau-Salle F, Gibbs A, Gown A, Hammar S, Litzky L, Marchevsky AM, Nicholson AG, Roggli V, Travis WD, Wick M, International Mesothelioma Interest Group. Guidelines for pathologic diagnosis of malignant mesothelioma: 2012 update of the consensus statement from the International Mesothelioma Interest Group. *Arch Pathol Lab Med.* 2013;137:647–67.
23. Mann S, Khawar S, Moran C, Kalhor N. Revisiting localized malignant mesothelioma. *Ann Diagn Pathol.* 2019;39:74–7.
24. Yao W, Yang H, Huang G, Yan Y, Wang H, Sun D. Massive localized malignant pleural mesothelioma (LMPM): manifestations on computed tomography in 6 cases. *Int J Clin Exp Med.* 2015;8:18367–74.
25. Hino T, Kamitani T, Sagiyama K, Yamasaki Y, Okamoto I, Tagawa T, Ijichi K, Yamamoto H, Yabuuchi H, Honda H. Localized malignant pleural mesothelioma mimicking an anterior mediastinal tumor. *Eur J Radiol Open.* 2019;6:72–7.
26. Kim K-C, Vo H-P. Localized malignant pleural sarcomatoid mesothelioma misdiagnosed as benign localized fibrous tumor. *J Thorac Dis.* 2016;8: E379–84.
27. Berzenji L, Van Schil PE, Carp L. The eighth TNM classification for malignant pleural mesothelioma. *Transl Lung Cancer Res.* 2018;7:543–9.
28. Qureshi NR, Rahman NM, Gleeson FV. Thoracic ultrasound in the diagnosis of malignant pleural effusion. *Thorax.* 2009;64:139–43.
29. Falaschi F, Romei C, Fiorini S, Lucchi M. Imaging of malignant pleural mesothelioma: it is possible a screening or early diagnosis program? – a systematic review about the use of screening programs in a population of asbestos exposed workers. *J Thorac Dis.* 2018;10:S262–8.
30. Wang ZJ, Reddy GP, Gotway MB, Higgins CB, Jablons DM, Ramaswamy M, Hawkins RA, Webb WR. Malignant pleural mesothelioma: evaluation with CT, MR imaging, and PET. *Radiographics.* 2004;24:105–19.
31. Jeong YJ, Kim S, Kwak SW, Lee NK, Lee JW, Kim KI, Choi KU, Jeon TY. Neoplastic and nonneoplastic conditions of serosal membrane origin: CT findings. *Radiographics.* 2008;28:801–17; discussion 817–8; quiz 912.
32. Bonomi M, De Filippis C, Lopci E, Gianoncelli L, Rizzardi G, Cerchiaro E, Bortolotti L, Zanello A, Ceresoli GL. Clinical staging of malignant pleural mesothelioma: current perspectives. *Lung Cancer.* 2017;8:127–39.
33. Hallifax RJ, Talwar A, Wrightson JM, Edey A, Gleeson FV. State-of-the-art: radiological investigation of pleural disease. *Respir Med.* 2017;124:88–99.
34. Kim YK, Kim JS, Lee KW, Yi CA, Goo JM, Jung S-H. Multidetector CT findings and differential diagnoses of malignant pleural mesothelioma and metastatic pleural diseases in Korea. *Korean J Radiol.* 2016;17: 545–53.
35. Metintas M, Ucgun I, Elbek O, Erginel S, Metintas S, Kolsuz M, Harmanci E, Alatas F, Hillerdal G, Ozkan R, Kaya T. Computed tomography features in malignant pleural mesothelioma and other commonly seen pleural diseases. *Eur J Radiol.* 2002;41:1–9.
36. Pessôa FMC, de Melo ASA, Souza AS Jr, de Souza LS, Hochegger B, Zanetti G, Marchiori E. Applications of magnetic resonance imaging of the thorax in pleural diseases: a state-of-the-art review. *Lung.* 2016;194:501–9.
37. Gill RR, Gerbaudo VH, Jacobson FL, Trotman-Dickenson B, Matsuoka S, Hunsaker A, Sugarbaker DJ, Hatabu H. MR imaging of benign and malignant pleural disease. *Magn Reson Imaging Clin N Am.* 2008;16: 319–39, x.
38. Pena E, Ojiaku M, Inacio JR, Gupta A, Macdonald DB, Shabana W, Seely JM, Rybicki FJ, Dennie C, Thornhill RE. Can CT and MR shape and textural features differentiate benign versus malignant pleural lesions? *Acad Radiol.* 2017;24:1277–87.
39. Coolen J, De Keyzer F, Naftoux P, De Wever W, Dooms C, Vansteenkiste J, Roebben I, Verbeken E, De Leyn P, Van Raemdonck D, Nackaerts K, Dymarkowski S, Verschakelen J. Malignant pleural disease: diagnosis by using diffusion-weighted and dynamic contrast-enhanced MR imaging-initial experience. *Radiology.* 2012;263(3):884–92.
40. Gill RR, Umeoka S, Mamata H, Tilleman TR, Stanwell P, Woodhams R, Padera RF, Sugarbaker DJ, Hatabu H. Diffusion-weighted MRI of malignant pleural mesothelioma: preliminary assessment of apparent diffusion coefficient in histologic subtypes. *AJR Am J Roentgenol.* 2010;195(2):W125–30.
41. Armato SG 3rd, Blyth KG, Keating JJ, Katz S, Tsim S, Coolen J, Gudmundsson E, Opitz I, Nowak AK. Imaging in pleural mesothelioma: a review of the 13th International Conference of the International Mesothelioma Interest Group. *Lung Cancer.* 2016;101:48–58.
42. Patel AM, Berger I, Wileyto EP, Khalid U, Torigian DA, Nachiappan AC, Barbosa EM Jr, Gefter WB, Galperin-Aizenberg M, Gupta NK, Simone CB 2nd, Haas AR, Alley EW, Singhal S, Cengel KA, Katz SI. The value of delayed phase enhanced imaging in malignant pleural mesothelioma. *J Thorac Dis.* 2017;9:2344–9.

43. Armato SG 3rd, Francis RJ, Katz SI, Ak G, Opitz I, Gudmundsson E, Blyth KG, Gupta A. Imaging in pleural mesothelioma: a review of the 14th International Conference of the International Mesothelioma Interest Group. *Lung Cancer*. 2019;130:108–14.
44. Vivoda Tomšič M, Bisdas S, Kovač V, Serša I, Šurlan Popovič K. Dynamic contrast-enhanced MRI of malignant pleural mesothelioma: a comparative study of pharmacokinetic models and correlation with mRECIST criteria. *Cancer Imaging*. 2019;19:10.
45. Gudmundsson E, Labby Z, Straus CM, Sensakovic WF, Li F, Rose B, Cunliffe A, Kindler HL, Armato SG 3rd. Dynamic contrast-enhanced CT for the assessment of tumour response in malignant pleural mesothelioma: a pilot study. *Eur Radiol*. 2019;29:682–8.
46. Armato SG, Nowak AK. Revised modified response evaluation criteria in solid tumors for assessment of response in malignant pleural mesothelioma (version 1.1). *J Thorac Oncol*. 2018;13:1012–21.
47. Murphy DJ, Mak SM, Mallia A, Jeljeli S, Stirling JJ, Goh V, Bille A, Cook GJR. Loco-regional staging of malignant pleural mesothelioma by integrated 18F-FDG PET/MRI. *Eur J Radiol*. 2019;115:46–52.
48. Kitajima K, Doi H, Kuribayashi K. Present and future roles of FDG-PET/CT imaging in the management of malignant pleural mesothelioma. *Jpn J Radiol*. 2016;34:537–47.
49. Tan C, Barrington S, Rankin S, Landau D, Pilling J, Spicer J, Cane P, Lang-Lazdunski L. Role of integrated 18-fluorodeoxyglucose position emission tomography-computed tomography in patients surveillance after multimodality therapy of malignant pleural mesothelioma. *J Thorac Oncol*. Elsevier; 2010;5:385–8.
50. Rusch VW, Giroux D, Kennedy C, Ruffini E, Cangir AK, Rice D, Pass H, Asamura H, Waller D, Edwards J, Weder W, Hoffmann H, van Meerbeeck JP, IASLC Staging Committee. Initial analysis of the international association for the study of lung cancer mesothelioma database. *J Thorac Oncol*. 2012;7:1631–9.
51. Gomez DR, Rimmer A, Simone CB, John Cho BC, de Perrot M, Adjei AA, Bueno R, Gill RR, Harpole DH Jr, Hestdorffer M, Hirsch FR, Jackson AA, Pass HI, Rice DC, Rusch VW, Tsao AS, Yorke E, Rosenzweig K. The use of radiation therapy for the treatment of malignant pleural mesothelioma: expert opinion from the National Cancer Institute Thoracic Malignancy Steering Committee, International Association for the Study of Lung Cancer, and Mesothelioma Applied Research Foundation. *J Thorac Oncol*. 2019;14:1172–83.
52. Miyazaki T, Yamasaki N, Tsuchiya T, Matsumoto K, Kamohara R, Hatachi G, Nagayasu T. Is pleurectomy/decortication superior to extrapleural pneumonectomy for patients with malignant pleural mesothelioma? A single-institutional experience. *Ann Thorac Cardiovasc Surg*. 2018;24:81–8.
53. Verma V, Ahern CA, Berlind CG, Lindsay WD, Sharma S, Shabason J, Culligan MJ, Grover S, Friedberg JS, Simone CB 2nd. National cancer database report on pneumonectomy versus lung-sparing surgery for malignant pleural mesothelioma. *J Thorac Oncol*. 2017;12:1704–14.
54. Odisio EG, Marom EM, Shroff GS, Wu CC, Benveniste APA, Truong MT, Benveniste MF. Malignant pleural mesothelioma: diagnosis, staging, pitfalls and follow-up. *Semin Ultrasound CT MR*. 2017;38:559–70.
55. Murthy V, Katzman D, Sterman DH. Intrapleural immunotherapy: an update on emerging treatment strategies for pleural malignancy. *Clin Respir J*. 2019;13:272–9.
56. Cramer G, Simone CB 2nd, Busch TM, Cengel KA. Adjuvant, neoadjuvant, and definitive radiation therapy for malignant pleural mesothelioma. *J Thorac Dis*. 2018;10:S2565–73.
57. Taioli E, Wolf AS, Camacho-Rivera M, Flores RM. Women with malignant pleural mesothelioma have a three-fold better survival rate than men. *Ann Thorac Surg*. 2014;98:1020–4.
58. van Gerwen M, Alpert N, Wolf A, Ohri N, Lewis E, Rosenzweig KE, Flores R, Taioli E. Prognostic factors of survival in patients with malignant pleural mesothelioma; an analysis of the National Cancer Data Base. *Carcinogenesis*. 2019;40(4):529–36.
59. Finn RS, Brims FJH, Gandhi A, Olsen N, Musk AW, Maskell NA, Lee YCG. Postmortem findings of malignant pleural mesothelioma: a two-center study of 318 patients. *Chest*. 2012;142:1267–73.
60. Jayaranagaiah A, Kariyanna PT, Chidella NKS, Singh N, Green J, Salifu MO, McFarlane S. Malignant pleural mesothelioma presenting with cardiac tamponade- a rare case report and review of the literature. *Clin Case Rep Rev* 2018;4(5).
61. Marom EM, Erasmus JJ, Pass HI, Patz EF Jr. The role of imaging in malignant pleural mesothelioma. *Semin Oncol*. 2002;29:26–35.
62. Robinson BWS, Lake RA. Advances in malignant mesothelioma. *N Engl J Med*. Massachusetts Medical Society; 2005;353:1591–603.
63. Bergamin S, Tio M, Stevens MJ. Prophylactic procedure tract radiotherapy for malignant pleural mesothelioma: a systematic review and meta-analysis. *Clin Transl Radiat Oncol*. 2018;13:38–43.
64. Clive AO, Taylor H, Dobson L, Wilson P, de Winton E, Panakis N, Pepperell J, Howell T, Stewart SA, Penz E, Jordan N, Morley AJ, Zahan-Evans N, Smith S, Batchelor TJP, Marchbank A, Bishop L, Ionescu AA, Bayne M, Cooper S, Kerry A, Jenkins P, Toy E, Vigneswaran V, Gildersleve J, Ahmed M, McDonald F, Button M, Lewanski C, Comins C, Dakshinamoorthy M, Lee YCG, Rahman NM, Maskell NA. Prophylactic radiotherapy for the prevention of procedure-tract metastases after surgical and large-bore pleural procedures in malignant pleural mesothelioma (SMART): a multicentre, open-label, phase 3, randomised controlled trial. *Lancet Oncol*. 2016;17:1094–104.
65. Ideguchi R, Ashizawa K, Akashi S, Shindo M, Minami K, Fukuda T, Uetani M. Malignant pleural mesothelioma with marked lymphatic involvement: a report of two autopsy cases. *Case Rep Oncol Med*. 2017;2017: 6195898.
66. Berger I, Cengel KA, Simone CB 2nd, Alley EW, Roshkovan L, Haas AR, Patel AM, Khalid U, Culligan MJ, McNulty S, Singhal S, Friedberg JS, Katz SI. Lymphangitic carcinomatosis: a common radiographic

- manifestation of local failure following extended pleurectomy/decortication in patients with malignant pleural mesothelioma. *Lung Cancer*. 2019;132:94–8.
67. Okten F, Köksal D, Onal M, Özcan A, Simşek C, Ertürk H. Computed tomography findings in 66 patients with malignant pleural mesothelioma due to environmental exposure to asbestos. *Clin Imaging*. 2006;30:177–80.
 68. Wu H, Tino G, Gannon FH, Kaiser LR, Pietra GG. Lepidic intrapulmonary growth of malignant mesothelioma presenting as recurrent hydropneumothorax. *Hum Pathol*. 1996;27:989–92.
 69. Rice D, Chansky K, Nowak A, Pass H, Kindler H, Shemanski L, Opitz I, Call S, Hasegawa S, Kernstine K, Atinkaya C, Rea F, Nafteux P, Rusch VW. Mesothelioma Domain of the IASLC Staging and Prognostic Factors Committee, advisory boards and participating institutions. The IASLC mesothelioma staging project: proposals for revisions of the N descriptors in the forthcoming eighth edition of the TNM classification for pleural mesothelioma. *J Thorac Oncol*. Elsevier; 2016;11:2100–11.
 70. Seely JM, Nguyen ET, Churg AM, Müller NL. Malignant pleural mesothelioma: computed tomography and correlation with histology. *Eur J Radiol*. 2009;70:485–91.
 71. Schouwink JH, Kool LS, Rutgers EJ, Zoetmulder FAN, van Zandwijk N, v d Vijver MJ, Baas P. The value of chest computer tomography and cervical mediastinoscopy in the preoperative assessment of patients with malignant pleural mesothelioma. *Ann Thorac Surg*. 2003;75:1715–8; discussion 1718–9.
 72. Ohno Y, Yui M, Aoyagi K, Kishida Y, Seki S, Koyama H, Yoshikawa T. Whole-body MRI: comparison of its capability for TNM staging of malignant pleural mesothelioma with that of coregistered PET/MRI, integrated FDG PET/CT, and conventional imaging. *AJR Am J Roentgenol*. 2019;212:311–9.
 73. Yamagishi T, Fujimoto N, Miyamoto Y, Asano M, Fuchimoto Y, Wada S, Kitamura K, Ozaki S, Nishi H, Kishimoto T. Brain metastases in malignant pleural mesothelioma. *Clin Exp Metastasis*. 2016;33:231–7.
 74. Lester T, Xu H. Malignant pleural mesothelioma with osseous metastases and pathologic fracture of femoral neck. *Appl Immunohistochem Mol Morphol*. 2008;16:507–9.
 75. Tanwar M, Simone CB 2nd, Newman S, Cengel K, Yu GH, Melhem ER, Mohan S. Perineural spread of malignant mesothelioma with spinal intramedullary involvement. *Clin Neurol Neurosurg*. 2014;120:116–9.
 76. Yao MJ, Ding L, Atay SM, Toubat O, Ebner P, David EA, McFadden PM, Kim AW. A modern reaffirmation of surgery as the optimal treatment for solitary fibrous tumors of the pleura. *Ann Thorac Surg*. 2019;107:941–6.
 77. Attanoos RL, Pugh MR. The diagnosis of pleural tumors other than mesothelioma. *Arch Pathol Lab Med*. 2018;142:902–13.
 78. Bishop AJ, Zagars GK, Demicco EG, Wang W-L, Feig BW, Guadagnolo BA. Soft tissue solitary fibrous tumor: combined surgery and radiation therapy results in excellent local control. *Am J Clin Oncol*. 2018;41:81–5.
 79. Song Z, Yang F, Zhang Y, Fan P, Liu G, Li C, Ding W, Zhang Y, Xu X, Ye Y. Surgical therapy and next-generation sequencing-based genetic alteration analysis of malignant solitary fibrous tumor of the pleura. *Onco Targets Ther*. 2018;11:5227–38.
 80. Liu CC, Wang HW, Li FY, Hsu PK, Huang MH, Hsu WH, Wang LS. Solitary fibrous tumors of the pleura: clinicopathological characteristics, immunohistochemical profiles, and surgical outcomes with long-term follow-up. *Thorac Cardiovasc Surg*. 2008;56:291–7.
 81. Hélage S, Revel MP, Chabi ML, Audureau É, Ferretti G, Laurent F, Alifano M, Mansuet-Lupo A, Buy JN, Vadrot D. Solitary fibrous tumor of the pleura: can computed tomography features help predict malignancy? A series of 56 patients with histopathological correlates. *Diagn Interv Imaging*. 2016;97:347–53.
 82. de Perrot M, Fischer S, Bründler MA, Sekine Y, Kes-havjee S. Solitary fibrous tumors of the pleura. *Ann Thorac Surg*. 2002;74(1):285–93.
 83. Erb CT, Johnson KM, Kim AW. Rare pleural tumors. *Clin Chest Med*. 2013;34:113–36.
 84. Ershadi R, Rahim M, Abbasi M, Erfanian R. Giant solitary fibrous tumor of the pleura. *J Surg Case Rep*. 2018;20188(11):rjy270.
 85. Abu Arab W. Solitary fibrous tumours of the pleura. *Eur J Cardiothorac Surg*. Narnia; 2012;41:587–97.
 86. Rosado-de-Christenson ML, Abbott GF, McAdams HP, Franks TJ, Galvin JR. From the archives of the AFIP: localized fibrous tumor of the pleura. *Radiographics*. 2003;23:759–83.
 87. Inaoka T, Takahashi K, Miyokawa N, Ohsaki Y, Aburano T. Solitary fibrous tumor of the pleura: apparent diffusion coefficient (ADC) value and ADC map to predict malignant transformation. *J Magn Reson Imaging*. 2007;26:155–8.
 88. Cardillo G, Carbone L, Carleo F, Masala N, Graziano P, Bray A, Martelli M. Solitary fibrous tumors of the pleura: an analysis of 110 patients treated in a single institution. *Ann Thorac Surg*. 2009;88:1632–7.
 89. Kohler M, Clarenbach CF, Kestenholz P, Kurrer M, Steinert HC, Russi EW, Weder W. Diagnosis, treatment and long-term outcome of solitary fibrous tumours of the pleura. *Eur J Cardiothorac Surg*. 2007;32:403–8.
 90. Robinson LA. Solitary fibrous tumor of the pleura. *Cancer Control*. 2006;13:264–9.
 91. Cortes J, Rodriguez J, Garcia-Velloso MJ, Rodriguez-Espiteri N, Boan JF, Castellano JM, Torre W. [(18)F]-FDG PET and localized fibrous mesothelioma. *Lung*. 2003;181:49–54.
 92. Shinya T, Masaoka Y, Sando M, Tanabe S, Okamoto S, Ihara H, Tanaka T, Otani S, Hiraki T, Kanazawa S. Imaging an intrapulmonary solitary fibrous tumor with CT and F-18 FDG PET/CT. *Radiol Case Rep*. 2019;14:755–8.
 93. Ginat DT, Bokhari A, Bhatt S, Dogra V. Imaging features of solitary fibrous tumors. *AJR Am J Roentgenol*. 2011;196:487–95.
 94. Tazeler Z, Tan G, Aslan A, Tan S. The utility of 18F-FDG PET/CT in solitary fibrous tumors of the pleura. *Rev Esp Med Nucl Imagen Mol*. 2016;35:165–70.

95. Yeom YK, Kim MY, Lee HJ, Kim SS. Solitary fibrous tumors of the pleura of the thorax: CT and FDG PET characteristics in a tertiary referral center. *Medicine*. 2015;94:e1548.
96. Chick JFB, Chauhan NR, Madan R. Solitary fibrous tumors of the thorax: nomenclature, epidemiology, radiologic and pathologic findings, differential diagnoses, and management. *AJR Am J Roentgenol*. 2013;200:W238–48.
97. Friis RB, Safwat A, Baad-Hansen T, Aggerholm-Pedersen N. Solitary fibrous tumour: a single institution retrospective study and further validation of a prognostic risk assessment system. *Clin Oncol*. 2018;30:798–804.
98. Arab WA. Solitary fibrous tumours of the pleura. *Eur J Cardiothorac Surg*. 2012;41:587–97.
99. Steiropoulos P, Kouliatsis G, Karpathiou G, Popidou M, Froudarakis ME. Rare cases of primary pleural Hodgkin and non-Hodgkin lymphomas. *Respiration*. 2009;77:459–63.
100. Bligh MP, Borgaonkar JN, Burrell SC, MacDonald DA, Manos D. Spectrum of CT findings in thoracic extranodal non-Hodgkin lymphoma. *Radiographics*. 2017;37:439–61.
101. Borie R, Wislez M, Antoine M, Cadranet J. Lymphoproliferative disorders of the lung. *Respiration*. 2017;94:157–75.
102. Arora N, Gupta A, Sadeghi N. Primary effusion lymphoma: current concepts and management. *Curr Opin Pulm Med*. 2017;23:365–70.
103. Castillo JJ, Beltran BE, Miranda RN, Young KH, Chavez JC, Sotomayor EM. EBV-positive diffuse large B-cell lymphoma, not otherwise specified: 2018 update on diagnosis, risk-stratification and management. *Am J Hematol*. 2018;93:953–62.
104. Nakatsuka S-I, Yao M, Hoshida Y, Yamamoto S, Iuchi K, Aozasa K. Pyothorax-associated lymphoma: a review of 106 cases. *J Clin Oncol*. 2002;20:4255–60.
105. Kligerman SJ, Franks TJ, Galvin JR. Primary extranodal lymphoma of the thorax. *Radiol Clin N Am*. 2016;54:673–87.
106. Bugalho A, Ferreira D, Dias SS, Schuhmann M, Branco JC, Marques Gomes MJ, Eberhardt R. The diagnostic value of transthoracic ultrasonographic features in predicting malignancy in undiagnosed pleural effusions: a prospective observational study. *Respiration*. 2014;87:270–8.
107. Sharma A, Fidas P, Hayman LA, Loomis SL, Taber KH, Aquino SL. Patterns of lymphadenopathy in thoracic malignancies. *Radiographics*. 2004;24:419–34.
108. Fan Y, Wang F, Li S, Ye C, Ying Y, Mao H. Pleural epithelioid hemangioendothelioma: a case report and literature review. *J Natl Med Assoc*. 2016;108:124–9.
109. Granville L, Laga AC, Allen TC, Dishop M, Roggli VL, Churg A, Zander DS, Cagle PT. Review and update of uncommon primary pleural tumors: a practical approach to diagnosis. *Arch Pathol Lab Med*. 2005;129:1428–43.



Tumors of the Chest Wall

*Elisa Baratella, Ilaria Fiorese, Sundeep M. Nayak,
and Stefano Lovadina*

- 9.1 Overview – 182**
 - 9.1.1 Epidemiology – 182
 - 9.1.2 Risk Factors – 182
 - 9.1.3 Diagnosis – 182
 - 9.1.4 Treatment – 194
 - 9.1.5 Prognosis – 197
- 9.2 Patterns of Local Spread – 198**
 - 9.2.1 Involvement of Adjacent Structures – 198
- 9.3 Lymph Node Involvement – 198**
 - 9.3.1 Lymphatic Drainage and Lymph Node Involvement – 198
- 9.4 Metastatic Spread – 198**
 - References – 198

9.1 Overview

Primary tumors of the chest wall are uncommon. Chest wall tumors, whether malignant or benign, are classified as primary or secondary (metastatic). The most common benign tumors are osteochondromas and chondromas. The most common malignant chest wall tumors are sarcomas.

Most primary tumors originate in the bones or muscles of the chest wall, though they can also arise from nerves and vessels. Less than half of malignant chest wall tumors are primary. Secondary tumors originate elsewhere in the body and spread (metastasize) to the chest wall. The most frequent secondary tumors of the chest wall spread from primary breast and lung cancer. In fact, they can either locally extend to the chest wall, or metastasize to it. Furthermore, other tumors that are not unfrequently spread to the pleura include those originating from ovary, kidney, uterus, head and neck, and testis. Therefore, almost all secondary tumors are malignant. Most chest wall tumors found in children are primary, while most found in adults are secondary [1, 2].

It is often difficult to make an accurate presurgical diagnosis and differentiate benign from malignant tumors. Most patients with primary chest wall tumor receive surgical biopsy or radical surgical resection [3].

9.1.1 Epidemiology

Primary chest wall tumors are rare and represent approximately 5% of all thoracic neoplasms [1, 4, 5]. The chest wall is composed of ten (10) layers which are, from superficial to deep, skin, superficial fascia, deep fascia, muscle (for example, serratus anterior, pectoralis major or minor, and latissimus dorsi), rib (including intercostal muscles, costal cartilage, and articulations), and endothoracic fascia. Benign and malignant tumors could arise in any of these layers [1, 6, 7].

It is practical to think of chest wall tumors as bone origin and non-bone origin. It is estimated that only 8% of primary bone tumors occur in the chest wall [8]. The most common primary malignant bony tumor histologies are, in order, chondrosarcoma, (35%), followed by solitary myeloma (25%), Ewing sarcoma (15%), osteosarcoma (15%), and lymphomas (10%) [3].

Symptomatic palpable lumps in the chest wall are more likely to be malignant. The clinical presentation of primary chest wall tumor is variable: chest wall tumors could manifest as painful and palpable lesions (80% of cases), or be asymptomatic (20%) and incidentally encountered on imaging acquired for unrelated reasons [3]. Symptoms when present could be related to chest wall invasion, such as chest pain or dyspnea, but some may also report nonspecific complaints like weight loss, fatigue, night sweats, and muscle aches [3, 8–10]. When present, symptoms are more often associated with malignant tumors [3, 11].

9.1.2 Risk Factors

Some predisposing risk factors for the development of chest wall tumors include immunosuppression therapy after organ transplantation, radiotherapy, AIDS (e.g., for leiomyosarcoma and lymphoma), Epstein-Barr virus (e.g., for leiomyosarcoma), chronic lymphedema and chemicals exposure (e.g., for angiosarcoma), radiation exposure (e.g., for malignant fibrous histiocytoma), bony lesions or Paget (e.g., for osteosarcoma) [12–14].

9.1.3 Diagnosis

A combination of clinical, radiological, and pathologic data is often required to make an accurate presurgical diagnosis. Although chest wall lesions may occasionally be detected on chest radiography, an imaging diagnosis is definitively made at both CT and MRI. CT is pivotal in determining the size of the lesion, its morphologic features, location, and invasion of the adjacent structures. The administration of intravenous iodinated or gadolinium-based contrast media assists in complete characterization of the tumor.

MRI helps characterize tissue composition and tumoral relationship with the adjacent structures, improving presurgical staging and perhaps in differentiation between nonaggressive and biologically aggressive chest wall tumors.

PET-CT has accuracy of 96% in staging patients with either sarcoma originating in bone and non-bone tissues.

However, definitive diagnosis requires a histologic evaluation through an excisional biopsy

(e.g., for tumors less than 5 cm in diameter), or an incisional biopsy (e.g., for larger lesions) [3].

9.1.3.1 Benign Tumors

Vascular Tumors

Cavernous Hemangioma

Cavernous hemangioma is typically in the skin layer and composed of dilated tortuous thin-walled vessels: it is not a true neoplasm but a vascular anomaly usually manifest before the age of 30 years [13].

At chest radiography, it appears as a soft-tissue mass with or without the erosion of the adjacent bones. Indeed, a speculated or sunburst appearance may be recognized [15].

At CT, the lesion content usually looks heterogeneous, due to the variable combination of neoplastic, fatty, fibrous, and vascular tissues. Cavernous hemangioma is characterized by the presence of phleboliths in 30% of cases [13].

Such a heterogeneity can be appreciated on MRI, which shows areas of high signal intensity on T1-weighted sequences due to fatty tissue within the mass. A high intensity signal is also characteristically present on T2-weighted images [3].

Intramuscular cavernous hemangioma is characterized by a signal like that of skeletal muscle on T1-weighted sequences, with linear hyperintense areas due to the presence of blood in the cavernous or cystic spaces (■ Fig. 9.1). If blood is present, a flow void can be seen on T2-weighted images, where the intramuscular cavernous hemangioma typically has a high intensity signal [13].

Glomus Tumor

Glomus tumor typically manifests in adulthood, with similar gender incidence rate. This tumor is generally painful due its tendency to erode the adjacent bones. The intramuscular location is frequent [13].

On MRI, the lesion is characterized by a heterogeneous signal due to its variable composition. The lesion may be circled by tortuous vessels and can displace the major vessels [13].

Langerhans Cell Histiocytosis

Langerhans cell histiocytosis may involve the bones of the chest wall. It accounts for 10–20% of benign tumors of the ribs. Its incidence is five times higher in males as compared to females. It usually manifests with pain, fever, and malaise [3].

The tumor characteristically destroys the cortex of the ribs, and new subperiosteal bone forma-

tion is typical [16]. These features can be easily seen on plain radiograph, which shows a lesion associated with an irregular cortex destruction and a subperiosteal reaction, thus mimicking malignancy or osteomyelitis [12].

Lymphangioma

Lymphangioma is a benign lymphomatous malformation that may be present at birth. At histology, it appears constituted of dilated lymphatic vessels. It is often located in the neck though it may also occur in the chest wall structures, particularly in pediatric subjects. When large in dimension, it can compress adjacent structures [3, 17]. In neonates, it can be easily detected with ultrasound where it appears as a multiloculated cystic mass [3].

On CT, most of lymphangiomas are homogeneous and cystic; sometimes the lesion can be inhomogeneous due to the presence of fluid, blood, fat, or proteinaceous components. Intralesional septa can be seldomly observed [18].

On MRI, the lesion displays a low signal intensity on T1-weighted sequences, and a high signal intensity (e.g., greater than that of fat) on T2-weighted sequences. After contrast administration, a thin and peripheral and septal enhancement is typical [17].

Osseous and Cartilaginous Tumors

Osteochondroma

Osteochondroma develops from an aberrant growth of normal tissue, typically arising from the metaphysis of the ribs. It represents 50% of all benign rib tumors and occurs in young subjects [17]. Pain is the most frequent symptom, though complications such as fractures, bone deformities and nerve compression, vascular injury, and malignant transformation may also occur.

It is characterized by cartilage-capped bony growth that projects from the surface of the affected bone.

On the chest radiograph, the tumor often appears as a pedunculated or sessile lesion in the metaphyseal regions of the long bones, with calcification of the cartilaginous cap. This feature appears more obvious on CT. Thus, osteochondroma appears as mineralized mass on CT. On MRI, the tumor shows an intermediate signal intensity on T1-weighted images, and the cartilaginous cap has a typical high intensity signal on T2-weighted sequences [12, 13, 17]. The cartilage

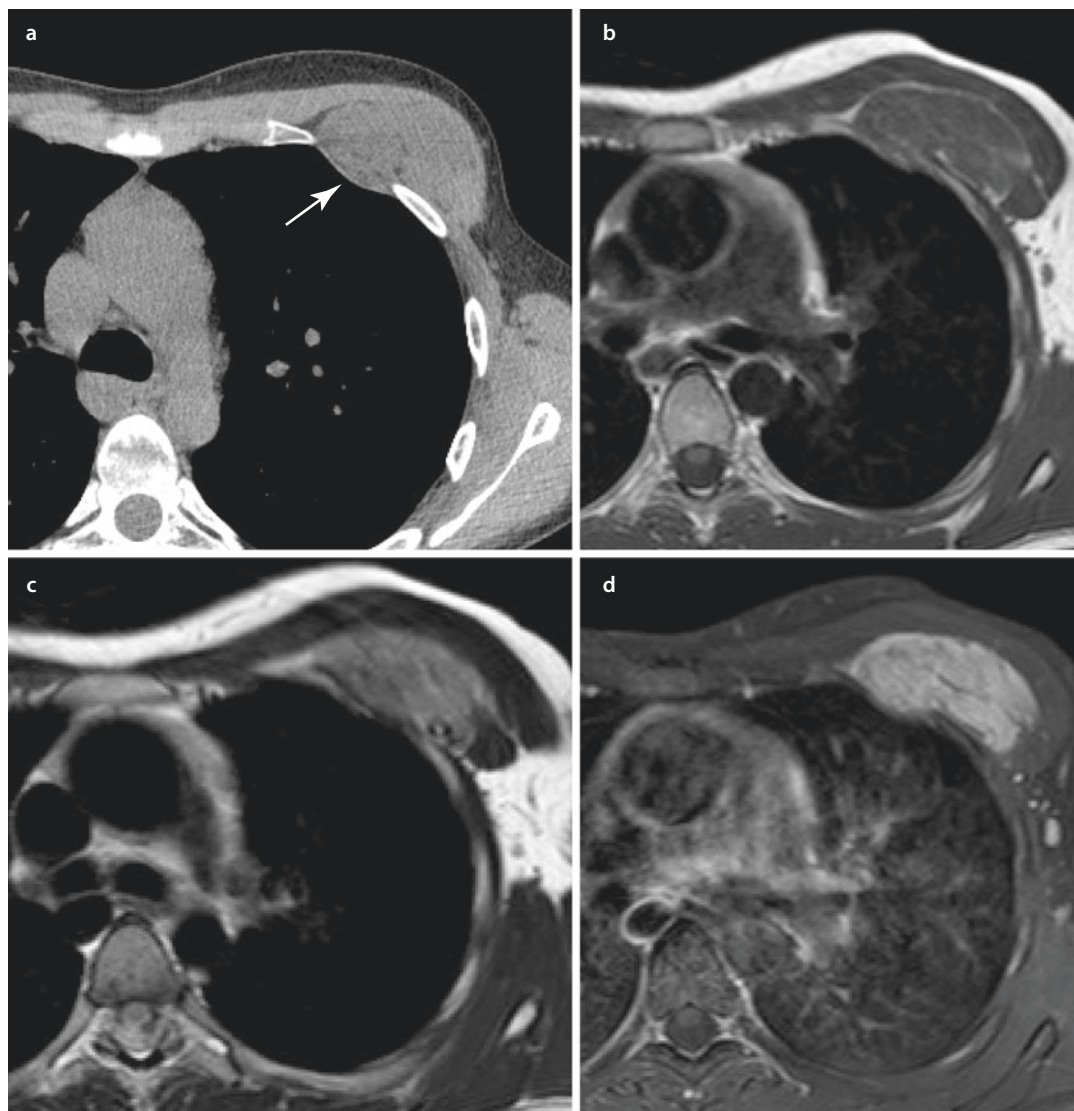


Fig. 9.1 Images courtesy of Department of Radiology, Gorizia's Hospital. Intramuscular cavernous hemangioma. (a) CT scan shows a soft tissue mass of the left anterior subpectoral chest wall (white arrow). (b, c) MRI shows that

it is isosignal to muscle on T1, b, and minimally hyperintense on T2-weighted imaging, c (d). After contrast media administration, fat-suppressed T1 image shows a homogenous moderate enhancement

cap thickness is a predictive factor of malignant transformation of the tumor. A cap exceeding 3 cm and 2 cm, in adults and children, respectively, is a sign predictive of malignant transformation into sarcoma [19].

Chondroma

This tumor constitutes 15–20% of benign chest wall lesions and is the most common benign tumor of the cartilage [3]. It typically manifests between 20 and 30 years of age, with an equal distribution among men and women. It is a slow

growing painless tumor that develops typically at the anterior costochondral junction. We speak of *enchondroma* when the chondroma arises from the medulla of the bone [17].

Chondroma manifests as a lytic area with sclerotic and well-defined margins on both chest radiograph and CT. At MRI, the tumor shows an intermediate to low signal intensity on T1-weighted images and a high signal intensity on T2-weighted ones, with a heterogeneous and variable enhancement after contrast media administration [12, 19].

Aneurysmal Bone Cyst

Aneurysmal bone cyst is a mass containing multiple blood-filled cysts lined by fibroblasts and giant cells of the osteoclast type [13]. A sclerotic margin usually surrounds the lesion. It typically manifests in patients younger than 30 years of age. Patients may present with pain, which may be of insidious onset or abrupt due to pathological fracture. Such features can make difficult the differential diagnosis with malignant tumors such as sarcoma. When located it develops in the chest wall and characteristically involves the posterior elements of the spine (e.g., articular processes, lamina and spinous processes).

At the chest radiograph, the aneurysmal bone cyst appears as an expansile osteolytic lesion, with well-defined margins. The bone cortex can appear either thinned or expanded [13]. CT demonstrates these findings to a greater degree. Furthermore, CT can show fluid-fluid levels consistent with hemorrhagic component that can be hardly appreciable on MRI. MRI shows a lobulated or septated mass, with an intermediate to low intensity signal on T1-weighted images and a heterogeneous high intensity signal on T2-weighted sequences. Either hemosiderin deposits or fibrosis appear as low intensity signal areas on T2-weighted images [12, 13, 19].

Fibrous Dysplasia of Bone

Fibrous dysplasia accounts for nearly 40% of benign chest wall lesion [3]. It is a developmental anomaly caused by the failure in morphologic differentiation and maturation of mesenchymal osteoblasts, resulting in fibrous tissue replacement within the bone [13]. Fibrous dysplasia is monostotic in approximately 80% of the cases, and polyostotic in the remainders. The latter subtype is more frequent in subjects of 20–30 years of age and may be part of the McCune-Albright syndrome [20].

Fibrous dysplasia is usually asymptomatic but can become painful when pathologic fractures supervene. Both ribs and clavicles are the most frequently involved bones [17].

The chest radiograph shows a fusiform enlargement and deformity of the bone, with a cortical thickening and increased trabeculation. Usually, the matrix of the lesion is smooth and relatively homogeneous, producing the so-called ground glass appearance. These features, along

with amorphous or irregular calcifications, are more clearly depicted by CT. MRI is useful to define the extent of the lesion. The signal intensity is variable: on T2-weighted images the intensity varies from low to high, while on T1-weighted images the signal is low [12, 13].

Ossifying Fibromyxoid Tumor

The origin of this tumor remains unknown. It preferentially involves the ribs and is constituted by fibrous stroma well vascularized that contains new bone trabeculation and multinucleated giant cells [13].

An intracortical bubble-shaped osteolytic area surrounded by a sclerotic band of tissue can be seen at the chest radiograph. On CT, ossifying fibromyxoid tumor manifests as an osteolytic bubble-shaped intracortical mass with sclerotic margins. On MRI, focal areas of high signal correspond to myxoid material on T2-weighted sequences. The tumor enhances after contrast media administration due to its high vascularization on MRI [13].

Giant Cell Tumor

Giant cell tumor, also known as osteoblastoma, is composed by vascular sinuses lined or filled with giant and spindle cells. It typically manifests in patients of 21–40 years of age, with a higher prevalence in women. It more frequently involves the subchondral region of sternum, clavicle, and the ribs. It may metastasize to the lung in 5% of cases [3].

The chest radiograph shows an eccentric osteolytic lesion. Surrounding sclerosis is not an established feature of the giant cell tumor.

CT is useful to better evaluate the cortical thinning and the relationship of the lesion with the surrounding structures (■ Fig. 9.2).

On MRI, the signal is characteristically of low intensity on T1-weighted images and high intensity on T2-weighted images [13].

Chondromyxoid Fibroma

Chondromyxoid fibroma is a rare tumor that typically affects older children and young adults.

The tumor comprises of a variable combination of chondroid, myxoid, and fibrous tissue components organized in a pseudo-lobulated architecture [3].

At the chest radiograph, it appears as a lytic lesion with well-delimited sclerotic borders. At

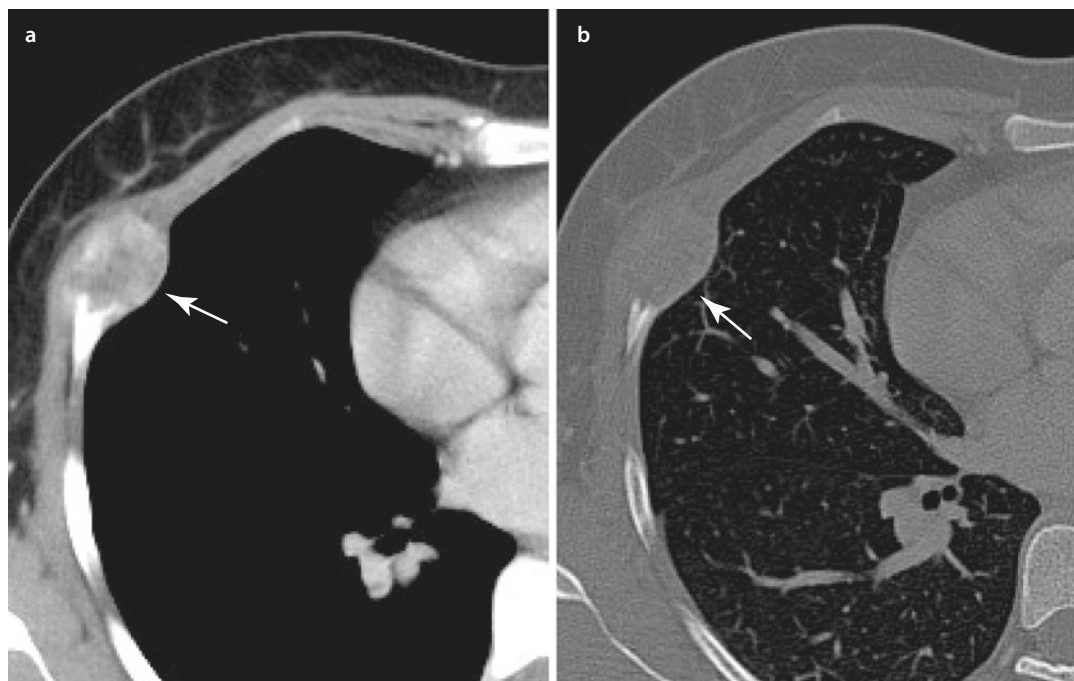


Fig. 9.2 Images courtesy of Department of Radiology, Gorizia's Hospital. Giant cell Tumor. (a, b) CT scan demon-

strates the presence of an expansile mass with internal ground glass matrix and cortical thinning (white arrow)

CT, it appears as a heterogeneous enhancing mass with lobulated margins, septations, and sclerotic rim. CT may better depict bone destruction. On MRI, chondromyxoid fibroma has a heterogeneous signal intensity on T2-weighted images and a diffuse enhancement on T1-weighted images after contrast media administration [13].

Osteoblastoma

Osteoblastoma is a rare tumor that typically manifests in patients of 20–30 years of age, with a slightly male predilection.

On both chest radiograph and CT, the lesion appears as an expansile osteolytic lesion with sclerotic margins, sometimes with intralesional calcifications.

On MRI, it shows an intermediate intensity signal, or a low intensity signal if calcifications are present, on both T1- and T2-weighted images. A high intensity signal rim due to the presence of edema around the soft tissue – also called “flare phenomenon” – may be seen. After contrast media administration, a strong enhancement is seen in either the lesion itself or in the surrounding tissue (■ Fig. 9.3) [19].

Chondroblastoma

Chondroblastoma is a rare benign tumor presenting in patients of 10–20 years of age. It typically originates from the costovertebral or costochondral junction of the ribs, or from the scapula. It usually causes joint swelling or tenderness. A well-defined lytic lesion with thin sclerotic margins is seen on both chest radiograph and CT.

On MRI, the areas of mineralization are of low signal intensity on T1-weighted images in a background of low intensity signal due to cartilage, while they appear as areas of low intensity signal in a background of high intensity signal due to cartilage on T2-weighted images. Fluid-fluid levels may be seen if aneurysmal bone cyst change occurs. Edema can be present in adjacent bone and soft tissue [19].

Adipose Tissue Tumors

Lipoma

Lipomas are masses of adipocytes very similar to normal fatty tissue, well circumscribed and encapsulated [3]. They occur in patients between 50 and 70 years of age, with a predilection for obese people. On X-ray, it appears as a radiolucent ovoid mass compared to other soft tissue

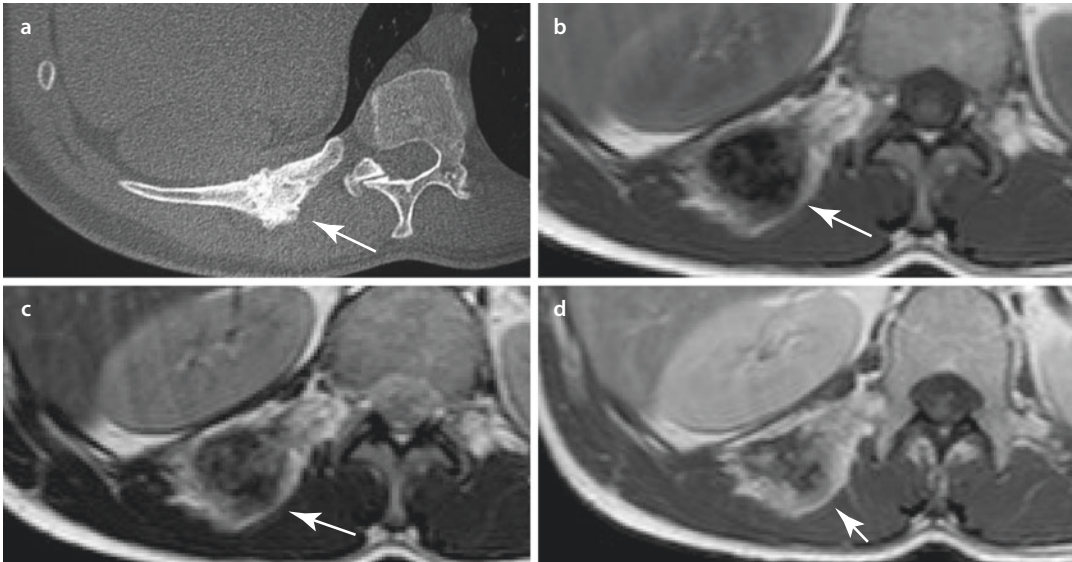


Fig. 9.3 Images courtesy of Department of Radiology, Gorizia's Hospital. Osteoblastoma. (a) CT scan shows an expansile sclerotic bone lesion of the posterior segment of a right rib (white arrow). (b, c) MRI images confirm the presence of a lesion with low intensity signal on T1- and

T2-weighted images due to the presence of calcifications and a high peripheral signal called "flare phenomenon" due to edema (arrow). (d) Post-contrast T1-weighted imaging shows enhancement in the periphery of the rib lesion and adjacent deep submuscular soft tissues

[15]. Both on CT and on MRI, lipomas are internally homogeneous, without enhancement after contrast media administration (▣ Fig. 9.4). Often multiple thin septa are present with a slight enhancement on CT and with signal suppression on fat-suppressed sequences on MRI [13]. In contrast, thickened internal septa and large size are both features that trigger the differential diagnosis with liposarcoma [21].

Spindle Cell Lipoma

It is a rare slow growing and painless tumor, due to the substitution of mature fat cells with collagen-forming spindle cells. It presents as a well-demarcated mass of 3–5 cm in subcutaneous tissue of the neck or shoulders, mostly in men older than 45 years of age. On MRI, both on T1- and T2-weighted images, it appears as a heterogeneous mass with a variable quantity of lipomatous and non-lipomatous components [13].

9.1.3.2 Malignant Tumors

Vascular Tumors

Angiosarcoma

Angiosarcoma is a malignant tumor originating from the vascular endothelium. It can be occasionally misdiagnosed as chronic hematomas, as it frequently presents as a painful, large, rapidly

growing mass. Sometimes it can be associated with hematologic disorders, such as anemia, or coagulopathy. In chest wall, it typically develops in the breast, sometimes following radiation therapy for breast carcinoma or in association with lymphedema.

MRI shows a heterogeneous mass, often associated with feeding vessels at its periphery. The mass enhances after contrast media administration. Other typical signs are fluid collections around the muscle, fibrous thickening, soft-tissue nodules, and increased attenuation in fatty tissue [14]. The prognosis is poor and only few patients are alive within 3 years after the diagnosis [22].

Osseous and Cartilaginous Tumors

Chondrosarcoma

Chondrosarcoma is the most common malignant primary tumor of the chest wall. The anterior part of the chest wall is more frequently involved, as the tumor arises from the costochondral arches (especially along the upper five ribs) or from the sternum in 60% of cases. As such, all tumors arising from the costal cartilages should be considered with suspicion of malignancy and treated with resection. In most of cases, chondrosarcoma occurs as a primary lesion, but can develop from preexisting benign tumors (e.g., chondroma or

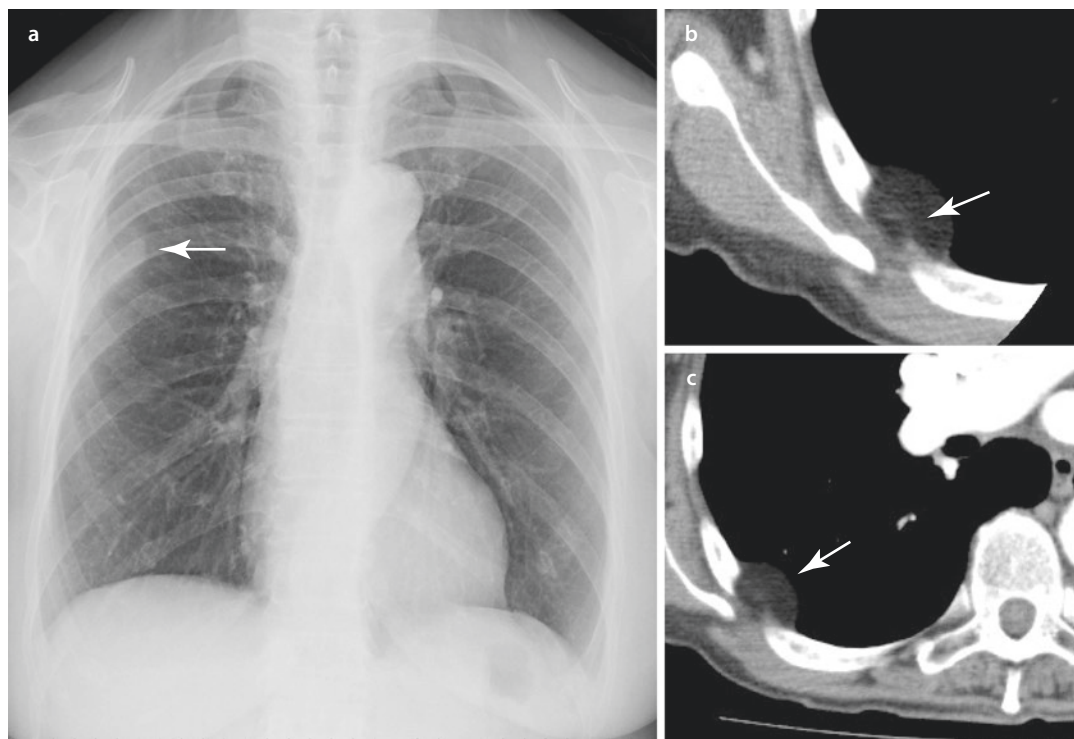


Fig. 9.4 Lipoma. (a) Chest X-ray shows asymmetric ill-defined opacity (white arrow) in the periphery of the right upper chest. (b) CT confirms the presence of

lipid-rich chest wall mass with an internal thin septum (white arrow), (c) with no post-contrast enhancement (white arrow)

osteochondroma) in 10% of cases [3, 12]. Lung metastases have been reported in nearly 10% of patients, and bone involvement may also be seen. It manifests with an incidence rate two times higher in men than in women and two peaks of age have been identified, respectively 20 and 50 years of age.

Chest radiographic features include endosteal scalloping, moth-eaten appearance with bone destruction, irregular contours, and intratumoral mineralization, with variable degree of calcification (e.g., rings and arcs, flocculent or stippled, or dense calcification).

On CT, chondrosarcoma manifests as a destructive low-attenuation mass of soft tissue. Calcification of the chondroid matrix may be characteristically appreciated on CT, though this may be also absent. A heterogeneous enhancement may be seen following contrast media (■ Fig. 9.5).

On MRI, T1-weighted images, the lesion shows a signal intensity like muscle, and a signal intensity rather than that of fat on T2-weighted images. After contrast media administration, the

enhancement is typically inhomogeneous, especially at the periphery [12, 14, 19].

The grade of the tumor, as well as an adequate surgical resection, seems the most important prognostic factors [23].

Osteosarcoma

Osteosarcoma represents 10–15% of malignant chest wall tumors. It can be either primary or secondary when arising from a preexisting bone lesion such as Paget disease, or after radiation therapy. It usually originates from the ribs, scapula, and clavicle [21].

It typically manifests as a painful and rapidly enlarging mass that tend to regionally recur after treatment or spreading to the lung or to the lymph nodes (in approximately 70% of cases). At diagnosis, most patients already have distant metastases. In fact, osteosarcoma is associated with a very poor prognosis [22].

The chest radiograph usually shows a mass with calcifications or with an osteoid bone matrix that can be lytic or sclerotic. A sunburst pattern is typical [12, 14].

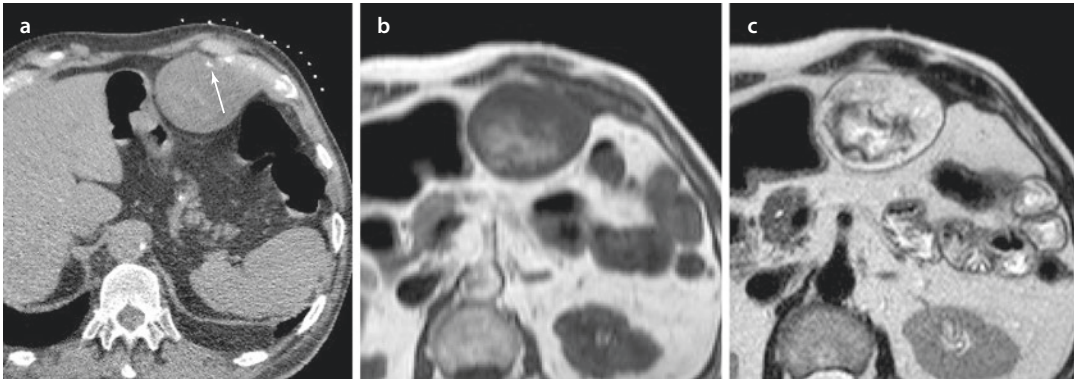


Fig. 9.5 Chondrosarcoma. (a) CT shows a well-circumscribed mass arising from the subcostal left inferior anterior chest wall, containing microcalcifications (arrow).

(b) MRI shows a mass with predominantly hypointense signal on T1-weighted image and (c) a heterogeneous hyperintense signal on T2-weighted MRI image

On CT, osteosarcoma appears as large mass including areas of mineralization that are more conspicuous in the center of the lesion. On CT, attenuation of the mass may look particularly heterogeneous due to the presence of areas of necrosis or hemorrhage [21].

On MRI, osteosarcoma shows a signal intensity greater than that of muscle on T1-weighted images, and a high signal intensity on T2-weighted sequences. Areas of mineralization have a low signal intensity both on T1- and T2-weighted sequences. Sometimes cystic components can be seen within the mass. A heterogeneous enhancement is also characteristic after contrast media administration [3, 12, 14, 19].

Osteosarcomas are usually high-grade tumors and combined treatment is required; despite this, they often metastasize, and survival is significantly lower as compared to other subgroups of primary malignant chest wall tumors [12, 14].

Adamantinoma

Adamantinoma accounts for 0.3–0.4% of all primary bone tumors, and it presents in patients with a mean of 30 years of age. It is a low-grade malignant tumor, arising from intraosseous epithelium. It is rarely found in the chest wall origin, where it more frequently arises from the ribs. It is constituted of solid cell nests, with variable proportion of epithelial and osteofibrous components. The tumor can be quite infiltrative, eroding the adjacent bones and spreading to distant organs such as the one in liver metastases [3].

On both CT and MRI, it generally manifests as an osteolytic lesion with sclerotic margins,

with a typical medullary and eccentric development [3].

In literature, due to the rarity of this tumor, there are no data regarding the prognosis.

Adipose Tissue Tumors

Liposarcoma

Chest wall origin is uncommon and can be seen in 10% of cases. It originates from lipoblasts that can be round and poorly differentiated or equal to that of mature adipose tissue. Liposarcoma can be divided into three subtypes, as follows: pleomorphic, myxoid, and the most frequent (40–45% of cases) well differentiated, or dedifferentiated liposarcoma [3]. On the chest radiograph, it may appear slightly radiolucent like a lipoma.

On CT, the lesion attenuation is moderately higher than that of normal fatty tissue, as the tumor contains both adipose and soft tissue. The variability in the cellularity of the tumor is expressed by a heterogeneous appearance. In the myxoid variant, calcifications and ossifications can be seen [14].

On MRI, myxoid liposarcoma has a moderately high signal intensity on T1-weighted images and high signal on T2-weighted images. Different features can be detected in case of round cells liposarcoma that shows a heterogeneous appearance with a low signal intensity on T1-weighted images, and a high signal intensity on T2-weighted images.

Given the tumor histologic composition, it may be difficult to distinguish well-differentiated liposarcoma from lipoma. Generally, a tumor composed entirely of fat can be identified as a

lipoma, while the presence of non-adipose components should increase the suspicion for malignancy. On MRI, the presence of intralesional septa of thickness greater than 2 mm is strongly indicative of liposarcoma [19].

If areas of high signal intensity on T2-weighted images and low signal intensity on T1-weighted sequences develop in a previously well-differentiated liposarcoma, a dedifferentiated liposarcoma should be suspected, particularly if these areas enhance after contrast media administration [14].

The outcome is like other soft-tissue sarcomas of the chest wall [3].

Muscular Tumors

Leiomyosarcoma

Leiomyosarcoma accounts for 1–5% of primary soft tissue sarcomas of the chest wall. It manifests as a painful mass occurring typically in adulthood (50–70 years), with a higher incidence rate in men than women [3].

CT shows a large mass that often displaces adjacent vessels that can be distorted. In addition, necrotic or cystic areas can be seen within the tumor. Calcifications are not a feature of this tumor (■ Fig. 9.6).

On MRI, a spindle shape is typical with low signal intensity on T1-weighted images and high

signal intensity on T2-weighted images. After contrast administration, the peripheral region of the lesion typically enhances, creating a hyperintense rim that encircles a central area of low signal intensity [14].

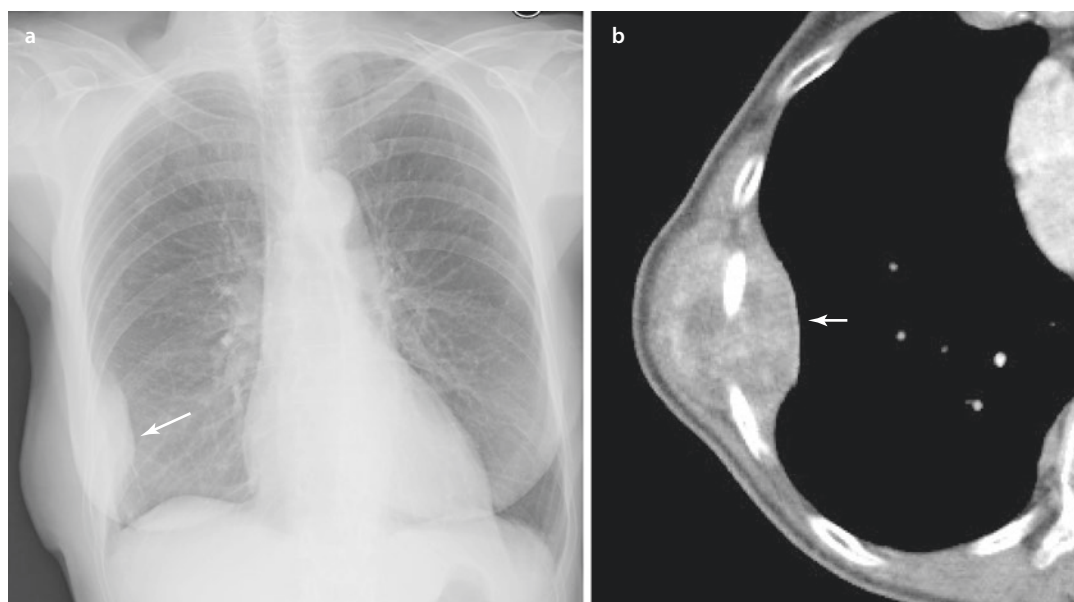
Rhabdomyosarcoma

This tumor accounts for 11% of the chest wall tumors [3]. It is a high-grade sarcoma showing a skeletal muscle differentiation that typically occurs in patients less than 45 years of age [14].

In the chest wall, it manifests as a nontender rapid growing mass that can cause pain or symptoms related to nerve compression. There are three different histologic subtypes: embryonal, alveolar, and pleomorphic. The alveolar subtype is the most frequently observed in the chest wall and is associated with the worst prognosis [3].

As reported by Gurney and Winer-Muram, rhabdomyosarcoma has an identical appearance to Askin tumor, presenting on the chest radiograph as a large, unilateral, and rapidly growing mass, with or without rib destruction. On CT, it manifests as a large and heterogeneous mass, due to intratumoral cystic, hemorrhagic, or necrotic components [3, 19].

On MRI, alveolar and pleomorphic subtypes show a specific aspect, with necrotic areas of low



■ Fig. 9.6 Leiomyosarcoma. (a) Chest X-ray shows asymmetrically increased density in the inferior lateral right chest with an “incomplete border” sign (white

arrow). (b) CT scan after contrast media administration confirms that the process is in the chest wall (arrow) with heterogeneous contrast enhancement

signal intensity not enhancing after contrast media administration, alternating with high signal intensity ring like areas that markedly enhance [3, 12, 17].

Embryonal type, typically occurring in children, can extend even in the anterior and lower chest wall.

The prognosis is related to the degree of differentiation of the tumor and to the histologic subtype: the alveolar subtype has a worst prognosis compared to both embryonal and pleomorphic subtypes [22].

Fibrous and Fibrohistiocytic Tumors

Malignant Fibrous Histiocytoma

MFH is the most common soft-tissue sarcoma in adults that rarely occurs in the chest wall. It arises from deep fascia or skeletal muscle and seldomly from the bones. It typically manifests as a nontender slow growing mass. Four histologic subtypes have been identified: pleomorphic, giant cell, myxoid, and inflammatory, which do not show typical features on X-ray. Two-thirds of patients are affected by storiform-pleomorphic MFH. On CT, this appears as a mass in the muscle and fascia planes with heterogeneous enhancement following contrast administration. The second most common type is myxoid MFH that has a typical aspect on CT due to its composition: the myxoid matrix in the center of the lesion is low attenuating, while the peripheral more cellularized components have a nodular enhancement.

On MRI, the tumor has a signal intensity equal to that of muscle on T1-weighted images, and signal intensity equal to or greater than that of fat on T2-weighted sequences. The tumor has a heterogeneous enhancement after contrast media administration [12, 14].

Due to the rarity of this tumor in the chest wall, no data in literature are available regarding the prognosis.

Aggressive Fibromatosis or Desmoid Tumor

Aggressive fibromatosis is an infiltrative lesion that does not metastasize (and may even undergo a spontaneous regression), originating from musculoaponeurotic structures and composed by patterns of elongated spindle-shaped cells infiltrating the surrounding tissue. The exact pathogenesis is still not clear, even if some predisposing factors have been identified, like trauma, scars, irradiation, endocrine disorders, and genetic factors. It can sometimes be associated with Gardner syn-

drome, even if this occurrence is more frequently seen in aggressive fibromatosis of the abdomen. Aggressive fibromatosis accounts for 54% of low-grade sarcomas of the chest wall, affecting prevalently adolescents and young adults, often with a female prevalence. Young patients are more frequently affected by tumor with an infiltrative pattern, while adults with a nodular one. Patients present with a palpable mass, associated with pain, paresthesia, hyperesthesia, and motor weakness if the thoracic inlet is involved. The tumor can locally recur, but it does not metastasize [3]. There are no typical radiographic findings.

On CT, the variable composition of the tumor is expressed in both attenuation and enhancement. Whereas confined to the muscles, it can encase adjacent vessels and nerves or extend into the pleural space with displacement of mediastinal viscera [14]. Bone invasion is rare but secondary compressive effects are seen.

MRI generally shows signal hypointensity on T1-weighted images and isosignal on T2-weighted images, which likely reflects collagen content [14].

Desmoid tumor is considered a low-grade fibrosarcoma, but it should be resected with wide margins to avoid recurrence, as all other primary malignant chest wall tumors; radiation therapy represents a proven and effective alternative or supplementary treatment [24].

Elastofibroma

Not a true neoplasm, elastofibroma arises secondary to idiopathic fibroblastic proliferation. It usually presents as a slow growing typically asymptomatic lesion, typically developing in the inferior subscapular region, deep to the serratus anterior, latissimus dorsi, and rhomboid muscles, and may be bilateral in 10%. It is seen around 60 years of age and is more common in women [3, 15, 17].

There are no typical radiographic findings. On CT, it appears as a soft-tissue mass, poorly circumscribed, and isoattenuating to muscle.

On MRI, it appears striated with linear strands of high signal on a background of T1 and T2 hypointensity, with low-grade heterogeneous enhancement [3, 15, 17, 19] (■ Fig. 9.7).

Hematologic Tumors

Malignant Lymphoma

Primary malignant chest wall lymphoma is rare, typically extranodal diffuse large B-cell lymphoma (DLBCL), and presents around the age of

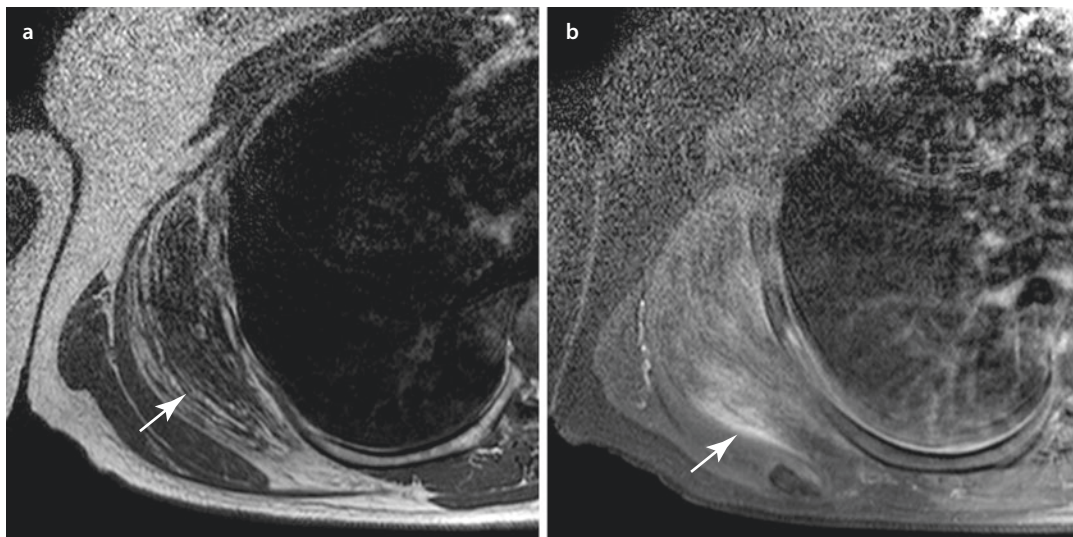


Fig. 9.7 Elastofibroma. (a) T1-weighted MRI image shows a low signal intensity process (white arrow) (b) with a low heterogeneous post-contrast enhancement (white arrow)

50 years [14]. It may be more commonly encountered in those with immunosuppressive therapy after transplantation, in AIDS, or after metallic orthopedic implants. It shows a multinodular or infiltrative pattern. Bone invasion may manifest after spreading from adjacent lymph nodes or from hematogenous spread [3].

On CT, the process mass is isoattenuating to muscle with moderate post-contrast enhancement.

On MRI, an intermediate signal is typical, with an intensity equal to that or slightly low than that of the adjacent muscle on T1-weighted images and with high signal intensity on T2-weighted images. Other features like infiltration of the neurovascular bundle and extension up to the subcutaneous tissue are commonly observed [14].

Solitary and Multiple Myeloma

Solitary and multiple myeloma are plasma cell tumors.

Solitary myeloma, or plasmacytoma, typically presents in patients with a mean age of about 50 years and manifests as a single mass that can progress to multiple myeloma [14].

Plasma cells produce an osteoclast-stimulating factor, thus determining multiple areas of osteolysis. On the chest radiograph, solitary myeloma manifest as an expansile mass with multiple cysts or as an osteolytic area with cortical thinning

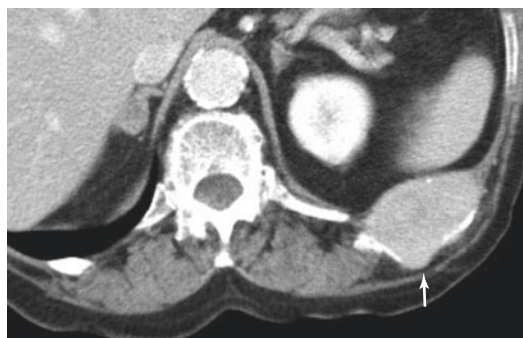


Fig. 9.8 Solitary multiple myeloma (Plasmacytoma). CT scan shows a single expansile lytic mass in the anterior chest wall, with post-contrast enhancement (white arrow)

without expansion. Extrasosseous solitary myeloma presents like a soft-tissue mass and progresses to multiple myeloma with a lower frequency.

Multiple myeloma manifests with a diffuse marrow involvement reflecting diffuse marrow space accumulation of plasma cells with multiple osteolytic lesions in the vertebral column, ribs, and clavicles. These lesions lead to pathologic fractures. Sclerosis may develop if pathologic fractures occur, but even after irradiation, chemotherapy, or without treatment.

CT scan demonstrates the presence of multiple (multiple myeloma) or single lytic lesions (plasmacytoma) (Fig. 9.8).

On MRI, the tumor has a low signal on T1-weighted images and a high signal on

T2-weighted images, although the signal intensity may be altered from secondary foci of hemorrhage or necrosis [12, 14, 18].

Localized solitary plasmacytoma is a rare tumor and surgery followed by adjuvant chemotherapy that is considered the best therapeutic approach. The most important factor affecting survival is the subsequent development of a multiple myeloma [25].

Cutaneous Tumors

Dermatofibrosarcoma Protuberans

Dermatofibrosarcoma protuberans is a rare tumor of the skin that tends to be locally invasive and recur locally (e.g., usually within 3 years after initial treatment) [14]. It typically manifests in adolescents as a slow growing violaceous nodule that is asymptomatic. There are two different variants of this tumor: a classic variant with an indolent course and an aggressive variant [26]. Metastases to regional lymph nodes are rare, accounting for 1–7% of cases. Distant metastases are rare as well, occurring in fewer than 5% of patients. The lung is the most frequent site involved, but metastases to the brain, pleura, pancreas, cervical lymph nodes, and orbit have also been observed. Distant metastases are more frequent with larger masses (>10 cm). This may reflect fibrosarcomatous changes (in 3–20% of cases) that are associated with a higher risk of local recurrence, metastasis, and death [27].

There are no typical radiographic findings. In the aggressive variant, CT shows a nodular subcutaneous lesion that appears well delineated with attenuation like that of skeletal muscle and with moderate enhancement after contrast media administration.

Nonspecific MRI is seen with heterogeneous signal owing to its variable composition, with foci of hemorrhage, myxoid change, or necrosis [14].

Other Tumors

Ewing Sarcoma Family of Tumors

Ewing sarcoma family includes both Askin tumor and Ewing sarcoma and is the most common malignant chest wall tumor in children and young adults. Both tumors probably originate from embryonal neural crest cells and express the same balanced translocation between chromosomes 11 and 22, t(11;22)(q24;q12) [21].

Ewing sarcoma may manifest as a solitary mass or as multiple masses with a typical eccen-

tric growth, which if expands could cause lung collapse or invasion. It originates from the ribs in a paravertebral region and then extends to the vertebral foramina. If smaller tumors displaces adjacent soft tissue, but larger ones invade or encase it.

Patients typically present with pain and systemic symptoms, like fever and malaise. Metastases to the lung or the bone are commonly found at diagnosis.

The chest radiograph shows the typical “onion peel” feature that is caused by subperiosteal bone formation but may also show periosteal elevation with osseous destruction with lytic and blastic foci [3, 12, 14].

CT of Ewing sarcoma demonstrates a large heterogeneous mass with extensive cystic degeneration along with occasional calcifications and sometimes hemorrhage or necrosis.

The tumor has a signal intensity equal to that of muscle on MRI T1-weighted images, showing a heterogeneous signal if areas of hemorrhage or necrosis are present. On T2-weighted images, heterogeneous signal intensity is seen. Significant post-contrast enhancement is present [12, 14, 19].

Ewing’s sarcoma of the chest wall is rare and usually considered as a systemic disease necessitating local as well as systemic therapy; despite this aggressive treatment, up to 40% of patients with localized disease will die [12, 14]. Indeed, distant metastases occur in about 75% and are associated with poor prognosis [22].

Synovial Sarcoma

Synovial sarcoma is a mesenchymal tumor that develops near joint capsules, bursae, and tendon sheaths of the extremities. Chest wall involvement is extremely rare and occurs in patients between 15 and 40 years of age, with possible metastases to lung, bones, or regional lymph nodes. The tumor is characterized by a specific translocation t(X;18)(p11;q11) [14].

There are no typical radiographic findings.

CT shows a soft-tissue mass with an attenuation similar or slightly higher to that of muscle that can infiltrate adjacent structures. In 20–30% of cases, intralesional calcifications are easily detected along with cortical bone erosion or invasion [28].

On MRI, a heterogeneous signal intensity is seen on T1-weighted images, predominantly

equal to that of muscle. In 45% of cases, small foci of hemorrhage are seen as foci of high T1 intensity. Fluid–fluid menisci may be present in 15–25% of patients [29]. These two features are associated with very poor prognosis, as they are associated with both larger and invasive tumors. On T2-weighted images, a marked heterogeneity is typical with internal septations, typical in larger tumors. In a third, a characteristic pattern on T2-weighted images with three different signal intensity levels: fluid (high signal), fat (intermediate), and low (fibrous tissue), when observed near a joint and accompanied by small foci of high intensity signal on T1-weighted images or calcifications, suggests the histological diagnosis [14].

Proximal-Type Epithelioid Sarcoma

Proximal-type epithelioid sarcoma is a tumor involving soft tissue of the extremities than occurring with a higher frequency in adolescents and young adults. It usually manifests as a lesion attached to the tendons, tendon sheaths, or fascial structure subcutaneously or deeply located. It clinically manifests as a subcutaneous or deep dermal mass [3].

There are no typical radiographic findings. On CT, stippled calcifications or ossification may be seen in 20–30% of cases [14].

On MRI on T1-weighted images, the tumor can be detected only because of its mass effect as it manifests with a signal intensity equal to that of muscle. A heterogeneous high intensity signal is evident on T2-weighted images. After contrast media administration, a strong and heterogeneous enhancement is observed [3, 14].

9.1.4 Treatment

Primary malignant chest wall tumors (PMCWT) are a heterogeneous group of tumors developing in the bones and soft tissues of the thoracic cage. They are usually considered as a group because the diagnostic and therapeutic problems they pose are similar. Their infrequency in this location generates a diagnostic and therapeutic challenge to the thoracic surgeon.

The approach to chest wall resection and reconstruction is similar to other major chest surgery, to balance the best option while minimizing surgical risk. A thorough medical history and physical examination form the basis for any fur-

ther investigation. Pulmonary function testing must be performed to evaluate patient reserves because a temporary compromise in respiratory function must be expected after resection. Several different techniques have been proposed to avoid paradoxical motion of the chest wall and impaired ventilation [6, 30, 31].

Although advanced surgical technique, use of prosthetic materials for reconstruction, and improvements in anesthesia and postoperative care have reduced the rates of mortality and morbidity, complications still occur in a fourth of cases with reported operative mortality up to 4% in some series. The most common complications are respiratory (some patients require prolonged ventilation and tracheostomy), wound infection, hematoma, seroma, partial flap loss, delayed wound healing, and, rarely, paradoxical motion of the chest wall [32].

9.1.4.1 Tissue Diagnosis

While obtaining tissue for diagnosis, some pitfalls must be recognized.

The skin incision on the Tru-Cut needle tract must not jeopardize subsequent skin flap. Hematoma must be avoided because it may propel sarcoma cells into and along soft tissue planes. The biopsy must be adequate for pathologic study. Necrotic tissue, hematoma, or inflammatory tissue may be submitted rather than tumor tissue. If the tissue specimen seems inadequate, a frozen section to confirm the cancerous tissue may be helpful.

Biopsy options include fine-needle aspiration (poor diagnostic yield), core-needle biopsy (superior accuracy of 88–95%), and incisional or excisional surgical biopsy.

Percutaneous core needle biopsy is effective and safe for the diagnosis of chest wall masses and may be performed with palpation or under sonographic or CT guidance. Besides being cost-effective, core needle biopsy limits the size of the biopsy tract that must be removed at the time of definitive wide or radical excision. If planned, induction therapy may be initiated immediately after without waiting for wound healing. However, it should be emphasized that while evaluating a patient with previous malignancy for suspected chest wall metastasis, fine needle aspiration for cytology should be enough for making a diagnosis.

Excisional (surgical) biopsy is appropriate for small lesions (2–4 cm) and lesions that appear to

benign on imaging. For tumors with unusual histologic pattern, it is important for the pathologist to know whether these patterns are present throughout the whole lesion or if they are confined to small areas of the tumor; in the latter, excisional (surgical) biopsy will be more informative. Open biopsy also appears to be superior for the diagnosis of cystic bone lesions. These lesions contain substantial amount of fluid, blood, and necrotic material, and sampling may not be sufficiently diagnostic without inclusion of a portion of the wall of the lesion. The biopsy access pathway must be planned to permit complete excision of its scar with primary tumor.

Less invasive biopsy procedures are preferred for larger tumors and for those tumors for which treatment is unlikely to be surgical (such as for Ewing's sarcoma, plasmacytoma, chest wall metastases). A presurgical diagnosis is critical before consideration of major chest wall resection or multimodality therapy.

9.1.4.2 Chest Wall Resection and Repair

Resection

Surgical policy in treating PMCWT is, in general, as follows: skin incision included the site of the previous biopsy, the invaded skin or previously irradiated tissue; wide resection of a lateral PMCWT included the affected ribs with at least 3–4 cm free margin proximally and distally to the tumors and the adjacent portions of one normal rib above and below the lesion; the extent of surgery in sternal PMCWT (partial sternectomy, subtotal sternectomy, or complete sternectomy) depends on the size and location of the tumors and, in all cases, resection included the adjacent sternocostal cartilages on each side; tumors extension into the chest cavity was evaluated during operation by VATS (video-assisted thoracic surgery) and any other structure involved in the tumor was also excised. In every case, care was paid during resection to spare unaffected muscles such as the latissimus dorsi (LD) and the lateral part of the pectoralis major (PM), both commonly used for reconstruction.

The importance of radical surgery in PMCWT is well known and has been demonstrated by several authors: Jean Philippe Berthet et al. analyzed 31 patients who underwent chest wall reconstruction between 2006 and 2011. In their series, they always checked the disease-free margin with

an accurate intraoperative examination; in particular for bone resection, they respected the limit of 3 cm macroscopic healthy tissue, wherever possible [33].

Resection and reconstruction were performed as a one-stage procedure in all cases. Every effort was made to wean patients rapidly from the ventilator. The need to perform induction chemotherapy or postoperative chemotherapy and radiotherapy in the case of high-grade sarcomas was discussed and planned with the medical oncologist and the radiotherapist in an oncological multidisciplinary group. Most of our operations were planned and performed by a team composed of a thoracic surgeon, a neurosurgeon (if the tumor is abutting the spine), and a plastic surgeon (if the need for a flap could be anticipated) [34, 35].

Reconstruction

The rule generally followed, as also we have applied, is not to reconstruct defects smaller than 5 cm in size in any location and those up to 10 cm in size posteriorly, while larger defects, most anterior defects, or defects in proximity to the tip of the scapula must be reconstructed.

In fact, chest wall defects posteriorly located, smaller than 7–10 cm in diameter, and covered by the scapula do not require reconstruction of the skeletal chest wall. If the tip of the scapula tends to intussuscept into the defect, surgical reintervention with reconstruction or partial scapular resection is mandatory.

Sometimes, when needed (large antero-lateral defects), chest-wall reconstruction was carried out with prosthetic material (non-rigid and rigid). In our experience, in the case of subtotal sternectomy, when a small part of the manubrium (with the sternoclavicular joint) or a part of the lower sternal body are conserved, a rigid reconstruction is not necessary; further, these defects can be replaced by nonrigid prostheses. In the case of large antero-lateral chest wall defects or in the case of a complete sternectomy, a reconstruction with rigid material is often mandatory to restore chest wall stability and to maintain the geometry of the thoracic cage [36–38].

Non-rigid material: mostly nonabsorbable polyethylene (Marlex) mesh, (Bard Inc., Murray Hill, NJ, USA), polypropylene (Prolene) mesh and polytetrafluoroethylene (ePTFE) patch (Gore Dualmesh Plus, W.L. Gore & Associates, Flagstaff,

AZ, USA), a prosthetic biomaterial combined with two antimicrobial preservative agents (chlorhexidine diacetate and silver carbonate, both active against Gram-positive and Gram-negative organisms), and also provided of a smooth visceral surface to minimize adhesions and a textured external surface for tissue ingrowth. Absorbable materials, in the past most often (Vicryl) mesh, are used in situations in which postoperative infection may be anticipated [36, 37].

Generally, a double layer of Marlex or Prolene mesh is cut in the shape of the defect, sewn to the ribs with interrupted nonabsorbable no. 1 or no. 2 sutures, and secured tightly by suture holes drilled in the rib edges or fixation superiorly and inferiorly around the ribs. The mesh is placed over the outer surface of the ribs to avoid scapular impingement. Before final fixation of the mesh, the patient is repositioned, a chest tube is placed, and the operative area is irrigated thoroughly with saline solution. A closed suction drain may be brought out from the mesh area through a puncture wound in the skin, and soft tissue coverage is accomplished.

Owing to the general absence of consensus, the type of allomaterial and the technique of reconstruction are largely dependent on the expertise and preference of the individual surgeon.

Recently, collagen matrixes harvested from human or animal sources and processed for medical use have emerged as an alternative. The implanted matrix undergoes remodeling with cellular infiltration, neovascularization, and exchange of extracellular matrix. Some of these materials have been chemically cross-linked to increase strength and durability. They are more expensive but very resistant to surgical site infections.

Many new biomaterials have been tested in other areas of surgery with good results. Cross-linked and noncross-linked swine or bovine dermal collagen prosthesis has been used to reconstruct musculofascial defects in the trunk with low infection and herniation rate. In all cases, we used a porcine collagen matrix mesh, and in all patients, it was covered by transposition of myocutaneous flap. The collagen material resulted in a durable and good to excellent chest wall stability in clinical follow-ups, and on computer tomography scans spanning over 3, 5 years. In conclusion: cross-linked acellular porcine dermal collagen matrix is a feasible and reliable biological patch material for recon-

struction of the thoracic wall. Excellent wound healing, long-term stability, low complication, and good pulmonary function are achieved even in large defects or complete sternal replacements. Permacol Biologic Implant (Covidien, Mansfield, MA) is a porcine dermal collagen matrix used in abdominal wall reconstruction and other surgical specialties. Structurally it is like human dermis. It is nonallergic and devoid of foreign body reaction and supports in growth and neovascularization. Veritas collagen matrix (Synovis, St Paul, MN) is a noncross-linked bovine pericardium that has been used over 5 years as a graft reinforcement in the treatment of uterine prolapse, urinary incontinence surgery, and urethral sling. It has demonstrated markedly less adhesion formation with underlying viscera. It also provides an ideal scaffold for reconstructive surgery. Its use has been reported in skeletal reconstructions of the chest wall [11]. Several reviews have been published regarding its utility as an alternative to other mesh. Our initial experience of using bioprosthetic patches for soft tissue reconstruction in thoracic surgery has proven satisfactory with overall acceptable results. The infection rates are low even when a proportion of procedures were performed under contaminated environments. Biologic prosthesis should be part of the surgical options to reconstruct soft tissues in thoracic surgery [39, 40].

Rigid reconstruction was carried out in some cases with Marlex mesh-methylmethacrylate sandwich (MMM) while other cases with the STRATOS (Strasbourg Thoracic Osteosyntheses System; MedXpert GmbH, Heitersheim, Germany) or different titanium bars systems and rib clips. However, the intraoperative preparation of the MMM requires time and, it is not very easy to handle and to adapt to the shape of the patient's chest and to set directly onto bony structures, particularly in nonexperienced hands. Moreover, even if the methylmethacrylate sandwich provides excellent chest wall stability and a low risk of respiratory complications, it is associated with a great number of wound complications; further, fracture, tilting, or extrusion of the implant are reported [37]. Nowadays, this new system consists of titanium rib clips available in different angles and connecting bars and its assembly is very simple and quick: once the ribs are isolated laterally to the margin of resection, the rib clips and the connecting bars can be bent to shape (by means of special

bending instruments, rib clip fixation, and cutting pliers) and fitted individually to reconstruct the chest defect. These rigid structures combine very well with any kind of mesh [41].

Once the chest wall has been stabilized, a soft-tissue coverage can be used to complete the reconstruction to control infection, obliterate dead space, and cover and separate the synthetic material.

The soft tissue transfer was always performed in close interaction with a plastic surgeon, involved in the preoperative selection of the flap as well as in the surgical procedure. PM (Pectoralis Major) is the most frequently selected muscle for sternectomy, because of its proximity, reliability, and versatility, and it can be used unilaterally or bilaterally, with skin advancement or as a musculocutaneous flap. We use a homolateral LD (latissimus dorsi) muscular flap for sternal reconstruction only in one case of PM that was unavailable because of previous irradiation. We reconstructed preferentially the antero-lateral chest wall defects with an LD muscle flap associated with skin advancement; the LD flap is easily transposed on thoracodorsal vessels and its length and bulk provide extensive coverage. The importance of a multidisciplinary approach in the treatment of PMCWTs is widely accepted and this need arises from the complexity of surgery (resection and subsequent reconstruction) (■ Fig. 9.9) as well as from the local and systemic aggressiveness of some histological types of PMCWTs. In our experience, most of the procedures were planned and performed with contributions from the plastic surgeon. In the same way, the indica-

tions to induction or adjuvant therapy were discussed and planned, together with the medical oncologist and the radiotherapist [30].

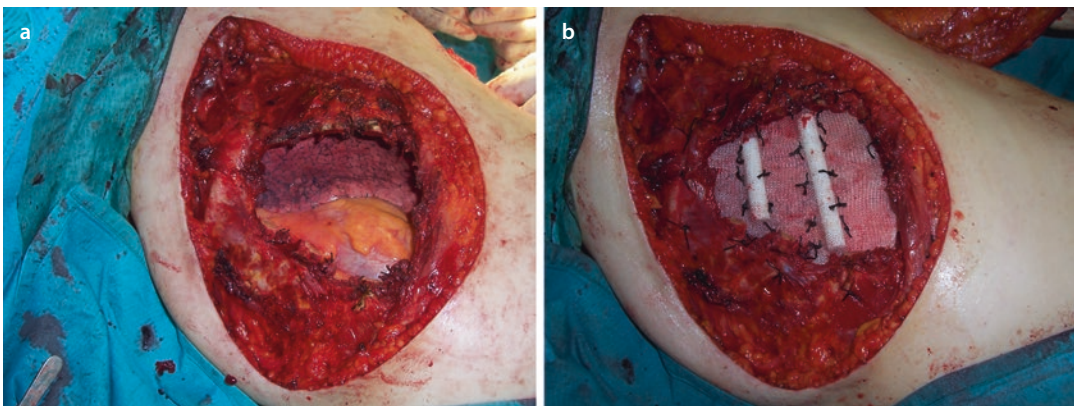
9.1.5 Prognosis

For PMCWTs, a 5-year survival range of 46–66% has been reported, with a wide difference between the various histologic types [32, 35, 36].

RIS (radiation-induced sarcoma) is an uncommon but increasing group of PMCWT; it develops commonly in patients previously irradiated for breast cancer or Hodgkin's disease and frequently arises or involves the thoracic outlet. Radical resection with adjuvant chemotherapy is advocated but, despite aggressive management, local and systemic recurrence rates are higher than other chest wall sarcomas [35].

Surgery is the cornerstone in the treatment of PMCWT: an adequate radical resection associated with the maintenance of chest stability, lung function, and an acceptable cosmetic result. Consequently, a critical point, in general in anterior chest wall resections, is a suitable prosthetic replacement, able to restore the rigidity of the chest and to prevent paradoxical motion, and a healthy soft-tissue coverage able to seal the pleural space, to protect the viscera and great vessels and to prevent infection [6].

Wide resection with tumor-free margins is necessary in PMCWT to minimize local recurrence and to contribute to long-term survival. To achieve satisfactory surgical results, the coordinated effort



■ **Fig. 9.9** (a) Surgical resection: full thickness antero-lateral chest wall resection for PMCWTs. (b) Reconstruction: partial chest wall reconstruction with the

combined use of polypropylene mesh and artificial methylmethacrylate ribs, prior to cover with musculocutaneous flap (b)

of a multidisciplinary surgical team is mandatory. Numerous advances over the years have made available various prosthetic materials and free or pedicled muscle flaps for chest wall replacement; the new mesh and the moldable titanium bars allows a firm reconstruction, simple to handle and to fix, and, in our opinion, represents a new option in the scenario of rigid or semirigid reconstruction. Despite the progress in multimodality treatment, survival in PMCWTs is very histology-dependent and durable long-term survival can be obtained only in the case of chondrosarcoma [6, 35, 36].

9.2 Patterns of Local Spread

9.2.1 Involvement of Adjacent Structures

Most chest wall tumors are often infiltrative. Neoplastic growth may determine invasion of the adjacent tissues, such as fat and bone.

For example, glomus tumor or cavernous hemangioma can erode adjacent bone when expanding. Similarly, aneurysmal bone cyst can markedly and rapidly expand in dimension, thus provoking bone destruction and extension to the adjacent tissues consequently. Desmoid tumor can encase adjacent vessels and nerves.

Malignant tumors can invade surrounding tissues secondary to their infiltrative nature to their high capability to infiltrate. Malignant fibrous histiocytoma and adamantinoma can infiltrate adjacent bones, while invasion of the lung is more frequently seen in Ewing sarcoma of family tumors [12, 14, 17, 19].

The involvement of neurologic structures typically manifest with the compression of the brachial plexus, of the long thoracic nerve (resulting in winged scapula) or with the involvement of sympathetic chain (resulting in Horner syndrome).

9.3 Lymph Node Involvement

9.3.1 Lymphatic Drainage and Lymph Node Involvement

Lymph nodes metastases from chest wall tumors are rare. Osteosarcoma spread to the lymphatics and lymph nodes in up to 70% of cases. Synovial sarcoma or dermatofibrosarcoma protuberans can

rarely metastasize to the pulmonary and regional lymph nodes (e.g., in 1–7% of cases) [14, 17].

Tumors developing in the thoracic inlet usually have a regional thoracic drainage (including supraclavicular nodes). Similarly, tumors arising from the lowest parts of the thorax may drain either into thoracic lymph nodes or into diaphragmatic ones.

Lymph nodes involvement can be well defined with FDG-PET. FDG-PET with CT imaging has demonstrable accuracy of 96% on nodal evaluation during tumor staging [3].

9.4 Metastatic Spread

Distant metastases are encountered with malignant chest wall tumors. Malignant peripheral nerve sheaths tumor, chondrosarcoma, osteosarcoma, neuroblastoma, dermatofibrosarcoma protuberans, giant cell tumor, and Ewing sarcoma of family tumors tend to metastasize to the lung, bone, and liver [3, 14, 17, 19]. Meguid and Brock reported cutaneous and liver metastases in advanced stages of leiomyosarcoma and hepatic involvement in one-third of patients with adamantinoma [3].

References

1. Siegel RL, Miller KD, Jemal A. Cancer statistics. *CA Cancer J Clin.* 2019;69:7–34.
2. Hemmati SH, Correa AM, Walsh GL, Swisher SG, Roth JA, Rice DC, Mehran RJ, Vaporciyan A. The prognostic factors of chest wall metastasis resection. *Eur J Cardiothorac Surg.* 2011;40(2):328–33.
3. Meguid RA, Brock MV. Chap. 18: Chest wall tumors. *John Hopkins textbook of cardiothoracic surgery.* 2014.
4. Graeber GM, Snyder RJ, Fleming AW, Head HD, Lough FC, Parker JS, Zajtchuk R, et al. Initial and long-term results in the management of primary chest wall neoplasms. *Ann Thorac Surg.* 1982;34:664–73.
5. Threlkel JB, Adkins RB. Primary chest wall tumors. *Ann Thorac Surg.* 1971;11:450–9.
6. Incarbone M, Pastorino U. Surgical treatment of chest wall tumors. *World J Surg.* 2001;25:218–30.
7. Anderson BO, Burt ME. Chest wall neoplasms and their management. *Ann Thorac Surg.* 1994;58:1774–81.
8. Pairolero PC, Arnold PG. Chest wall tumors experience with 100 consecutive patients. *J Thorac Cardiovasc Surg.* 1985;90:367–72.
9. Stelzer P, Gay WA. Tumors of the chest wall. *Surg Clin North Am.* 1980;60:779–91.
10. Sabanathan S, Shah R, Mearns AJ. Surgical treatment of primary malignant chest wall tumors. *Eur J Cardiothorac Surg.* 1997;11:1011.

11. Hsu PK, Lee HC, Hsieh CC, Wu YC, Wang LS, Huang BS, Hsu WH, Huang MH. Management of primary chest wall tumors: 14 years' clinical experience. *J Chin Med Assoc.* 2006;69(8):377–82.
12. Shah AA, D'Amico TA. Primary chest wall tumors. *J Am Coll Surg.* 2010;210:360–6.
13. Tateishi U, Gladish GW, Kusumoto M, et al. Chest wall tumors: radiologic findings and pathologic correlation. Part 1. Benign tumors. *Radiographics.* 2003;23:1477–90.
14. Tateishi U, Gladish GW, Kusumoto M, et al. Chest wall tumors: radiologic findings and pathologic correlation. Part 2. Malignant tumors. *Radiographics.* 2003;23:1491–508.
15. Mullan CP, Madan R, Trotman-Diskenson B, et al. Radiology of chest wall masses. *Am J Roentgenol.* 2011;197:460–70.
16. Shimoyama T, Kimura B, Nakamura K, Yamada T, Kawachi H. Langerhans cell histiocytosis of the rib in adult male. *Kyobu Geka.* 2011;64(2):135–8.
17. Nam SJ, Lim BJ, Yoon CS, et al. Imaging of primary chest wall tumors with radiologic-pathologic correlation. *Radiographics.* 2011;3:749–70.
18. Faul JL, Berry GJ, Colby TV, Ruoss SJ, Walter MB, Rosen GD, Raffin TA. Thoracic lymphangiomas, lymphangiectasis, lymphangiomatosis, and lymphatic dysplasia syndrome. *Am J Respir Crit Care Med.* 2000;161(3 Pt 1):1037–46.
19. Antunes N, Serrado MA, Santos R, et al. Primary chest wall tumors: a pictorial essay. *ECR.* 2016, poster n. C-1832.
20. Defilippi C, Chiappetta D, Marzari D, Mussa A, Lala R. Image diagnosis in McCune-Albright syndrome. *J Pediatr Endocrinol Metab.* 2006;19(Suppl 2):561–70.
21. Carter BW, Benveniste MF, Betancourt SL, de Groot PM, Lichtenberger JP 3rd, Amini B, Abbott GF. Imaging evaluation of malignant chest wall neoplasms. *Radiographics.* 2016;36:1285–306.
22. Gladish GW, Sabloff BM, Munden RF, et al. Primary thoracic sarcomas. *Radiographics.* 2002;22:621–37.
23. Marullia G, Durantib L, Cardillo G, et al. Primary chest wall chondrosarcomas: results of surgical resection and analysis of prognostic factors. *Eur J Cardiothorac Surg.* 2014;45:e194–201.
24. Kabiria EH, Al Aziza S, El Maslout A, et al. Desmoid tumors of the chest wall. *Eur J Cardiothorac Surg.* 2001;19:580–3.
25. Jia R, Xue L, Liang H. Surgery combined with radiotherapy for the treatment of solitary plasmacytoma of the rib: a case report and review of the literature. *J Cardiothorac Surg.* 2015;10:125.
26. Torreggiani WC, Al-ismail K, Munk PL, et al. Dermatofibrosarcoma protuberans: MR imaging features. *AJR Am J Roentgenol.* 2002;178(4):989–93.
27. Li X, Zhang W, Xiao L, et al. Computed tomographic and pathological findings of dermatofibrosarcoma protuberans. *J Comput Assist Tomogr.* 2012; 36(4):462–8.
28. Sanchez Reyes JM, Alcaraz Mexia M, Quinones Tapia D, Aramburu JA. Extensively calcified synovial sarcoma. *Skelet Radiol.* 1997;26:671–3.
29. Jones BC, Sundaram M, Kransdorf MJ. Synovial sarcoma: MR imaging findings in 34 patients. *AJR Am J Roentgenol.* 1993;161:827–30.
30. Lardinois D, Muller M, Furrer M, Banic A, Gugger M, Krueger T, Ris HB. Functional assessment of chest wall integrity after methylmethacrylate reconstruction. *Ann Thorac Surg.* 2000;69:919–23.
31. Gonfiotti A, Santini PF, Campanacci D, Innocenti M, Ferrarello S, Caldarella A, Janni A. Malignant primary chest-wall tumors: techniques of reconstruction and survival. *Eur J Cardiothorac Surg.* 2010;38(1):39–45.
32. Athanassiadi K, Kalavrouziotis G, Rondogianni D, Loutsidis A, Hatzimi-chalis A, Bellenis I. Primary chest wall tumors: early and long-term results of surgical treatment. *Eur J Cardiothorac Surg.* 2001; 19:589–93.
33. Berthet JP, Wihlm JM, Canaud L, Joyeux F, Cosma C, Hireche K, Alric P, Marty-Ané CH. The combination of polytetrafluoroethylene mesh and titanium ribs implants: an innovative process for reconstructing large full thickness chest wall defects. *Eur J Cardiothorac Surg.* 2012;42:444–53.
34. Mansour KA, Thourani VH, Losken A, Reeves JG, Miller JI Jr, Carlson GW, Jones GE. Chest wall resection and reconstruction: a 25-year experience. *Ann Thorac Surg.* 2002;73:1720–5.
35. Burt M. Primary malignant tumors of the chest wall: the Memorial Sloan—Kettering Cancer Center experience. *Chest Surg Clin N Am.* 1994;49:363–9.
36. Weyant M, Bains M, Venkatraman E, Downey R, Park B, Flores R, Rizk N, Rusch V. Results of chest wall resection and reconstruction with and without rigid prosthesis. *Ann Thorac Surg.* 2006;81:279–85.
37. Chapelier A, Macchiarini P, Rietjens M, Lenot B, Margulis A, Petit JY, Darteville P. Chest wall reconstruction following resection of large primary malignant tumors. *Eur J Cardiothorac Surg.* 1994;8:351–7.
38. Chapelier AR, Missana MC, Couturaud B, Fadel E, Fabre D, Mussot S, Pouillart P, Darteville PG. Sternal resection and reconstruction for primary malignant tumors. *Ann Thorac Surg.* 2004;77:1001–7.
39. Barua A, Catton JA, Socci L, Raurell A, Malik M, Interullo E, Martin-Ucar AE. Initial experience with the use of biological implants for soft tissue and chest wall reconstruction in thoracic surgery. *Ann Thorac Surg.* 2012;94:1701–5.
40. Schmidt J, Redwan B, Koesek V, Heitplatz B, Bedetti B, Aebert H, Wiebe K. Thoracic wall reconstruction with acellular porcine dermal collagen matrix. *Thorac Cardiovasc Surg.* 2016;64(3):245–51.
41. Gonfiotti A, Santini PF, Campanacci D, Innocenti M, Ferrarello S, Janni A. Use of moldable titanium bars and rib clips for total sternal replacement: a new composite technique. *J Thorac Cardiovasc Surg.* 2009;138:1248–50.